

Copyright  
by  
Craig E. Michoski  
2009

The Dissertation Committee for Craig E. Michoski  
certifies that this is the approved version of the following dissertation:

## **Evolution Equations in Physical Chemistry**

Committee:

---

Alexis F. Vasseur, Supervisor

---

John F. Stanton, Supervisor

---

Irene M. Gamba

---

Robert E. Wyatt

---

Panagiotis E. Souganidis

---

Graeme Henkelman

# **Evolution Equations in Physical Chemistry**

by

**Craig E. Michoski, B.A.**

## **DISSERTATION**

Presented to the Faculty of the Graduate School of

The University of Texas at Austin

in Partial Fulfillment

of the Requirements

for the Degree of

## **DOCTOR OF PHILOSOPHY**

THE UNIVERSITY OF TEXAS AT AUSTIN

May 2009

Dedicated to my parents, Thomas and Beverly Michoski.



## Acknowledgments

I would like to express my heartfelt gratitude to my advisor, Alexis Vassuer. Without his enduring patience and gracious generosity none of this work would have been possible. I would like to, in particular, thank him for sharing his great wealth of knowledge in his art and science, for his willingness to engage in a complicated research tract; but most of all, for his inconspicuous encouragement, insouciant veracity, and gentle wisdom. I would also like to thank John Stanton for his continued support and patience throughout this work. Without his sponsorship it would not have been possible to perform this unique interdisciplinary program. I would also like to extend my thanks to Bob Wyatt, for his extensive help in understanding quantum hydrodynamics, his passion for chemistry and learning and also for all of his helpful and useful advice. I would additionally like to thank my close collaborators and friends, John Evans and Phillip Schmitz. Without their guidance and friendship I would not have found my way through the forest. I would also like to thank Ruth Shear and Harshal Gupta for the substantial moral support that they have tendered throughout this work.

I would finally like to thank my family for their constant love and support. It is within your adamantine enclave that I have dwelled.

# Evolution Equations in Physical Chemistry

Publication No. \_\_\_\_\_

Craig E. Michoski, Ph.D.

The University of Texas at Austin, 2009

Supervisors: Alexis F. Vasseur  
John F. Stanton

We analyze a number of systems of evolution equations that arise in the study of physical chemistry. First we discuss the well-posedness of a system of mixing compressible barotropic multicomponent flows. We discuss the regularity of these variational solutions, their existence and uniqueness, and we analyze the emergence of a novel type of entropy that is derived for the system of equations.

Next we present a numerical scheme, in the form of a discontinuous Galerkin (DG) finite element method, to model this compressible barotropic multifluid. We find that the DG method provides stable and accurate solutions to our system, and that further, these solutions are energy consistent; which is to say that they satisfy the classical entropy of the system in addition to an additional integral inequality. We discuss the initial-boundary problem and the existence of *weak entropy* at the boundaries. Next we extend these results to include more complicated transport properties (i.e. mass diffusion), where exotic acoustic and chemical inlets are explicitly shown.

We continue by developing a mixed method discontinuous Galerkin finite element method to model quantum hydrodynamic fluids, which emerge

in the study of chemical and molecular dynamics. These solutions are solved in the conservation form, or Eulerian frame, and show a notable scale invariance which makes them particularly attractive for high dimensional calculations.

Finally we implement a wide class of chemical reactors using an adapted discontinuous Galerkin finite element scheme, where reaction terms are analytically integrated locally in time. We show that these solutions, both in stationary and in flow reactors, show remarkable stability, accuracy and consistency.

# Table of Contents

<b>Acknowledgments</b>	<b>v</b>
<b>Abstract</b>	<b>vi</b>
<b>List of Tables</b>	<b>x</b>
<b>List of Figures</b>	<b>xi</b>
<b>Chapter 1. Introduction</b>	<b>1</b>
<b>Chapter 2. A Well-posed System for Compressible Multicomponent Flows</b>	<b>9</b>
2.1 Introduction . . . . .	9
2.2 Statement of Result . . . . .	17
2.3 Energy Inequalities . . . . .	21
2.3.1 Additional Energy Inequality . . . . .	24
2.4 Establishing the Existence Theorem . . . . .	25
2.4.1 Bounds on the Density . . . . .	27
2.4.2 Bounds for the Velocity . . . . .	37
2.4.3 Bounds on the Mass Fraction . . . . .	42
2.4.4 Proof of the Existence Half of the Theorem . . . . .	42
2.5 Establishing the Uniqueness Theorem . . . . .	44
<b>Chapter 3. Numerical Solutions to Generalized Compressible Multicomponent Flows</b>	<b>50</b>
3.1 Introduction . . . . .	50
3.2 The Generalized $n$ -fluid . . . . .	53
3.3 Towards a Generalized Boundary Treatment . . . . .	61
3.4 Numerical Test Cases . . . . .	69

3.5	Example: 2-fluid with chemical inlet . . . . .	75
3.6	Example: k-th order in time n-fluid . . . . .	79
3.7	Energy Consistency of Scheme . . . . .	82
3.8	Fick's Diffusion with Acoustic BCs . . . . .	87
<b>Chapter 4. Quantum Hydrodynamics with Chemical Applications</b>		<b>93</b>
4.1	Introduction . . . . .	93
4.2	Conservation Formulation of Quantum Hydrodynamics . . . .	98
4.3	Boundary Treatment . . . . .	105
4.4	A Numerical Test Case . . . . .	111
4.5	Tunneling in TDSE and QHD . . . . .	114
4.6	Recovering $\psi$ and $S$ in both frames . . . . .	124
<b>Chapter 5. Chemical Reactor Models</b>		<b>128</b>
5.1	Introduction . . . . .	128
5.2	Basic Stationary Chemical Reactors . . . . .	130
5.3	Basic Flow Reactors . . . . .	140
5.4	General Chemical Reactors . . . . .	146
<b>Chapter 6. Conclusions and Future Work</b>		<b>152</b>
<b>Appendices</b>		<b>157</b>
<b>Appendix A.</b>		<b>158</b>
<b>Appendix B.</b>		<b>162</b>
<b>Bibliography</b>		<b>164</b>
<b>Vita</b>		<b>197</b>

## List of Tables

3.1	<i>Choice of boundary conditions</i> . . . . .	65
3.2	<i>Runge-Kutta <math>k</math>-th order in time</i> . . . . .	82
4.1	<i>Runge-Kutta <math>k</math>-th order in time</i> . . . . .	115
5.1	All approximate values given at STP. (1) was measured via chronoamperometry as shown in Ref. [241]. (2) was measured using oscillating disc viscometry in Ref. [242]. (3) was determined via the single component Chapman-Enskog experimental fits in Ref. [243]. (4) was calculated using diffusion denuders in Ref. [244]. The remaining approximate coefficients are adapted using relative magnitude arguments from simple collisional theory [12] (viz. $\nu \propto m$ and $\mathcal{D} \propto \sigma^{-1}$ ). . . . .	132

## List of Figures

3.1	The discretization of $\Omega$ , distinguishing nodes, elements, and neighbors with the boundary $\partial\Omega = \{a, b\}$ . . . . .	58
3.2	A plot of the solutions $\rho_s = \rho_{RvL} - \rho_{LFO}$ and $u_s = u_{RvL} - \rho_{LFO}$ minus the analytic steady state solutions $\rho_a = 1$ and $u_a = 1$ . .	72
3.3	The top two graphs show the solution to (3.36) in terms of the local Lax-Friedrich's flux and the van Leer limiter, denoted by $u_s$ and $\rho_s$ versus the exact solution $u_a = \tan x$ and $\rho_a = (\tan x)^{-1}$ . The bottom two graphs show the solution to (3.36) in terms of the linear Riemann flux and the Osher limiter, denoted $u_r$ and $\rho_r$ , again versus the exact solution. . . . .	73
3.4	The left plot shows miscible species at $t = 12$ given the “characteristic” chemical inlet conditions from (3.42) with $\mathcal{C} = 0.9$ and on the boundary $a = 0$ , with transmissive conditions on $b = x_{ne}$ (see Figure 3.1). The right plot shows the same solution using the <i>weak entropy</i> formulation. Here we have a miscible solution of methanol and water at $\vartheta = 500\text{K}$ and initial $\mu_1 = \mu_2 = 0.5$ , while both solutions use $\tilde{\Phi}_{LFL}$ and the van Leer limiter. . . . .	76
3.5	Here we show the difference between specie one of the <i>weak entropy</i> $\mu_{1,w}$ versus “characteristic” $\mu_{1,c}$ solutions, where $\xi = \mu_{1,w} - \mu_{1,c}$ . . . . .	77
3.6	Here we have the complementary difference between species two of the <i>weak entropy</i> $\mu_{2,w}$ and “characteristic” $\mu_{2,c}$ solutions, where $\eta = \mu_{2,w} - \mu_{2,c}$ . . . . .	78
3.7	Here we show the first and last timesteps of the mass fractions at $\vartheta = 293\text{K}$ using periodic boundary conditions with Runge-Kutta order $k = 2$ . Initial conditions set $\rho = 5 + 20e^{-(x-10)^2/8} + 20e^{-(x-30)^2/8}$ and $u = \sin(6\pi x/x_{ne})$ , with $\mu_1 = 0.07 + 0.3e^{-(x-27.5)^2/12}$ , $\mu_2 = 0.1 + 0.3e^{-(x-10.5)^2/8}$ , $\mu_3 = 0.06 + 0.3e^{-(x-22.5)^2/8}$ , $\mu_4 = 0.05 + 0.3e^{-(x-30.5)^2/10}$ and solvent $\mu_5 = 1 - \sum_{n=1}^4 \mu_i$ . . . . .	80
3.8	Here we show the time evolution over the entire solution space of the same problem from Figure 3.7. . . . .	81

3.9	Here we plot the integral forms $\mathcal{S}_T$ and $\tilde{\mathcal{S}}_T$ for $C = 1$ and $\alpha = 0.9$ , where $\int_{\Omega} \mathcal{H}_0 dx$ and $\int_{\Omega} \tilde{\mathcal{H}}_0 dx$ are represented by the first timestep. The spatial mesh is chosen with $ne = 100$ with $\Delta t = 0.01$ . . . . .	84
3.10	Here we compare the viscosity $\nu$ , density $\rho$ and pressure $p$ of the periodic 5-fluid from §3.6 with $\alpha = 0.9$ , $C = 0.5$ , 150 meshpoints and $\Delta t = .006$ . . . . .	86
3.11	A <i>weak entropy</i> solution to an oscillating pressure front propagating through a 5-component low density ( $\sim 100$ molecules per cm) gas at $\vartheta = 20\text{K}$ . The chemical constituents are comprised of species found in dark interstellar molecular clouds, where representative fractional abundances are adopted and the solution space is appropriately scaled; with corresponding initial conditions: $\text{H}_2 \sim 80\%$ , $\text{He} \sim 19.9\%$ , and trace $\text{CO}$ , $\text{H}$ (atomic hydrogen), and $\text{HC}_3\text{N}$ (cyanoacetylene). . . . .	89
3.12	A “characteristic” solution to the same oscillating pressure front presented in 3.11. . . . .	90
3.13	Here we plot the relative difference between the <i>weak entropy</i> pressure $p_w$ and the “characteristic” pressure $p_c$ . . . . .	92
4.1	Here we have the intramolecular rearrangement of the aryl radical 2, 4, 6-tri- <i>tert</i> -butylephenyl to 3, 5-di- <i>tert</i> -butylneophyl (see Ref. [210] for details). . . . .	94
4.2	Here we show an enzymatic catalysis – an aromatic amine dehydrogenase (AADH) with a tryptophan tryptophyl quinone (TTQ) prosthetic group catalyzing the oxidative deamination of tryptamine with an electron transfer to an arsenate reductase enzyme (see Ref. [210] and Ref. [212] for details, PDB codes: 1nwp (azurin), 2agy (AADH)). . . . .	95
4.3	Here we show the relative error introduced by the <i>weak entropy</i> boundary conditions for $a = 0$ and both $b = 10$ and $b = 50$ . The boundary data (the graphs on the right) show only the relative error on element $b$ of $\partial\Omega$ for $b = 10$ and $b = 50$ , respectively. . . . .	112
4.4	The top graphs compare solutions to the TDSE and QHD system in the so-called “eyeball norm,” using the forward Euler scheme. The bottom solution shows the nontrivial formal difference. Here $x$ refers to the $x$ -th meshpoint. . . . .	116
4.5	We show the diffusive noise profile $\min(\rho_{\text{QHD}}, 10^{-3})$ in the QHD solution, and the difference $\min(\rho_{\text{TDSE}}, 10^{-3}) - \min(\rho_{\text{QHD}}, 10^{-3})$ . Here $x$ refers to the $x$ -th meshpoint. . . . .	118



4.6	We show the absolute difference between the QHD solution using the approximate boundary data from Figure 4.4 denoted $\rho_\psi$ with the transmissive boundary formulation from (4.44) denoted $\rho_T$ . Here $x$ refers to the $x$ -th meshpoint. . . . .	119
4.7	We solve the accumulated density trajectories from (4.42) using the transmissive solutions from $\rho_T$ in Figure 4.6. . . . .	120
4.8	Here we show mass conservation in the QHD regime given transmissive boundaries, where $bf = \int_{[0,T)} \int_{\partial\Omega} \rho dx dt$ is the boundary flux. . . . .	122
4.9	Here we show the remarkable spatial invariance of the solution. These represent the same solution as that given in Figure 4.4, except the left graph is with 25 meshpoints and 100 timesteps, and the right at 50 meshpoints and 200 timesteps. . . . .	124
4.10	We graph the quantum trajectories using (4.45) to solve for $\vec{r}$ , which can be compared with the accumulated mass trajectories shown in Figure 4.7. . . . .	125
4.11	The Eulerian solution $\rho(t, x)$ and the corresponding Lagrangian solution $\rho(t, \vec{r})$ for the same initial condition settings as in figure 4.7 using the conservation form of the trajectories (4.42).. . . .	125
4.12	A graph of the Eulerian solution $S(t, x)$ and the corresponding Lagrangian solution $S(t, \vec{r})$ for the same initial condition settings as in figure 4.11 using the conservation form of the trajectories (4.42). . . . .	126
5.1	We show the hypergolic ignition reaction from 5.7, where initial conditions are given by $\alpha_{1,0} = 0.49 \exp\left(-\frac{(x-60)^2}{800}\right)$ , $\alpha_{2,0} = 1 \times 10^{-5}$ , $\alpha_{3,0} = 0.49 \exp\left(-\frac{(x-40)^2}{800}\right)$ and $\alpha_{4,0} = 1 \times 10^{-5}$ , where transmissive boundaries are used. . . . .	135
5.2	The top graphs compare solutions to $\alpha_3$ with respect to the constant vector $\mathcal{D}_i$ (on the top left), and the Chapman-Enskog matrix $\mathcal{D}_{ij}$ (on the top right). The bottom left is a difference map between these two solutions, and the bottom right shows the noise occurring near both the reagent interfaces and near the ( <i>weak entropy</i> ) boundary of the domain, $\partial\Omega$ . . . . .	137

5.3	The top left graph shows the depletion of the nitrous dioxide, the compound with the largest heat capacity index as approximated by the ideal gas assumption. Hence, the speed of sound is highest in the region of highest NO <sub>2</sub> concentration, as seen in the top right graph. The bottom graph shows that the velocity field $u$ ( <i>color</i> ) breaks through the speed of sound ( <i>light grey</i> ) in the region containing MMH, causing a shock front to propagate through the solution. . . . .	143
5.4	Here we show the supersonic nozzle with a propagating hypergolic reaction mechanism. . . . .	145
B.1	On the top we show the quantum trajectories using the offset method solution of the same problem in Figure 4.10 with $r = 1$ ; and on the bottom we show the same trajectories using $r = 2$ . . . . .	162

# Chapter 1

## Introduction

Evolution equations can generally be thought of as the objects comprising any theoretical model system whose parameter space evolves dynamically through time. Most generally, the study of evolution equations can be shown to span nearly every theoretical field that employs quantitative models; from mathematics [1], physics [2], chemistry [3], engineering [4] and biology [5], to informatics [6], quantitative psychology [7], economics [8], analytic philosophy [9] and metamathematics [10] — just to mention a sparse subclass of examples.

In particular, we are concerned in this work with the study of evolution equations which arise in physical chemistry, chemical physics, mathematical physics, as well as applied and numerical mathematics and engineering. More specifically, we address a subset of evolution equations that emerge in these fields, but which find direct application to model systems of particular importance in physical chemistry.

Studying evolution equations in theoretical and computational physical chemistry presents a unique set of interdisciplinary challenges. First, the study of “realistic” chemical systems — which is to say, systems which include “as many natural, or physical, variables as possible” — often requires extensive and complicated functionally-coupled mathematical systems. These systems may not only be difficult and subtle to model numerically, but may also be (and often are) extremely difficult to pose in a consistent and non-degenerate way

analytically; which is to say, a way which does not lead to “nonphysical” and spurious behavior.

More specifically, evolution equations comprise the substrate, *in essence*, of the study of chemical kinetics (for example see Ref. [11]). Here rate laws can be seen as one of the most immediate examples of an evolution equation arising in chemical systems, i.e. a source field — the local componentwise concentration of the molecular constituents of the system — evolving in time. As reaction kinetics are so fundamental to the study of many, if not most, chemical systems, it becomes immediately clear how pervasive these techniques are in the study of chemical and biochemical systems.

A more complicated evolution equation which arises in physical chemistry applications include the class of transport, or advection equations. A prime example of such an equation is given by the mixing of (inert) multi-component fluids and gases (see Chapter 2 and 3 for examples) along the characteristics of a flow field. These transport equations (such as Fick’s law) are used to describe the transport properties (viscosity, conductivity, thermal diffusion, etc. [12]) that characterize the behaviors of bulk materials.

In fact, in order to include the effects of equilibrium thermodynamics on the mixing (which arises in standard physical chemistry [11]), one must include the time-evolving Gibb’s free energy of mixing,  $G$ . This already introduces a substantial technical difficulty at the level of mathematical representation, since these systems, which may be modeled using the Allen-Cahn [13] or Cahn-Hilliard [14] equations, exhibit second and fourth order differential dependencies on the evolution parameters. Nevertheless, these types of systems are very common in physical chemistry experiments, where they may describe spinodal decomposition, colloidal chemistry, nucleation and crystal-

lization events, and the complicated interspecies phase dynamics of mixtures (e.g. in dense polymeric fluids, nanocrystals, and solar cell fabrication [4, 15–17]).

When these transported properties are coupled to conservation laws, nonlinear fluid dynamical models emerge, such as the Euler system of partial differential equations, or the Navier-Stokes system of partial differential equations (PDEs). These coupled systems of PDEs quickly become quite complicated, as they are invariably determined from  $k$  equations and  $k$  unknowns. For example, the Euler equations solve a system of three equations (mass, momentum, and energy conservation) and three unknowns (density  $\rho$ , velocity  $u$ , and total energy  $E$ ). This system of PDEs is highly nonlinear and admits naturally discontinuous solutions (i.e. shockwaves). Similarly the Navier-Stokes system introduces viscous effects and rotational field effects, such as turbulence; which immediately introduce additional mathematical complications into the solution space. The coupling of higher order transport effects (as mentioned above) to these conservation laws lead to elaborate systems of partial differential equations, such as seen in Korteweg-type fluid equations [18], surface tension phase-field models [19], quantum hydrodynamics [20] and magnetofluid models [21, 22]. All of these systems arise commonly in physical chemistry, in the form of interfacial diffusion [23], multiphase dynamics (e.g. bubbles in water) [24], (quantum) chemical kinetics [20], and the dynamics of strongly (or weakly) ionized multicomponent gases [25, 26], respectively.

The theoretical foundation of the above mentioned fluid models may be derived from molecular collision theory (see Ref. [12, 27]). In fact, fluid models may be viewed as  $\ell$ -th order moment expansions that emerge from the molecular description of fluids, given by the Boltzmann equation [28] (or

the Vlasov equation for neutral plasmas [29]). That is, we may consider the statistical “flow field” of the probability density  $f$  of individual particles in phase space, which comprise the well-known kinetic theory of liquids and gases (see Ref. [30–32]), and in the Chapman-Enskog expansion, these lead in  $\ell = 0$  to the Euler equations, in  $\ell = 1$  to the Navier-Stokes equations, in  $\ell = 2$  to the Burnett equations, in  $\ell = 3$  to the super-Burnett equations [33], etc.

In the present work, we focus on the chemical dynamics of systems which are either in a stationary state, or those which follow the flow fields of “fluids” (for us, either gases, plasmas, liquids or electronic probability densities) which obey compressible fluid mechanics. Compressible fluid mechanics are distinguished from incompressible fluid mechanics, in that the divergence (source or sink) of the velocity vector vanishes in incompressible fluids:  $\nabla \cdot \mathbf{u} = 0$ . The concept of a compressible fluid in continuum mechanics should not, however, be confused with the concept of the compressibility  $Z$  of a “real gas” in equilibrium thermodynamics. For instance, in Chapter 2 we will be concerned with a time evolving compressible flow of an idealized gas whose pressure is a function of the density  $p = p(\rho)$ , and whose compressibility factor  $Z = 1$ .

More specifically, in this work we cover a large family of continuum processes which are described by conservation form partial differential equations of mixed hyperbolic-parabolic type. We are generally interested in a diverse set of initial-boundary value problems which can accommodate a large number of physically and chemically relevant contexts. Where possible, we have stayed as close as possible to the concept of “mathematical well-posedness,” in the sense of Hadamard. We find, and demonstrate, that this not only improves the stability of our results, but also the accuracy and consistency of our solutions.

In Chapter 2 we address the issue of well-posedness directly. Here we show the existence, uniqueness and regularity results for a compressible barotropic flow comprised of miscible (and reactively inert) chemical constituents. We rely heavily on the previous results of Solonnikov [34], Vasseur [35], Mellet [36], Desjardins [37] and Bresch [38], and demonstrate how the fluid obeys a novel multicomponent *entropy* with functional concentration dependent viscosity, which in tandem with the *classical entropy* is enough to control variational (or weak) solutions in the  $L^2$ -norm globally in time. Some of the work in this chapter is duplicated from Ref. [39].

We proceed in Chapter 3 by presenting a computationally well-posed discontinuous Galerkin finite element implementation of the system from Chapter 2. That is to say, we present a local variational formulation of a slightly generalized form of the system from Chapter 2, where as many underlying assumptions, approximations and implementational nuances are made as completely explicit as possible, with an eye towards making these systems exactly numerically reproducible. Along these lines, a special emphasis is made on the consistent treatment of boundary data. We show how one may generally introduce so-called *weak entropy* boundary conditions, which are aptly named, versus the so-called “characteristic treatment” of boundary data; which also introduce local perturbations in the solution space. Here we explicitly introduce some physically relevant boundary conditions, such as chemical and acoustic inlets, and perform some extensive numerical experiments on these physical systems. We further show how our discontinuous Galerkin scheme not only conserves mass, momentum and species (for inert constituents), but also conserves both entropy inequalities from Chapter 2, as long as the Courant-Friedrichs-Lewy (CFL) condition is satisfied (which is a standard restriction

on the timestep in terms of the spacial resolution of the solution for explicit solutions). Finally we introduce more physics into the system, by adding the Fick’s mass diffusion to the species equation, which yields a flow field which not only mixes, but whose concentration dependent viscosity and mass diffusion allow for a slow local homogenization effect to proceed across the domain, and we analyze some chemically pertinent numerical experiments. Some of the work in this chapter is duplicated in Ref. [3].

In Chapter 4 we shift our attention to conservation form quantum hydrodynamics. Quantum hydrodynamics is generally viewed as a natural outcropping of time-dependent quantum mechanics (in relation to the time-dependent Schrödinger equation), leading to a direct formal equivalence to a system of conservation law continuum mechanics, comprised of a continuity equation and a conservation of momentum equation that contains the so-called Bohmian quantum potential (in honour of one of the early pioneers of the field, David Bohm [40,41]). This system has recently received substantial attention in chemical and molecular dynamics, and in particular, to the study of quantum (or  $\hbar$ ) resolution chemical kinetics occurring over complicated high-dimensional potential energy surfaces [20]. These systems are also of importance in modeling semiconductor systems [42] as well as diffuse interfacial phase dynamics [43]. We show a novel mixed discontinuous Galerkin finite element scheme for solving the conservation (or Eulerian frame) form of these equations in their full generality.

We view our solution as a complement to the more standard Lagrangian frame (or characteristic) based solutions. Again our approach emphasizes boundary conditions, and the importance and recurring nuances which arise with respect to boundary data in the implementation of systems of partial dif-



ferential equations. We also show explicitly ways of recovering the “Bohmian trajectories,” or pathlines of the flow field. We perform a number of numerical experiments and show some careful analysis of these results, including explicitly measuring our solutions against those well established by Wyatt et al. in Ref. [20], to analyze accuracy, efficiency, and convergence properties of our results. A nice feature of our mixed method solution, is that it displays a remarkable scale invariance, making solutions over extremely small meshes qualitatively equivalent to solutions over much larger meshes, and thus yielding a realistic time scaling for complicated high dimensional problems. Some of the work in this chapter is duplicated in Ref. [44].

Finally, in Chapter 5 we return to the classical and semi-classical evolution equations, and look at chemical reactors in a generalized setting. We define a chemical reactor model as any time-evolving system that models chemical reactions. In particular, we emphasize reaction-diffusion systems of partial differential equations, which are of importance in physical chemistry [30, 45], as well as in chemical and aerospace engineering [46, 47]. We present an adapted discontinuous Galerkin finite element scheme, which solves for the reacting source locally in time by direct integration. We use this methodology to analyze stationary chemical reactors (which arise in studies of chemical vapour deposition and flame theory, for example), as well as compressible flow reactors. We implement our scheme explicitly for a simple hypergolic ignition reaction, and look at stationary behavior, catalytic shockwave formation and supersonic nozzle inlet boundary conditions via numerical experiment. Finally we extend our results to full dimension, while showing stability, accuracy and consistency of solutions.

Let us conclude with a brief, though necessary, apologia. Throughout

this work we often find ourselves at a bifurcation between two incongruous set of conventions, and thus in the delicate position of having to choose one over another. A prime example of such a convention, which may have already precipitated concern amongst the chemical readership of this thesis, is the habitual use of the nominative plural “we,” in place of the far more standard passive voice convention used in physical chemistry. In this instance we have adopted the mathematics convention, where “we” is used interchangeably to denote any number of usages from a diverse family of pronouns; that is, it may denote: the collective set of individuals in some sense *explicitly* behind the present work, the collective and inclusive scientific body as a connected and interdependent institution of research, the collective presence of the current audience (i.e. the objective, though time-dependent, “us” of the readership), and so forth. With this in mind, it then naturally follows for single author texts to regularly adopt the plural nominative “we;” and do so as a choice of convention.

In contrast we have adopted the chemistry convention on the bibliography, where references are numbered by order of appearance, as opposed to by the first author’s last name. Additionally we use a mathematics convention for the given entropy  $\mathcal{S}$  a convex function, as well as for the sign of the Bohmian quantum potential  $\mathcal{Q}$ . When cases such as these arise in the the body of the text, the given convention is explicitly stated once, and then taken as implicit.

## Chapter 2

### A Well-posed System for Compressible Multicomponent Flows

#### 2.1 Introduction

In this chapter we show the well-posedness of a global strong solution to a multifluid problem over  $\mathbb{R}^+ \times \mathbb{R}$  characterized by the one-dimensional compressible barotropic Navier-Stokes equations. That is, we consider the following system of equations,

$$\partial_t \rho + \partial_x(\rho u) = 0, \quad (2.1)$$

$$\partial_t(\rho u) + \partial_x(\rho u^2) + \partial_x p(\rho, \mu) - \partial_x(\nu(\rho, \mu) \partial_x u) = 0, \quad (2.2)$$

$$\partial_t(\rho \mu) + \partial_x(\rho u \mu) = 0, \quad (2.3)$$

with initial conditions given by:

$$\rho|_{t=0} = \rho_0 > 0, \quad \rho u|_{t=0} = m_0, \quad \mu|_{t=0} = \mu_0.$$

The conservation of mass (2.1), conservation of momentum (2.2) and conservation of species (2.3) describe the flow of a barotropic compressible viscous fluid defined for  $(t, x) \in \mathbb{R}^+ \times \mathbb{R}$ . Here the *density* is given as  $\rho$ , the *velocity* as  $u$ , the *momentum* as  $m$ , and the *mass fraction*  $\mu$  denotes the relative weighting for each fluid component of the *adiabatic exponent*  $\gamma(\mu) \in \mathbb{R}$  associated to the generalized *pressure*  $p(\rho, \mu)$ , thus effectively tracking the “mixing” of the

fluid components. In one dimension the shear viscosity and the bulk viscosity collapse into a single coefficient function depending on  $\rho$  and  $\mu$  which we denote here  $\nu(\rho, \mu)$ . Monofluid one-dimensional compressible Navier-Stokes equations have been studied by many authors when the viscosity coefficient  $\nu$  is a positive constant. The existence of weak solutions was first established by A. Kazhikhov and V. Shelukhin in Ref. [48] for smooth enough data close to the equilibrium (bounded away from zero). The case of discontinuous data (still bounded away from zero) was addressed by V. Shelukhin [49, 50] and then by D. Serre[51, 52] and D. Hoff [53]. First results concerning vanishing initial density were also obtained by V. Shelukhin [54]. In Ref. [55], D. Hoff proved the existence of global weak solutions with large discontinuous initial data, possibly having different limits at  $x = \pm\infty$ . He proved moreover that the constructed solutions have strictly positive densities (vacuum states cannot form in finite time). In dimension greater than two, similar results were obtained by A. Matsumura and T. Nishida [56–58] for smooth data and D. Hoff [59] for discontinuous data close to the equilibrium. The first global existence result for an initial density that is allowed to vanish was due to P.-L. Lions (see Ref. [60]). The result was later improved by B. Desjardins[61] and E. Feireisl et al. (See Ref. [62–64] and [65]). The class of solutions was then extended by A. Zlotnik, G.-Q. Chen, D. Hoff, B. Ducomet, and K. Trivisa in Ref. [66–70] and [71] to the case of a thermally active compressible flow coupled by the systems chemical kinetics, where global existence results are shown for an Arrhenius type biphasic combustion reaction tracking only the reactants level of consumption. Y. Amirat and V. Shelukhin have further provided in Ref. [72] weak solutions for the case of a miscible flow in porous media.

The problem of regularity and uniqueness of solutions was first analyzed

by V. Solonnikov [34] for smooth initial data and for small time. However, the regularity may blow-up as the solution gets close to vacuum. This leads to another interesting question of whether vacuum may arise in finite time. D. Hoff and J. Smoller [73] show that any weak solution of the Navier-Stokes equations in one space dimension do not exhibit vacuum states, provided that no vacuum states are present initially.

Interfacial multicomponent flows have been extensively studied in the literature, and span a rich array of applied topics with natural analogues in continuum dynamics. For example, there has been numerous work on multicomponent flows in biological systems, including bifurcating vascular flows [74, 75] and pulsatile hemodynamics [76], *in vitro* tissue growth [77] and the “amoeboid motion” of cells by way of surface polymerization [78], chemotactic transport [79] in aqueous media under chemical mixing (e.g. varying relative concentrations) applied to specialized cell types [80], as well as biological membrane dynamics due to local gradients in surface tension caused by flux in local boundary densities [2]. Another important and popular field of application is that of dispersed nanoparticles in colloidal media (e.g. aerosols, emulsifications, sols, foams, etc. [81–83]) applied to, for example, electrospray techniques in designing solar cells [4], or more generally to diagnostic and flow analysis in the applied material sciences [84, 85]. In addition, phase separation and spinodal decomposition have received a great deal of attention [14, 17, 86], especially with respect to morphological engineering [87]. Another field which is heavily weighted with multifluid applications is that of combustion dynamics [46] and chemical kinetics [12, 45], where the conservation of species equation (2.3) is regularly invoked, including numerous topics in reaction diffusion dynamics and phase mixing, spanning many essential topics in the atmospheric

[88, 89] and geophysical [90, 91] sciences. In electrochemistry and chemical engineering recent work has been done on porous multiphase fuel cells [92, 93], and in sonochemistry recent studies have shown acoustically induced transport properties across interfacial phase changes [24, 94], Finally in the fields of astronomy and astrophysics exotic multicomponent magnetohydrodynamic plasmas are studied [21, 95].

Many applied results exist for computational methods and schemes for solving multicomponent flows. Let us briefly mention some notable examples. An early generalized numerical approach in multiphase modeling was presented by F. Harlow and A. Amsden in Ref. [96], which provides an extensive system of dynamically coupled phases using a conservation of species (2.3) equation obeying a number of relevant physical boundary conditions and which applies, in particular, to compressible flows. In Ref. [97] J. Dukowicz implements a particle-fluid model for incompressible sprays, an approach extended by G. Faeth in Ref. [98, 99] to combustion flows. D. Youngs then, in Ref. [100], expanded numerical mixing regimes to include interfacial turbulent effects. These basic schemes and approaches have been applied by a large number of authors to a large number of fields, modeling an extremely diverse number of natural phenomenon, from star formation [101] to volcanic eruptions [102]. Some good reviews of the foundational numerics of these approaches can be found in the books of C. Hirsch [103], P. Shih-I and L. Shijun [104], and M. Feistauer, J. Felcman, and I. Straškraba [105].

Let us briefly outline the physical meaning of the subject of this Chapter, namely, the system of equations (2.1)-(2.3). Here we have a barotropic system with the flow driven by a pressure  $p$  that depends on the density  $\rho$  and the mass fraction  $\mu$  of each chemical/phase component of the system. Since

the function  $\gamma(\mu)$  depends on the constant heat capacity ratios  $\gamma_i > 1$  of each component of the multifluid, the pressure  $p(\rho, \mu)$  effectively traces the thermodynamic “signature” of mixing chemicals/phases in solution. Note that this is very similar, for example, to the system of equations set out in Ref. [46], except here, for simplicity, we have neglected the associated diffusion and chemical kinetics which break the strict (and mathematically convenient) conservation in the species equation (2.3). Another important facet of the system (2.1)-(2.3) is that the viscosity  $\nu$  is a function of the pressure  $p$ . Much recent work has been done by M. Franta, M. Bulíček, J. Málek, and K. Rajagopal in providing results on these type of viscosity laws [106–109]. Moreover, since the form of the pressure  $p$  is chosen up to any state equation that satisfies the assumptions given in §2, the formulation is general enough to include, for example, multi-nuclear regimes. That is, in addition to describing the flow of mixing fluids characterized by their concentrations with respect to their heat capacity ratios, this construction also educes applications in nuclear hydrodynamics, where one can derive the pressure law using the time-dependent *Hartree-Fock approximation* [110]. Such a *nuclear fluid* obeying the assumptions given by the *Eddington Standard Model* for stellar phenomena has a pressure law [63] that takes the form,  $p(\rho) = C_1\rho^3 - C_2\rho^2 + C_3\rho^{7/4}$  where  $C_1, C_2$  and  $C_3$  are positive constants. In particular, this exotic pressure law can be shown to model nontrivial physical phenomena; such as spin and isospin wavefront propagation in nuclear fluids. It has further been shown to be in good agreement with nuclear hydrodynamic models of the sun [63]. Thus the result in §2 allows us to extend the above to *nuclear multifluids* that satisfies

$$p(\rho, \mu) = C_1\rho^{\gamma_i(\mu)} - C_2\rho^{\gamma_j(\mu)} + C_3\rho^{\gamma_k(\mu)},$$

as long as it verifies the conditions given in §2. It however remains to be seen

if quantum multi-molecular fluids [20] have an analogous formulation.

At the level of the mathematical results, incompressible (for general background on the incompressible Navier-Stokes equations see Ref. [111]) multicomponent flows have been addressed by a number of authors. First S. Antontsev and A. Kazhikhov in Ref. [112], A. Kazhikhov in Ref. [113], S. Antontsev, A. Kazhikhov and V. Monakhov in Ref. [114], and B. Desjardins in Ref. [61] show results for mixing flows where homogenization of the density  $\rho$  is allowed. These solutions can be seen in contrast with P.L. Lions' and R. DiPerna's solutions in Ref. [115, 116] which provide a multiphase solution for immiscible inhomogenizable flows given discrete constant densities for each component. A. Nouri, F. Poupaud and Y. Demay [116, 117] extend these results to functional densities where boundary components  $\partial\Omega_i$  are set between each fluid domain  $\Omega_i$  that satisfy the so-called *kinematic condition*, which restricts the viscosity  $\nu$  to obey  $\partial_t \nu + u \cdot \nabla \nu = 0$  (see Ref. [118] for further discussion on the kinematic condition). These results apply to immiscible flows with boundary surfaces that effectively fix the number of fluid particles on the interface. These solutions were then further extended by N. Tanaka [119, 120], V. Solonnikov and A. Tani [121–125] to include boundary conditions tracking both the surface tension at the interface using a mean curvature flow on the interfacial surface, as well as the inclusion of self-gravitating parcels.

In this Chapter we consider viscosity coefficients depending on the pressure satisfying a barotropic-type pressure law, a result based upon the paper of A. Mellet and A. Vasseur in Ref. [35] and extended to the multifluid case with a viscosity functional  $\nu(p)$  given no *a priori* uniform bound from below. Thus, in addition to modeling the miscible multiflow regimes that have generated substantial physical interest (see above), our result further incorporates a very



inclusive form of the generalized viscosity. We show the global existence with uniqueness result for a one-dimensional compressible barotropic multicomponent Navier-Stokes problem. In order to acquire the existence result, we rely heavily on an energy inequality provided by D. Bresch and B. Desjardins (see for example Ref. [18] and [126]). This beautiful and powerful tool is central to our result, and, as it turns out, the breakdown of this calculation is the only (known) obstruction to acquiring similar results in dimension greater than one. Next we obtain the uniqueness result by adapting a proof of Solonnikov's [34] to the case of the barotropic system (2.1)-(2.2) coupled to the species conservation equation (2.3).

Let us take this opportunity to discuss difficulties and related systems of equations in higher dimension. Again, the present result relies heavily on the calculation of an energy inequality (see §3) as provided by D. Bresch and B. Desjardins [37, 38, 127]. However, in dimension  $n \geq 2$ , the derivation of this entropy inequality leads to an unnatural form of the viscosity coefficient  $\nu(\rho, \mu)$ ; which is to say, the calculation no longer demonstrates the type of symmetry which leads to the essential *cancellation of singularities* (for example see Ref. [55]) required in the calculation (see Ref. [36] for the monofluid case).

We briefly recall some exciting results known for compressible fluids in higher dimension, and note that extending these to multifluid regimes introduces both beautiful and difficult mathematics, while also addressing very important and physically relevant questions in the applied fields. For example, a result of A. Valli and W. Zajackowski [128] shows global weak solutions to the multidimensional problem for a heat conducting fluid with inflow and outflow conditions on the boundary. In Ref. [129] A. Solonnikov and A. Tani offer a uniqueness proof for an isentropic compressible problem given a free

boundary in the presence of surface tension. D. Hoff and E. Tsyganov next provide a very nice extension of the system to find weak solutions to the compressible magnetohydrodynamics regime in Ref. [130]. G. Chen and M. Kratka in Ref. [131] further show a free boundary result for a heat-conducting flow given spherically symmetric initial data and a constant viscosity coefficient in higher dimension; a result which is extended by E. Feireisl's work [63] under the notion of the *variational solution* for heat-conducting flows in multiple dimensions; though this result restricts the form of the equation of state. Further existence results are provided by B. Ducomet and E. Feireisl [1, 132] for gaseous stars and the compressible heat-conducting magnetohydrodynamic regime. Further, D. Donatelli and K. Trivisa [133, 134] have extended the existence results for the coupled chemical kinetics system mentioned above to higher dimensions. In Ref. [82], A. Mellet and A. Vasseur provide global weak solutions for a compressible barotropic regime coupled to the Vlasov-Fokker-Planck equation, which characterizes the evolution of dispersed particles in compressible fluids, such as with spray phenomenon. Finally, important results of D. Bresch and B. Desjardins, in a very recent paper [135], has worked to extend the existence results to a more general framework (using their energy inequality) for a viscous compressible heat-conducting fluid.

We conclude by noting a number of important and interesting results related to vacuum solutions. That is, though in this work we are concerned with densities that obey uniform bounds in  $\mathbb{R}$ , a number of nice results exist for the case where over some open  $U \subset \mathbb{R}$ ,

$$\int_U \rho_0 dx \geq 0;$$

which is to say, solutions that incorporate vacuum states. For example, T. Yang and C. Zhu show in Ref. [136] global existence for a 1D isentropic fluid con-

nected continuously to a vacuum state boundary with a density dependent viscosity. Additionally, in dimension one, a recent result by C. Cho and H. Kim [137] provides unique strong local solutions to a viscous polytropic fluid, where they utilize a compatibility condition on the initial data.

## 2.2 Statement of Result

Let us first state the hypothesis we make on the pressure and viscosity functional  $p(\rho, \mu)$  and  $\nu(\rho, \mu)$ . First we assume that the pressure  $p(\rho, \mu)$  is an increasing function of the density  $\rho$  such that a.e.,

$$\partial_\rho p(\rho, \mu) \geq 0. \quad (2.4)$$

The viscosity coefficient  $\nu(\rho, \mu)$  is chosen such that it satisfies the following relation,

$$\nu(\rho, \mu) = \rho \partial_\rho p(\rho, \mu) \psi'(p(\rho, \mu)), \quad (2.5)$$

where  $\psi(p)$  is a function of the pressure restricted only by the form of its derivative in  $p$ .

We consider a multifluid for which the pressure functional does not change too much with respect to the fractional mass. Namely, Consider two  $\check{\gamma} > 1$  and  $\hat{\gamma} > 1$ , where  $\check{\gamma} < \gamma < \hat{\gamma}$  up to the constraint that,

$$\frac{\hat{\gamma} - 1/2}{\check{\gamma}} < \frac{\check{\gamma} + 1/2}{\hat{\gamma}}, \quad (2.6)$$

$$\frac{\check{\gamma} - 1/2}{\hat{\gamma}} > \frac{\hat{\gamma} + 1/2}{\check{\gamma}} - 1. \quad (2.7)$$

These relations are satisfied when  $\hat{\gamma} = 1.4$  and  $\check{\gamma} = 1.3$ , for example.

Then, we ascribe the existence of constants  $C \geq 0$  such that the following conditions hold:

$$\begin{aligned}\psi'(p) &\geq C \sup(p^{-\underline{\alpha}}, p^{-\bar{\alpha}}), \\ \rho^{\tilde{\gamma}}/C &\leq p(\rho, \mu) \leq C\rho^{\hat{\gamma}} \quad \text{for } \rho \geq 1, \mu \in \mathbb{R}, \\ \rho^{\hat{\gamma}}/C &\leq p(\rho, \mu) \leq C\rho^{\tilde{\gamma}} \quad \text{for } \rho \leq 1, \mu \in \mathbb{R},\end{aligned}\tag{2.8}$$

where  $\underline{\alpha}$  and  $\bar{\alpha}$  are such that

$$\frac{\hat{\gamma} - 1/2}{\tilde{\gamma}} < \underline{\alpha} \leq \frac{\tilde{\gamma} + 1/2}{\hat{\gamma}},\tag{2.9}$$

$$\frac{\tilde{\gamma} - 1/2}{\hat{\gamma}} > \bar{\alpha} \geq \frac{\hat{\gamma} + 1/2}{\tilde{\gamma}} - 1.\tag{2.10}$$

Note that the existence of  $\underline{\alpha}$  and  $\bar{\alpha}$  comes from (2.6) and (2.7).

Next we set conditions on the derivatives of the pressure in  $\rho$  and  $\mu$ ; given first in  $\rho$  by,

$$\begin{aligned}\rho^{\tilde{\gamma}-1}/C &\leq \partial_{\rho}p(\rho, \mu) \leq C\rho^{\hat{\gamma}-1} \quad \text{for } \rho \geq 1, \mu \in \mathbb{R}, \\ \rho^{\hat{\gamma}-1}/C &\leq \partial_{\rho}p(\rho, \mu) \leq C\rho^{\tilde{\gamma}-1} \quad \text{for } \rho \leq 1, \mu \in \mathbb{R},\end{aligned}\tag{2.11}$$

and in  $\mu$  by,

$$\begin{aligned}\partial_{\mu}p(\rho, \mu) &\leq C\rho^{\hat{\gamma}} \quad \text{for } \rho \geq 1, \mu \in \mathbb{R}, \\ \partial_{\mu}p(\rho, \mu) &\leq C\rho^{\tilde{\gamma}} \quad \text{for } \rho \leq 1, \mu \in \mathbb{R}.\end{aligned}\tag{2.12}$$

Notice that a simple pressure which satisfies these conditions is,  $p(\rho, \mu) = C(\mu)\rho^{\gamma(\mu)}$  where  $1/C \leq C(\mu) \leq C$  and with two constants  $\gamma_1$  and  $\gamma_2$  such that,

$$\tilde{\gamma} < \gamma_1 \leq \gamma(\mu) \leq \gamma_2 < \hat{\gamma}.$$

In particular note that (2.4), (2.5), (2.8), and (2.11)-(2.12) are quite general assumptions, while the strong conditions, (2.6) and (2.7), have the effect of constraining the amount  $p(\rho, \mu)$  can change with respect to  $\mu$ .

For the sake of clarity we define  $\dot{H}^1(\mathbb{R})$  as the space consisting of all functions  $\rho$  for which,

$$\int_{\mathbb{R}} (\partial_x \rho)^2 dx \leq C.$$

This Chapter is dedicated to the proof of the following theorem.

**Theorem 2.2.1.** *Assume a pressure  $p(\rho, \mu)$  and viscosity  $\nu(\rho, \mu)$  satisfying (2.5), (2.8), and (2.11)-(2.12) where the adiabatic limits  $\hat{\gamma}$  and  $\check{\gamma}$  verify (2.6)-(2.7), and take initial data  $(\rho_0, u_0, \mu_0)$  for which there exists positive constants  $\underline{\varrho}(0)$  and  $\bar{\varrho}(0)$  such that*

$$\begin{aligned} 0 < \underline{\varrho}(0) \leq \rho_0 \leq \bar{\varrho}(0) < \infty, \\ \rho_0 \in \dot{H}^1(\mathbb{R}), \quad u_0 \in H^1(\mathbb{R}), \quad \mu_0 \in H^1(\mathbb{R}), \\ \int_{\mathbb{R}} \mathcal{E}(\rho_0, \mu_0) dx < +\infty, \\ |\partial_x \mu_0| \leq C \rho_0, \end{aligned}$$

where  $\mathcal{E}$  is the internal energy as defined in (2.14). We additionally assume the existence of constants  $R, S > 0$  and  $\tilde{\rho}, \tilde{\mu} > 0$  where  $\rho_0 \equiv \tilde{\rho}$  for  $|x| > R$  and  $\mu_0 \equiv \tilde{\mu}$  for  $|x| > S$ . Then there exists a global strong solution to (2.1)-(2.3) on  $\mathbb{R}^+ \times \mathbb{R}$  such that for every  $T > 0$  we have

$$\begin{aligned} \rho &\in L^\infty(0, T; \dot{H}^1(\mathbb{R})), \quad \partial_t \rho \in L^2((0, T) \times \mathbb{R}), \\ u &\in L^\infty(0, T; H^1(\mathbb{R})) \cap L^2(0, T; H^2(\mathbb{R})), \quad \partial_t u \in L^2((0, T) \times \mathbb{R}), \\ \mu_x &\in L^\infty(0, T; L^\infty(\mathbb{R})), \quad \partial_t \mu \in L^\infty(0, T; L^2(\mathbb{R})). \end{aligned}$$

Furthermore, there exist positive constants  $\underline{\varrho}(T)$  and  $\bar{\varrho}(T)$  depending only on  $T$ , such that

$$0 < \underline{\varrho}(T) \leq \rho(t, x) \leq \bar{\varrho}(T) < \infty, \quad \forall (t, x) \in (0, T) \times \mathbb{R}.$$

Additionally, when  $\psi''(p)$ ,  $\partial_{\rho\rho} p(\rho, \mu)$ , and  $\partial_{\rho\mu} p(\rho, \mu)$  are each locally bounded then this solution is unique in the class of weak solutions satisfying the entropy inequalities of §3.

It is worth remarking that our results are slightly stronger than those presented in the statement of the theorem above. Namely, the conditions  $\rho_0 \equiv \tilde{\rho}$  for  $|x| > R$  and  $\mu_0 \equiv \tilde{\mu}$  for  $|x| > S$  with respect to constants  $R$  and  $S$  can be relaxed, such that simply choosing  $\rho_0$  and  $\mu_0$  close to the reference values  $\tilde{\rho}$  and  $\tilde{\mu}$  is permissible as long as the internal energy  $\mathcal{E}(\rho, \mu)$  remains integrable at  $t = 0$ .

We additionally use the existence of the short-time solution to the system (2.1)-(2.3), which follows from Ref. [34]. That is, as we show explicitly in §4, applying (2.8) and (2.11) to (2.5) provides that for every  $(\rho, \mu)$  the viscosity coefficient  $\nu(\rho, \mu) \geq C$ , for a positive constant  $C$ . This leads to the following proposition.

**Proposition 2.2.2.** *(Solonnikov) For initial data  $(\rho_0, u_0, \mu_0)$  taken with respect to the positive constants  $\bar{\varrho}(0)$  and  $\underline{\varrho}(0)$  satisfying*

$$0 < \underline{\varrho}(0) \leq \rho_0 \leq \bar{\varrho}(0) < \infty,$$

$$\rho_0 \in \dot{H}^1(\mathbb{R}), \quad u_0 \in H^1(\mathbb{R}), \quad \mu_0 \in H^1(\mathbb{R}),$$

*and assuming that  $\nu(\rho, \mu) \geq C$  for a positive constant  $C$ , then there exists a  $T_s > 0$  for each such that (2.1)-(2.3) has a unique solution  $(\rho, u, \mu)$  on  $(0, T_s)$  for each  $T_r < T_s$  satisfying*

$$\rho \in L^\infty(0, T_r; \dot{H}^1(\mathbb{R})), \quad \partial_t \rho \in L^2((0, T_r) \times \mathbb{R}),$$

$$u \in L^2(0, T_r; H^2(\mathbb{R})), \quad \partial_t u \in L^2((0, T_r) \times \mathbb{R}),$$

$$\mu_x \in L^\infty(0, T_r; L^\infty(\mathbb{R})), \quad \partial_t \mu \in L^\infty((0, T_r); L^2(\mathbb{R}));$$

*and there exists two positive constants,  $\underline{\varrho}_r > 0$  and  $\bar{\varrho}_r < \infty$ , such that  $\underline{\varrho}_r \leq \rho(x, t) \leq \bar{\varrho}_r$  for all  $t \in (0, T_s)$ .*

The proof of Solonnikov's proposition 2.2 as presented in Ref. [34] follows with the addition of equation (2.3) by applying Duhamel's principle to

the transport equation in  $\mu$  given the regularity which we demonstrate in §4, in much the same way Duhamel's principle is applied to  $\rho$  in Ref. [34] for the continuity equation. The rest of the proof then pushes through directly by virtue of the calculation shown in §5 of this work.

## 2.3 Energy Inequalities

In this section we derive two inequalities in order to gain enough control over (2.1)-(2.3) to prove the theorem. That is, from these inequalities we obtain *a priori* estimates that hold for smooth solutions and then prove the existence result using Solonnikov's short-time solution. The first inequality we show is the classical entropy inequality adapted to the context of a multfluid, while the second is an additional energy inequality derived using a technique discovered by D. Bresch and B. Desjardins that effectively fixes the form of the viscosity coefficient  $\nu(\rho, \mu)$ .

A simple calculation is required in order to obtain the classical entropy inequality (in the sense of Ref. [126] and [36]). That is, multiplying the momentum equation (2.2) by  $u$  and integrating we find,

$$\frac{d}{dt} \int_{\mathbb{R}} \left\{ \rho \frac{u^2}{2} + \mathcal{E}(\rho, \mu) \right\} dx + \int_{\mathbb{R}} \nu(\rho, \mu) |\partial_x u|^2 dx \leq 0. \quad (2.13)$$

Here  $\mathcal{E}(\rho, \mu)$  is the *internal energy* functional effectively tempered by a fixed constant reference density  $\tilde{\rho} < \infty$  and a fixed constant reference mass fraction  $\tilde{\mu} \leq C$ , given by

$$\mathcal{E}(\rho, \mu) = \rho \int_{\tilde{\rho}}^{\rho} \left\{ \frac{p(s, \mu) - p(\tilde{\rho}, \mu)}{s^2} \right\} ds + p(\tilde{\rho}, \tilde{\mu}) - p(\tilde{\rho}, \mu). \quad (2.14)$$

Let us make this calculation precise. First we restrict to the first two

terms of (2.2) to notice that,

$$\partial_t(\rho u) + \partial_x(\rho u^2) = \rho \partial_t u + \rho u \partial_x u + u(\partial_t \rho + \partial_x(\rho u)),$$

where subsequently multiplying through by a factor of  $u$  and integrating gives,

$$\int_{\mathbb{R}} \left\{ u^2 (\partial_t \rho + \partial_x(\rho u)) + \frac{1}{2} (\rho \partial_t u^2 + \rho u \partial_x u^2) \right\} dx.$$

This can be easily rewritten using (2.1), as

$$\int_{\mathbb{R}} (u \partial_t(\rho u) + u \partial_x(\rho u^2)) dx = \frac{1}{2} \int_{\mathbb{R}} \left\{ \partial_t(\rho u^2) + \partial_x(\rho u^3) \right\} dx.$$

Likewise the pressure term  $p_x$  from (2.2) is multiplied through by a factor of  $u$  and integrated. In particular, the form this term takes in (2.13) is derived from a pressure  $p(\rho, \mu)$  that satisfies a conservation law (shown in §4) for a tempered internal energy  $\mathcal{E}(\rho, \mu)$ . To see this, first notice that for any function of  $\rho$  and  $\mu$  we have,

$$\begin{aligned} \int_{\mathbb{R}} \partial_t \mathcal{E}(\rho, \mu) dx &= \int_{\mathbb{R}} \partial_\rho \mathcal{E}(\rho, \mu) \partial_t \rho dx + \int_{\mathbb{R}} \partial_\mu \mathcal{E}(\rho, \mu) \partial_t \mu dx \\ &= - \int_{\mathbb{R}} u \partial_\mu \mathcal{E}(\rho, \mu) \partial_x \mu dx - \int_{\mathbb{R}} \partial_\rho \mathcal{E}(\rho, \mu) \partial_x(\rho u) dx \\ &= - \int_{\mathbb{R}} u \partial_\mu \mathcal{E}(\rho, \mu) \partial_x \mu dx - \int_{\mathbb{R}} \rho \partial_\rho \mathcal{E}(\rho, \mu) \partial_x u dx \\ &\quad - \int_{\mathbb{R}} u \partial_\rho \mathcal{E}(\rho, \mu) \partial_x \rho dx. \end{aligned}$$

But here, since  $\partial_x \mathcal{E}(\rho, \mu) = \partial_\rho \mathcal{E} \partial_x \rho + \partial_\mu \mathcal{E} \partial_x \mu$ , we can write,

$$\begin{aligned} \int_{\mathbb{R}} \partial_t \mathcal{E}(\rho, \mu) dx &= - \int_{\mathbb{R}} u \partial_\mu \mathcal{E}(\rho, \mu) \partial_x \mu dx - \int_{\mathbb{R}} \rho \partial_\rho \mathcal{E}(\rho, \mu) \partial_x u dx \\ &\quad - \int_{\mathbb{R}} u \partial_\rho \mathcal{E}(\rho, \mu) \partial_x \rho dx \\ &= - \int_{\mathbb{R}} u \partial_x \mathcal{E}(\rho, \mu) dx - \int_{\mathbb{R}} \rho \partial_\rho \mathcal{E}(\rho, \mu) \partial_x u dx \\ &= \int_{\mathbb{R}} \partial_x u \left\{ \mathcal{E}(\rho, \mu) - \rho \partial_\rho \mathcal{E}(\rho, \mu) \right\} dx, \end{aligned}$$



which gives,

$$\int_{\mathbb{R}} \partial_t \mathcal{E}(\rho, \mu) dx = \int_{\mathbb{R}} u \partial_x \left\{ \rho \partial_\rho \mathcal{E}(\rho, \mu) - \mathcal{E}(\rho, \mu) \right\} dx. \quad (2.15)$$

Using (2.14) we find

$$\mathcal{E}(\rho, \mu) = \rho \partial_\rho \mathcal{E}(\rho, \mu) + p(\tilde{\rho}, \tilde{\mu}) - p(\rho, \mu), \quad \text{where} \quad \mathcal{E}(\tilde{\rho}, \tilde{\mu}) = 0, \quad (2.16)$$

such that computing  $\rho \partial_\rho \mathcal{E}(\rho, \mu) - \mathcal{E}(\rho, \mu)$  arrives with the desired equality,

$$\frac{d}{dt} \int_{\mathbb{R}} \mathcal{E}(\rho, \mu) dx = \int_{\mathbb{R}} u \partial_x p(\rho, \mu) dx. \quad (2.17)$$

This internal energy  $\mathcal{E}$  over  $\mathbb{R}$  arises in Ref. [55] for the single component case, where there  $G(\rho, \rho')$  is set as the *potential energy density* and treated in a similar fashion. Note that as  $\mathcal{E}(\rho, \mu)$  is tempered with respect to a reference density  $\tilde{\rho}$  and a reference fractional mass  $\tilde{\mu}$ , this is all that is needed to control the sign on the internal energy  $\mathcal{E}(\rho, \mu)$ , with the only qualification coming from §3 which gives cases on the limits of integration.

It is further worth mentioning that the above terms comprise an entropy  $\mathcal{S}(\rho, u, \mu)$  of the system (as well as the entropy term of inequality (2.13)), where we write the integrable function,

$$\mathcal{S}(\rho, u, \mu) = \frac{m^2}{2\rho} + \mathcal{E}(\rho, \mu).$$

The final step in recovering (2.13) is to calculate the remaining diffusion term, which follows directly upon integration by parts. That is, after multiplying through by  $u$  and integrating by parts we see that

$$- \int_{\mathbb{R}} u \partial_x (\nu(\rho, \mu) \partial_x u) dx = \int_{\mathbb{R}} \nu(\rho, \mu) (\partial_x u)^2 dx$$

which leads to the result; namely (2.13).

### 2.3.1 Additional Energy Inequality

The following lemma provides the second energy inequality that we use in order to prove the theorem.

**Lemma 2.3.1.** *For solutions of (2.1)-(2.3) we have*

$$\frac{d}{dt} \int_{\mathbb{R}} \left\{ \frac{\rho}{2} |u + \rho^{-1} \partial_x \psi(p)|^2 + \mathcal{E}(\rho, \mu) \right\} dx + \int_{\mathbb{R}} \rho^{-1} \psi'(p) (\partial_x p(\rho, \mu))^2 dx = 0, \quad (2.18)$$

providing the following constraint on the viscosity  $\nu(\rho, \mu)$ :

$$\nu(\rho, \mu) = \rho \partial_\rho p \psi'(p). \quad (2.19)$$

*Proof.* Take the continuity equation and the transport equation in  $\mu$  and multiply through by derivatives of a function of the pressure  $\psi(p)$  such that,

$$\begin{aligned} \partial_\rho \psi(p) \left\{ \partial_t \rho + \partial_x(\rho u) \right\} &= 0, \\ \partial_\mu \psi(p) \left\{ \partial_t \mu + u \partial_x \mu \right\} &= 0, \end{aligned}$$

where adding the components together gives,

$$\partial_t \psi(p) + u \partial_x \psi(p) + \rho \partial_\rho \psi(p) \partial_x u = 0.$$

A derivation in  $x$  provides that

$$\partial_t (\partial_x \psi(p)) + \partial_x (u \partial_x \psi(p)) + \partial_x (\rho \partial_\rho \psi(p) \partial_x u) = 0,$$

which we expand to

$$\partial_t (\rho \rho^{-1} \partial_x \psi(p)) + \partial_x (\rho \rho^{-1} u \partial_x \psi(p)) + \partial_x (\rho \partial_\rho \psi(p) \partial_x u) = 0,$$

such that adding it back to the momentum equation (2.2) and applying condition (2.19) arrives with

$$\partial_t (\rho \{u + \rho^{-1} \partial_x \psi(p)\}) + \partial_x (\rho u \{u + \rho^{-1} \partial_x \psi(p)\}) + \partial_x p(\rho, \mu) = 0.$$

Multiplying this by  $(u + \rho^{-1}\partial_x\psi(p))$  then gives,

$$\begin{aligned} \frac{1}{2}\partial_t\{\rho|u + \rho^{-1}\partial_x\psi(p)|^2\} + \frac{1}{2}\partial_x\{\rho u|u + \rho^{-1}\partial_x\psi(p)|^2\} \\ + \{u + \rho^{-1}\partial_x\psi(p)\}\partial_x p(\rho, \mu) = 0, \end{aligned}$$

which when integrated becomes

$$\frac{d}{dt} \int_{\mathbb{R}} \left\{ \frac{\rho}{2} |u + \rho^{-1}\partial_x\psi(p)|^2 + \mathcal{E}(\rho, \mu) \right\} dx + \int_{\mathbb{R}} \rho^{-1}\psi'(p) (\partial_x p(\rho, \mu))^2 dx = 0,$$

completing the proof.  $\square$

## 2.4 Establishing the Existence Theorem

In this section our aim is to apply the inequalities in §3 predicated on the formulation in §2 to acquire the existence half of the theorem. However, in order to do this we must first confirm that the energy inequalities satisfy the appropriate bounds. Let us demonstrate this principle for both (2.13) and (2.18) in the form of the following lemma.

**Lemma 2.4.1.** *For any solution  $(\rho, u, \mu)$  of (2.1)-(2.3) verifying,*

$$\int_{\mathbb{R}} \left\{ \rho_0 \frac{u_0^2}{2} + \mathcal{E}(\rho_0, \mu_0) \right\} dx < +\infty \quad (2.20)$$

and

$$\int_{\mathbb{R}} \left\{ \frac{\rho_0}{2} \left| u_0 + \frac{\partial_x \psi(p_0)}{\rho_0} \right|^2 + \mathcal{E}(\rho_0, \mu_0) \right\} dx < +\infty, \quad (2.21)$$

we have that

$$\text{ess sup}_{[0, T]} \int_{\mathbb{R}} \left\{ \rho \frac{u^2}{2} + \mathcal{E}(\rho, \mu) \right\} dx + \int_0^T \int_{\mathbb{R}} \nu(\rho, \mu) |\partial_x u|^2 dx dt \leq C, \quad (2.22)$$

and

$$\text{ess sup}_{[0, T]} \int_{\mathbb{R}} \left\{ \frac{\rho}{2} \left| u + \frac{\partial_x \psi(p)}{\rho} \right|^2 + \mathcal{E}(\rho, \mu) \right\} dx + \int_0^T \int_{\mathbb{R}} \frac{\psi'(p)}{\rho} |\partial_x p|^2 dx dt \leq C. \quad (2.23)$$

*Proof.* It suffices if every term on the left side of both inequality (2.22) and (2.23) can be shown to be nonnegative.

First notice that we clearly have that  $\rho u^2 \geq 0$  for any barotropic fluid over  $\mathbb{R}$ , since  $\rho$  is strictly nonnegative. To check that  $\mathcal{E}(\rho, \mu) \geq 0$  we simply refer to the definition given in (2.16). Indeed  $\left(\frac{p(s, \mu) - p(\tilde{\rho}, \mu)}{s^2}\right) \geq 0$  when  $\rho \geq \tilde{\rho}$  and  $\left(\frac{p(s, \mu) - p(\tilde{\rho}, \mu)}{s^2}\right) \leq 0$  for  $\rho \leq \tilde{\rho}$ , which implies

$$\int_{\tilde{\rho}}^{\rho} \frac{p(s, \mu) - p(\tilde{\rho}, \mu)}{s^2} ds \geq 0.$$

Together with (2.14) this gives that  $\mathcal{E}(\rho, \mu) \geq 0$ .

Next we check the viscosity coefficient  $\nu(\rho, \mu)$ . Here the positivity follows from (2.5), where again the pressure is increasing in  $\rho$  satisfying (2.4) and the density is positive definite away from the vacuum solution (which we show is forbidden due to proposition 2.4.2), so for a  $\psi'(p)$  satisfying (2.8) we see that  $\psi'(p) \geq 0$ . Similarly, the last term on the right in (2.23) follows away from vacuum, where again we only rely upon the fact from §2 that  $\psi'(p) \geq 0$ .  $\square$

These results provide the estimates that we use for the remainder of the Chapter. That is, it is well-known (for example see Theorem 7.2 in Ref. [60] and the results in Ref. [35]) that the existence of a global strong solution to the system (2.1)-(2.2) follows by regularity analysis in tandem with (2.13) and (2.18). Below we present a similar approach for the case of a mixing multicomponent fluid (2.1)-(2.3) using only what we have found above; namely, that (2.13) and (2.18) provide the following *a priori* bounds:

$$\begin{aligned} \|\sqrt{\nu(\rho, \mu)} \partial_x u\|_{L^2(0, T; L^2(\mathbb{R}))} &\leq C, \\ \|\sqrt{\rho} u\|_{L^\infty(0, T; L^2(\mathbb{R}))} &\leq C, \\ \|\mathcal{E}(\rho, \mu)\|_{L^\infty(0, T; L^1(\mathbb{R}))} &\leq C, \end{aligned} \tag{2.24}$$

along with,

$$\begin{aligned} \|(\partial_x \psi(p)/\sqrt{\rho})\|_{L^\infty(0,T;L^2(\mathbb{R}))} &\leq C, \\ \|(\psi'(p)/\rho)^{1/2} \partial_x p(\rho, \mu)\|_{L^2(0,T;L^2(\mathbb{R}))} &\leq C. \end{aligned} \quad (2.25)$$

We will use these inequalities extensively for the remainder of the Chapter.

As a remark, if we denote the *internal energy density*  $e$  as being characterized by the relations,

$$\begin{aligned} \rho e &= \rho \int_{\tilde{\rho}}^{\rho} \frac{\partial e(s, \mu)}{\partial \rho} ds \quad \text{with} \quad e(\tilde{\rho}, \mu) = 0, \\ \text{and} \quad \partial_\rho e(\rho, \mu) &= \rho^{-2} p(\rho, \mu) - \rho^{-2} p(\tilde{\rho}, \mu), \end{aligned} \quad (2.26)$$

then  $e$  is closely related to the *specific internal energy*  $e_s$ , defined by

$$e_s(\rho) \equiv \int_1^{\rho} \frac{p(s)}{s^2} ds,$$

which is provided for the single barotropic compressible fluid case in Ref. [118] and [63]; but in the multifluid context, since the internal energy  $\mathcal{E}$  is tempered up to some constant reference density  $\tilde{\rho}$ , the usual form of the specific internal energy inherits a tempering in  $\tilde{\rho}$  as well, which is what is provided here by the function  $e$ . We also note that the tempered internal energy  $\mathcal{E}$  now satisfies the following conservation form as mentioned in §3,

$$\partial_t \mathcal{E}(\rho, \mu) + \partial_x (\mathcal{E}(\rho, \mu) u) + \left\{ \rho^2 \partial_\rho e(\rho, \mu) + p(\tilde{\rho}, \mu) - p(\tilde{\rho}, \tilde{\mu}) \right\} \partial_x u = 0, \quad (2.27)$$

where it is easy to confirm that upon integration this recovers (2.17).

### 2.4.1 Bounds on the Density

For the existence theorem we need to establish a bound for the density in the space  $L^\infty(0, T; \dot{H}^1(\mathbb{R}))$ . To achieve this we first establish uniform bounds on the density.

**Proposition 2.4.2.** *For every  $T > 0$  there exist two distinct positive constants  $\underline{\varrho}$  and  $\bar{\varrho}$  such that*

$$\underline{\varrho} \leq \rho(t, x) \leq \bar{\varrho} \quad \forall (t, x) \in [0, T] \times \mathbb{R}. \quad (2.28)$$

Showing this proposition requires the following three lemmas which provide the groundwork for its subsequent proof.

**Lemma 2.4.3.** *Let  $\mathcal{F} \geq 0$  be a function defined on  $[0, +\infty) \times \mathbb{R}$  where  $\mathcal{F}(\cdot, x)$  is uniformly continuous with respect to  $x \in \mathbb{R}$  and where there exists a  $\delta > 0$  with  $\mathcal{F}(0, x) > \delta$  for any  $x$ . Then there exists an  $\epsilon > 0$  such that for any constant  $\bar{C} > 0$  there exists a constant  $K > 0$  so that for any nonnegative function  $f$  verifying  $\int_{\mathbb{R}} \mathcal{F}(f(x), x) dx \leq \bar{C}$ , and for any  $x_0 \in \mathbb{R}$ , there exists a point  $x_1 \in I = [x_0 - K, x_0 + K]$  such that  $f(x_1) > \epsilon$ .*

*Proof.* For any fixed  $\mathcal{F}$  there exists a  $\tilde{C}$  such that for all  $y \leq \epsilon$  we have,

$$\mathcal{F}(y, x) \geq \frac{1}{2\tilde{C}}$$

since  $\mathcal{F}(0, x) > \delta$  for any  $x$  and  $\mathcal{F}$  is uniformly continuous in  $x$ . Let us fix  $\bar{C} > 0$  and define

$$K = 2\bar{C}\tilde{C}. \quad (2.29)$$

We show that this  $K$  verifies the desired properties. Here we utilize a proof by contradiction in the spirit of Ref. [36]. Assume that we can find a nonnegative function  $f$  verifying  $\int_{\mathbb{R}} \mathcal{F}(f(x), x) dx \leq \bar{C}$  and an  $x_0 \in \mathbb{R}$  with

$$\operatorname{ess\,sup}_{x \in I} f \leq \epsilon,$$

where  $I = [x_0 - K, x_0 + K]$ . Since  $\mathcal{F} \geq 0$  this implies

$$\bar{C} \geq \int_{\mathbb{R}} \mathcal{F}(f(x), x) dx \geq \int_I \mathcal{F}(f(x), x) dx \geq \int_I \frac{1}{2\tilde{C}} dx,$$

which yields  $\bar{C} \geq K/\tilde{C}$  in contradiction to (2.29).  $\square$

Additionally we require the following technical lemma.

**Lemma 2.4.4.** *Providing (2.8) then (2.14) yields,*

$$\begin{aligned}\rho^{\hat{\gamma}} + C\rho &\leq C + 1 \quad \text{for } \rho \leq 1, \\ \rho^{\tilde{\gamma}} + \frac{\rho}{C} &\leq C + C\mathcal{E}(\rho, \mu) \quad \text{for } \rho \geq 1.\end{aligned}$$

*Proof.* Trivially, when  $\rho \leq 1$  we have that  $\rho^{\hat{\gamma}} + C\rho \leq C + 1$ . When  $\rho \geq 1$  we use (2.8) to expand  $\mathcal{E}(\rho, \mu)$  where (2.14) gives that as  $\rho \rightarrow \infty$  the  $\rho^{\tilde{\gamma}}$  dominates such that scaling the constant correctly provides the result.  $\square$

Now we are able to find uniform positive bounds  $\underline{\varrho}$  and  $\bar{\varrho}$  on the density which inherently preclude the vacuum and concentration states.

**Lemma 2.4.5.** *Assume that (2.6), (2.7) and (2.8)-(2.12) are satisfied and let*

$$\partial_x \xi(\rho) = \mathbb{1}_{\{\rho \leq 1\}} \partial_x \rho^{-\eta} + \mathbb{1}_{\{\rho \geq 1\}} \partial_x \rho^{\sigma}. \quad (2.30)$$

*Then there exists an  $\eta > 0$  and  $\sigma > 0$  such that for any  $K > 0$  there exists a  $C_K$  with*

$$\|\partial_x \xi(\rho)\|_{L^\infty(0,T;L^1(I))} \leq C_K \quad (2.31)$$

*for every  $x_0 \in \mathbb{R}$  and  $I = [x_0 - K, x_0 + K]$ .*

*Proof.* First recall that the pressure satisfies

$$\partial_x p(\rho, \mu) = \partial_\rho p(\rho, \mu) \partial_x \rho + \partial_\mu p(\rho, \mu) \partial_x \mu.$$

Here we are concerned with two cases, namely when  $\rho \leq 1$  and when  $\rho \geq 1$ . For the case when  $\rho \leq 1$  we multiply through by  $\rho^{-1/2} p(\rho, \mu)^{-\underline{\alpha}}$  where  $\underline{\alpha}$  is given by (2.9), which yields

$$\frac{\partial_\rho p(\rho, \mu) \partial_x \rho}{\sqrt{\rho} p(\rho, \mu)^{\underline{\alpha}}} = \frac{\partial_x p(\rho, \mu)}{\sqrt{\rho} p(\rho, \mu)^{\underline{\alpha}}} - \frac{\partial_\mu p(\rho, \mu) \partial_x \mu}{\sqrt{\rho} p(\rho, \mu)^{\underline{\alpha}}}. \quad (2.32)$$

Likewise for  $\rho \geq 1$  we multiply through by  $p(\rho, \mu)^{-\bar{\alpha}} \rho^{-1/2}$  given  $\bar{\alpha}$  from (2.10) such that

$$\frac{\partial_\rho p(\rho, \mu) \partial_x \rho}{\sqrt{\rho} p(\rho, \mu)^{\bar{\alpha}}} = \frac{\partial_x p(\rho, \mu)}{\sqrt{\rho} p(\rho, \mu)^{\bar{\alpha}}} - \frac{\partial_\mu p(\rho, \mu) \partial_x \mu}{\sqrt{\rho} p(\rho, \mu)^{\bar{\alpha}}}. \quad (2.33)$$

In order to demonstrate the lemma we will control the right hand side of both (2.32) and (2.33) such that each is bounded in  $L^\infty(0, T; L^1_{loc}(\mathbb{R}))$ .

Towards this, we first show that  $\rho^{-1} \partial_x \mu$  is bounded in  $L^\infty(0, T; L^\infty(\mathbb{R}))$ . That is, take a derivation in  $x$  of (2.3) in order to write

$$\partial_t(\rho \rho^{-1} \partial_x \mu) + \partial_x(\rho u \rho^{-1} \partial_x \mu) = 0, \quad (2.34)$$

such that multiplying through by a function  $\vartheta'(\rho^{-1} \partial_x \mu) = \vartheta'$  achieves

$$\partial_t(\rho \vartheta(\rho^{-1} \partial_x \mu)) + \partial_x(\rho u \vartheta(\rho^{-1} \partial_x \mu)) = 0.$$

Take  $\vartheta(y) = (|y| - M)_+$  for positive  $M \in \mathbb{R}$ . Upon integration this implies

$$\int_0^T \frac{d}{dt} \int_{\mathbb{R}} \rho \vartheta(\rho^{-1} \partial_x \mu) dx dt = 0,$$

such that for an appropriate choice of initial condition, where  $\rho_0^{-1} \partial_x \mu_0 \in [-M, M]$ , we find

$$\text{ess sup}_{[0, T]} \int_{\mathbb{R}} \rho \vartheta(\rho^{-1} \partial_x \mu) dx = 0.$$

This implies that  $\rho \vartheta(\rho^{-1} \partial_x \mu) = 0$  almost everywhere for all  $(t, x) \in (0, T) \times \mathbb{R}$ , and so we can conclude that the argument of  $\vartheta$  takes values over the interval, or more clearly that for  $\rho$  a.e.  $|\rho^{-1} \partial_x \mu| \leq M$ . This is then enough to educe the norm:

$$\|\rho^{-1} \partial_x \mu\|_{L^\infty(0, T; L^\infty(\mathbb{R}))} \leq M.$$

However, this is not yet enough to control the last term on the right for the two cases. In (2.32) applying (2.8) and (2.12) further provides

$$\frac{\sqrt{\rho} \partial_\mu p(\rho, \mu)}{p(\rho, \mu)^\alpha} \leq C_0 \rho^{\tilde{\gamma} - \alpha \hat{\gamma} + \frac{1}{2}} \quad \text{for} \quad \rho \leq 1$$



for a positive constant  $C_0$ . Using (2.9) from above we have that  $\tilde{\gamma} \geq \underline{\alpha}\hat{\gamma} - 1/2$ , and so the positivity of the exponent gives

$$C_0 \rho^{\tilde{\gamma} - \underline{\alpha}\hat{\gamma} + \frac{1}{2}} \leq C \quad \text{for} \quad \rho \leq 1,$$

which leads to,

$$\left\| \mathbb{1}_{\{\rho \leq 1\}} \frac{\sqrt{\rho} \partial_\mu p(\rho, \mu)}{p(\rho, \mu)^\alpha} \right\|_{L^\infty(0, T; L^\infty(\mathbb{R}))} \leq C. \quad (2.35)$$

Similarly for (2.33) we apply (2.8) and (2.12) to see that,

$$\frac{\sqrt{\rho} \partial_\mu p(\rho, \mu)}{p(\rho, \mu)^{\bar{\alpha}}} \leq C_0 \rho^{\hat{\gamma} - \bar{\alpha}\tilde{\gamma} + \frac{1}{2}} \quad \text{for} \quad \rho \geq 1.$$

Notice that since (2.10) provides  $\tilde{\gamma} \geq \hat{\gamma} - \bar{\alpha}\tilde{\gamma} + 1/2$ , then applying lemma 2.4.4 implies

$$\mathbb{1}_{\{\rho \geq 1\}} \left( \frac{\sqrt{\rho} \partial_\mu p(\rho, \mu)}{p(\rho, \mu)^{\bar{\alpha}}} \right) \leq C + C \mathcal{E}(\rho, \mu).$$

Integrating over  $I$  gives

$$\int_I \left| \mathbb{1}_{\{\rho \geq 1\}} \frac{\sqrt{\rho} \partial_\mu p(\rho, \mu)}{p(\rho, \mu)^{\bar{\alpha}}} \right| dx \leq 2KC + C \int_{\mathbb{R}} \mathcal{E}(\rho, \mu) dx,$$

such that applying (2.24) establishes

$$\left\| \mathbb{1}_{\{\rho \geq 1\}} \frac{\sqrt{\rho} \partial_\mu p(\rho, \mu)}{p(\rho, \mu)^{\bar{\alpha}}} \right\|_{L^\infty(0, T; L^1_{loc}(\mathbb{R}))} \leq C_K,$$

for  $C_K$  a constant depending only on  $K$ .

Now consider the  $\partial_x p$  term in (2.32) where here again we treat the two cases  $\rho \leq 1$  and  $\rho \geq 1$  separately. For the case  $\rho \leq 1$  notice that we have by the bound on  $\psi'(p)$  in (2.8) that

$$\left| \mathbb{1}_{\{\rho \leq 1\}} \frac{\partial_x p(\rho, \mu)}{\sqrt{\rho} p(\rho, \mu)^\alpha} \right| = C |\mathbb{1}_{\{\rho \leq 1\}} \rho^{-1/2} \partial_x p(\rho, \mu)^{1-\alpha}| \leq C |\mathbb{1}_{\{\rho \leq 1\}} \rho^{-1/2} \partial_x \psi(p)|.$$

Upon integration (2.25) gives

$$\begin{aligned} \int_{\mathbb{R}} |\mathbb{1}_{\{\rho \leq 1\}} \rho^{-1/2} \partial_x p(\rho, \mu)^{1-\alpha}|^2 dx &\leq C \int_{\mathbb{R}} |\mathbb{1}_{\{\rho \leq 1\}} \rho^{-1/2} \partial_x \psi(p)|^2 dx \\ &\leq C, \end{aligned}$$

and so we obtain

$$\|\mathbb{1}_{\{\rho \leq 1\}} \rho^{-1/2} p(\rho, \mu)^{-\alpha} \partial_x p(\rho, \mu)\|_{L^\infty(0,T;L^2(\mathbb{R}))} \leq C.$$

Similarly for  $\rho \geq 1$  we apply (2.8), giving

$$\left| \mathbb{1}_{\{\rho \geq 1\}} \frac{\partial_x p(\rho, \mu)}{\sqrt{\rho p(\rho, \mu)^\alpha}} \right| = C |\mathbb{1}_{\{\rho \geq 1\}} \rho^{-1/2} \partial_x p(\rho, \mu)^{1-\bar{\alpha}}| \leq C |\mathbb{1}_{\{\rho \geq 1\}} \rho^{-1/2} \partial_x \psi(p)|,$$

such that integrating and utilizing (2.25) yields

$$\begin{aligned} \int_{\mathbb{R}} \left| \mathbb{1}_{\{\rho \geq 1\}} \frac{\partial_x p(\rho, \mu)}{\sqrt{\rho p(\rho, \mu)^\alpha}} \right| dx &\leq C \int_{\mathbb{R}} |\mathbb{1}_{\{\rho \geq 1\}} \rho^{-1/2} \partial_x \psi(p)| dx \\ &\leq C, \end{aligned}$$

and so

$$\|\mathbb{1}_{\{\rho \geq 1\}} \rho^{-1/2} p(\rho, \mu)^{-\bar{\alpha}} \partial_x p(\rho, \mu)\|_{L^\infty(0,T;L^1(\mathbb{R}))} \leq C.$$

Combining these results we have thus acquired the important bound on the left sides of (2.32) and (2.33):

$$\begin{aligned} &\|\mathbb{1}_{\{\rho \leq 1\}} \rho^{-1/2} p(\rho, \mu)^{-\alpha} \partial_\rho p(\rho, \mu) \partial_x \rho\|_{L^\infty(0,T;L^2_{loc}(\mathbb{R}))} \\ &+ \|\mathbb{1}_{\{\rho \geq 1\}} \rho^{-1/2} p(\rho, \mu)^{-\bar{\alpha}} \partial_\rho p(\rho, \mu) \partial_x \rho\|_{L^\infty(0,T;L^1(I))} \leq C_K. \end{aligned} \tag{2.36}$$

It remains to show that for all  $\rho$  we have bounds on some power of the spatial derivative  $\rho_x$ . First notice that when  $\rho \leq 1$  applying (2.8) and (2.11) to the left of (2.32) provides

$$\left| \mathbb{1}_{\{\rho \leq 1\}} \frac{\partial_\rho p(\rho, \mu) \partial_x \rho}{\sqrt{\rho p(\rho, \mu)^\alpha}} \right| \geq C |\mathbb{1}_{\{\rho \leq 1\}} \rho^{\hat{\gamma}-\alpha\check{\gamma}-3/2} \partial_x \rho| = C |\mathbb{1}_{\{\rho \leq 1\}} \rho^{\hat{\gamma}-\alpha\check{\gamma}-3/2}| |\partial_x \rho|,$$

such that upon squaring and integrating we find

$$\begin{aligned} C \int_{\mathbb{R}} |\mathbb{1}_{\{\rho \leq 1\}} \rho^{\hat{\gamma} - \underline{\alpha}\hat{\gamma} - 3/2} \partial_x \rho|^2 dx &\leq \int_{\mathbb{R}} \left| \mathbb{1}_{\{\rho \leq 1\}} \frac{\partial_\rho p(\rho, \mu) \partial_x \rho}{\sqrt{\rho} p(\rho, \mu)^{\underline{\alpha}}} \right|^2 dx \\ &\leq C. \end{aligned}$$

This provides what we desire by way of the following equality:

$$\begin{aligned} \|\mathbb{1}_{\{\rho \leq 1\}} \rho^{\hat{\gamma} - \underline{\alpha}\hat{\gamma} - 3/2} \partial_x \rho\|_{L^\infty(0, T; L^2_{loc}(\mathbb{R}))} &= C \|\mathbb{1}_{\{\rho \leq 1\}} \partial_x \rho^{\hat{\gamma} - \underline{\alpha}\hat{\gamma} - 1/2}\|_{L^\infty_{loc}(0, T; L^2(\mathbb{R}))} \\ &\leq C. \end{aligned} \tag{2.37}$$

Thus when applying the condition from (2.6) it follows that  $\eta$  satisfies

$$\eta = \underline{\alpha}\check{\gamma} - \hat{\gamma} + \frac{1}{2}. \tag{2.38}$$

Likewise when  $\rho \geq 1$  applying (2.8) and (2.11) provides

$$\left| \mathbb{1}_{\{\rho \geq 1\}} \frac{\partial_\rho p(\rho, \mu) \partial_x \rho}{\sqrt{\rho} p(\rho, \mu)^{\bar{\alpha}}} \right| \geq C |\mathbb{1}_{\{\rho \geq 1\}} \rho^{\check{\gamma} - \bar{\alpha}\hat{\gamma} - 3/2} \partial_x \rho| = C |\mathbb{1}_{\{\rho \geq 1\}} \rho^{\check{\gamma} - \bar{\alpha}\hat{\gamma} - 3/2}| |\partial_x \rho|,$$

such that integrating over  $I$  gives by (2.36) that

$$\begin{aligned} C \int_I |\mathbb{1}_{\{\rho \geq 1\}} \rho^{\check{\gamma} - \bar{\alpha}\hat{\gamma} - 3/2} \partial_x \rho| dx &\leq \int_I \left| \mathbb{1}_{\{\rho \geq 1\}} \frac{\partial_\rho p(\rho, \mu) \partial_x \rho}{\sqrt{\rho} p(\rho, \mu)^{\bar{\alpha}}} \right| dx \\ &\leq C_K. \end{aligned}$$

Here this yields

$$\|\mathbb{1}_{\{\rho \geq 1\}} \rho^{\check{\gamma} - \bar{\alpha}\hat{\gamma} - \frac{3}{2}} \partial_x \rho\|_{L^\infty(0, T; L^1(I))} = C \|\mathbb{1}_{\{\rho \geq 1\}} \partial_x \rho^{\check{\gamma} - \bar{\alpha}\hat{\gamma} - \frac{1}{2}}\|_{L^\infty(0, T; L^1(I))} \leq C_K. \tag{2.39}$$

Thus using the condition from (2.7) establishes

$$\sigma = \check{\gamma} - \bar{\alpha}\hat{\gamma} - \frac{1}{2}. \tag{2.40}$$

In order to complete the proof all that remains is to add (2.37) and (2.39) together and apply Minkowski's inequality, which gives

$$\|\partial_x \xi(\rho)\|_{L^\infty(0, T; L^1(I))} \leq C_K.$$

□

We are now able to show Proposition 2.4.2 by applying the preceding results.

*Proof of Proposition 2.4.2.* For  $t$  fixed set

$$\mathcal{F}(y, x) = \begin{cases} \mathcal{E}(y, \mu(t, x)) & \text{for } y \leq 1 \\ \mathcal{E}(1, \mu(t, x)) & \text{for } y \geq 1 \end{cases}$$

such that  $y = \rho$ . Next (2.14) together with (2.8) shows that  $\mathcal{F}(y, x)$  is continuous in  $\rho$  uniformly with respect to  $x$ , and (2.24) assures that

$$\int_{\mathbb{R}} \mathcal{F}(\rho(t, x), x) dx \leq C.$$

Then the hypothesis of lemma 2.4.3 is satisfied as long as there exists a  $\delta > 0$  such that  $\mathcal{F}(0, x) > \delta$ . But for  $\rho \leq 1$  we can apply (2.8) to the form of the internal energy (2.14) to see that as  $\rho \rightarrow 0$  we have  $\mathcal{E}(\rho, \mu) \geq C$ . Likewise when  $\rho = 1$  we see that  $\mathcal{E}(1, \mu) \geq C_1$  for  $C_1$  a constant. So we have for a positive  $\delta < \inf\{C, C_1\}$  that the hypothesis of lemma 2.4.3 is satisfied. Then for any  $x \in \mathbb{R}$  with  $x_0 = x$  from lemma 2.4.3 there exists an  $x_1 \in I = [x-K, x+K]$  such that  $\rho(t, x_1) > \epsilon$ . Note that  $K$  does not depend on  $t$  since  $\int_{\mathbb{R}} \mathcal{F}(\rho(t, x), x) dx$  does not depend on time thanks to (2.24). Then the fundamental theorem provides:

$$|\mathbb{1}_{\{\rho \leq 1\}} \rho^{-\eta}(x)| \leq |\epsilon^{-\eta}| + \int_I |\mathbb{1}_{\{\rho \leq 1\}} \partial_x \rho^{-\eta}| dx.$$

Since  $K$  does not depend on time, lemma 2.4.5 gives that the right hand side is bounded uniformly in  $x$  and  $t$ .

For the upper bound, again fix  $t$  and now set

$$\mathcal{F}(y, x) = \mathcal{E}\left(\frac{1 + \tilde{\rho}}{1 + y}, \mu(t, x)\right) \quad \forall y \geq 0$$

such that  $y = 1/\rho$ . Again (2.14) and (2.8) provide that  $\mathcal{F}(y, x)$  is continuous in  $\rho$  uniformly with respect to  $x$ . Additionally we find that both  $\mathcal{F}(1/\tilde{\rho}, x) = \mathcal{E}(\tilde{\rho}, \mu) \geq C$  and that  $\mathcal{F}(0, x) > C_1$  by applying (2.8) to (2.14), which provides an admissible  $\delta$ . Now, upon defining a function  $\varpi = \rho(1 + \tilde{\rho})/(\rho + 1)$ , then there exists a constant  $C > 0$  such that

$$\mathcal{E}(\varpi, \mu) \leq C\mathcal{E}(\rho, \mu),$$

which can be shown using (2.14) and checking the formula for  $|\rho - \tilde{\rho}| \leq \frac{\tilde{\rho}}{2}$ ,  $\rho \leq \frac{\tilde{\rho}}{2}$  and  $\rho \geq \frac{3}{2}\tilde{\rho}$  thanks to (2.11). Then (2.24) is enough to deduce that

$$\int_{\mathbb{R}} \mathcal{F}(\rho(t, x)^{-1}, x) dx \leq C.$$

Hence for any  $x \in \mathbb{R}$  we can use lemma 2.4.3 setting  $x_0 = x$  such that there exists an  $x_1 \in [x - K, x + K]$  with  $\rho(t, x_1) \leq \epsilon^{-1}$ . Again notice that  $K$  does not depend on  $t$  since (2.24) is uniform in time. Then by the fundamental theorem and lemma 2.4.5 we obtain

$$|\mathbb{1}_{\{\rho \geq 1\}} \rho^\sigma(x)| \leq |\epsilon^{-\sigma}| + \int_I |\mathbb{1}_{\{\rho \geq 1\}} \partial_x \rho^\sigma| dx.$$

Again since  $K$  does not depend on time, lemma 2.4.5 gives the right side bounded uniformly in  $x$  and  $t$  which completes the proof of proposition 2.4.2.  $\square$

We proceed by showing the important corollary to this proposition.

**Corollary 2.4.6.** *Assume that (2.6)-(2.8) and (2.11)-(2.12) are satisfied, then*

$$\rho \in L^\infty(0, T; \dot{H}^1(\mathbb{R})).$$

*Proof.* Lemma 2.4.5 provides the appropriate framework. Thus we will show the bound separately for the cases  $\rho \leq 1$  and  $\rho \geq 1$ .

For  $\rho \leq 1$  applying (2.8), (2.11) and (2.12) we calculate

$$\begin{aligned}
\partial_x \rho^{-\eta} &= \rho^{-\eta-1} \partial_x \rho \\
&= \rho^{-\eta-1} \left( \frac{\partial_x p(\rho, \mu) - \partial_\mu p(\rho, \mu) \partial_x \mu}{\partial_\rho p(\rho, \mu)} \right) \\
&\leq \rho^{-\eta-1} \left( \frac{\partial_x p(\rho, \mu)}{C \rho^{\hat{\gamma}-1}} \right) - C \rho^{-\eta-\hat{\gamma}} \partial_\mu p(\rho, \mu) \partial_x \mu \\
&\leq C \rho^{-\alpha\hat{\gamma}-1/2} \partial_x p(\rho, \mu) - C \rho^{-\eta-\hat{\gamma}+\hat{\gamma}+1} \left( \frac{\partial_x \mu}{\rho} \right).
\end{aligned} \tag{2.41}$$

Squaring both sides gives

$$(\partial_x \rho)^2 \leq \rho^{2+2\eta} \left( C \rho^{-\alpha\hat{\gamma}-1/2} \partial_x p(\rho, \mu) - C \rho^{-\eta-\hat{\gamma}+\hat{\gamma}+1} \left( \frac{\partial_x \mu}{\rho} \right) \right)^2.$$

Integrating, applying (2.8) and utilizing Hölder's inequality yields,

$$\begin{aligned}
\int_{\mathbb{R}} \mathbb{1}_{\{\rho \leq 1\}} (\partial_x \rho)^2 dx &\leq \check{C} \int_{\mathbb{R}} \mathbb{1}_{\{\rho \leq 1\}} \left| \frac{\partial_x p}{\sqrt{\rho} \rho^{\alpha\hat{\gamma}}} \right|^2 dx - \check{C} \left( \int_{\mathbb{R}} \mathbb{1}_{\{\rho \leq 1\}} \left| \frac{\partial_x p}{\sqrt{\rho} \rho^{\alpha\hat{\gamma}}} \right|^2 dx \right. \\
&\times \left. \int_{\mathbb{R}} \mathbb{1}_{\{\rho \leq 1\}} \left| \rho^{\hat{\gamma}(1-\alpha)+\frac{1}{2}} \left( \frac{\partial_x \mu}{\rho} \right) \right|^2 dx \right)^{\frac{1}{2}} + C \int_{\mathbb{R}} \mathbb{1}_{\{\rho \leq 1\}} \left| \rho^{\hat{\gamma}(1-\alpha)+\frac{1}{2}} \left( \frac{\partial_x \mu}{\rho} \right) \right|^2 dx \\
&\leq \check{C}_0 \int_{\mathbb{R}} \mathbb{1}_{\{\rho \leq 1\}} \left| \frac{\partial_x \psi(p)}{\sqrt{\rho}} \right|^2 dx - \check{C}_0 \left( \int_{\mathbb{R}} \mathbb{1}_{\{\rho \leq 1\}} \left| \frac{\partial_x \psi(p)}{\sqrt{\rho}} \right|^2 dx \right. \\
&\times \left. \bar{\varrho}^{\hat{\gamma}(1-\alpha)+\frac{1}{2}} \int_{\mathbb{R}} \mathbb{1}_{\{\rho \leq 1\}} |\rho^{-1} \partial_x \mu|^2 dx \right)^{\frac{1}{2}} + C \bar{\varrho}^{\hat{\gamma}(1-\alpha)+\frac{1}{2}} \int_{\mathbb{R}} \mathbb{1}_{\{\rho \leq 1\}} |\rho^{-1} \partial_x \mu|^2 dx \\
&\leq C,
\end{aligned}$$

which concludes the proof for  $\rho \leq 1$ .

For the case  $\rho \geq 1$  we follow an almost identical calculation, except

that now after applying (2.8), (2.11) and (2.12); (2.41) becomes

$$\begin{aligned}
\partial_x \rho^\sigma &= \rho^{\sigma-1} \partial_x \rho \\
&= \rho^{\sigma-1} \left( \frac{\partial_x p(\rho, \mu) - \partial_\mu p(\rho, \mu) \partial_x \mu}{\partial_\rho p(\rho, \mu)} \right) \\
&\leq \rho^{\sigma-1} \left( \frac{\check{C} \partial_x p(\rho, \mu)}{\rho^{\check{\gamma}-1}} \right) - C \rho^{\sigma-\check{\gamma}} \partial_\mu p(\rho, \mu) \partial_x \mu \\
&\leq \check{C} \rho^{-\bar{\alpha}\check{\gamma}-1/2} \partial_x p(\rho, \mu) - C \rho^{\sigma-\check{\gamma}+\check{\gamma}+1} \left( \frac{\partial_x \mu}{\rho} \right).
\end{aligned} \tag{2.42}$$

Squaring both sides now gives

$$(\partial_x \rho)^2 \leq \rho^{2-2\sigma} \left( \check{C} \rho^{-\bar{\alpha}\check{\gamma}-1/2} \partial_x p(\rho, \mu) - C \rho^{\hat{\gamma}(1-\bar{\alpha})+\frac{1}{2}} \left( \frac{\partial_x \mu}{\rho} \right) \right)^2.$$

Again integrating and applying (2.8) with Hölder's inequality establishes,

$$\begin{aligned}
\int_{\mathbb{R}} \mathbb{1}_{\{\rho \geq 1\}} (\partial_x \rho)^2 dx &\leq \hat{C} \int_{\mathbb{R}} \mathbb{1}_{\{\rho \geq 1\}} \left| \frac{\partial_x p}{\sqrt{\rho} \rho^{\bar{\alpha}\check{\gamma}}} \right|^2 dx - \tilde{C} \left( \int_{\mathbb{R}} \mathbb{1}_{\{\rho \geq 1\}} \left| \frac{\partial_x p}{\sqrt{\rho} \rho^{\bar{\alpha}\check{\gamma}}} \right|^2 dx \right. \\
&\times \left. \int_{\mathbb{R}} \mathbb{1}_{\{\rho \geq 1\}} \left| \rho^{\hat{\gamma}(1-\bar{\alpha})+\frac{1}{2}} \left( \frac{\partial_x \mu}{\rho} \right) \right|^2 dx \right)^{\frac{1}{2}} + C \int_{\mathbb{R}} \mathbb{1}_{\{\rho \geq 1\}} \left| \rho^{\hat{\gamma}(1-\bar{\alpha})+\frac{1}{2}} \left( \frac{\partial_x \mu}{\rho} \right) \right|^2 dx \\
&\leq \hat{C}_0 \int_{\mathbb{R}} \mathbb{1}_{\{\rho \geq 1\}} \left| \frac{\partial_x \psi(p)}{\sqrt{\rho}} \right|^2 dx - \tilde{C}_0 \left( \int_{\mathbb{R}} \mathbb{1}_{\{\rho \geq 1\}} \left| \frac{\partial_x \psi(p)}{\sqrt{\rho}} \right|^2 dx \right. \\
&\times \left. \bar{\varrho}^{\hat{\gamma}(1-\bar{\alpha})+\frac{1}{2}} \int_{\mathbb{R}} \mathbb{1}_{\{\rho \geq 1\}} |\rho^{-1} \partial_x \mu|^2 dx \right)^{\frac{1}{2}} + C \bar{\varrho}^{\hat{\gamma}(1-\bar{\alpha})+\frac{1}{2}} \int_{\mathbb{R}} \mathbb{1}_{\{\rho \geq 1\}} |\rho^{-1} \partial_x \mu|^2 dx \\
&\leq C,
\end{aligned}$$

which due to Minkowski's inequality completes the proof.  $\square$

## 2.4.2 Bounds for the Velocity

It is now possible to find bounds on the velocity by applying the uniform bounds achieved above.

**Proposition 2.4.7.** *Assume that (2.5)-(2.8) and (2.11)-(2.12) are satisfied, then*

$$u \in L^2(0, T; H^2(\mathbb{R})) \quad \text{and} \quad \partial_t u \in L^2(0, T; L^2(\mathbb{R})). \tag{2.43}$$

*Proof.* First notice that the second estimate in (2.24) in tandem with the uniform bounds on the density gives

$$\|u\|_{L^\infty(0,T;L^2(\mathbb{R}))} \leq C. \quad (2.44)$$

Also notice that the uniform bounds on  $\rho$  applied to (2.5) show that there exists a constant  $C$  such that  $\nu(\rho, \mu)^{-1} \leq C$ . That is, applying (2.8) and (2.11) to (2.5) for  $\rho \leq 1$  gives  $\nu(\rho, \mu) \geq C\rho^{\hat{\gamma}-\underline{\alpha}\check{\gamma}}$  so that using the uniform bounds on  $\rho$  provides

$$\nu(\rho, \mu)^{-1} \leq C\rho^{\underline{\alpha}\check{\gamma}-\hat{\gamma}} \leq C\underline{\varrho}^{\underline{\alpha}\check{\gamma}-\hat{\gamma}} \leq C. \quad (2.45)$$

For  $\rho \geq 1$  it follows in the same way that  $\nu(\rho, \mu) \geq C\rho^{\check{\gamma}-\bar{\alpha}\hat{\gamma}}$  provides

$$\nu(\rho, \mu)^{-1} \leq C\rho^{\bar{\alpha}\hat{\gamma}-\check{\gamma}} \leq C\underline{\varrho}^{\bar{\alpha}\hat{\gamma}-\check{\gamma}} \leq C. \quad (2.46)$$

Thus for all  $\rho$  we have  $\nu(\rho, \mu)^{-1} \leq C$ , which when applied to (2.24) yields

$$\|u\|_{L^2(0,T;H^1(\mathbb{R}))} \leq C. \quad (2.47)$$

Further, observing the continuity equation with respect to (2.47) implies that  $\partial_t \rho$  is bounded in  $L^2((0, T) \times \mathbb{R})$  as denoted in the theorem. We proceed by controlling the following form of the momentum equation (after multiplication through by  $\rho^{-1}$ ):

$$\partial_t u - \partial_x (\rho^{-1} \nu(\rho, \mu) \partial_x u) = -u \partial_x u - \rho^{-1} \partial_x p(\rho, \mu) - \nu(\rho, \mu) \partial_x u \partial_x \rho^{-1}. \quad (2.48)$$

We want to control the right side of (2.48) in such a way as to apply classical regularity results for parabolic equations.

Consider first the second term on the right in (2.48). This term is bounded in  $L^\infty(0, T; L^2(\mathbb{R}))$  as an immediate consequence of proposition 2.4.2,



the corollary, and condition (2.8). This follows since (2.8) gives  $p(\rho, \mu) \leq C\rho^{\hat{\gamma}}$  for  $\rho \geq 1$  and  $p(\rho, \mu) \leq C\rho^{\check{\gamma}}$  for  $\rho \leq 1$ . Then we can expand the pressure term as  $\rho^{\hat{\gamma}-2}\partial_x\rho$  and  $\rho^{\check{\gamma}-2}\partial_x\rho$ , such that for  $\rho \geq 1$  the corollary and proposition 2.4.2 provide that

$$\begin{aligned} \int_{\mathbb{R}} \mathbb{1}_{\{\rho \geq 1\}} |\rho^{-1} \partial_x p(\rho, \mu)|^2 dx &\leq C \left( \operatorname{ess\,sup}_{\{x \in \mathbb{R}; \rho \geq 1\}} |\rho^{2\hat{\gamma}-4}| \right) \left( \int_{\mathbb{R}} \mathbb{1}_{\{\rho \geq 1\}} |\partial_x \rho|^2 dx \right) \\ &\leq C, \end{aligned}$$

and likewise for  $\rho \leq 1$  the corollary and proposition 2.4.2 give

$$\begin{aligned} \int_{\mathbb{R}} \mathbb{1}_{\{\rho \leq 1\}} |\rho^{-1} \partial_x p(\rho, \mu)|^2 dx &\leq C \left( \operatorname{ess\,sup}_{\{x \in \mathbb{R}; \rho \leq 1\}} |\rho^{2\check{\gamma}-4}| \right) \left( \int_{\mathbb{R}} \mathbb{1}_{\{\rho \leq 1\}} |\partial_x \rho|^2 dx \right) \\ &\leq C. \end{aligned}$$

Minkowski's inequality then provides the result.

For the third term on the right we again use the fact from above that  $\nu(\rho, \mu)^{-1} \leq C$ , and so because of the uniform bounds on  $\rho$  we acquire

$$|\nu(\rho, \mu) \partial_x u \partial_x \rho^{-1}| \leq C |\partial_x u \partial_x \rho|.$$

Hence, due to results on parabolic equations (see Ref. [138]) we have reduced the problem to finding for the third term on the right in (2.48) that  $\rho_x u_x$  is bounded in  $L^2(0, T; L^{4/3}(\mathbb{R}))$  and similarly for the first term on the right that  $u u_x$  is in  $L^2(0, T; L^{4/3}(\mathbb{R}))$ . To get this, we adapt a subtle calculation from Ref. [36] that relies on correctly weighting the norms in order to establish that  $u_x \in L^2(0, T; L^\infty(\mathbb{R}))$ . That is, using Hölder's inequality we can write:

$$\begin{aligned} &\|u u_x\|_{L^2(0, T; L^{4/3}(\mathbb{R}))} + \|\rho_x u_x\|_{L^2(0, T; L^{4/3}(\mathbb{R}))} \\ &\leq \left\{ \|u\|_{L^\infty(0, T; L^2(\mathbb{R}))} + \|\rho_x\|_{L^\infty(0, T; L^2(\mathbb{R}))} \right\} \|u_x\|_{L^2(0, T; L^4(\mathbb{R}))}. \end{aligned} \tag{2.49}$$

Now for some function  $f$  with constant  $a \in \mathbb{R}$  we have  $(f^a)_x = af^{a-1}f_x$  such that we may infer by Hölder's inequality that

$$\|\partial_x(f^{3/2})\|_{L^1(\mathbb{R})} \leq C\|f^{1/2}\|_{L^4(\mathbb{R})}\|f_x\|_{L^{4/3}(\mathbb{R})}. \quad (2.50)$$

Next we infer a bound in  $L^{8/3}(\mathbb{R})$  given by

$$\|f^{3/2}\|_{L^{8/3}(\mathbb{R})} \leq C\|f^{3/2}\|_{L^{4/3}(\mathbb{R})}^{1/2}\|\partial_x(f^{3/2})\|_{L^1(\mathbb{R})}^{1/2},$$

which follows since

$$\|\partial_x(f^{3/2})\|_{L^1(\mathbb{R})}^{1/2} \geq C\|f^{3/2}\|_{L^\infty(\mathbb{R})}^{1/2}.$$

Thus invoking (2.50) we can write

$$\begin{aligned} \|f\|_{L^4(\mathbb{R})}^{3/2} &\leq C\|f\|_{L^2(\mathbb{R})}^{3/4}\|f_x\|_{L^{4/3}(\mathbb{R})}^{1/2}\|\sqrt{f}\|_{L^4(\mathbb{R})}^{1/2} \\ &\leq C\|f\|_{L^2(\mathbb{R})}\|f_x\|_{L^{4/3}(\mathbb{R})}^{1/2}, \end{aligned}$$

where both sides raised to the power  $n = 2/3$  clearly implies that

$$\|f\|_{L^4(\mathbb{R})} \leq C\|f\|_{L^2(\mathbb{R})}^{2/3}\|f\|_{W^{1,4/3}}^{1/3}.$$

Hence, if we set  $u_x = f$  then (2.49) leads to

$$\begin{aligned} &\left\{\|u\|_{L^\infty(0,T;L^2(\mathbb{R}))} + \|\rho_x\|_{L^\infty(0,T;L^2(\mathbb{R}))}\right\}\|u_x\|_{L^2(0,T;L^4(\mathbb{R}))} \\ &\leq C\|u\|_{L^\infty(0,T;L^2(\mathbb{R}))}\|u_x\|_{L^2(0,T;L^2(\mathbb{R}))}^{2/3}\|u_x\|_{L^2(0,T;W^{1,4/3}(\mathbb{R}))}^{1/3} \\ &\quad + C\|\rho_x\|_{L^\infty(0,T;L^2(\mathbb{R}))}\|u_x\|_{L^2(0,T;L^2(\mathbb{R}))}^{2/3}\|u_x\|_{L^2(0,T;W^{1,4/3}(\mathbb{R}))}^{1/3} \\ &\leq C\|u_x\|_{L^2(0,T;W^{1,4/3}(\mathbb{R}))}^{1/3}, \end{aligned}$$

since  $u$  and  $\rho_x$  are given by (2.47) and the corollary. But then regularity results (see theorem 4.2 in Chapter III of Ref. [138]) for equations of the form (2.48),

given the bounds established above and that  $\nu(\rho, \mu)$  is a coefficient function satisfying uniform parabolicity, imply that since

$$\|\partial_x u\|_{L^2(0,T;W^{1,4/3}(\mathbb{R}))} \leq C + C\|u_x\|_{L^2(0,T;W^{1,4/3}(\mathbb{R}))}^{1/3},$$

we have

$$\|\partial_x u\|_{L^2(0,T;W^{1,4/3}(\mathbb{R}))} \leq C. \quad (2.51)$$

Now, we want to show that

$$u_x \in L^2(0, T; L^\infty(\mathbb{R})). \quad (2.52)$$

Indeed for any  $x \in \mathbb{R}$  and  $t \in [0, T]$  if we set  $\varsigma = u_x$  from lemma 2.4.8 (which is given following this proof) and notice that

$$\|u_x(t, x)\|^2 \leq 2\|u_x(t, \cdot)\|_{L^2(\mathbb{R})}^2 + \|u_{xx}(t, \cdot)\|_{L^{4/3}(\mathbb{R})}^2$$

for any  $t \in [0, T]$ , then integrating in time gives (2.52).

It follows as a consequence that the entire right hand side of (2.48) is bounded in  $L^2(0, T; L^2(\mathbb{R}))$ . Applying the classical regularity results for parabolic equations then yields:

$$\|u\|_{L^2(0,T;H^2(\mathbb{R}))} \leq C \quad \text{and} \quad \|\partial_t u\|_{L^2(0,T;L^2(\mathbb{R}))} \leq C.$$

□

**Lemma 2.4.8.** *Let  $\varsigma \in L^2(\mathbb{R})$  with  $\partial_x \varsigma \in L^1_{loc}(\mathbb{R})$ . Then for any  $x \in \mathbb{R}$*

$$|\varsigma(x)|^2 \leq 2\|\varsigma\|_{L^2(\mathbb{R})}^2 + 2\left(\int_I |\partial_x \varsigma| dz\right)^2,$$

where  $I = [x, x + 1]$ .

*Proof.* It follows by the fundamental theorem that

$$|\varsigma(x)| \leq |\varsigma(y)| + \int_x^y |\partial_x \varsigma| dz \leq |\varsigma(y)| + \int_I |\partial_x \varsigma| dz,$$

for any  $y \in I$ . Squaring both sides and integrating over  $\mathbb{R}$  in  $y$  yields:

$$|\varsigma(x)|^2 \leq 2\|\varsigma\|_{L^2(\mathbb{R})}^2 + 2 \left( \int_I |\partial_x \varsigma| dz \right)^2.$$

□

### 2.4.3 Bounds on the Mass Fraction

All that remains in order to conclude the proof of the existence half of the theorem is to establish the bounds on  $\mu$ . However, this is now an easy consequence of the bounds we have already established above.

**Lemma 2.4.9.** *Given proposition 2.4.2 and 2.4.7 there exist constants such that,*

$$\|\mu_x\|_{L^\infty(0,T;L^\infty(\mathbb{R}))} \leq C \quad \text{and} \quad \|\partial_t \mu\|_{L^\infty(0,T;L^2(\mathbb{R}))} \leq C.$$

*Proof.* We have from lemma 2.4.5 that

$$\|\rho^{-1/2} \partial_x \mu\|_{L^\infty(0,T;L^\infty(\mathbb{R}))} \leq C, \tag{2.53}$$

and so thanks to the uniform bounds on the density from proposition 4.2, this yields that  $\partial_x \mu$  is in  $L^\infty(0,T;L^\infty(\mathbb{R}))$ . Now using (2.44) and the above with (2.3) we find that  $\partial_t \mu$  is in  $L^\infty(0,T;L^2(\mathbb{R}))$ . □

### 2.4.4 Proof of the Existence Half of the Theorem

We now apply the preceeding results in §4 in order to prove the existence theorem.

*Proof of existence half of the theorem.* In view of the *a priori* estimates that we have now, the only difficulty that remains is to deal with the fact that  $\nu$  is not uniformly bounded by below with respect to  $\rho$ . This is needed to apply the short-time existence result of Solonnikov (proposition 4.2.2). To solve this problem let us fix any  $T > 0$ . Then we define an approximation to  $\nu$  by,

$$\tilde{\nu}(y, z) = \begin{cases} \nu(y, z) & \text{if } y \geq \frac{\underline{\varrho}(T)}{2} \\ \nu\left(\frac{\underline{\varrho}(T)}{2}, z\right) & \text{if } y \leq \frac{\underline{\varrho}(T)}{2} \end{cases}$$

where  $\underline{\varrho}(T)$  is defined by proposition 4.4.2. Now let  $(\tilde{\rho}, \tilde{u}, \tilde{\mu})$  be a strong solution of (2.1)-(2.3), where  $\nu$  is replaced by  $\tilde{\nu}$ ; giving

$$\begin{aligned} \partial_t \tilde{\rho} + \partial_x(\tilde{\rho} \tilde{u}) &= 0, \\ \partial_t(\tilde{\rho} \tilde{u}) + \partial_x(\tilde{\rho} \tilde{u}^2) + \partial_x p(\tilde{\rho}, \tilde{\mu}) - \partial_x(\tilde{\nu}(\tilde{\rho}, \tilde{\mu}) \partial_x \tilde{u}) &= 0, \\ \partial_t(\tilde{\rho} \tilde{\mu}) + \partial_x(\tilde{\rho} \tilde{u} \tilde{\mu}) &= 0. \end{aligned}$$

By (2.5), (2.8), and (2.11) the approximate function  $\tilde{\nu}$  is bounded from below, thus proposition 4.2.2 provides that such a solution exists for all  $t \in (0, T_s)$ . Consider  $\tilde{T} \leq T$  the biggest time such that

$$\inf_x(\tilde{\rho}(t, \cdot)) \geq \frac{\underline{\varrho}(T)}{2}.$$

Then on  $[0, \tilde{T}]$ , it follows that  $\tilde{\nu} = \nu$ . Now assume that  $\tilde{T} < T$ . From proposition 4.4.2, on  $[0, \tilde{T}]$

$$\inf_x \tilde{\rho}(t, \cdot) \geq \underline{\varrho}(T) > \frac{\underline{\varrho}(T)}{2},$$

which contradicts the fact that  $\tilde{T} < T$ . Hence we have constructed the solution of (2.1)-(2.3) up to time  $T$ , and this for any  $T > 0$ , which completes the proof.  $\square$

## 2.5 Establishing the Uniqueness Theorem

Now we address the uniqueness half of the theorem. Thanks to Ref. [34] this result follows fairly directly.

**Theorem 2.5.1.** *(The uniqueness half of theorem 2.1) Let  $\psi''(p)$ ,  $\partial_{\rho\rho}p(\rho, \mu)$  and  $\partial_{\rho\mu}p(\rho, \mu)$  be locally bounded. Then a solution of (2.1)-(2.3) verifying proposition 2.4.2, proposition 2.4.7, and lemma 2.4.9 is uniquely determined.*

*Proof.* Let  $(\rho_1, u_1, \mu_1)$  and  $(\rho_2, u_2, \mu_2)$  be two solutions to the system (2.1)-(2.3), and define  $\chi = \mu_1 - \mu_2$ ,  $\tau = \rho_1 - \rho_2$ ,  $\zeta = u_1 - u_2$ ,  $p_\ell = p(\rho_1, \mu_1) - p(\rho_2, \mu_2)$  and  $\nu_\ell = \nu(\rho_1, \mu_1) - \nu(\rho_2, \mu_2)$  such that from (2.1)-(2.3) we can write:

$$\partial_t \tau + \partial_x(\rho_1 u_1 - \rho_2 u_2) = 0,$$

$$\rho_1 \partial_t u_1 - \rho_2 \partial_t u_2 + \rho_1 u_1 \partial_x u_1 - \rho_2 u_2 \partial_x u_2 + \partial_x p_\ell - \partial_x(\nu_1 \partial_x u_1 - \nu_2 \partial_x u_2) = 0,$$

$$\partial_t \chi + (u_1 \partial_x \mu_1 - u_2 \partial_x \mu_2) = 0.$$

By rearranging we get

$$\partial_t \tau + \partial_x(\tau u_1 + \rho_2 \zeta) = 0, \tag{2.54}$$

$$\begin{aligned} \rho_1(\partial_t \zeta + u_1 \partial_x \zeta + \zeta \partial_x u_2) + \tau(\partial_t u_2 + u_2 \partial_x u_2) \\ + \partial_x p_\ell - \partial_x(\nu_\ell \partial_x u_1) - \partial_x(\nu_2 \partial_x \zeta) = 0, \end{aligned} \tag{2.55}$$

$$\partial_t \chi + \zeta \partial_x \mu_1 + u_2 \partial_x \chi = 0. \tag{2.56}$$

First let us consider equation (2.54). Here we multiply through by  $\tau$  and integrate in  $x$ . To begin with, note that the first term on the left satisfies

$$\int_{\mathbb{R}} \tau \partial_t \tau dx = \frac{1}{2} \int_{\mathbb{R}} \partial_t \tau^2 dx. \tag{2.57}$$

For the  $(\tau u_1)_x$  term we use proposition 2.4.7 as applied in (2.52) by setting  $u = u_1$  to see that

$$\left| \int_{\mathbb{R}} \tau(\tau u_1)_x dx \right| \leq \frac{1}{2} \|\tau^2 \partial_x u_1\|_{L^1(\mathbb{R})} \leq \frac{1}{2} \|\tau\|_{L^2(\mathbb{R})}^2 \|\partial_x u_1\|_{L^\infty(\mathbb{R})} \leq B_1(t) \|\tau\|_{L^2(\mathbb{R})}^2. \quad (2.58)$$

For the  $(\rho_2 \zeta)_x$  term notice that we can write:

$$\left| \int_{\mathbb{R}} \tau \partial_x (\rho_2 \zeta) dx \right| \leq \left| \int_{\mathbb{R}} \tau \rho_2 \partial_x \zeta dx \right| + \left| \int_{\mathbb{R}} \tau \zeta \partial_x \rho_2 dx \right|.$$

Applying proposition 2.4.2 and Cauchy's inequality to the first term on the right provides,

$$\begin{aligned} \left| \int_{\mathbb{R}} \tau \rho_2 \partial_x \zeta dx \right| &\leq C \int_{\mathbb{R}} |\tau \partial_x \zeta| dx \leq C \|\tau\|_{L^2(\mathbb{R})} \|\zeta_x\|_{L^2(\mathbb{R})} \\ &\leq C^2 (4\epsilon_1)^{-1} \|\tau\|_{L^2(\mathbb{R})}^2 + \epsilon_1 \|\zeta_x\|_{L^2(\mathbb{R})}^2. \end{aligned} \quad (2.59)$$

For the second term on the right Hölder's inequality with the corollary implies that

$$\begin{aligned} \left| \int_{\mathbb{R}} \tau \zeta \partial_x \rho_2 dx \right| &\leq \left( \int_{\mathbb{R}} |\tau|^2 dx \right)^{1/2} \left( \int_{\mathbb{R}} |\partial_x \rho_2|^2 dx \right)^{1/2} \left( \operatorname{ess\,sup}_{\mathbb{R}} |\zeta| \right) \\ &\leq C \left( \int_{\mathbb{R}} |\tau|^2 dx \right)^{1/2} \left( \operatorname{ess\,sup}_{\mathbb{R}} |\zeta| \right). \end{aligned} \quad (2.60)$$

Now we utilize lemma 2.4.8 by setting  $\varsigma = \zeta$ . Since  $|\zeta| \leq |u_1| + |u_2|$  the bounds in (2.44) provide that  $\zeta \in L^\infty(0, T; L^2(\mathbb{R}))$ . Furthermore, proposition 2.4.7 gives that since  $|\zeta_x|^2 \leq 2|\partial_x u_1|^2 + 2|\partial_x u_2|^2$  we have  $\zeta_x \in L^2(0, T; L^2(\mathbb{R}))$ . Thus noticing that  $\|\zeta\|_{L^1(I)} \leq \|\zeta\|_{L^2(I)}$  since  $|I| = 1$  from lemma 2.4.8, it follows that

$$|\zeta(x)| \leq \|\zeta\|_{L^2(\mathbb{R})} + \|\zeta_x\|_{L^1(I)} \leq \|\zeta\|_{L^2(\mathbb{R})} + \|\zeta_x\|_{L^2(\mathbb{R})},$$

allowing us to deduce,

$$\|\zeta\|_{L^\infty(\mathbb{R})} \leq \|\zeta\|_{L^2(\mathbb{R})} + \|\partial_x \zeta\|_{L^2(\mathbb{R})}.$$

By Cauchy's inequality this finally yields

$$\begin{aligned} & C\|\tau\|_{L^2(\mathbb{R})}\|\zeta\|_{L^\infty(\mathbb{R})} \\ & \leq \epsilon_2\|\zeta_x\|_{L^2(\mathbb{R})}^2 + \left\{\frac{C^2}{4\epsilon_2} + \frac{C}{2}\right\} \left(\|\tau\|_{L^2(\mathbb{R})}^2 + \|\zeta\|_{L^2(\mathbb{R})}^2\right). \end{aligned} \quad (2.61)$$

Thus combining (2.57), (2.58) and (2.61) allows us to write for (2.54):

$$\begin{aligned} & \frac{1}{2} \frac{d}{dt} \int_{\mathbb{R}} \tau^2 dx - \{\epsilon_1 + \epsilon_2\} \int_{\mathbb{R}} (\partial_x \zeta)^2 dx \\ & \leq \left\{B_1(t) + \frac{C^2}{4\epsilon_1} + \frac{C^2}{4\epsilon_2} + \frac{C}{2}\right\} \left(\|\tau\|_{L^2(\mathbb{R})}^2 + \|\zeta\|_{L^2(\mathbb{R})}^2\right). \end{aligned} \quad (2.62)$$

Next we want to multiply (2.55) through by  $\zeta$  and integrate in  $\mathbb{R}$ . For the first two terms in the first part of (2.55) we find:

$$\begin{aligned} \int_{\mathbb{R}} \rho_1 \zeta (\partial_t \zeta + u_1 \partial_x \zeta) dx &= \int_{\mathbb{R}} \frac{\rho_1}{2} (\partial_t \zeta^2 + u_1 \partial_x \zeta^2) dx \\ &= \frac{1}{2} \frac{d}{dt} \int_{\mathbb{R}} \rho_1 \zeta^2 dx - \int_{\mathbb{R}} \frac{\zeta^2}{2} (\partial_t \rho_1 + \partial_x (\rho_1 u_1)) dx \\ &= \frac{1}{2} \frac{d}{dt} \int_{\mathbb{R}} \rho_1 \zeta^2 dx. \end{aligned} \quad (2.63)$$

For the  $\rho_1 \zeta \partial_x u_2$  term in (2.55) we use the same calculation given in (2.58) which is formulated in (2.52) by setting  $u = u_2$  such that,

$$\left| \int_{\mathbb{R}} \rho_1 \zeta^2 \partial_x u_2 dx \right| \leq C \|\zeta\|_{L^2(\mathbb{R})}^2 \|\partial_x u_2\|_{L^\infty(\mathbb{R})} \leq B_2(t) \|\zeta\|_{L^2(\mathbb{R})}^2. \quad (2.64)$$

Now, for the  $\tau(\partial_t u_2 + u_2 \partial_x u_2)$  part of (2.55) we utilize a calculation similar to that employed for the term in (2.60). Here we simply substitute the  $\partial_x \rho_2$  term from (2.60) with  $\omega = \partial_t u_2 + u_2 \partial_x u_2$ , noting that proposition 2.4.7 along with (2.52) assure that  $\omega$  is bounded in  $L^2(0, T; L^2(\mathbb{R}))$ . Thus we obtain

$$B(t) \|\tau\|_{L^2(\mathbb{R})} \|\zeta\|_{L^\infty(\mathbb{R})} \leq \epsilon_3 \|\zeta_x\|_{L^2(\mathbb{R})}^2 + \epsilon_3^{-1} B_3(t) \left( \|\tau\|_{L^2(\mathbb{R})}^2 + \|\zeta\|_{L^2(\mathbb{R})}^2 \right), \quad (2.65)$$



where here  $B_3(t) = \epsilon_3 B(t)/2 + B(t)^2/4$ .

Next consider the pressure term  $p_\ell$  in (2.55). Here set

$$\int_{\mathbb{R}} \zeta \partial_x p_\ell dx = - \int_{\mathbb{R}} \left\{ p(\rho_1, \mu_1) - p(\rho_2, \mu_2) \right\} \partial_x \zeta dx.$$

The uniform bounds on  $\rho$  along with (2.11) and (2.12) give that  $|\partial_\rho p(\rho, \mu)| \leq C$  and  $|\partial_\mu p(\rho, \mu)| \leq C$ , and so

$$|p(\rho_2, \mu_2) - p(\rho_1, \mu_1)| \leq C(|\tau| + |\chi|).$$

Thus

$$\int_{\mathbb{R}} \zeta \partial_x p_\ell dx \leq C \int_{\mathbb{R}} (|\tau| + |\chi|) \partial_x \zeta dx,$$

which gives by Cauchy's inequality,

$$\int_{\mathbb{R}} \zeta \partial_x p_\ell dx \leq 2\epsilon_4 \int_{\mathbb{R}} (\partial_x \zeta)^2 dx + \frac{C^2}{4\epsilon_4} \int_{\mathbb{R}} |\tau|^2 dx + \frac{C^2}{4\epsilon_4} \int_{\mathbb{R}} |\chi|^2 dx. \quad (2.66)$$

Finally we consider the viscosity terms in (2.55). For the  $(\nu_\ell \partial_x u_1)_x$  term

$$- \int_{\mathbb{R}} \zeta \partial_x (\nu_\ell \partial_x u_1) dx = \int_{\mathbb{R}} \nu_\ell \partial_x \zeta \partial_x u_1 dx.$$

Since  $\psi''(p)$ ,  $\partial_{\rho\rho} p(\rho, \mu)$  and  $\partial_{\rho\mu} p(\rho, \mu)$  are locally bounded, then from (2.5) we have  $\nu_\ell \leq C(|\tau| + |\chi|)$ , which gives

$$- \int_{\mathbb{R}} \zeta \partial_x (\nu_\ell \partial_x u_1) dx \leq C \int_{\mathbb{R}} (|\tau| + |\chi|) \partial_x \zeta \partial_x u_1 dx,$$

and leads to,

$$- \int_{\mathbb{R}} \zeta (\nu_\ell \partial_x u_1)_x dx \leq 2\epsilon_5 \int_{\mathbb{R}} \zeta_x^2 dx + \frac{C^2}{4\epsilon_5} \int_{\mathbb{R}} |\partial_x u_1|^2 \tau^2 dx + \frac{C^2}{4\epsilon_5} \int_{\mathbb{R}} |\partial_x u_1|^2 \chi^2 dx.$$

Next we again use the fact that  $\partial_x u_1$  is bounded in  $L^2(0, T; L^\infty(\mathbb{R}))$  by (2.52).

It subsequently follows that,

$$- \|\zeta (\nu_\ell \partial_x u_1)_x\|_{L^1(\mathbb{R})} \leq 2\epsilon_5 \|\partial_x \zeta\|_{L^2(\mathbb{R})}^2 + \frac{B_4(t)}{2\epsilon_5} (\|\tau\|_{L^2(\mathbb{R})}^2 + \|\chi\|_{L^2(\mathbb{R})}^2). \quad (2.67)$$

For the  $(\nu_2 \zeta_x)_x$  term we simply multiply through by  $\zeta$  and integrate, yielding

$$-\int_{\mathbb{R}} \zeta \partial_x (\nu_2 \partial_x \zeta) dx = \int_{\mathbb{R}} \nu_2 (\partial_x \zeta)^2 dx \geq C \int_{\mathbb{R}} (\partial_x \zeta)^2 dx \quad (2.68)$$

when using that  $\nu_2 \geq C$ .

Hence combining (2.63)-(2.68) we have:

$$\begin{aligned} \frac{1}{2} \frac{d}{dt} \int_{\mathbb{R}} \rho_1 \zeta^2 dx + (C - \epsilon_3 - 2\epsilon_4 - 2\epsilon_5) \int_{\mathbb{R}} |\partial_x \zeta|^2 dx \\ \leq \left\{ B_2(t) + \frac{B_3(t)}{\epsilon_3} + \frac{B_4(t)}{4\epsilon_5} + \frac{C^2}{4\epsilon_4} \right\} \left( \|\tau\|_{L^2(\mathbb{R})}^2 + \|\zeta\|_{L^2(\mathbb{R})}^2 \right). \end{aligned} \quad (2.69)$$

All that is left is to find a compatible form of equation (2.56). Here we multiply through by  $\chi$  and integrate in  $\mathbb{R}$  such that the first term gives

$$\int_{\mathbb{R}} \chi \partial_t \chi dx = \frac{1}{2} \frac{d}{dt} \int_{\mathbb{R}} \chi^2 dx. \quad (2.70)$$

The second term in (2.56) is treated in a similar way as (2.60) and (2.65), where here we have

$$\begin{aligned} \left| \int_{\mathbb{R}} \chi \zeta \partial_x \mu_1 dx \right| &\leq \left( \int_{\mathbb{R}} |\chi|^2 dx \right)^{1/2} \left( \int_{\mathbb{R}} |\zeta|^2 dx \right)^{1/2} \left( \operatorname{ess\,sup}_{\mathbb{R}} |\partial_x \mu_1| \right) \\ &\leq C \left( \int_{\mathbb{R}} |\chi|^2 dx \right)^{1/2} \left( \int_{\mathbb{R}} |\zeta|^2 dx \right)^{1/2}. \end{aligned} \quad (2.71)$$

Thus we obtain,

$$C \|\chi\|_{L^2(\mathbb{R})} \|\zeta\|_{L^2(\mathbb{R})} \leq \frac{C}{2} \left( \|\chi\|_{L^2(\mathbb{R})}^2 + \|\zeta\|_{L^2(\mathbb{R})}^2 \right). \quad (2.72)$$

For the last term in (2.56) we use (2.52) with  $u = u_2$  to see

$$\left| \int_{\mathbb{R}} \chi u_2 \partial_x \chi dx \right| \leq C \|\chi\|_{L^2(\mathbb{R})}^2 \|\partial_x u_2\|_{L^\infty(\mathbb{R})} \leq B_5(t) \|\chi\|_{L^2(\mathbb{R})}^2. \quad (2.73)$$

Thus putting (2.70), (2.72) and (2.73) together yields,

$$\frac{1}{2} \frac{d}{dt} \int_{\mathbb{R}} \chi^2 dx \leq \left\{ C/2 + B_5(t) \right\} \left( \|\chi\|_{L^2(\mathbb{R})}^2 + \|\zeta\|_{L^2(\mathbb{R})}^2 \right). \quad (2.74)$$

Finally, combining (2.62), (2.68) and (2.74) along with defining,

$$\begin{aligned}
\mathcal{C} &= C - \epsilon_1 + \epsilon_2 + \epsilon_3 + 2\epsilon_4 + 2\epsilon_5, \\
\mathcal{B}_1(t) &= B_1(t) + C^2(4\epsilon_1)^{-1} + C^2(4\epsilon_2)^{-1} + C/2, \\
\mathcal{B}_2(t) &= B_2(t) + B_3(t)(\epsilon_3)^{-1} + C^2(4\epsilon_4)^{-1} + B_4(2\epsilon_5)^{-1}, \\
\mathcal{B}_3(t) &= B_5(t) + C/2, \\
\mathcal{A}(t) &= \mathcal{B}_1(t) + \mathcal{B}_2(t) + \mathcal{B}_3(t) \\
\mathcal{X}(t) &= (\tau^2 + \rho_1 \zeta^2 + \chi^2),
\end{aligned}$$

yields:

$$\frac{1}{2} \frac{d}{dt} \int_{\mathbb{R}} \mathcal{X}(t) dx + \mathcal{C} \int_{\mathbb{R}} |\partial_x \zeta|^2 dx \leq \mathcal{A}(t) \left( \|\chi\|_{L^2(\mathbb{R})}^2 + \|\zeta\|_{L^2(\mathbb{R})}^2 + \|\tau\|_{L^2(\mathbb{R})}^2 \right).$$

Since proposition 2.4.2, proposition 2.4.7 and lemma 2.4.9 confirm by above that  $\mathcal{A}(t) \in L^2(0, T)$ , and as  $\mathcal{C}$  is positive, then at  $t = 0$  since

$$\int_{\mathbb{R}} \mathcal{X}(t_0) dx = \int_{\mathbb{R}} \tau_0^2 + \rho_1|_{t=0} \zeta_0^2 + \chi_0^2 dx = 0,$$

then Gronwall's lemma gives that  $\int_{\mathbb{R}} \mathcal{X}(t) dx \equiv 0$  over  $[0, T]$ , which establishes that  $\tau$ ,  $\zeta$ , and  $\chi$  are each zero.  $\square$

## Chapter 3

# Numerical Solutions to Generalized Compressible Multicomponent Flows

### 3.1 Introduction

Much work has been done in the study of the numerics of multicomponent flows. An example of an early yet comprehensive study of computational multiphase mechanics was given by Harlow and Amsden in Ref. [96], where they developed an implicit finite differencing technique for extremely generalized multicomponent settings of both compressible and incompressible flows, including phenomena ranging from bubble formation and cavitation effects, to the formation of atmospheric precipitation and mixing jets. Subsequent and related work in multicomponent flows followed with, for example, the work of J. Dukowicz in Ref. [97] for particle-fluid models of incompressible sprays, an approach extended by G. Faeth in [98, 99] to combustion flows and by D. Youngs in Ref. [100] to interfacial turbulent type flows.

Owing to some of these pioneering works, recent work has demonstrated a resurgence of interest in multicomponent flows, approaches and numerical techniques [139–158]. The importance of fluid-flows comprised of more than one phase, specie or component is represented by a vast array of applications that range across a number of fields. For example, multicomponent flows are essential for any flow demonstrating even rudimentary chemistry; hence, for all (nontrivial) “chemical fluids” [45, 46]. Likewise biological flows often require

phase separations, in order to resolve membrane dynamics and interfacial behaviors in cells and cell organelles [2] and medical applications desire estimates in local componentwise variations in blood serosity, which effect the viscosity and flow parameters involved with pulsatile hemodynamics [76, 159]. Likewise we find numerous examples of multicomponent flow applications in the atmospheric [88, 89] and geophysical [90, 91] sciences; as well as in acoustics [24, 94] and astrophysics [21, 95], just to mention a few.

Here we present a new multicomponent numerical scheme based on a mathematically well-posed [39] compressible barotropic system with functional viscosity depending on both the density  $\rho$  and the mass fraction  $\mu_i$  of each fluid component. It is well-known, both experimentally and theoretically, that viscosity has a functional relationship to the density and specie type (for examples see the NIST thermophysical properties server or [12]). In addition, these types of mathematical models (with functional transport coefficients) are well understood from the point of view of continuum dynamics, having been extensively studied by Málek, Rajagopal et al. in Ref. [106, 108, 109, 160, 161] and [107]. It is further seen in Ref. [39] that the analytic model used in this work *a priori* satisfies two essential entropy inequalities, much like the shallow water equations [126], which serve as important tools for numerical analysis and implementation. Mathematically, the existence and regularity of the strong solutions owes enormously to Ref. [35, 48, 60, 65, 66, 68, 70, 82, 114, 116, 119, 122, 130, 132, 134, 135, 137].

In this Chapter we implement a discontinuous Galerkin (DG) finite element method, employing piecewise polynomial approximations which do not enforce or require any type of continuity between the interfaces of “neighboring” elements. This particular implementation is primarily motivated by the

works of Cockburn, Shu et al. (see Ref. [162–166]) and Feistauer, Dolejší et al. (see Ref. [105, 167–172]). We implement a generalized formulation that is designed to accommodate an arbitrary choice of inviscid, viscous, and supplementary numerical fluxes. We use explicit time discretization methods as described in Ref. [162], which necessitate a conditional stability requirement; namely the time discretization must satisfy the CFL condition. Up to the CFL stability condition we find our method to be very robust and to deal well with arbitrary numbers of fluid components of arbitrary type — up to the additional assumption that a barotropic pressure law is applicable. On the domain boundary data we again strive to generalize our setting. We show two different implementations of boundary conditions, which demonstrate different solvency with respect to interior solutions, initial conditions and phenomenologically relevant contexts. In both cases arbitrary Robin type BCs may be set.

In §3.2 we give the general governing system of equations, the mathematical regularity, and the discrete formulation of the problem. In §3.3 we demonstrate a general way of dealing with boundary conditions by way of the method of characteristics, or alternatively, by way of setting arbitrary  $L^\infty$  data on the boundary. We provide an explicit formulation of the characteristic technique and show the generalized behavior of these types of “characteristic” boundary conditions, while subsequently discussing a number of alternative approaches. In §3.4 we implement two test cases with exact solutions, which are restrictions placed on the multifluid barotropic governing equations, and show that they are exact up to the possible exception of the boundary data. In §3.5 we show an example of a bifluid solution using the forward Euler method. We then show the difference between boundary conditions by way

of *weak entropy* solutions versus that of “characteristic” boundary solutions. The next section, §3.6, is used to generalize the setting to  $n$ -fluid components and  $k$ -th order Runge-Kutta schemes, where the example of an  $n = 5$  fluid is shown explicitly. Then in §3.7 we analyse the energy consistency of the modelisation with respect to two entropy inequalities derived in Ref. [39]; one the classical entropy  $\mathcal{S}$  and the second a closely related entropy  $\tilde{\mathcal{S}}$  discovered by Bresch and Desjardins (see Ref. [18, 37, 61, 126, 127, 135]), where it turns out that the numerical scheme from §3.2 can be arbitrarily scaled (by means of the CFL condition) to satisfy both energy relations. Finally in §3.8 we extend the results to include Fick’s diffusion law, where we inspect the exotic physical setting of a pressure wave traveling through a gas comprised partially of polyynes, and discuss some applications.

## 3.2 The Generalized $n$ -fluid

We consider a compressible barotropic  $n$ -fluid system governed by the following system of equations:

$$\partial_t \rho + \partial_x(\rho u) = 0, \tag{3.1}$$

$$\partial_t(\rho u) + \partial_x(\rho u^2) + \partial_x p - \partial_x(\nu \partial_x u) = 0, \tag{3.2}$$

$$\partial_t(\rho \mu_i) + \partial_x(\rho u \mu_i) = 0, \tag{3.3}$$

with initial conditions,

$$\rho|_{t=0} = \rho_0 > 0, \quad \rho u|_{t=0} = m_0, \quad (\rho \mu_i)|_{t=0} = \rho_{i,0}.$$

The multicomponent barotropic pressure  $p = p(\rho \mu_1, \dots, \rho \mu_n)$  is chosen to satisfy,

$$p = \sum_{i=1}^n (\rho \mu_i)^{\gamma_i}, \tag{3.4}$$

where  $\sum_{i=1}^n \mu_i = 1$ . The mass conservation (3.1), momentum conservation (3.2), species conservation (3.3), and barotropic equation of state (3.4) describe the flow of a barotropic compressible viscous fluid defined for  $(t, x) \in \mathbb{R}^+ \times \mathbb{R}$ . Here the *density* is given as  $\rho$ , the *velocity* as  $u$ , the *momentum* by  $m$ , and the *mass fraction* of each component (chemical specie, phase element, etc.) of the fluid is given by  $\mu_i$ , respectively, where  $\gamma_i > 1$  corresponds to the empirically determined adiabatic exponent uniquely characterizing each of the  $n$  species. Furthermore, adopting the notation throughout this chapter that  $\rho_i = \rho \mu_i$ , the form of the viscosity functional  $\nu = \nu(\rho_1, \dots, \rho_n)$  is fixed to satisfy

$$\nu = \psi'(p) \sum_{i=1}^n \rho_i \partial_{\rho_i} p, \quad (3.5)$$

for  $\psi'(p) = Cp^{-\alpha}$  given  $\alpha \in (0, 1)$  and  $C > 0$  as empirically determined constants (see Ref. [106, 108, 109, 160]) and §7).

The mathematical well-posedness of such a system is given by the following theorem, which was proven in Ref. [39]:

**Theorem 3.2.1.** *Given (3.4) and (3.5) satisfying the conditions in Ref. [39] with initial data  $(\rho_0, u_0, \mu_0)$  satisfying*

$$\begin{aligned} 0 < \underline{\varrho}(0) \leq \rho_0 \leq \bar{\varrho}(0) < \infty, \\ \rho_0 \in \dot{H}^1(\mathbb{R}), \quad u_0 \in H^1(\mathbb{R}), \quad \mu_0 \in H^1(\mathbb{R}), \\ \int_{\Omega} \mathcal{E}(\rho_0, \mu_0) dx < +\infty, \\ |\partial_x \mu_0| \leq C \rho_0, \end{aligned}$$

*with  $\bar{\varrho}(0), \underline{\varrho}(0)$  positive constants and  $\mathcal{E}_0$  the internal energy as in Ref. [39], there exists a global strong solution to (3.1)-(3.3) on  $\mathbb{R}^+ \times \mathbb{R}$  such that for*



every  $T > 0$  we have

$$\begin{aligned}\rho &\in L^\infty(0, T; \dot{H}^1(\mathbb{R})), \quad \partial_t \rho \in L^2((0, T) \times \mathbb{R}), \\ u &\in L^\infty(0, T; H^1(\mathbb{R})) \cap L^2(0, T; H^2(\mathbb{R})), \quad \partial_t u \in L^2((0, T) \times \mathbb{R}), \\ \mu_x &\in L^\infty(0, T; L^\infty(\mathbb{R})), \quad \partial_t \mu \in L^\infty(0, T; L^2(\mathbb{R})).\end{aligned}$$

Furthermore, there exist positive constants  $\underline{\varrho}(T)$  and  $\bar{\varrho}(T)$  depending only on  $T$ , such that

$$0 < \underline{\varrho}(T) \leq \rho(t, x) \leq \bar{\varrho}(T) < \infty, \quad \forall (t, x) \in (0, T) \times \mathbb{R}.$$

Additionally, when  $\psi''(p)$ ,  $\partial_{\rho\rho}p(\rho, \mu)$ , and  $\partial_{\rho\mu}p(\rho, \mu)$  are each locally bounded then this solution is unique.

Using this result, notice that for an  $n$ -fluid written with respect to conservation variables, the state vector  $\mathbf{U}$  can be written as the transpose of the  $1 \times m$  row vector

$$\mathbf{U} = (\rho, \rho u, \rho_1, \dots, \rho_n)^T,$$

where  $m = n + 2$  characterizes the degrees of freedom of our chosen system of equations. Note however that we make this choice of a state vector for the sake of flexibility of representation and implementation (see for example §8), where the strict degrees of freedom of the system (3.1)-(3.3), due to the multiplicity of (3.1) in the conservation form of (3.3), is just  $n + 1$ . Nevertheless, consistent with our choice of an  $(n + 2) \times 1$  state vector  $\mathbf{U}$ , we obtain that the  $m \times 1$  inviscid flux vector  $\mathbf{f}$  satisfies

$$\mathbf{f}(\mathbf{U}) = (\rho u, \rho u^2 + p, \rho_1 u, \dots, \rho_n u)^T,$$

while the  $m \times 1$  viscous flux  $\mathbf{g}$  is given by

$$\mathbf{g}(\mathbf{U}, \mathbf{U}_x) = (0, \nu u_x, 0, \dots, 0)^T,$$

such that in this notation (3.1)-(3.3) can be expressed as

$$\mathbf{U}_t + \mathbf{f}_x = \mathbf{g}_x, \quad (3.6)$$

where the notation  $(\cdot)_\iota$  corresponds to component-wise derivations with respect to the variable  $\iota$ .

The Jacobian matrix of the inviscid flux  $J_{\mathbf{U}}\mathbf{f}(\mathbf{U}) = \mathbf{\Gamma}(\mathbf{U})$  can be written as the  $m \times m$  matrix:

$$\mathbf{\Gamma}(\mathbf{U}) = \left( \begin{array}{cc|ccc} 0 & 1 & 0 & \cdots & 0 \\ -u^2 & 2u & \partial_{\rho_1} p & \cdots & \partial_{\rho_n} p \\ \hline -u\mu_1 & \mu_1 & & & \\ \vdots & \vdots & & & \\ -u\mu_n & \mu_n & & & \end{array} \right), \quad (3.7)$$

where  $\mathbb{I}_n$  is the  $n \times n$  identity matrix. An important feature of the barotropic pressure law (3.4) is that it is not a homogeneous function in  $\rho_i$ , and thus the Jacobian  $\mathbf{\Gamma}$  is *not* formulated to satisfy  $\mathbf{\Gamma}\mathbf{U} = \mathbf{f}$ . This contrasts, for example, with the compressible Navier-Stokes equations when using the monofluid form of the ideal gas law  $p = R\rho\vartheta$  (see Ref. [105, 173]). It should be noted that some numerical fluxes and schemes are designed or derived by specifically exploiting this homogeneity with respect to the Jacobian matrix of the flux function (for example, see the Vijayasundaram flux as used in Ref. [105, 167]). Nevertheless, our numerical fluxes will be defined independently of the homogeneity property of the corresponding map, where  $\mathbf{\Gamma}$  simply satisfies  $\mathbf{f}_x = \mathbf{\Gamma}\mathbf{U}_x$ .

For the viscous flux  $\mathbf{g}$  we define the  $m \times m$  matrix,

$$\mathcal{K}(\mathbf{U}) = \nu \left( \begin{array}{cc|cc} 0 & 0 & \mathbf{0} & \\ -\frac{u}{\rho} & \frac{1}{\rho} & \mathbf{0} & \\ \hline \mathbf{0} & \mathbf{0} & \mathbf{0} & \end{array} \right), \quad (3.8)$$

where here and below the  $\mathbf{0}$ 's are zero matrices of the appropriate sizes. Clearly then (3.6) satisfies

$$\mathbf{U}_t + \mathbf{\Gamma} \mathbf{U}_x - (\mathcal{K} \mathbf{U}_x)_x = 0. \quad (3.9)$$

Finally, in order to posit a consistent system of equations, we introduce the function  $\mathbf{\Sigma}$  such that we are concerned with solving the coupled system:

$$\begin{aligned} \mathbf{U}_t + \mathbf{\Gamma} \mathbf{U}_x - (\mathcal{K} \mathbf{\Sigma})_x &= 0 \\ \mathbf{\Sigma} - \mathbf{U}_x &= 0. \end{aligned} \quad (3.10)$$

Consider the following discretization scheme motivated by Ref. [105, 174] (and illustrated in the one dimensional case in Figure 3.1). Take an open  $\Omega \subset \mathbb{R}$  with boundary  $\partial\Omega = \Gamma$ , given  $T > 0$  such that  $\mathcal{Q}_T = ((0, T) \times \Omega)$  for  $\hat{\Omega}$  the closure of  $\Omega$ . Let  $\mathcal{T}_h$  denote the partition of the closure  $\Omega$ , such that taking  $\hat{\Omega} = [a, b]$  provides the partition

$$a = x_0 < x_1 \dots < x_{ne} = b$$

comprised of elements  $\mathcal{G}_i = (x_{i-1}, x_i) \in \mathcal{T}_h$  such that  $\mathcal{T}_h = \{\mathcal{G}_1, \mathcal{G}_2, \dots, \mathcal{G}_{ne}\}$ . The mesh diameter  $h$  is given by  $h = \sup_{\mathcal{G} \in \mathcal{T}_h} (x_i - x_{i-1})$  such that a discrete approximation to  $\Omega$  is given by the set  $\Omega_h = \cup_i \mathcal{G}_i \setminus \{a, b\}$ . Each element of the partition has a boundary set given by  $\partial\mathcal{G}_i = \{x_{i-1}, x_i\}$ , where elements sharing a boundary point  $\partial\mathcal{G}_i \cap \partial\mathcal{G}_j \neq \emptyset$  are characterized as neighbors and generate the set  $\mathcal{K}_{ij} = \partial\mathcal{G}_i \cap \partial\mathcal{G}_j$  of interfaces between neighboring elements. The boundary  $\partial\Omega = \{a, b\}$  is characterized in the mesh as  $\partial\Omega = \{x_0, x_{ne}\}$  and indexed by elements  $B_j \in \partial\Omega$  such that  $\hat{\Omega} = \mathcal{T}_h \cup \mathcal{K}_{ij} \cup \partial\Omega$ . Now for  $I \subset \mathbb{Z}^+ = \{1, 2, \dots\}$  define the indexing set  $r(i) = \{j \in I : \mathcal{G}_j \text{ is a neighbor of } \mathcal{G}_i\}$ , and for  $I_B \subset \mathbb{Z}^- = \{-1, -2, \dots\}$  define  $s(i) = \{j \in I_B : \mathcal{G}_i \text{ contains } B_j\}$ . Then for  $S_i = r(i) \cup s(i)$ , we have  $\partial\mathcal{G}_i = \cup_{j \in S(i)} \mathcal{K}_{ij}$  and  $\partial\mathcal{G}_i \cap \partial\Omega = \cup_{j \in s(i)} \mathcal{K}_{ij}$ .

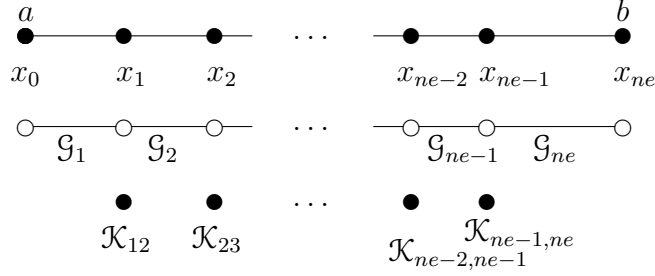


Figure 3.1: The discretization of  $\Omega$ , distinguishing nodes, elements, and neighbors with the boundary  $\partial\Omega = \{a, b\}$ .

We define the broken Sobolev space over the partition  $\mathcal{T}_h$  as

$$W^{k,2}(\Omega_h, \mathcal{T}_h) = \{v : v|_{\mathcal{G}_i} \in W^{k,2}(\mathcal{G}_i) \quad \forall \mathcal{G}_i \in \mathcal{T}_h\}.$$

Further, approximate solutions to (3.1)-(3.3) will exist in the space of discontinuous piecewise polynomial functions over  $\Omega$  restricted to  $\mathcal{T}_h$ , given as

$$S_h^d(\Omega_h, \mathcal{T}_h) = \{v : v|_{\mathcal{G}_i} \in \mathcal{P}^d(\mathcal{G}_i) \quad \forall \mathcal{G}_i \in \mathcal{T}_h\}$$

for  $\mathcal{P}^d(\mathcal{G}_i)$  the space of degree  $\leq d$  polynomials on  $\mathcal{G}_i$ .

Choosing a degree  $d$  set of polynomial basis functions  $N_\ell \in \mathcal{P}^d(\mathcal{G}_i)$  for  $\ell = 0, \dots, d$  we can denote the state vector at the time  $t$  over  $\Omega_h$ , by

$$\mathbf{U}_h(t, x) = \sum_{\ell=0}^d \mathbf{U}_\ell^i(t^n) N_\ell^i(x), \quad \forall x \in \mathcal{G}_i,$$

where the  $N_\ell^i$ 's are the finite element shape functions, and the  $\mathbf{U}_\ell^i$ 's correspond to the nodal unknowns. Likewise the test functions  $\boldsymbol{\varphi}_h, \boldsymbol{\vartheta}_h \in W^{2,2}(\Omega, \mathcal{T}_h)$  are characterized by

$$\boldsymbol{\varphi}_h(x) = \sum_{\ell=0}^d \boldsymbol{\varphi}_\ell^i N_\ell^i(x) \quad \text{and} \quad \boldsymbol{\vartheta}_h(x) = \sum_{\ell=0}^d \boldsymbol{\vartheta}_\ell^i N_\ell^i(x) \quad \forall x \in \mathcal{G}_i,$$

for  $\boldsymbol{\varphi}_\ell^i$  and  $\boldsymbol{\vartheta}_\ell^i$  the nodal values of the test function in each  $\mathcal{G}_i$ .

Letting  $\mathbf{U}$  be a classical solution to (3.10) and multiplying through by test functions  $\boldsymbol{\varphi}_h$  and  $\boldsymbol{\vartheta}_h$  and integrating elementwise by parts yields:

$$\begin{aligned} \frac{d}{dt} \int_{\mathcal{G}_i} \mathbf{U} \cdot \boldsymbol{\varphi}_h dx + \int_{\mathcal{G}_i} (\mathbf{f} \cdot \boldsymbol{\varphi}_h)_x dx - \int_{\mathcal{G}_i} \mathbf{f} \cdot \boldsymbol{\varphi}_x^h dx - \int_{\mathcal{G}_i} \mathbf{g}_x \cdot \boldsymbol{\varphi}_h dx &= 0, \\ \int_{\mathcal{G}_i} \boldsymbol{\Sigma} \cdot \boldsymbol{\vartheta}_h dx - \int_{\mathcal{G}_i} (\mathbf{U} \cdot \boldsymbol{\vartheta}_h)_x dx + \int_{\mathcal{G}_i} \mathbf{U} \cdot \boldsymbol{\vartheta}_x^h dx &= 0. \end{aligned} \quad (3.11)$$

Let  $\varphi|_{\mathcal{K}_{ij}}$  and  $\varphi|_{\mathcal{K}_{ji}}$  denote the values of  $\varphi$  on  $\mathcal{K}_{ij}$  considered from the interior and the exterior of  $\mathcal{G}_i$ , respectively. It should be noted that for  $\mathcal{K}_{ij} \in \Gamma$ , the restricted functions  $\boldsymbol{\varphi}_h|_{\mathcal{K}_{ji}}$  are determined up to a choice of boundary condition, which we will discuss in more detail in §3. Then we approximate the first term of (3.11) by,

$$\frac{d}{dt} \int_{\mathcal{G}_i} \mathbf{U}_h \cdot \boldsymbol{\varphi}_h dx \approx \frac{d}{dt} \int_{\mathcal{G}_i} \mathbf{U} \cdot \boldsymbol{\varphi}_h dx, \quad (3.12)$$

the second term in (3.11) by the inviscid numerical flux  $\Phi_i$ ,

$$\begin{aligned} \tilde{\Phi}_i(\mathbf{U}_h|_{\mathcal{K}_{ij}}, \mathbf{U}_h|_{\mathcal{K}_{ji}}, \boldsymbol{\varphi}_h) &= \sum_{j \in S(i)} \int_{\mathcal{K}_{ij}} \Phi(\mathbf{U}_h|_{\mathcal{K}_{ij}}, \mathbf{U}_h|_{\mathcal{K}_{ji}}, n_{ij}) \cdot \boldsymbol{\varphi}_h|_{\mathcal{K}_{ij}} d\mathcal{K} \\ &\approx \int_{\mathcal{K}_{ij}} \mathbf{f}_h \cdot n_{ij} \boldsymbol{\varphi}_h|_{\mathcal{K}_{ij}} d\mathcal{K}, \end{aligned} \quad (3.13)$$

for  $n_{ij}$  the unit outward pointing normal; and the third term on the left in (3.11) by,

$$\Theta_i(\mathbf{U}_h, \boldsymbol{\varphi}_h) = \int_{\mathcal{G}_i} \mathbf{f}_h \cdot (\boldsymbol{\varphi}_h)_x dx \approx - \int_{\mathcal{G}_i} \mathbf{f} \cdot (\boldsymbol{\varphi}_h)_x dx. \quad (3.14)$$

The viscous term in (3.11) integrates by parts to give:

$$\begin{aligned} \int_{\mathcal{G}_i} \mathbf{g}_x \cdot \boldsymbol{\varphi}_h dx &= \int_{\mathcal{G}_i} (\mathbf{g} \cdot \boldsymbol{\varphi}_h)_x dx - \int_{\mathcal{G}_i} \mathbf{g} \cdot \boldsymbol{\varphi}_x^h dx \\ &= \int_{\mathcal{G}_i} (\mathcal{K} \boldsymbol{\Sigma} \cdot \boldsymbol{\varphi}_h)_x dx - \int_{\mathcal{G}_i} \mathcal{K} \boldsymbol{\Sigma} \cdot \boldsymbol{\varphi}_x^h dx. \end{aligned} \quad (3.15)$$

For the first term on the right in (3.15) we approximate using a generalized viscous flux  $\hat{\mathcal{G}}$  (see Ref. [175] for a review of choices in the DG framework). We write here for the general viscous flux

$$\begin{aligned}\mathcal{G}_i(\boldsymbol{\Sigma}_h, \mathbf{U}_h, \boldsymbol{\varphi}_h) &= \int_{\mathcal{K}_{ij}} \hat{\mathcal{G}}(\boldsymbol{\Sigma}_h|_{\mathcal{K}_{ij}}, \boldsymbol{\Sigma}_h|_{\mathcal{K}_{ji}}, \mathbf{U}_h|_{\mathcal{K}_{ij}}, \mathbf{U}_h|_{\mathcal{K}_{ji}}, n_{ij}) \cdot \boldsymbol{\varphi}_h|_{\mathcal{K}_{ij}} d\mathcal{K} \\ &\approx \int_{\mathcal{K}_{ij}} \mathbf{g}_h \cdot n_{ij} \boldsymbol{\varphi}_h|_{\mathcal{K}_{ij}} d\mathcal{K},\end{aligned}\tag{3.16}$$

while the second term is approximated by:

$$\mathcal{N}_i(\boldsymbol{\Sigma}_h, \mathbf{U}_h, \boldsymbol{\varphi}_h) = \int_{\mathcal{G}_i} \mathbf{g}_h \cdot (\boldsymbol{\varphi}_h)_x dx \approx \int_{\mathcal{G}_i} \mathbf{g} \cdot \boldsymbol{\varphi}_x^h dx.\tag{3.17}$$

Finally for the second equation in (3.10) we expand it such that the approximate solution satisfies:

$$\begin{aligned}\mathcal{Q}_i(\hat{\mathbf{U}}, \boldsymbol{\Sigma}_h, \mathbf{U}_h, \boldsymbol{\vartheta}_h, \boldsymbol{\vartheta}_x^h) &= \int_{\mathcal{G}_i} \boldsymbol{\Sigma}_h \cdot \boldsymbol{\vartheta}_h dx + \int_{\mathcal{G}_i} \mathbf{U}_h \cdot \boldsymbol{\vartheta}_x^h dx \\ &\quad - \sum_{j \in S(i)} \int_{\mathcal{K}_{ij}} \hat{\mathbf{U}}(\mathbf{U}_h|_{\mathcal{K}_{ij}}, \mathbf{U}_h|_{\mathcal{K}_{ji}}, \boldsymbol{\vartheta}_h|_{\mathcal{K}_{ij}}) d\mathcal{K},\end{aligned}\tag{3.18}$$

where,

$$\begin{aligned}\mathcal{U}_i(\mathbf{U}_h, \boldsymbol{\vartheta}_h) &= \sum_{j \in S(i)} \int_{\mathcal{K}_{ij}} \hat{\mathbf{U}}(\mathbf{U}_h|_{\mathcal{K}_{ij}}, \mathbf{U}_h|_{\mathcal{K}_{ji}}, \boldsymbol{\vartheta}_h|_{\mathcal{K}_{ij}}) d\mathcal{K} \\ &\approx \int_{\mathcal{K}_{ij}} \mathbf{U} \cdot n_{ij} \boldsymbol{\vartheta}_h|_{\mathcal{K}_{ij}} d\mathcal{K}\end{aligned}$$

given that  $\hat{\mathbf{U}}$  is the generalized flux term associated with the discontinuous Galerkin method determined up to a congeries of options (please see Ref. [175] for a unified analysis), and using the approximate relations:

$$\int_{\mathcal{G}_i} \boldsymbol{\Sigma}_h \cdot \boldsymbol{\vartheta}_h dx \approx \int_{\mathcal{G}_i} \boldsymbol{\Sigma} \cdot \boldsymbol{\vartheta}_h dx, \quad \text{and} \quad \int_{\mathcal{G}_i} \mathbf{U}_h \cdot \boldsymbol{\vartheta}_x^h dx \approx \int_{\mathcal{G}_i} \mathbf{U} \cdot \boldsymbol{\vartheta}_x^h dx.$$

Combining (3.13), (3.14), (3.16), (3.17) and (3.18) and setting,

$$\mathcal{X} = \sum_{\mathcal{G}_i \in \mathcal{T}_h} \mathcal{X}_i,$$

given the inner product

$$(\mathbf{a}_h^n, \mathbf{b}_h)_{\Omega_{\mathcal{G}}} = \sum_{\mathcal{G}_i \in \mathcal{T}_h} \int_{\mathcal{G}_i} \mathbf{a}_h^n \cdot \mathbf{b}_h dx,$$

we define an approximate solution to (3.11) as functions  $\mathbf{U}_h$  and  $\boldsymbol{\Sigma}_h$  for all  $t \in (0, T)$  satisfying:

- 1)  $\mathbf{U}_h \in C^1([0, T]; S_h^d)$ ,  $\boldsymbol{\Sigma}_h \in S_h^d$ ,
- 2)  $\frac{d}{dt}(\mathbf{U}_h, \boldsymbol{\varphi}_h)_{\Omega_{\mathcal{G}}} + \tilde{\Phi}(\mathbf{U}_h, \boldsymbol{\varphi}_h) - \Theta(\mathbf{U}_h, \boldsymbol{\varphi}_h) - \mathcal{G}(\boldsymbol{\Sigma}_h, \mathbf{U}_h, \boldsymbol{\varphi}_h) + \mathcal{N}(\boldsymbol{\Sigma}_h, \mathbf{U}_h, \boldsymbol{\varphi}_h) = 0$ , (3.19)
- 3)  $\mathcal{Q}(\hat{\mathbf{U}}, \boldsymbol{\Sigma}_h, \mathbf{U}_h, \boldsymbol{\vartheta}_h, \boldsymbol{\vartheta}_x^h) = 0$ ,
- 4)  $\mathbf{U}_h(0) = \mathbf{U}_0$ .

We find below that up to a (possibly arbitrary) choice of boundary data, these solutions are quite well-behaved, extremely robust for arbitrary choice of  $n$  fluids (we show  $n = 1, 2$  and  $5$  here, and have tested up to  $n = 11$  elsewhere) and readily extended to more complicated systems (e.g. §8).

### 3.3 Towards a Generalized Boundary Treatment

Specifying arbitrary boundary data with respect to our approximate solution (3.19) is a delicate issue which requires a nuanced understanding of barotropic solutions and the mathematical techniques used to pose them. That is, we wish to determine the nature of an arbitrary boundary state  $\mathbf{U}|_{\partial\Omega}$  in a way which is well-posed with respect to the system (3.1)-(3.3); which is to say, in such a way that the uniqueness of the solution is maintained.

However, practically speaking, recovering boundary data of an arbitrary nature on  $\partial\Omega$  poses well-established difficulties with respect to the *a priori* estimates established in Ref. [39], which serve as the cornerstone to the existence and uniqueness result stated in Theorem 2.1. That is, recovering the *a priori* estimates on the solution is reduced, in the first step, to recovering two entropy inequalities (see §3.7 for explicit forms) which serve as positive definite functionals over  $(0, T) \times \Omega$ . However, when explicit boundary data is given, these inequalities acquire the addition of the following two unsigned boundary components, respectively (see Ref. [39] for the explicit calculation):

$$\int_{\Omega} (\rho u^3)_x dx \quad \text{and} \quad \int_{\Omega} (\rho u(u + \rho^{-1} \psi_x)^2)_x dx,$$

having the consequence of rendering a formulation which spans any type of boundary data difficult to establish. Instead we offer a number of pragmatic approximate approaches that generalize the solution up to some important restrictions, and then discuss some alternative approaches that are aimed at certain specialized types of settings. First we review some known results.

It has been shown by Strikwerda [176], Gustaf'sson and Sundstrom [177] that incompletely parabolic systems, such as the shallow water equations and the full Navier-Stokes equations, may be well-posed with respect to a broad set of initial-boundary data. These works additionally demonstrate the appropriate number of boundary conditions expected on incompletely parabolic systems, which differ from completely hyperbolic systems such as Euler's equations. As the barotropic system (3.1)-(3.2) maintains a formal equivalence to the viscous shallow water equations (see for example Ref. [36, 126]), we might expect (3.1)-(3.2) to behave as an incompletely parabolic system due to Ref. [177]. However, the dependencies of the  $p$  and



$\nu$  on the mass fractions make showing this nontrivial and requires a careful analysis of either incompletely parabolic systems [176], or hyperbolic-parabolic systems [178].

The implementation of both incompletely parabolic and hyperbolic systems often rely upon the so-called “characteristic treatment.” In these systems we use characteristic directions to extrapolate values of the system variables on the boundary, while the others become constrained by a set of characteristic relations (see Ref. [179] and Ref. [180] for the hyperbolic regime). These types of treatments have been extended to treat the full Navier-Stokes equations [181, 182], the viscous shallow water equations [183], and multifluid systems [184].

We want to consider what we will refer to here and below as “characteristic” type boundary solutions, which we view as a reduced hyperbolic system (as presented in Ref. [105, 177]). That is, let  $\mathbf{q} = \mathbf{U}$  be a characteristic variable such that upon linearizing (3.6) on the boundary we arrive with:

$$\frac{\partial \mathbf{q}}{\partial t} + \mathbf{\Gamma}(\mathbf{q}_h^n) \frac{\partial \mathbf{q}}{\partial x} - \mathbf{g}_x(\mathbf{q}_{h,x}^n \mathbf{q}_h^n) = 0. \quad (3.20)$$

The initial conditions are given by

$$\mathbf{q}_h(0, x_1) = \mathbf{q}_h^n, \quad \text{for } x \in (-\infty, 0), \quad (3.21)$$

while the boundary data satisfies

$$\mathbf{q}_h(t, 0) = \mathbf{q}_b^n, \quad \text{for } t \in (0, \infty). \quad (3.22)$$

Since  $\mathbf{\Gamma}$  is diagonalizable we have that  $\mathbf{\Gamma}_h \mathbf{c}_j = \varsigma_j \mathbf{c}_j$ , where  $\mathbf{c}_j$  are the eigenvectors of  $\mathbf{\Gamma}$  associated to eigenvalues  $\varsigma_j$  (see §3.4 for an example), which are used to formulate the solution in the form

$$\mathbf{q}(x_1, t) = \sum_{j=1}^m \lambda_j(x_1, t) \mathbf{c}_j, \quad (3.23)$$

where the initial and boundary data, respectively, satisfy

$$\mathbf{q}_h^n = \sum_{j=1}^m \alpha_j \mathbf{c}_j, \quad \text{and} \quad \mathbf{q}_b^n = \sum_{j=1}^m \beta_j \mathbf{c}_j. \quad (3.24)$$

Now, the diffusion term  $\mathbf{g}_x$  is chosen with respect to the viscous ansatz  $\zeta_j$ , such that the following relation holds:

$$\nu u_{xx}^n \varpi_j \mathbf{c}_j = \zeta_j \mathbf{c}_j - \nu_x^n u_x^n \varpi_j \mathbf{c}_j \quad \text{on} \quad \partial\Omega, \quad (3.25)$$

where  $e_2 = \sum_j \varpi_j \mathbf{c}_j$  with  $e_2 = (0, 1, 0, \dots, 0)$ . This notation should not be misleading here, where all we have written is the viscous flux in (3.16) in the characteristic basis restricted to the boundary element.

It then follows (from Ref. [105] chapter 3, for example) that (3.20) can be written as  $j$  initial-boundary value scalar problems:

$$\begin{aligned} \frac{\partial \lambda_j}{\partial t} + \varsigma_j \frac{\partial \lambda_j}{\partial x} - \zeta_j &= 0 \quad \text{in } (0, \infty) \times (-\infty, 0), \\ \lambda_j(x_1, 0) &= \alpha_j, \quad \text{for } x_1 \in (-\infty, 0), \\ \lambda_j(0, t) &= \beta_j \quad \text{for } t \in (0, \infty). \end{aligned} \quad (3.26)$$

The scalar problems (3.26) may be solved via the method of characteristics, from which we obtain the solution,

$$\lambda_j(x_1, t) = \begin{cases} \alpha_j(t - x_1/\varsigma_j) + t\zeta_j, & \text{for } t - x_1/\varsigma_j \geq 0, \\ \beta_j(x_1 - t\varsigma_j) + x_1\zeta_j/\varsigma_j, & \text{for } x_1 - t\varsigma_j > 0, \end{cases} \quad (3.27)$$

which provides an explicit form to (3.23). Plugging this state vector  $\mathbf{q}$  back into the viscous and inviscid fluxes we are able to prescribe consistent boundary conditions. Here, by “consistent” we mean in the sense of the solution being linearized around the current interior state values such that perturbations around those values break up into small amplitude waves in the characteristic

Table 3.1: *Choice of boundary conditions*

Boundary type		Restrictions	Free	Fixed
Subsonic $u \cdot \mathbf{n} > -c$	inlet $u \cdot \mathbf{n} < 0$	$\mu_1 + \dots + \mu_n = 1, \rho > 0$ and the appropriate supplementary conditions associated with a choice of boundary data, including: $\rho, u, \mu_i, p, \nu, m, \rho\mu_i$ , etc.	$\beta_2, \dots, \beta_m,$	$\alpha_1$
Supersonic $u \cdot \mathbf{n} \leq -c$	inlet $u \cdot \mathbf{n} < 0$		$\beta_1, \dots, \beta_m,$	none
Subsonic $u \cdot \mathbf{n} < c$	outlet $u \cdot \mathbf{n} > 0$		$\beta_2$	$\alpha_1, \alpha_3,$ $\dots, \alpha_m$
Supersonic $u \cdot \mathbf{n} \geq c$	outlet $u \cdot \mathbf{n} > 0$		none	$\alpha_1,$ $\dots, \alpha_m$
Membrane $u \cdot \mathbf{n} = 0$	wall $u \cdot \mathbf{n} = 0$	$\rho, u, \mu_i, p, \nu, m, \rho\mu_i$ , etc.	$\beta_2$	$\alpha_1, \alpha_3,$ $\dots, \alpha_m$

directions provided by the eigenbasis. The amplitudes of the incoming waves (negative eigendirections) form the physical boundary conditions and can be chosen, while the outgoing waves propagate to form the numerical boundary conditions, which are determined from the interior state.

It turns out that for (3.1)-(3.5) we can reduce this method to that of the essential choices listed in Table 3.1. This corresponds with what we know of hyperbolic systems as shown in Ref. [105] and Ref. [179], with respect to the number of free and fixed conditions on the boundaries. That is, the  $\alpha_j$ 's are determined below the characteristic line  $t = x_1/\varsigma_j$ , which has the effect of reducing the degrees of freedom on the inlet and outlet states for eigenvalues which satisfy  $\varsigma_j \geq 0$ ; and otherwise the  $\beta_j$ 's determined the free states of the system.

As an example consider the subsonic outlet condition  $u \cdot \mathbf{n} < c$ . Then at  $x = 0$  (see appendix A for the full formulation) we solve for the  $\alpha_j$ 's and  $\beta_j$ 's via,

$$(\alpha_1 - t\zeta_1, \beta_2, \alpha_3 - t\zeta_3, \dots, \alpha_n - t\zeta_n)^T = \mathbf{V}^{-1}\mathbf{U} \quad (3.28)$$

where we show  $\mathbf{V}$  and its inverse for  $\mathbf{\Gamma}$  in appendix A. From this we find that  $\alpha_1 = \rho/2 - t\zeta_1$  while  $\alpha_\ell = t\zeta_\ell$  for  $\ell = 3, \dots, n$ , and consequently solving (3.24) is immediate. Once the fixed components are determined, all that remains is characterizing the nature of the desired boundary, and then solving for the  $\beta_j$ 's to fix the desired condition, upon which we simply plug  $\mathbf{q}$  back into the appropriately chosen inviscid flux on  $\partial\Omega$ . For example, we may consider the dynamic viscosity condition  $\nu_b = \mathcal{V}$  prescribed on  $\partial\Omega$  which must satisfy  $C \sum_{i=1}^n \gamma_i \rho_i^{\gamma_i} = \mathcal{V} p^\alpha$ , thus reducing to prescription upon  $\rho$  and the  $\mu_i$ 's. In this case it is interesting to note that since  $\nu$  is a function of the primitive variables  $\rho$  and  $\mu_i$ , the form of the viscous ansatz  $\zeta_j$  in no way precludes a choice of  $\nu$  on  $\partial\Omega$ .

In addition to employing these “characteristic” solutions, we notice that the form of (3.20) satisfies the *weak entropy* solutions of Ref. [162, 185] and Ref. [186]) for hyperbolic systems, since the ansatz  $\zeta$  can be viewed as a source term in this context. These solutions provide even greater flexibility to our choice of boundary conditions. However, as we show in §3.4, even though these two types of solutions are both consistent, they do not display equivalent numerical behavior.

Nevertheless these two choices of boundary data, the “characteristic” and *weak entropy* solutions, are not ideal since (3.1)-(3.3) is *not* a hyperbolic system, and thus only represent approximate solutions on the boundary up to a choice of linearization. These restrictions however do not exhaust our

options for solving (3.1)-(3.3) on the boundary. For example, we may alternatively consider the route of positing boundary data by a simple extension of the results of Zlotnik (see Ref. [187]) to see that the barotropic system is parabolic in the sense of Petrovskii upon addition of the “quasihydrodynamic” or “quasigasdynamic” auxilliary function  $w$  (see Ref. [22, 188]) on  $\partial\Omega$ :

$$w = \omega (uu_x + \rho^{-1}\partial_\rho p \rho_x - F) \quad \text{on} \quad \partial\Omega,$$

for a mass force function  $F$  and  $\omega = \nu/pS$ , where  $S$  is the Schmidt number. In the quasihydrodynamic barotropic monofluid treatment,  $w$  is viewed as a stabilization parameter with respect to the usual Navier-Stokes equations, and  $\omega$  is weighted in such a manner as to scale like the atomic mean free path, in the sense of the kinetics theory (see Ref. [27, 188]), where (3.1) becomes

$$\rho_t + (\rho u)_x = (\rho w)_x.$$

Using this approximation we easily recover the initial-boundary problem of Ref. [176] with the additional conditions provided in Proposition 3 of Ref. [187]. That is equations (3.1)-(3.2) now directly satisfy Proposition 3 of Ref. [187] with the help of Ref. [39], then applying this to (3.1)-(3.3) and using the formulation of Ref. [176] immediately yields the result. Alternatively we may adapt  $w$  to include a parameter dependent on  $\mu_x$  in the multicomponent setting, where

$$w = \omega (uu_x + \rho^{-1}p_x - F) \quad \text{on} \quad \partial\Omega,$$

corresponding to a nontrivial species-dependent diffusion velocity (see Ref. [46] appendix C.2), in which case a careful treatment is required (e.g. set  $\phi' = \nu\partial_\mu p/\rho p$  to find the parabolic component in the advection form  $\partial_t\mu_i + u\partial_x\mu_i = w\partial_x\mu_i$  to satisfy  $\phi\partial_{xx}\mu_i$  in the leading symbol) to confirm that the system obeys a Petrovskii parabolicity condition.

However it should be additionally cautioned that the quasigasdynamic condition may be strongly nonideal for some physically relevant systems, being more dissipative than the traditional compressible Navier-Stokes system. On the other hand, it is interesting to cite that in the so-called quasi-compressible regime of Ref. [189] a similar dissipative type component emerges in the mass conservation law. Here the velocity component of the system is decomposed via extensive phenomenological arguments (see Ref. [189]) into a mass velocity  $u_m$  and the usual volume velocity  $u$ , satisfying the constitutive law  $u - u_m = K(\log \rho)_x$  with  $K$  a phenomenological coefficient, and 3.1 consequently becomes

$$\rho_t + (\rho u)_x = (K \rho_x)_x,$$

a parabolic equation. However, in this regime again, it is unclear how to deal with the hyperbolic equation (3.3).

More generally, there exists a large back catalogue of results on compressible barotropic systems with varying initial-boundary data; some of which utilizing fairly exotic conditions on the boundary. For example, for barotropic inflow problems we can refer to both Ref. [190] and Ref. [191], where in both cases results from Ref. [39] are required and additional extensions are needed to move into the multiphase regime. Likewise solutions exist for free boundary barotropic problems [129], surface tension type boundaries [122], Navier boundary type conditions [192], and various Dirichlet type problems near vacuum states [60, 193, 194]; however, again, all of these results are only strictly satisfied for monofluidic systems, and thus require subtle analysis in order to extend them to the full multifluid regime. In many cases however, such as in Ref. [187], the extension is relatively straightforward.

### 3.4 Numerical Test Cases

We inspect two analytic test cases to verify the accuracy of the numerical method presented in §3.2 and §3.3. In both cases we solve a monofluid restriction of (3.1)-(3.3) from the bifluid case ( $n = 2$ ), with  $\mu_1 = 1$  and  $\mu_2 = 0$  in  $N = 1$  spatial dimension.

Now we can easily define the three vectors  $\mathbf{U} = (\rho, \rho u, \rho_1, \rho_2)^T$ ,  $\mathbf{f}(\mathbf{U}) = (\rho u, \rho u^2 + p, \rho_1 u, \rho_2 u)^T$  and  $\mathbf{g}(\mathbf{U}, \mathbf{U}_x) = (0, \nu u_x, 0)^T$  such that (3.1)-(3.3) are expressed as

$$\mathbf{U}_t + \mathbf{f}_x = \mathbf{g}_x, \quad (3.29)$$

whereby setting  $n = 2$  in (3.7) and using (3.8) it then follows that

$$\mathbf{U}_t + \mathbf{\Gamma} \mathbf{U}_x = (\mathcal{K} \mathbf{U}_x)_x. \quad (3.30)$$

We can thus write a weak form of (3.1)-(3.3) in the same way as (3.11).

To solve the system we must first specify the inviscid flux  $\Phi$ . We test for two choices here. First we implement the local Lax-Friedrich's flux  $\Phi_{LF}$  which satisfies

$$\begin{aligned} \int_{\mathcal{K}_{ij}} \Phi_{LF} \cdot \varphi_h d\mathcal{K} &= \frac{1}{2} \int_{\mathcal{K}_{ij}} (\mathbf{f}(\mathbf{U}_h)|_{\mathcal{K}_{ij}} + \mathbf{f}(\mathbf{U}_h)|_{\mathcal{K}_{ji}}) \cdot n_{ij} \varphi_h|_{\mathcal{K}_{ij}} d\mathcal{K} \\ &\quad - \frac{1}{2} \int_{\mathcal{K}_{ij}} (\text{Spec}_r(\mathbf{\Gamma}))((\mathbf{U}_h)|_{\mathcal{K}_{ij}} - (\mathbf{U}_h)|_{\mathcal{K}_{ji}}) \cdot n_{ij} \varphi_h|_{\mathcal{K}_{ij}} d\mathcal{K}, \end{aligned}$$

for  $n_{ij}$  the outward unit normal and  $\text{Spec}_r(\mathbf{\Gamma})$  the spectral radius of  $\mathbf{\Gamma}$ . Summing over each of the elements of the mesh this term may be written as

$$\begin{aligned} 2\tilde{\Phi}_{LF}(\mathbf{U}_h, \varphi_h) &= \sum_{\mathcal{G}_i \in \mathcal{T}_h} \sum_{j \in S(i)} \int_{\mathcal{K}_{ij}} (\mathbf{f}(\mathbf{U}_h)|_{\mathcal{K}_{ij}} + \mathbf{f}(\mathbf{U}_h)|_{\mathcal{K}_{ji}}) \cdot n_{ij} \varphi_h|_{\mathcal{K}_{ij}} d\mathcal{K} \\ &\quad - \sum_{\mathcal{G}_i \in \mathcal{T}_h} \sum_{j \in S(i)} \int_{\mathcal{K}_{ij}} (\text{Spec}_r(\mathbf{\Gamma}))((\mathbf{U}_h)|_{\mathcal{K}_{ij}} - (\mathbf{U}_h)|_{\mathcal{K}_{ji}}) \cdot n_{ij} \varphi_h|_{\mathcal{K}_{ij}} d\mathcal{K}. \end{aligned} \quad (3.31)$$

As our second choice of inviscid flux we implement a standard approximate Riemann solver, with flux  $\Phi_R$  satisfying:

$$\begin{aligned} \int_{\mathcal{K}_{ij}} \Phi_R \cdot \varphi_h d\mathcal{K} &= \frac{1}{2} \int_{\mathcal{K}_{ij}} (\mathbf{f}(\mathbf{U}_h)|_{\mathcal{K}_{ij}} + (\mathbf{f}(\mathbf{U}_h)|_{\mathcal{K}_{ji}}) \cdot n_{ij} \varphi_h|_{\mathcal{K}_{ij}} d\mathcal{K} \\ &\quad - \frac{1}{2} \int_{\mathcal{K}_{ij}} (V(\{\mathbf{U}_h\})|\Lambda(\{\mathbf{U}_h\})|V^{-1}(\{\mathbf{U}_h\}) \cdot n_{ij} \varphi_h|_{\mathcal{K}_{ij}} d\mathcal{K}, \end{aligned}$$

where  $V$  and  $V^{-1}$  are found from the eigendecomposition given in appendix A, and  $\Lambda(\{\mathbf{U}_h\})$  is given by the diagonal matrix of eigenvalues  $\text{diag}(\varsigma_i)$  — as also enumerated in appendix A — such that peicewise averages are taken; e.g.

$$\varsigma_1(\{\mathbf{U}_h\}) = \{u_h\} + (\gamma_1\{(\rho\mu_1)_h/\rho_h\}\{\rho\mu_1\} + \dots + \gamma_n\{(\rho\mu_n)_h/\rho_h\}\{(\rho\mu_n)_h\})^{1/2},$$

where the average is given by

$$\{\mathbf{U}_h\} = \frac{1}{2} (\mathbf{U}_h|_{\mathcal{K}_{ij}} + \mathbf{U}_h|_{\mathcal{K}_{ji}}).$$

Summing over the mesh we find

$$\begin{aligned} 2\tilde{\Phi}_R(\mathbf{U}_h, \varphi_h) &= \sum_{\mathcal{G}_i \in \mathcal{T}_h} \sum_{j \in S(i)} \int_{\mathcal{K}_{ij}} (\mathbf{f}(\mathbf{U}_h)|_{\mathcal{K}_{ij}} + (\mathbf{f}(\mathbf{U}_h)|_{\mathcal{K}_{ji}}) \cdot n_{ij} \varphi_h|_{\mathcal{K}_{ij}} d\mathcal{K} \\ &\quad - \sum_{\mathcal{G}_i \in \mathcal{T}_h} \sum_{j \in S(i)} \int_{\mathcal{K}_{ij}} (V(\{\mathbf{U}_h\})|\Lambda(\{\mathbf{U}_h\})|V^{-1}(\{\mathbf{U}_h\}) \cdot n_{ij} \varphi_h|_{\mathcal{K}_{ij}} d\mathcal{K}. \end{aligned} \tag{3.32}$$

Next we specify the viscous flux  $\mathcal{G}$ . Here we use a formulation similar to that presented in Ref. [195], but we adapt it to include the functional dependencies present in the viscosity. We choose

$$\int_{\mathcal{K}_{ij}} \hat{\mathcal{G}}_b \cdot n_{ij} \varphi_h d\mathcal{K} = \frac{1}{2} \int_{\mathcal{K}_{ij}} ((\mathcal{K}\Sigma_h)|_{\mathcal{K}_{ij}} + (\mathcal{K}\Sigma_h)|_{\mathcal{K}_{ji}}) \cdot n_{ij} \varphi_h|_{\mathcal{K}_{ij}} d\mathcal{K},$$

which summed over elements gives:

$$\mathcal{G}_b(\Sigma_h, \mathbf{U}_h, \varphi_h) = \frac{1}{2} \sum_{\mathcal{G}_i \in \mathcal{T}_h} \sum_{j \in S(i)} \int_{\mathcal{K}_{ij}} (\mathcal{K}\Sigma_h)|_{\mathcal{K}_{ij}} + (\mathcal{K}\Sigma_h)|_{\mathcal{K}_{ji}} \cdot n_{ij} \varphi_h|_{\mathcal{K}_{ij}} d\mathcal{K}. \tag{3.33}$$



For the numerical flux  $\hat{\mathbf{U}}$  we use the Bassi-Rebay form, as shown in Ref. [195] and Ref. [175], which gives

$$\int_{\mathcal{K}_{ij}} \hat{\mathbf{U}}_{BR}(\mathbf{U}_h, \boldsymbol{\vartheta}_h) d\mathcal{K} = \frac{1}{2} \int_{\mathcal{K}_{ij}} ((\mathbf{U}_h)|_{\mathcal{K}_{ij}} + (\mathbf{U}_h)|_{\mathcal{K}_{ji}}) \cdot n_{ij} \boldsymbol{\vartheta}_h|_{\mathcal{K}_{ij}} d\mathcal{K},$$

so that over elements we find

$$\mathcal{U}_{BR}(\mathbf{U}_h, \boldsymbol{\vartheta}_h) = \frac{1}{2} \sum_{\mathcal{G}_i \in \mathcal{T}_h} \sum_{j \in S(i)} \int_{\mathcal{K}_{ij}} ((\mathbf{U}_h)|_{\mathcal{K}_{ij}} + (\mathbf{U}_h)|_{\mathcal{K}_{ji}}) \cdot n_{ij} \boldsymbol{\vartheta}_h|_{\mathcal{K}_{ij}} d\mathcal{K}. \quad (3.34)$$

Now we discretize in time, denoting a partition of  $[0, T]$  by

$$0 = t^0 < t^1 \dots < t^T = T,$$

for a timestep given as  $\Delta t^n = t^{n+1} - t^n$ , and implement the forward Euler scheme:

$$\frac{\partial \mathbf{U}_h}{\partial t} \approx \frac{\mathbf{U}_h^{n+1} - \mathbf{U}_h^n}{\Delta t^n},$$

along with a slope limiting scheme in the conservation variables  $(\rho, \rho u)$ , where van Leer's MUSCL scheme (as shown in Ref. [196] and Ref. [197]) has been adopted.

Now we solve explicitly for (3.19). In particular, we show an explicit scheme using the Riemann flux, which is formulated to read: for every  $n \geq 0$  find  $\mathbf{U}_h^{n+1}$  such that

$$\begin{aligned} 1) \quad & \mathbf{U}_h^n \in S_h^d, \quad \boldsymbol{\Sigma}_h^n \in S_h^d, \\ 2) \quad & \left( \frac{\mathbf{U}_h^{n+1} - \mathbf{U}_h^n}{\Delta t^n}, \boldsymbol{\varphi}_h \right)_{\Omega_{\mathcal{G}}} + \tilde{\Phi}_R(\mathbf{U}_h^n, \boldsymbol{\varphi}_h) - \Theta(\mathbf{U}_h^n, \boldsymbol{\varphi}_h) \\ & - \mathcal{G}_b(\boldsymbol{\Sigma}_h^n, \mathbf{U}_h^n, \boldsymbol{\varphi}_h) + \mathcal{N}(\boldsymbol{\Sigma}_h^n, \mathbf{U}_h^n, \boldsymbol{\varphi}_h) = 0, \quad (3.35) \\ 3) \quad & \mathcal{Q}(\hat{\mathbf{U}}_{RB}, \boldsymbol{\Sigma}_h^n, \mathbf{U}_h^n, \boldsymbol{\vartheta}_h, \boldsymbol{\vartheta}_x^h) = 0, \\ 4) \quad & \mathbf{U}_0^h = \mathbf{U}_h(0). \end{aligned}$$

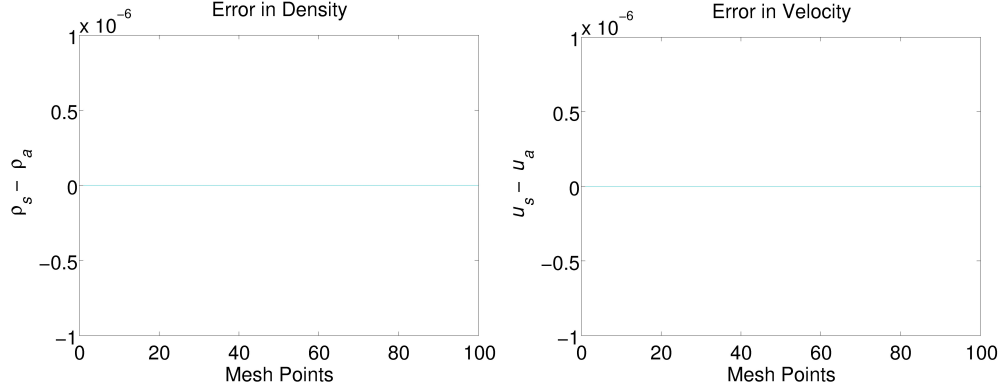


Figure 3.2: A plot of the solutions  $\rho_s = \rho_{RvL} - \rho_{ILFO}$  and  $u_s = u_{RvL} - \rho_{ILFO}$  minus the analytic steady state solutions  $\rho_a = 1$  and  $u_a = 1$ .

We inspect the first of two numerical test cases. First consider the monofluid steady state case of (3.1)-(3.3), by setting the initial data to  $\rho_0 = \mu_{1,0}^{-1} = u_0 = \gamma_i = 1$  and  $\mu_{2,0} = 0$ . Clearly here the pressure reduces to unity  $p_0 = 1$  and the viscosity to a constant  $\nu_0 = C_0$ . Next we set the periodic boundary condition

$$\mathbf{U}^n(a, t) = \mathbf{U}^n(b, t).$$

The exact solution shows constant solutions in the primitive variables.

Figure (3.2) shows an implementation of 3.35 to this system, comparing the solutions using the approximate Riemann Flux with the van Leer MUSCL scheme (denoted by  $\mathbf{U}_{RvL}$ ) versus the local Lax-Friedrich's flux with the Osher MUSCL scheme (denoted  $\mathbf{U}_{ILFO}$ ). It is evident that the scheme yields the expected behavior, showing no fluctuation about the steady state in all four of the primitive variables  $\rho, u$  and  $\mu_i$ .

For the second of our test cases, we consider the monofluidic restriction of (3.1)-(3.3) given by taking  $\mu_{1,0} = 1$ ,  $\mu_{2,0} = 0$  and  $\gamma_i = 1$  with the additional

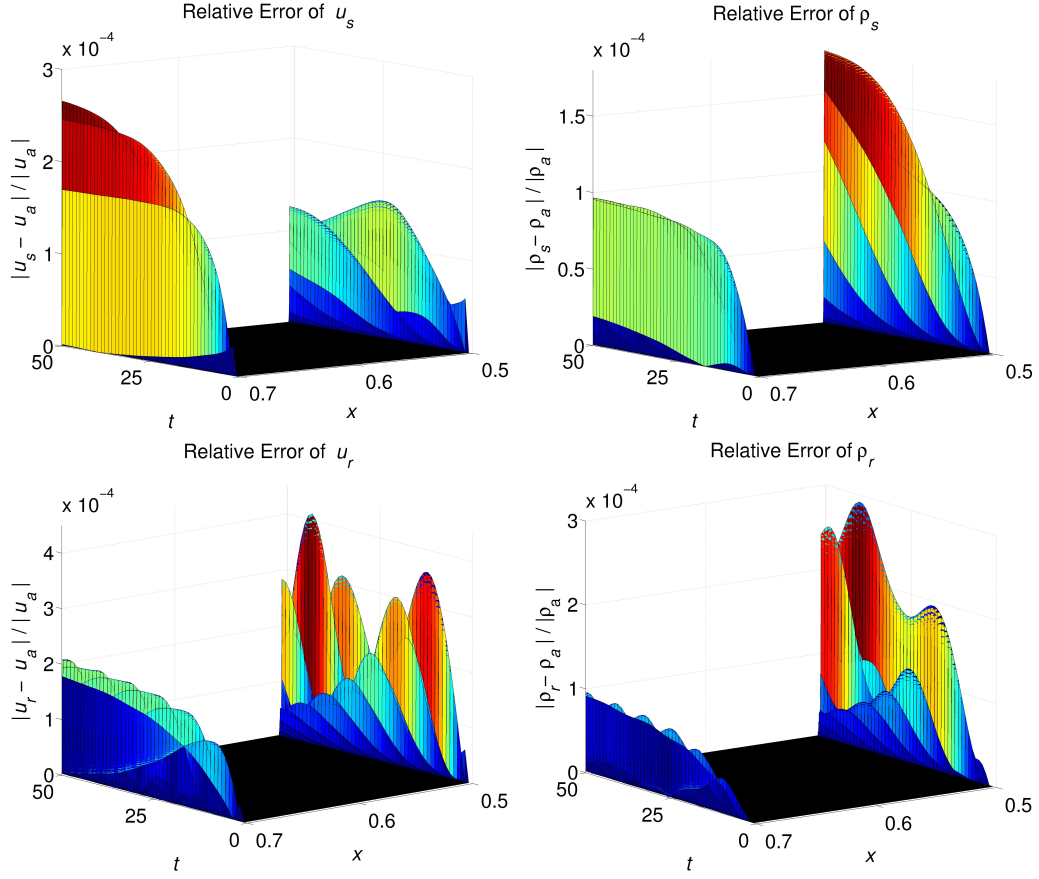


Figure 3.3: The top two graphs show the solution to (3.36) in terms of the local Lax-Friedrich's flux and the van Leer limiter, denoted by  $u_s$  and  $\rho_s$  versus the exact solution  $u_a = \tan x$  and  $\rho_a = (\tan x)^{-1}$ . The bottom two graphs show the solution to (3.36) in terms of the linear Riemann flux and the Osher limiter, denoted  $u_r$  and  $\rho_r$ , again versus the exact solution.

relations:

$$p = \rho = u^{-1}, \quad \text{and} \quad \nu = \rho.$$

Solving this system immediately yields

$$\rho^{-1} + \rho - \rho \partial_x \rho^{-1} = -C,$$

for  $C \in \mathbb{R}$ , which leads to the ordinary differential equation

$$u_x = u^2 + 1 - Cu. \quad (3.36)$$

Setting  $C = 0$  the noting that solution is independent of time, we solve the ODE yielding:  $u = \tan x$ . Setting the initial data to

$$\rho_0 = (\tan x)^{-1}, \quad m_0 = 1, \quad \text{and} \quad (\rho\mu_1)_0 = \rho_0,$$

with the Dirichlet boundary data provided in the weak entropy sense of §3.3 via,

$$\rho_b = 1/u_b, \quad m_b = 1 \quad \text{and} \quad (\rho\mu_1)_b = \rho_b,$$

we inspect the solution over the domain  $[a, b]$ , with  $a = 0.5$  and  $b = 0.7$ . Here we compare the exact solution to the solution obtained using the Lax-Friedrich's flux with the van Leer monotonicity scheme (denoted  $\rho_s$  in 3.3) to the Riemann flux with the Osher scheme (denoted  $\rho_r$  in (3.3)).

From inspection of Figure 3.3, it is clear that the relative error over fifty timesteps is three orders of magnitude smaller than the resolution of the mesh. Here we take  $a = 0.5$  and  $b = 0.7$  where  $h = 2 \times 10^{-4}$ . The relative error is zero across the solution at the first timestep, as expected, and remains nearly constant in the interior of the domain in both cases, while the weak entropy implementation displays fluctuations in time of the order of the interior error. These boundary fluctuations are neither monotonic nor generally increasing, but show complicated temporal perturbations at the weak entropy boundary points and are seen to weakly propagate into the interior as a function of the timestep. Neither of the formulations,  $\mathbf{U}_s$  or  $\mathbf{U}_r$ , show significantly better error behavior, though both are well within working precision of the exact solution given in Theorem 1, up to the weak entropy boundary data.

### 3.5 Example: 2-fluid with chemical inlet

Let us show a simple application of the system outlined in §3.2 and §3.3 evaluated over two distinct species. Consider the bifluid system,

$$\partial_t \rho + \partial_x(\rho u) = 0, \quad (3.37)$$

$$\partial_t(\rho u) + \partial_x(\rho u^2) + \partial_x p - \partial_x(\nu \partial_x u) = 0, \quad (3.38)$$

$$\partial_t(\rho \mu_i) + \partial_x(\rho u \mu_i) = 0, \quad (3.39)$$

with initial conditions:

$$\rho|_{t=0} = \rho_0 > 0, \quad m|_{t=0} = m_0 \quad \text{and} \quad \mu|_{t=0} = \mu_0.$$

The pressure is given by  $p = \rho_1^{\gamma_1} + \rho_2^{\gamma_2}$  and the viscosity by  $\nu = \psi'(\gamma_1 \rho_1^{\gamma_1} + \gamma_2 \rho_2^{\gamma_2})$  for  $\psi' = Cp^{-\alpha}$  and  $\alpha \in (0, 1)$  with  $C > 0$ .

Now as in §3.4 we easily recover the form

$$\mathbf{U}_t + \mathbf{F}\mathbf{U}_x = (\mathcal{K}\mathbf{U}_x)_x, \quad (3.40)$$

which integrates to (3.11). Again we solve for our system in a form equivalent to (3.19). We employ the local Lax-Friedrich's inviscid flux  $\mathbf{\Phi}_{LLF}$ , the Bassi-Rebay numerical flux  $\hat{\mathbf{U}}_{RB}$ , and the usual viscous flux  $\mathcal{G}_b$  such that the formulation of the problem reads: for every  $n \geq 0$  find  $\mathbf{U}_h^{n+1}$  such that

$$\begin{aligned} 1) \quad & \mathbf{U}_h^n \in S_h^d, \quad \mathbf{\Sigma}_h^n \in S_h^d, \\ 2) \quad & \left( \frac{\mathbf{U}_h^{n+1} - \mathbf{U}_h^n}{\Delta t^n}, \boldsymbol{\varphi}_h \right)_{\Omega_{\mathcal{G}}} + \tilde{\mathbf{\Phi}}_{LLF}(\mathbf{U}_h^n, \boldsymbol{\varphi}_h) - \mathbf{\Theta}(\mathbf{U}_h^n, \boldsymbol{\varphi}_h) \\ & - \mathcal{G}_b(\mathbf{\Sigma}_h^n, \mathbf{U}_h^n, \boldsymbol{\varphi}_h) + \mathcal{N}(\mathbf{\Sigma}_h^n, \mathbf{U}_h^n, \boldsymbol{\varphi}_h) = 0, \quad (3.41) \\ 3) \quad & \mathcal{Q}(\hat{\mathbf{U}}_{RB}, \mathbf{\Sigma}_h^n, \mathbf{U}_h^n, \boldsymbol{\vartheta}_h, \boldsymbol{\vartheta}_x^h) = 0, \\ 4) \quad & \mathbf{U}_h(0) = \mathbf{U}_0^h. \end{aligned}$$

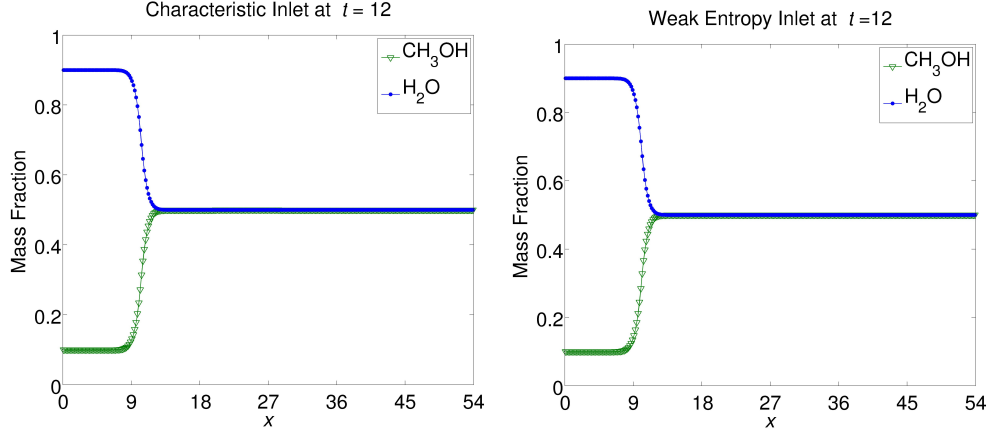


Figure 3.4: The left plot shows miscible species at  $t = 12$  given the “characteristic” chemical inlet conditions from (3.42) with  $\mathcal{C} = 0.9$  and on the boundary  $a = 0$ , with transmissive conditions on  $b = x_{ne}$  (see Figure 3.1). The right plot shows the same solution using the *weak entropy* formulation. Here we have a miscible solution of methanol and water at  $\vartheta = 500\text{K}$  and initial  $\mu_1 = \mu_2 = 0.5$ , while both solutions use  $\tilde{\Phi}_{ILF}$  and the van Leer limiter.

All that remains is determining the boundary states  $\mathbf{U}_{|\partial\Omega}^n$  in the characteristic sense of §3.3. Let us take a subsonic inlet  $u \cdot \mathbf{n} < 0$  on the boundary. Now, suppose we want a chemical inlet such that chemical specie one,  $\mu_1$ , is characterized by an influx condition  $\mu_{1,b} = \mathcal{C}$  on  $\{a\}$  and a transmissive condition on  $\{b\}$ . For  $n = 2$  we can easily write (3.28) and solve for  $\alpha_1$  as in §3.3 which yields that  $\alpha_1 = \rho/2 - t\zeta_1$ . In order to maintain consistency of the equations, we must also enforce both that  $\mu_{2,b} = 1 - \mathcal{C}$  and that  $\rho > 0$ . To meet these conditions requires us to solve for  $\beta_2, \beta_3$  and  $\beta_4$ . A standard calculation using (3.24) yields that for any  $\epsilon > 0$  where  $\xi = \partial_{\rho_1} p - \partial_{\rho_2} p$ , the consistent choice of parameters obeying  $\mu_{1,b} = \mathcal{C}$  is given by:

$$\beta_2 = -\rho/2 - \beta_3 + \epsilon, \quad \beta_3 = \beta_4 \xi \quad \text{and} \quad \beta_4 = \epsilon(\mu_1 - \mathcal{C})/c^2. \quad (3.42)$$

The behavior of such a “chemical inlet” is shown in Figure 3.4. Here it

follows that  $\epsilon$  may be chosen to weight  $\rho_b$ , and can be chosen as any smooth strictly positive function, for example. By comparison the *weak entropy* solutions discussed in §3.3 to (3.37)-(3.39) are also well-posed for an arbitrary collection of  $L^\infty((0, T) \times \partial\Omega)$  boundary data. So, in contrast to using the “characteristic” solutions to find a consistent set of boundary data, we may simply assign  $\mu_{1,b} = \mathcal{C}$ ,  $\mu_{2,b} = 1 - \mathcal{C}$ ,  $\rho_b = \epsilon$  and  $u_b = u_0$  to obtain a similar solution. Comparing the behavior of  $\mu_{1,w}$  in Figure 3.4 to  $\mu_{1,c}$  yields Figures 3.5 and 3.6. Notice that the two boundary solutions do not yield the same numerical result. In particular, the weak entropy  $\mu_1$  grows more rapidly at the boundary; while the dynamically coupled “characteristic” solution adapts to the influx of specie/density by producing a velocity outflow, which effectively

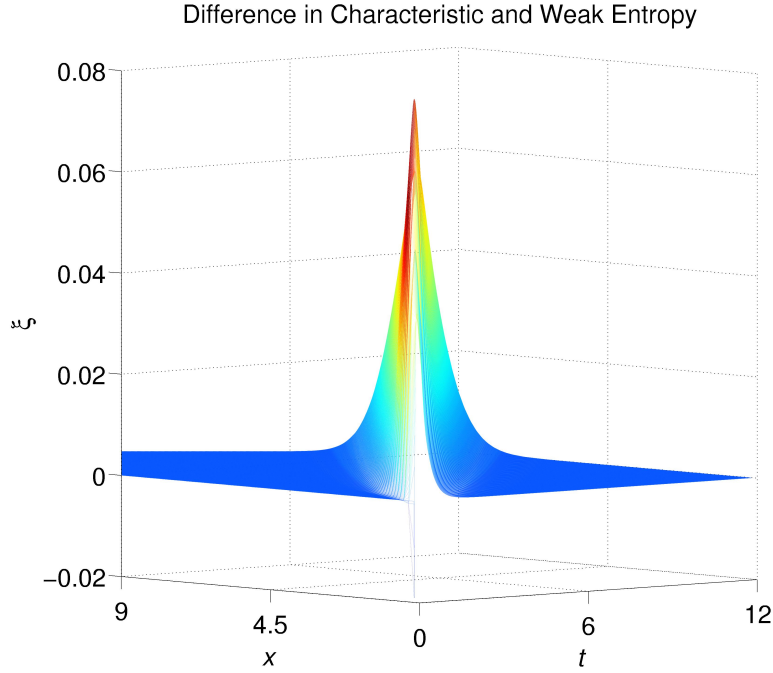


Figure 3.5: Here we show the difference between specie one of the *weak entropy*  $\mu_{1,w}$  versus “characteristic”  $\mu_{1,c}$  solutions, where  $\xi = \mu_{1,w} - \mu_{1,c}$ .

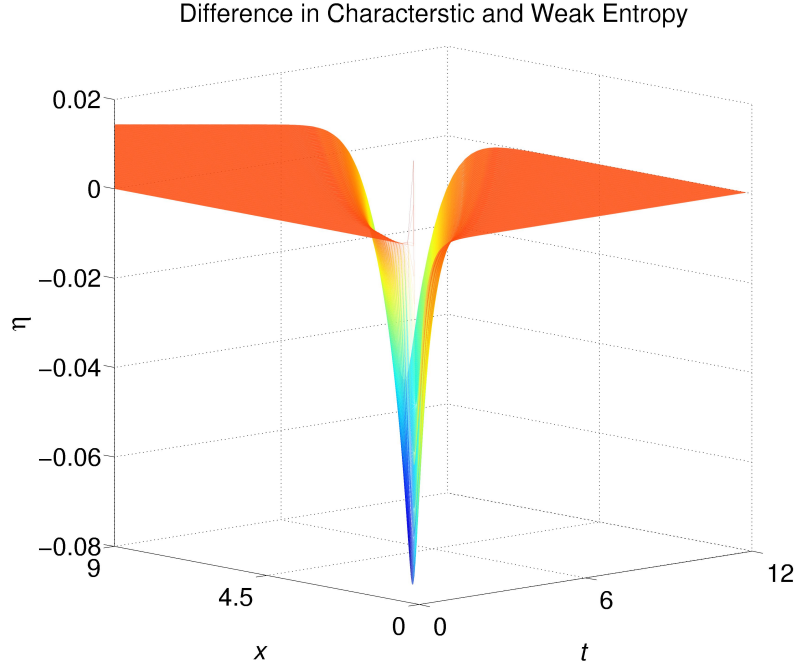


Figure 3.6: Here we have the complementary difference between species two of the *weak entropy*  $\mu_{2,w}$  and “characteristic”  $\mu_{2,c}$  solutions, where  $\eta = \mu_{2,w} - \mu_{2,c}$

reduces the “chemical influx” as a function of time.

In practice it is often physically pertinent to ascribe more boundary data than the free  $\beta$ ’s can consistently control. For example, a closely related case to the above is for a chemical inlet where  $u_b \equiv 0$  represents a fixed semipermeable membrane. In cases such as these, where only one characteristic direction is free, *weak entropy* solutions are essential in order to even characterize such a chemical inlet. Heuristically we say that “characteristic” solutions demonstrate a relatively weaker forcing on  $\partial\Omega$ , while *weak entropy* solutions have greater flexibility of representation by way of establishing stronger forcing on  $\partial\Omega$ .



### 3.6 Example: k-th order in time n-fluid

We wish to generalize the example in §3.5 to  $n$ -fluid components and a  $k$ -th order in time Runge-Kutta time discretization. Let us start with an  $n = 5$  system, which then can be easily generalized. Consider

$$\partial_t \rho + \partial_x(\rho u) = 0, \quad (3.43)$$

$$\partial_t(\rho u) + \partial_x(\rho u^2) + \partial_x p - \partial_x(\nu \partial_x u) = 0, \quad (3.44)$$

$$\partial_t(\rho \mu_i) + \partial_x(\rho u \mu_i) = 0, \quad (3.45)$$

with initial conditions,

$$\rho|_{t=0} = \rho_0 > 0, \quad \rho u|_{t=0} = m_0, \quad \text{and} \quad (\rho \mu_i)|_{t=0} = \rho_{i,0},$$

given the pressure

$$p = \rho_1^{\gamma_1} + \rho_2^{\gamma_2} + \rho_3^{\gamma_3} + \rho_4^{\gamma_4} + \rho_5^{\gamma_5}, \quad (3.46)$$

and viscosity

$$\nu = \psi'(\rho_1 \partial_{\rho_1} p + \rho_2 \partial_{\rho_2} p + \rho_3 \partial_{\rho_3} p + \rho_4 \partial_{\rho_4} p + \rho_5 \partial_{\rho_5} p). \quad (3.47)$$

We explicitly take the three vectors:

$$\mathbf{U} = (\rho, \rho u, \rho_1, \rho_2, \rho_3, \rho_4, \rho_5)^T,$$

$$\mathbf{f}(\mathbf{U}) = (\rho u, \rho u^2 + p, \rho_1 u, \rho_2 u, \rho_3 u, \rho_4 u, \rho_5 u)^T,$$

$$\mathbf{g}(\mathbf{U}, \mathbf{U}_x) = (0, \nu u_x, 0, 0, 0, 0, 0)^T,$$

such that again we arrive with

$$\mathbf{U}_t + \mathbf{\Gamma} \mathbf{U}_x - (\mathcal{K} \mathbf{U}_x)_x = 0, \quad (3.48)$$

which is easily posed in the form of (3.19).

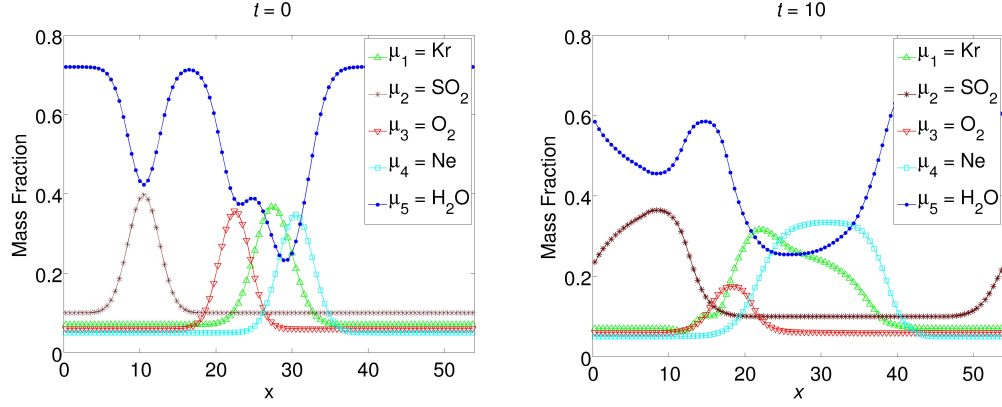


Figure 3.7: Here we show the first and last timesteps of the mass fractions at  $\vartheta = 293\text{K}$  using periodic boundary conditions with Runge-Kutta order  $k = 2$ . Initial conditions set  $\rho = 5 + 20e^{-(x-10)^2/8} + 20e^{-(x-30)^2/8}$  and  $u = \sin(6\pi x/x_{ne})$ , with  $\mu_1 = 0.07 + 0.3e^{-(x-27.5)^2/12}$ ,  $\mu_2 = 0.1 + 0.3e^{-(x-10.5)^2/8}$ ,  $\mu_3 = 0.06 + 0.3e^{-(x-22.5)^2/8}$ ,  $\mu_4 = 0.05 + 0.3e^{-(x-30.5)^2/10}$  and solvent  $\mu_5 = 1 - \sum_{n=1}^4 \mu_i$ .

Again we employ the local Lax-Friedrich's flux (3.31) and the Bassi-Rebay numerical flux (3.34), but now we generalize to a Runge-Kutta time discretization. That is, notice that we can rewrite (3.19) as a system of ordinary differential equations,

$$\frac{d}{dt}\mathbf{U}_h = L_h(\mathbf{U}_h).$$

We solve this system using an explicit Runge-Kutta method (for example, see Ref. [162] and Ref. [198]). That is, set the value of the current timestep to  $\mathbf{U}_h^0$ , and decompose this timestep into  $k$  substeps such that for  $i = 1, \dots, k$  we have the intermediate solutions

$$\mathbf{U}_h^i = \sum_{l=0}^{i-1} c_{il} \mathbf{U}_h^l + d_{il} \Delta t^n L_h(\mathbf{U}_h^l),$$

where the  $c$ 's and  $d$ 's are given in Table 3.2. Then setting  $\mathbf{U}_h^{n+1} = \mathbf{U}_h^k$  for each

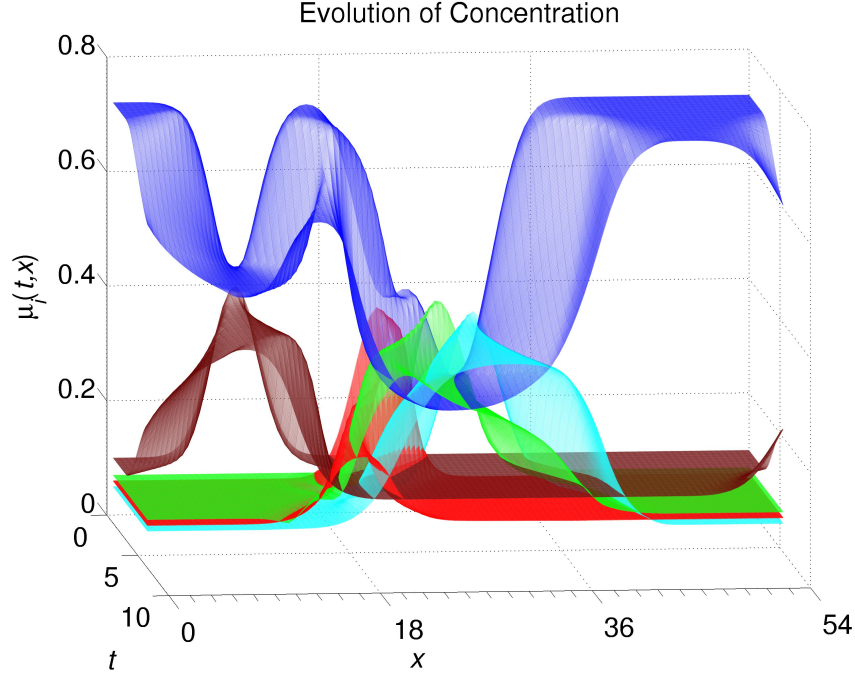


Figure 3.8: Here we show the time evolution over the entire solution space of the same problem from Figure 3.7.

$n \geq 0$  we arrive with:

$$\begin{aligned}
 & 1) \mathbf{U}_h^n \in S_h^d, \quad \Sigma_h^n \in S_h^d, \\
 & 2) (\mathbf{U}_h^i, \varphi_h)_{\Omega_g} - \sum_{l=0}^{i-1} \left\{ (c_{il} \mathbf{U}_h^l, \varphi_h)_{\Omega_g} + d_{il} \Delta t^n \left[ \tilde{\Phi}_{ILF}(\mathbf{U}_h^l, \varphi_h) - \Theta(\mathbf{U}_h^l, \varphi_h) \right. \right. \\
 & \quad \left. \left. - \mathcal{G}_b(\Sigma_h^l, \mathbf{U}_h^l, \varphi_h) + \mathcal{N}(\Sigma_h^l, \mathbf{U}_h^l, \varphi_h) \right] \right\} = 0, \quad \text{for } i = 1, \dots, k, \\
 & 3) \mathcal{Q}(\hat{\mathbf{U}}_{RB}, \Sigma_h^l, \mathbf{U}_h^l, \vartheta_h, \vartheta_x^h) = 0, \quad \text{for } i = 0, \dots, k-1, \\
 & 4) \mathbf{U}_h(0) = \mathbf{U}_0^h.
 \end{aligned} \tag{3.49}$$

This method follows for any  $n$ -fluid of the form (3.1)-(3.5) of Runge-Kutta order  $k$ .

Table 3.2: *Runge-Kutta k-th order in time*

Parameter	k=2	k=3
$c_{il}$	$\begin{pmatrix} 1 & 0 \\ 1/2 & 1/2 \end{pmatrix}$	$\begin{pmatrix} 1 & 0 & 0 \\ 3/4 & 1/4 & 0 \\ 1/3 & 0 & 2/3 \end{pmatrix}$
$d_{il}$	$\begin{pmatrix} 1 & 0 \\ 0 & 1/2 \end{pmatrix}$	$\begin{pmatrix} 1 & 0 & 0 \\ 0 & 1/4 & 0 \\ 0 & 0 & 2/3 \end{pmatrix}$

The behavior of this system is shown in Figure 3.7, where we have set the simple periodic boundary condition,

$$\mathbf{U}^n(a, t) = \mathbf{U}^n(b, t).$$

It is worth noting that the composition of this mixture does not tend towards homogeneous equilibrium, since there is both no inter-specie diffusion (see §3.8) and the species are not “chemically miscible” (in that they do not mix in all proportions). Nevertheless there is significant mixing from the state of the initial conditions, and it can be seen that the fluid is *more* homogenized, relatively speaking, at timestep  $t = 10$  that it was in the initial state. Most importantly, this scheme now immediately extends to an arbitrary  $n$ -fluid.

### 3.7 Energy Consistency of Scheme

In Ref. [39] it is shown that any solution for which Theorem 2.1 holds should satisfy two closely related entropy inequalities. The first, a classical integral inequality taking the form

$$\frac{1}{2} \frac{d}{dt} \int_{\mathbb{R}} \{\rho u^2 + 2\mathcal{E}\} dx + \int_{\mathbb{R}} \nu |u_x|^2 dx \leq 0, \quad (3.50)$$

and the second owing to Bresch and Desjardins (see Ref. [18, 37, 61, 126, 127, 135]), as

$$\frac{1}{2} \frac{d}{dt} \int_{\mathbb{R}} \{ \rho |u + \rho^{-1} \psi_x|^2 + 2\mathcal{E} \} dx + \int_{\mathbb{R}} \rho^{-1} \psi' |p_x|^2 dx \leq 0, \quad (3.51)$$

where the internal energy  $\mathcal{E} = \mathcal{E}(\rho_1, \dots, \rho_n)$  is specified as:

$$\mathcal{E} = \sum_{i=1}^n \frac{\rho_i^{\gamma_i}}{\gamma_i - 1}.$$

Entropy consistent numerical schemes are often formulated in the literature in order to explicitly enforce entropy inequalities such as (3.50) and (3.51) over all of  $\mathcal{Q}_T$  (viz. Ref. [173, 199–201]). For example enforcing (3.50) is done by utilizing a change of variables of the conservation variable form of the state vector  $\mathbf{U}$ , into the so-called entropy variable form  $\mathbf{W}$ , which is achieved by writing the entropy functional  $\mathcal{H} = \rho u^2/2 + \mathcal{E}$  and then setting the state vector as the partial with respect to the conservation variables  $\mathbf{W} = \mathcal{H}_{\mathbf{U}}$ . The difficulty of implementation of these energy schemes, which are inherently implicit methods, underscores the importance of conserving energy consistency of the solution, and further serves as motivation for testing how our explicit scheme behaves with respect to (3.50) and (3.51).

Here we inspect the entropy consistency from three perspectives. First, from the point of view of the global strong solution and Ref. [39] we do not necessarily expect local energy consistency with some arbitrary free boundary inlet condition for an arbitrary uniform timestep  $\Delta t$ , as locally this perturbs the magnitude and behavior of the entropy, which is a global property of the strong solution. However, we do expect energy conservation given periodic or transmissive boundary conditions, which are able to recover in some basic sense the global behavior of the solution. From the numerical perspective,

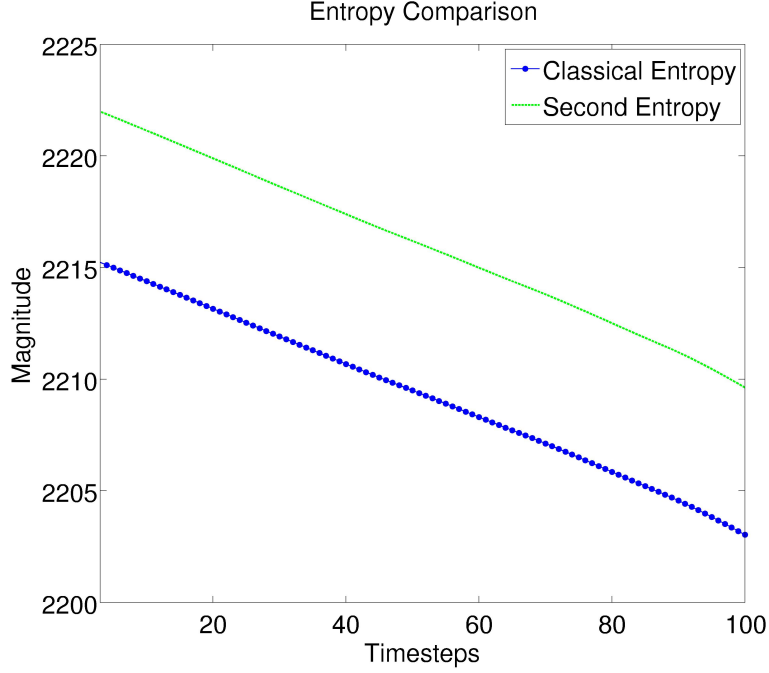


Figure 3.9: Here we plot the integral forms  $\mathcal{S}_T$  and  $\tilde{\mathcal{S}}_T$  for  $C = 1$  and  $\alpha = 0.9$ , where  $\int_{\Omega} \mathcal{H}_0 dx$  and  $\int_{\Omega} \tilde{\mathcal{H}}_0 dx$  are represented by the first timestep. The spatial mesh is chosen with  $ne = 100$  with  $\Delta t = 0.01$ .

we expect our solution (3.19) to obey entropy consistency regardless of the boundary data up to a restriction of the CFL stability condition, which for inviscid flows scale as  $\tilde{C}_1 h / \text{Spec}_r \Gamma \geq \Delta t$  and for the complementary viscous flows like  $\tilde{C}_2 h^2 / \max(\nu, 1) \geq \Delta t$ , where the CFL constants are characterized by  $\tilde{C}_1, \tilde{C}_2 \in (0, 1)$ . Finally, from the purely phenomenological perspective we expect the entropy to be satisfied in both the sense of the solution of Ref. [39] as well as the  $\Delta t$  restriction provided by the CFL scaling, but to in addition demonstrate behavior which is phenomenologically consistent with the modeling regime (ie. the  $C$  in  $\nu(t, x)$  should be chosen to reflect the physical viscosities of mixtures on time scales that are numerically tractable).

Here we use the  $n = 5$  fluid scheme from §3.5 (shown in Figure 3.7) as a test case for these issues where again the periodic boundary conditions are employed.

For our numerical scheme (3.19) the two inequalities (3.50) and (3.51) are adapted in the following way. The prescribed initial conditions are evaluated as  $\mathcal{H}_0$  and  $\tilde{\mathcal{H}}_0 = \frac{1}{2}\rho_0|u_0 + \rho_0^{-1}\partial_x\psi_0|^2 + \mathcal{E}_0$ , such that we evaluate the spacetime integrated functionals:

$$\mathcal{S}_T = \int_{\Omega} \mathcal{H}_T dx + \int_0^T \int_{\Omega} \nu |u_x|^2 dx dt \leq \int_{\Omega} \mathcal{H}_0 dx, \quad (3.52)$$

and

$$\tilde{\mathcal{S}}_T = \int_{\Omega} \tilde{\mathcal{H}}_T dx + \int_0^T \int_{\Omega} \rho^{-1} \psi' |p_x|^2 dx dt \leq \int_{\Omega} \tilde{\mathcal{H}}_0 dx. \quad (3.53)$$

We show the results of this calculation for an arbitrarily chosen set of parameters in Figure 3.9. As is clear from the graph, both (3.52) and (3.53) are satisfied. In fact we confirm that (3.19) satisfies (3.52) and (3.53) whenever the viscous CFL condition is satisfied, up to the choice of a constant. It is interesting to note that both of these inequalities are satisfied for an arbitrary choice of  $\alpha$  and  $C$  in the numerical setting. This confirms that the mathematical result from Ref. [39] is substantially more restrictive than the numerical one, where in Ref. [39] the choice of  $\alpha$  is bounded above and below by the limits of the adiabatic constants  $\gamma_i$ , such that given  $\check{\gamma} < \gamma_i < \hat{\gamma}$  for all  $i$ , it was shown that

$$\begin{aligned} \check{\gamma}^{-1}(\hat{\gamma} - 1/2) &< \underline{\alpha} \leq \hat{\gamma}^{-1}(\check{\gamma} + 1/2) \\ \hat{\gamma}^{-1}(\check{\gamma} - 1/2) &> \bar{\alpha} \geq \check{\gamma}^{-1}(\hat{\gamma} + 1/2) - 1. \end{aligned} \quad (3.54)$$

It is further worth mentioning that the behavior of the entropy is phenomenologically consistent with the behavior of the fluid mixtures. That is, we may estimate the magnitude of  $C$  in  $\nu$  by a weighted average  $C \approx \sum_i^n \mu_i \eta_i$

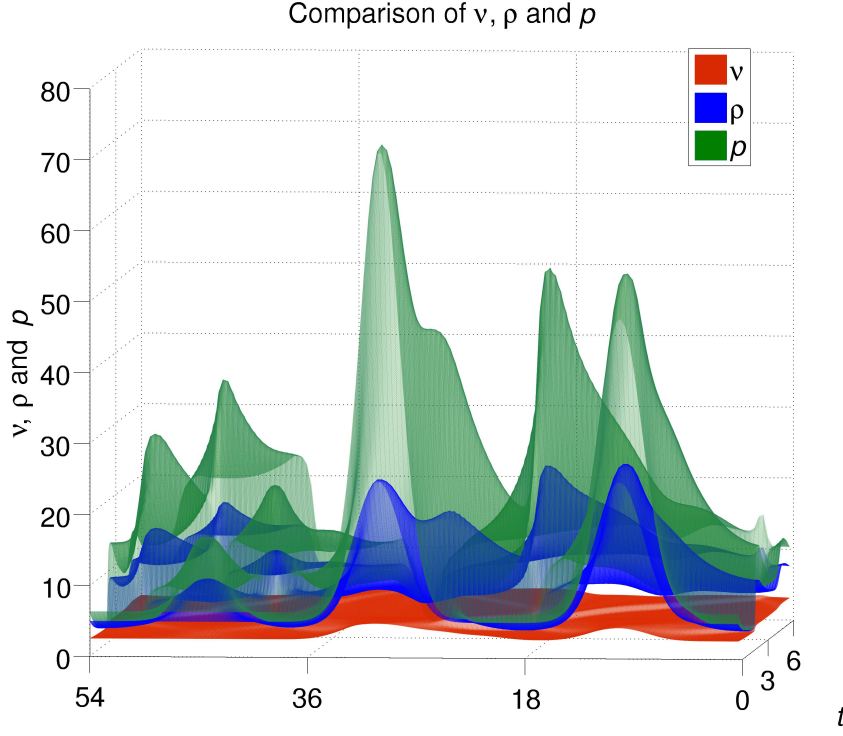


Figure 3.10: Here we compare the viscosity  $\nu$ , density  $\rho$  and pressure  $p$  of the periodic 5-fluid from §3.6 with  $\alpha = 0.9$ ,  $C = 0.5$ , 150 meshpoints and  $\Delta t = .006$ .

with  $\eta_i$  each of the components respective constant viscosity coefficient as approximated at constant temperature  $\vartheta$ . In SI units ( $\text{Pa} \cdot \text{s}$ ) this leads to extremely tractable CFL conditions for most liquid and gas mixtures (certainly all aqueous ones). However using  $C \approx \sum_i^n \mu_i \eta_i$  is unnecessary, and certainly not always well justified (e.g. supercritical solutions as in Ref. [202, 203], or more general formulations found in Ref. [30]), in which case the  $C$  coefficient may be appropriately, and relatively easily, rescaled.

The functional behavior of the viscosity is a relatively unique property of our system (3.1)-(3.3), which is to say that commonly compressible Navier-



Stokes systems utilize constant viscosity coefficients (eg. see Ref. [105] chapter 4) and thus the energy consistency and the CFL condition is not dynamically coupled to the solution components. However, for our system, since the viscosity is a function of time, the CFL condition must update to reflect the local viscosity magnitude at each timestep. We show this functional relationship in Figure 3.10, where a comparison plot between the visocosity  $\nu$ , the density  $\rho$  and the pressure  $p$  of the system is given.

### 3.8 Fick's Diffusion with Acoustic BCs

Although Theorem 2.1 only applies to systems of the form (3.1)-(3.3), the particular numerical scheme outlined in §3.2 can be easily extended to more complicated systems; and indeed can be extended with similar numerical behaviors. As an example let us consider the 5-fluid,

$$\partial_t \rho + \partial_x(\rho u) = 0, \quad (3.55)$$

$$\partial_t(\rho u) + \partial_x(\rho u^2) + \partial_x p - \partial_x(\nu \partial_x u) = 0, \quad (3.56)$$

$$\partial_t(\rho \mu_i) + \partial_x(\rho u \mu_i) - \partial_x(\mathcal{D}_i \partial_x \mu_i) = 0, \quad (3.57)$$

with initial conditions:

$$\rho|_{t=0} = \rho_0 > 0, \quad \rho u|_{t=0} = m_0, \quad \text{and} \quad (\rho \mu_i)|_{t=0} = \rho_{i,0},$$

given (3.46), (3.47) and  $\mathcal{D}_i$  the diffusivity constants of each respective species. Here the system is equivalent to that in §3.6, except we have added the Fick's diffusion law term to the advection equation in  $\mu$ . Thus the state vector and inviscid flux remain unchanged, while the vector  $\mathbf{g}$  becomes

$$\mathbf{g}(\mathbf{U}, \mathbf{U}_x) = (0, \nu u_x, \mathcal{D}_1 \mu_x, \dots, \mathcal{D}_n \mu_n)^T, \quad (3.58)$$

such that the corresponding visous flux matrix yields:

$$\mathcal{K}(\mathbf{U}) = \frac{1}{\rho} \begin{pmatrix} 0 & 0 & 0 & \dots & \dots & 0 \\ -\nu u & \nu & 0 & \dots & \dots & 0 \\ -\mathcal{D}_1 \mu_1 & 0 & \mathcal{D}_1 & 0 & \dots & 0 \\ -\mathcal{D}_2 \mu_2 & \vdots & 0 & \mathcal{D}_2 & \ddots & \vdots \\ \vdots & \vdots & \vdots & \ddots & \ddots & 0 \\ -\mathcal{D}_n \mu_n & 0 & 0 & \dots & 0 & \mathcal{D}_n \end{pmatrix}. \quad (3.59)$$

We set an acoustic inlet condition, which is equivalent to identifying the sound pressure on  $\partial\Omega$ . We set corresponding weak entropy conditions on  $\partial\Omega$ . That is, consider a classical solution to the acoustic wave equation at a boundary located at the origin such that the total pressure on the boundary satisfies  $p_b = p_0 + A_0 \sin(\omega t)$  for a driving amplitude  $A_0$  and an ambient reference pressure  $p_0 = \sum_i^n (\rho_0 \mu_{i,0})^{\gamma_i}$ , where  $\omega$  is the angular frequency of the acoustic wave; or, similarly we may consider the total solution from the point of a view of a solution to the Helmholtz equation at any  $x$  in  $\Omega$  corresponding to a fixed radiating acoustic source. Since in the barotropic case the total pressure satisfies  $p_b = \sum_i^n \rho_i^{\gamma_i}$ , we use the MATLAB® (2008a, The Math-Works, Natick, MA., USA) `fzero/fsolve` function to solve for roots in  $\rho_b$  of the following equation:

$$f(\rho_b) = \sum_i^n (\rho_b \mu_{i,b})^{\gamma_i} - (p_0 + A_0 \sin(\omega t)). \quad (3.60)$$

For the *weak entropy* solutions, to restrict to the pressure front inlet, we set the initial wall boundary condition  $u_0 \cdot \mathbf{n} = 0$ , where in addition the  $\mu_i$ 's are simply chosen from their initial concentrations on  $\partial\Omega$ . We allow antisymmetric inlets on  $\partial\Omega = \{a, b\}$  leading to the formation of supernodes within the fluid domain. The solution is plotted in Figure 3.11.

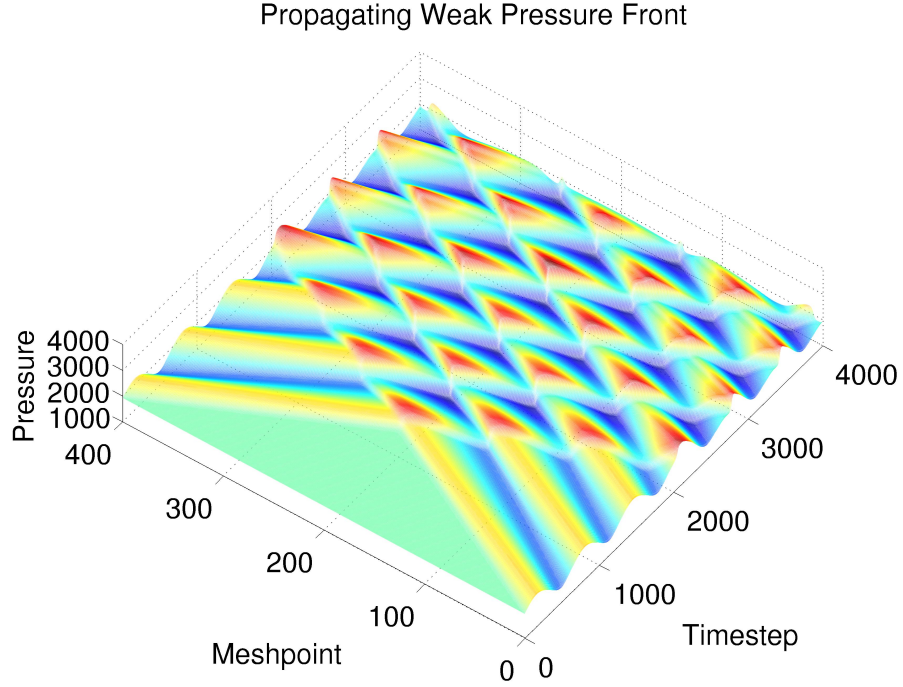


Figure 3.11: A *weak entropy* solution to an oscillating pressure front propagating through a 5-component low density ( $\sim 100$  molecules per cm) gas at  $\vartheta = 20\text{K}$ . The chemical constituents are comprised of species found in dark interstellar molecular clouds, where representative fractional abundances are adopted and the solution space is appropriately scaled; with corresponding initial conditions:  $\text{H}_2 \sim 80\%$ ,  $\text{He} \sim 19.9\%$ , and trace  $\text{CO}$ ,  $\text{H}$  (atomic hydrogen), and  $\text{HC}_3\text{N}$  (cyanoacetylene).

By comparison we solve the “characteristic” boundary solution presented in §3.3. In order to solve this system we must dynamically switch between the five regimes listed in Table 3.1, since the pressure oscillation pulls the velocity between transonic inlet and outlet conditions. That is, the values of the conservation variables on the boundary must satisfy a system of linear equations. The nature of this system depends on the number of free and fixed conservation variables in the particular type of characteristic boundary

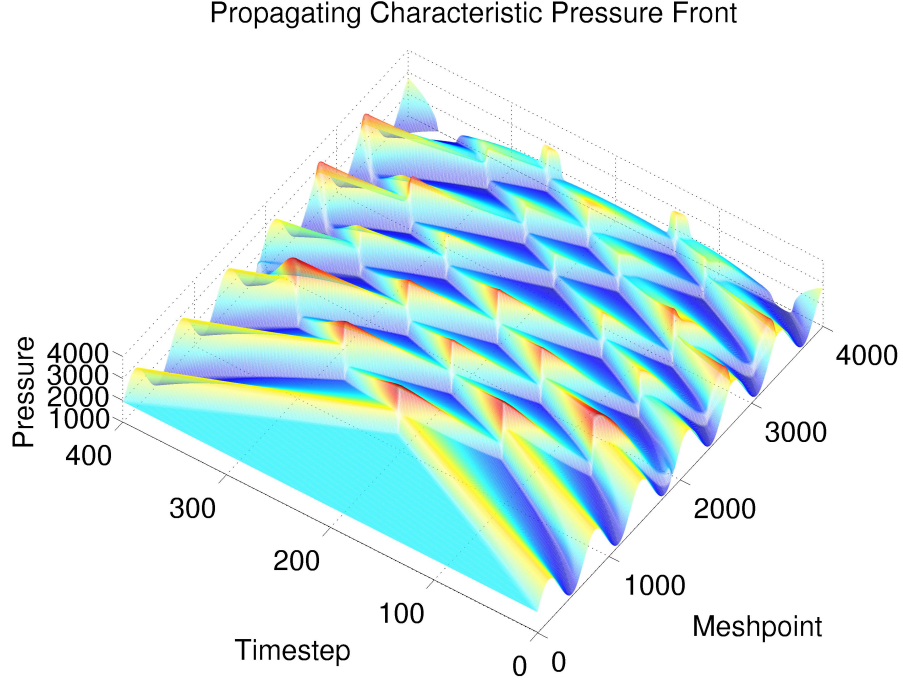


Figure 3.12: A “characteristic” solution to the same oscillating pressure front presented in 3.11.

condition as detailed in Table 3.1. There are four basic types of calculations corresponding to 0, 1,  $m - 1$  and  $m$  fixed  $\alpha_i$ . We take a single row from the augmented matrix  $[\mathbf{V}^{-1} \mid \boldsymbol{\alpha} + \Delta t^n \boldsymbol{\zeta}]$  for each  $\alpha_i$  appearing in Table 3.1, while those corresponding to each  $\beta_i$  are replaced by a single row from  $[\mathbb{I}_m \mid \mathbf{U}_b]$  containing the type of prescribed data on the boundary, where  $\mathbf{U}_b$  is formed from the appropriate number of prescribed primitive variables. Further notice that (3.25) no longer makes sense, but is replaced by the vector  $\boldsymbol{\zeta}$  with respect to (3.58)-(3.59):

$$\boldsymbol{\zeta} = \mathbf{V}^{-1} \mathbf{g} \quad \text{on} \quad \partial\Omega. \quad (3.61)$$

For example, in the case of the subsonic acoustic outlet the second row would

be replaced by  $[1\ 0\ \cdots\ 0\ |\ \rho_b]$ , consequently ensuring that any solution is assigned that particular density, whereas in the case of a chemical inlet we might use  $[0\ 0\ 1\ 0\ \cdots\ 0\ |\ \mu_{1,b}]$  instead to prescribe the mass fraction of the first fluid. Further note that since allowing complete freedom with respect to fluid proportions can lead to a violation of  $\sum_{i=1}^n \mu_i = 1$ , one of the rows corresponding to  $\rho\mu_i$  is replaced by  $[1\ 0\ -1\ \cdots\ -1\ |\ 0]$  which serves to enforce that requirement.

The solution to the resulting combined system of  $m$  equations then provides the values of the conservation variables consistent with both the choices on the boundary as well as the propagated values from the interior; from the one extreme of a supersonic inlet where the boundary values can be chosen subject only to the physical consistency conditions  $\sum_{i=1}^n \mu_i = 1$  and  $\rho > 0$ , through the two mixed subsonic cases, to the other extreme of a supersonic outlet where all the values are propagated from the interior. As the velocity and the speed of sound near the boundary changes with time, the type of linear system that needs to be solved changes as one switches between the different regimes of inlet and outlet.

It can be confirmed by inspection of Figure 3.12 and 3.13 that the “characteristic” solution initially demonstrates significantly sharper profiles that decay more quickly in time than the analogous profiles in the *weak entropy* solution. By contrast, the difference between the “characteristic” and *weak entropy* solutions for the chemical inlet shown in §3.5 are extremely small, and qualitatively indistinguishable. However, in the present case, with pressures and velocities fluctuating rapidly and doing so with large relative magnitudes, the difference between the two regimes is relatively extreme. From Figure 3.13 we can further see that the “characteristic” solution has steeper nodal peaks with greater amplitudes than the *weak entropy* solution. It is not clear *a priori*

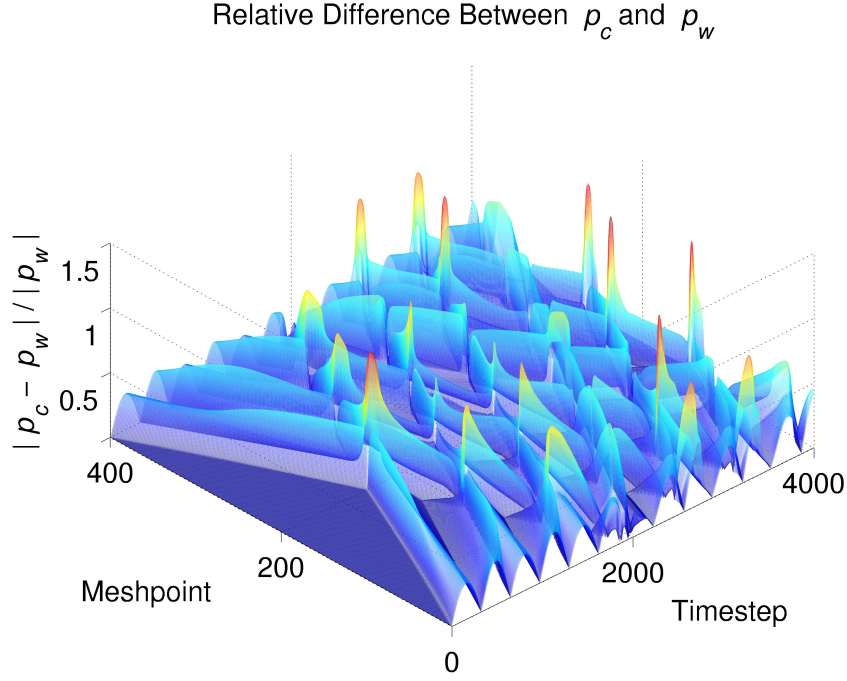


Figure 3.13: Here we plot the relative difference between the *weak entropy* pressure  $p_w$  and the “characteristic” pressure  $p_c$ .

which solution is more phenomenologically sound.

Here we have solved (3.55)-(3.57) using a formulation which is meant to weakly mimic some of the conditions found in interstellar media. The solution is shown in Figure 3.11, where it is notable that the traveling sound field  $p_b$  dynamically responds to the changing speed of sound  $c$  throughout the medium – which scales like the root of the local change in pressure up to the local species concentration. The initial conditions were estimated using Ref. [204], the diffusivities were estimated with the help of Ref. [205–207], and motivation for propagating pressure waves can be found in Ref. [208].

# Chapter 4

## Quantum Hydrodynamics with Chemical Applications

### 4.1 Introduction

Quantum hydrodynamics (QHD) has engendered substantial activity in the field of theoretical chemical dynamics, where one may refer to Wyatt et al. [20] for a comprehensive introductory overview of the numerous recent results emerging from this blossoming field.

The basic idea emerging from quantum chemistry in the context of QHD is to employ the time-dependent Schrödinger equation (TDSE) to solve for the dynamical properties (probability densities, “particle” velocities, etc.) of chemical systems. In the same spirit in which the de Broglie-Bohm interpretation (see Ref. [40, 41, 209]) of quantum mechanics may be used to recover “trajectories” of individual fluid elements along the characteristics of motion of the solution, the QHD equations of Madelung and Bohm are derived as formally equivalent to the TDSE and thus comprise an alternative route to solutions which generate quantum trajectories that follow particles along their respective paths (see Ref. [20] and Ref. [42] for a comprehensive overview).

These solutions hold particular significance, where, in the context of the QHD formulation, it is possible to resolve the chemical dynamics of a vast number of reaction mechanisms known to have pathways dominated by quantum tunneling regimes. Some of these systems include proton transfer

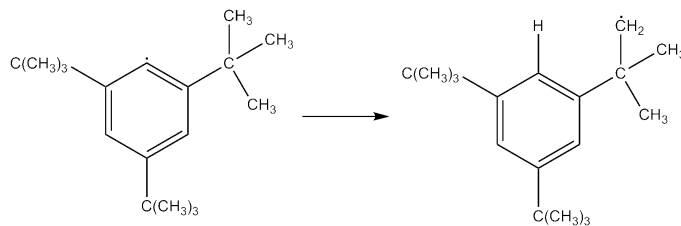


Figure 4.1: Here we have the intramolecular rearrangement of the aryl radical 2,4,6-tri-*tert*-butylphenyl to 3,5-di-*tert*-butylneophyl (see Ref. [210] for details).

reactions (for example see figure 4.1), conformational inversions, biologically important redox reactions in enzymatic catalysis reactions (see figure 4.2), and proton-coupled electron transfer reactions (refer to Ref. [211] and Ref. [212]). It is not yet clear if these types of methods may also have application at higher energies, for example in the halo nuclei tunneling occurring in fusion reactions (as seen, for example, in Ref. [213]).

Substantial research has been done in quantum hydrodynamics to find the best and fastest computational methodology for solving this system of equations. In the standard methodology presented using the quantum trajectory method (QTM), for example, solutions to the QHD equations are found by transforming the system of equations, which is generally posited in the Eulerian fixed coordinate framework (see Ref. [42, 214–216]), into the same set of equations in the Lagrangian coordinate framework, which effectively follows solutions along particle trajectories; or along so-called “Bohmian trajectories.” The transformation from the Eulerian to the Lagrangian frame leads to a set of coupled equations which solve for two unknowns: the *quantum action*  $S(t, \vec{r})$  and the probability density or *quantum amplitude*  $\sqrt{\varrho(t, \vec{r})} = R(t, \vec{r})$  along the trajectories  $\vec{r}(t, \boldsymbol{x})$  (e.g. see Ref. [20] box 1.2). The obvious advantage of the Lagrangian framework is reduced computational times, since solutions are only



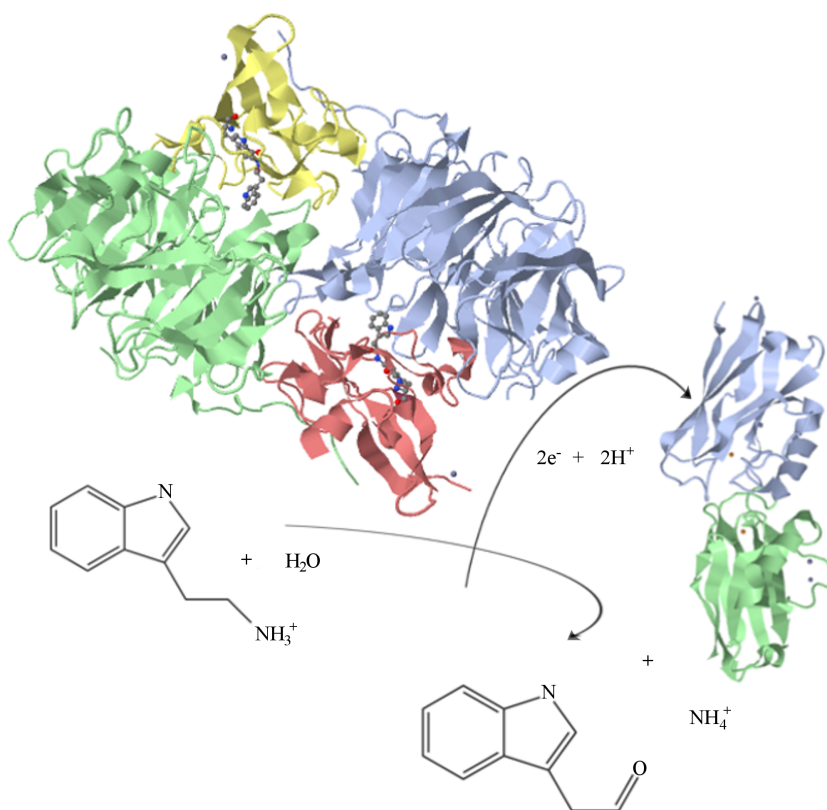


Figure 4.2: Here we show an enzymatic catalysis – an aromatic amine dehydrogenase (AADH) with a tryptophan tryptophyl quinone (TTQ) prosthetic group catalyzing the oxidative deamination of tryptamine with an electron transfer to an arsenate reductase enzyme (see Ref. [210] and Ref. [212] for details, PDB codes: 1nwp (azurin), 2agy (AADH)).

computed along a set of chosen trajectories; while clearly the disadvantage is the possibility of obscuring structure hidden within the continuum of the full solution, which may only emerge properly in convergent numerical schemes, and also the increased complications of transposing into more complicated settings: such as with functional or time dependencies on the potential term  $V$ , or including dissipative or rotational vector fields.

In addition, the numerical solutions to the above mentioned Lagrangian formulations have demonstrated characteristic behaviors which introduce certain technical difficulties at the level of formal analysis. First, the system of equations are *stiff*, which is to say, solutions to the system may locally or globally vary rapidly enough to become numerical unstable without reducing numerically to extremely small timesteps. Furthermore, there exists the so-called “node problem,” which is characterized by singularity formation (see Ref. [20] for characterization of node types) along particle trajectories. Another issue which arises is obtaining unique solutions, since there is not a unique choice of trajectories in the Lagrangian formulation (see for example §4.6 and appendix A). And finally, boundary data is often treated without regard to the (often substantial) numerical residuals introduced in the weak entropy case, or taking into account consistency between the TDSE and the QHD system of equations (see for example Ref. [174] and §4.3).

We introduce an alternative formulation to the standard solutions described above in  $\varrho$  and  $S$  and tracked with respect to the Lagrangian coordinate frame which is motivated by work of Gardner, Cockburn, et al. (see Ref. [215, 217, 218]). Instead, we keep the system in its conservation form (instead of in a primitive variable form) in the Eulerian coordinate system (see Ref. [214]), and solve for the density  $\varrho = \varrho(t, \mathbf{x})$  and the particle *velocity*  $\mathbf{v} = \mathbf{v}(t, \mathbf{x})$  (instead of the *quantum action*  $S$ ). We show that these solutions may be used to easily recover the variables  $S$  and  $\psi$  in a single step; and may with little difficulty be transformed into their Lagrangian coordinate frame counterpart solutions  $\varrho(t, \vec{r}), \mathbf{v}(t, \vec{r}), S(t, \vec{r})$  and  $\psi(t, \vec{r})$ , using the conservation equation (continuity equation), or by solving for pathlines in the sense of classical mechanics, or by any number of alternative so-called “offset methods.”

Additionally, our solutions demonstrate a type of resolution invariance, which is to say that the behavior of our solutions are qualitatively equivalent at varying spatial resolutions, and compare favorably with solutions to the formally equivalent TDSE. As a consequence, our conservation-based formulation is computationally competitive with Lagrangian formulations, up to a type of “formal accuracy” in the trajectory solutions.

Our solutions, as the Lagrangian formulated solutions mentioned above, still demonstrate a *stiff* behavior. However, also as the Lagrangian solutions above, and similarly to the classical CFL condition in fluid mechanics, we consider this a prohibitive but not insurmountable computational difficulty. On the other hand, our solutions to the conservation form of QHD do not demonstrate the node problem (at least on Gaussian wavepackets) as expected, as the only type of node our formulation exhibits is for  $\varrho \equiv 0$ , which never occurs if we add a numerical ambient density  $\varrho_A$  to the initial density  $\rho|_{t=0}$ . The solution is stable when the ambient density is set to  $\sim 11$  orders of magnitude smaller than  $\max_{\Omega}(\varrho)$  over a computational domain  $\Omega$ . We maintain that the addition of  $\varrho_A$  to the initial density does not significantly change the numerical solution of the system of partial differential equations, while introducing the substantial benefit of significantly improving its stability. Again, this behavior compares favorably with solutions to the TDSE, which also do not demonstrate the node problem. On the other hand, computing solutions in the Lagrangian frame still offers substantial computational efficiency when compared to those in the Eulerian frame; due simply to relative density of solutions.

We begin in §4.2 by presenting the governing equations, then rescaling these equations in time for substantial improvement of numerical tractability. Next we present the details of a computationally well-posed finite element

discretization scheme leading to our approximate (numerical) solution. The scheme is based on a discontinuous Galerkin method for the QHD conservation laws and a mixed finite element method for the Bohmian quantum potential, which is inspired by Ref. [219]. In §4.3 we briefly derive the basic equations, and discuss the rather strong dependence on the formal and numerical equivalencies in the boundary data. In §4.4 we derive an analytic test case which allows us to find the relative error in the discontinuous Galerkin mixed method, which shows that our formulation is near to numerically exact everywhere but at the boundaries (which is expected). We proceed in §4.5 by testing the standard case of a hydrogen atom tunneling through an Eckart potential barrier, compare these results to a finite difference scheme for the TDSE, and then show how to use the continuity equation to recover the Lagrangian, or Bohmian, trajectories. Next, in §4.6, we show how to compute pathlines, recover the variables  $\rho, \mathbf{u}, \psi$  and  $S$  in both the Eulerian and Lagrangian frames, and compare the way in which these solutions relate to each other.

## 4.2 Conservation Formulation of Quantum Hydrodynamics

Consider the following system of equations for  $(s, x) \in T_s \times \Omega$ , motivated by Ref. [20], where we have transformed the solution space from the usual Lagrangian coordinate frame into the conservation form of the Eulerian coordinate frame:

$$\partial_s \varrho + \nabla_x \cdot (\varrho \mathbf{v}) = 0, \quad (4.1)$$

$$\partial_s (\varrho m \mathbf{v}) + \nabla_x \cdot \Pi + \varrho \nabla_x V = 0, \quad (4.2)$$

with initial conditions

$$\varrho_{s=0} = \varrho_0, \quad \text{and} \quad \mathbf{v}_{s=0} = \mathbf{v}_0$$

where  $\varrho = \varrho(s, \mathbf{x})$  is the probability density corresponding to conservation equation (4.1), and  $\mathbf{v} = \mathbf{v}(s, \mathbf{x})$  is the volume velocity corresponding to the momentum density  $\varrho \mathbf{p} = \varrho m \mathbf{v}$  in equation (4.2), where the mass  $m$  is constant. Here  $V$  corresponds to the potential surface, where in keeping with the usual formulation in chemical applications in one dimension  $V$  may be generally thought of as a model potential (e.g. an Eckart, Lennard-Jones or electrostatic potential).

The quantum stress  $\Pi$  is given to obey,

$$\Pi = \varrho m \mathbf{v} \otimes \mathbf{v} + \varrho^{-1} \left\{ \frac{\hbar^2}{4m} (\nabla_x \varrho)^2 \right\} - \frac{\hbar^2}{4m} \nabla_x^2 \varrho,$$

or alternatively

$$m^{-1} \Pi = \varrho \mathbf{v} \otimes \mathbf{v} - \frac{\varrho \hbar^2}{4m^2} \nabla_x^2 \log \varrho,$$

with the Bohmian quantum potential given as  $\mathcal{Q} = \left( \frac{\hbar^2}{2m} \Delta_x \sqrt{\varrho} \right) / \sqrt{\varrho}$  (note that this term is only defined up to a sign convention, see for example Ref. [42, 220] versus Ref. [20]), such that the nonlinear dispersion relation is given by,

$$\frac{\varrho \hbar^2}{2m} \nabla_x \left( \frac{\Delta_x \sqrt{\varrho}}{\sqrt{\varrho}} \right) = \frac{\hbar^2}{4m} \nabla \cdot (\varrho \nabla_x^2 \log \varrho), \quad (4.3)$$

yielding the alternative form of (4.2):

$$\partial_t(\varrho m \mathbf{v}) + \nabla_x \cdot (\varrho m \mathbf{v} \otimes \mathbf{v}) - \varrho \nabla_x \mathcal{Q} + \varrho \nabla_x V = 0. \quad (4.4)$$

Let us rescale (4.1) and (4.4) by setting  $s = \sqrt{m}t$  and solving for a rescaled solution  $\mathbf{u}$  and  $\rho$  in the time variable  $t$ , such that our new variables

satisfy  $\mathbf{u}(t, x) = \sqrt{m}\mathbf{v}(\sqrt{m}t, x)$  and  $\rho(t, x) = \varrho(\sqrt{m}t, x)$  such that (4.1) and (4.4) for  $(t, x) \in T \times \Omega$  become:

$$\partial_t \rho + \nabla_x \cdot (\rho \mathbf{u}) = 0, \quad (4.5)$$

$$\partial_t (\rho \mathbf{u}) + \nabla_x \cdot (\rho \mathbf{u} \otimes \mathbf{u}) - \rho \nabla_x \mathcal{Q} + \rho \nabla_x V = 0. \quad (4.6)$$

We solve (4.5)-(4.6) using a mixed discontinuous Galerkin finite element method. We define the state vector

$$\mathbf{U} = (\rho, \rho \mathbf{u})^T,$$

the inviscid flux vector

$$\mathbf{f} = (\rho \mathbf{u}, \rho \mathbf{u} \otimes \mathbf{u})^T,$$

and the source vector

$$\mathbf{S} = (0, \rho \nabla_x (V - \mathcal{Q}))^T.$$

Then we can rewrite (4.1)-(4.2) as

$$\mathbf{U}_t + \mathbf{f}_x + \mathbf{S} = 0. \quad (4.7)$$

Consider the following discretization scheme motivated by [105, 174] (and illustrated in the one dimensional case in Figure 3.1). Take an open  $\Omega \subset \mathbb{R}$  with boundary  $\partial\Omega = \Gamma$ , given  $T > 0$  such that  $\mathcal{Q}_T = ((0, T) \times \Omega)$  for  $\hat{\Omega}$  the closure of  $\Omega$ . Let  $\mathcal{T}_h$  denote the partition of the closure  $\Omega$ , such that taking  $\hat{\Omega} = [a, b]$  provides the partition

$$a = x_0 < x_1 \dots < x_{ne} = b$$

comprised of elements  $\mathcal{G}_i = (x_{i-1}, x_i) \in \mathcal{T}_h$  such that  $\mathcal{T}_h = \{\mathcal{G}_1, \mathcal{G}_2, \dots, \mathcal{G}_{ne}\}$ . The mesh diameter  $h$  is given by  $h = \sup_{\mathcal{G} \in \mathcal{T}_h} (x_i - x_{i-1})$  such that a discrete

approximation to  $\Omega$  is given by the set  $\Omega_h = \cup_i \mathcal{G}_i \setminus \{a, b\}$ . Each element of the partition has a boundary set given by  $\partial \mathcal{G}_i = \{x_{i-1}, x_i\}$ , where elements sharing a boundary point  $\partial \mathcal{G}_i \cap \partial \mathcal{G}_j \neq \emptyset$  are characterized as neighbors and generate the set  $\mathcal{K}_{ij} = \partial \mathcal{G}_i \cap \partial \mathcal{G}_j$  of interfaces between neighboring elements. The boundary  $\partial \Omega = \{a, b\}$  is characterized in the mesh as  $\partial \Omega = \{x_0, x_{ne}\}$  and indexed by elements  $B_j \in \partial \Omega$  such that  $\hat{\Omega} = \mathcal{T}_h \cup \mathcal{K}_{ij} \cup \partial \Omega$ . Now for  $I \subset \mathbb{Z}^+ = \{1, 2, \dots\}$  define the indexing set  $r(i) = \{j \in I : \mathcal{G}_j \text{ is a neighbor of } \mathcal{G}_i\}$ , and for  $I_B \subset \mathbb{Z}^- = \{-1, -2, \dots\}$  define  $s(i) = \{j \in I_B : \mathcal{G}_i \text{ contains } B_j\}$ . Then for  $S_i = r(i) \cup s(i)$ , we have  $\partial \mathcal{G}_i = \cup_{j \in S(i)} \mathcal{K}_{ij}$  and  $\partial \mathcal{G}_i \cap \partial \Omega = \cup_{j \in s(i)} \mathcal{K}_{ij}$ .

We define the broken Sobolev space over the partition  $\mathcal{T}_h$  as

$$W^{k,2}(\Omega_h, \mathcal{T}_h) = \{v : v|_{\mathcal{G}_i} \in W^{k,2}(\mathcal{G}_i) \quad \forall \mathcal{G}_i \in \mathcal{T}_h\}.$$

Further, approximate solutions to (4.1)-(4.2) will exist in the space of discontinuous piecewise polynomial functions over  $\Omega$  restricted to  $\mathcal{T}_h$ , given as

$$S_h^d(\Omega_h, \mathcal{T}_h) = \{v : v|_{\mathcal{G}_i} \in \mathcal{P}^d(\mathcal{G}_i) \quad \forall \mathcal{G}_i \in \mathcal{T}_h\}$$

for  $\mathcal{P}^d(\mathcal{G}_i)$  the space of degree  $\leq d$  polynomials on  $\mathcal{G}_i$ .

Choosing a set of degree  $d$  polynomial basis functions  $N_\ell \in \mathcal{P}^d(\mathcal{G}_i)$  for  $\ell = 0, \dots, d$  we can denote the state vector at the time  $t$  over  $\Omega_h$ , by

$$\mathbf{U}_h(t, x) = \sum_{\ell=0}^d \mathbf{U}_\ell^i(t) N_\ell^i(x), \quad \forall x \in \mathcal{G}_i, \quad (4.8)$$

where the  $N_\ell^i$ 's are the finite element shape functions in the DG setting, and the  $\mathbf{U}_\ell^i$ 's correspond to the nodal unknowns. We characterize the finite dimensional test functions

$$\boldsymbol{\varphi}_h \in W^{2,2}(\Omega_h, \mathcal{T}_h), \quad \text{by} \quad \boldsymbol{\varphi}_h(x) = \sum_{\ell=0}^d \boldsymbol{\varphi}_\ell^i N_\ell^i(x)$$

where  $\varphi_\ell^i$  are the nodal values of the test functions in each  $\mathcal{G}_i$ .

Assuming that the source term  $\mathbf{S}$  is sufficiently smooth, we let  $\mathbf{U}$  be a classical solution to (4.7) and multiply through by  $\varphi_h$  and integrating such that:

$$\frac{d}{dt} \int_{\mathcal{G}_i} \mathbf{U} \cdot \varphi_h dx + \int_{\mathcal{G}_i} \mathbf{f}_x \cdot \varphi_h dx = - \int_{\mathcal{G}_i} \mathbf{S} \cdot \varphi_h dx. \quad (4.9)$$

Integrating (4.9) by parts gives

$$\frac{d}{dt} \int_{\mathcal{G}_i} \mathbf{U}_h \cdot \varphi_h dx + \int_{\mathcal{G}_i} (\mathbf{f} \cdot \varphi_h)_x dx - \int_{\mathcal{G}_i} \mathbf{f} \cdot \varphi_x^h dx = - \int_{\mathcal{G}_i} \mathbf{S} \cdot \varphi_h dx. \quad (4.10)$$

Let  $\varphi|_{\mathcal{K}_{ij}}$  and  $\varphi|_{\mathcal{K}_{ji}}$  denote the values of  $\varphi$  on  $\mathcal{K}_{ij}$  considered from the interior and the exterior of  $\mathcal{G}_i$ , respectively. It should be noted that for  $\mathcal{K}_{ij} \in \Gamma$ , the restricted functions  $\varphi_h|_{\mathcal{K}_{ji}}$  are determined up to a choice of boundary condition, which we will discuss in more detail in §3. We approximate the first term in (4.10) by,

$$\frac{d}{dt} \int_{\mathcal{G}_i} \mathbf{U}_h \cdot \varphi_h dx \approx \frac{d}{dt} \int_{\mathcal{G}_i} \mathbf{U} \cdot \varphi_h dx, \quad (4.11)$$

the second term using an inviscid numerical flux  $\Phi_i$ , by

$$\begin{aligned} \tilde{\Phi}_i(\mathbf{U}_h|_{\mathcal{K}_{ij}}, \mathbf{U}_h|_{\mathcal{K}_{ji}}, \varphi_h) &= \sum_{j \in S(i)} \int_{\mathcal{K}_{ij}} \Phi(\mathbf{U}_h|_{\mathcal{K}_{ij}}, \mathbf{U}_h|_{\mathcal{K}_{ji}}, n_{ij}) \cdot \varphi_h|_{\mathcal{K}_{ij}} d\mathcal{K} \\ &\approx \int_{\mathcal{K}_{ij}} \sum_{l=1}^N (\mathbf{f}_h)_l \cdot (n_{ij})_l \varphi_h|_{\mathcal{K}_{ij}} d\mathcal{K}, \end{aligned} \quad (4.12)$$

for  $n_{ij}$  the unit outward pointing normal and where  $l$  is the dimension, and the third term on the left in (4.10) by:

$$\Theta_i(\mathbf{U}_h, \varphi_h) = - \int_{\mathcal{G}_i} \mathbf{f}_h \cdot (\varphi_h)_x dx \approx - \int_{\mathcal{G}_i} \mathbf{f} \cdot (\varphi_h)_x dx. \quad (4.13)$$



Using (4.11)-(4.13), taking the convention that

$$\mathcal{X} = \sum_{\mathcal{G}_i \in \mathcal{T}_h} \mathcal{X}_i,$$

and setting the inner product

$$(\mathbf{a}_h, \mathbf{b}_h)_{\Omega_{\mathcal{G}}} = \sum_{\mathcal{G}_i \in \mathcal{T}_h} \int_{\mathcal{G}_i} \mathbf{a}_h \cdot \mathbf{b}_h dx,$$

we define an approximate solution to (4.9)-(4.17) as  $\mathbf{U}_h$  for all  $t \in (0, T)$  satisfying:

*Discontinuous Galerkin Method for the QHD Conservation Laws*

- 1)  $\mathbf{U}_h \in C^0([0, T]; S_h^d)$ ,
  - 2)  $\frac{d}{dt}(\mathbf{U}_h, \boldsymbol{\varphi}_h)_{\Omega_{\mathcal{G}}} + \tilde{\Phi}(\mathbf{U}_h, \boldsymbol{\varphi}_h) + \Theta(\mathbf{U}_h, \boldsymbol{\varphi}_h) + (\mathbf{S}_h, \boldsymbol{\varphi}_h)_{\Omega_{\mathcal{G}}} = 0$ ,
  - 3)  $\mathbf{U}_h(0) = \mathbf{U}_0$ .
- (4.14)

To compute the source term  $\mathbf{S}$ , we approximate the Bohmian quantum potential using a mixed finite element method. In particular, we know that at each time  $t$ , the quantum potential  $\mathcal{Q}$  satisfies the equations:

$$\mathcal{Q} = \frac{\hbar^2}{2m} \frac{\nabla_x \cdot \mathbf{q}}{\sqrt{\rho}} \quad \text{and} \quad \mathbf{q} = \nabla_x \sqrt{\rho}. \quad (4.15)$$

Let  $\vartheta \in L^2(\Omega)$  and  $\varsigma \in H(\text{div}, \Omega)$ . Then multiplying (4.15) by  $\vartheta$  and  $\varsigma$ , respectively, and integrating by parts over  $\Omega$  results in:

$$\int_{\Omega} \mathcal{Q} \vartheta dx = \int_{\Omega} \frac{\hbar^2}{2m} \frac{\nabla_x \cdot \mathbf{q}}{\sqrt{\rho}} \vartheta dx, \quad (4.16)$$

$$\int_{\Omega} \mathbf{q} \cdot \varsigma dx = - \int_{\Omega} \sqrt{\rho} \nabla_x \varsigma dx + \int_{\Gamma} \sqrt{\rho} \varsigma \cdot \mathbf{n} d\Gamma. \quad (4.17)$$

Choosing finite dimensional subspaces  $\mathcal{L}^h \subset L^2(\Omega)$  and  $\mathcal{H}^h \subset H(\text{div}, \Omega)$ , a mixed finite element method for the Bohmian quantum potential is then: find  $\mathcal{Q}^h : [0, T] \times \Omega \rightarrow \mathbb{R}$ ,  $\mathbf{q}^h : [0, T] \times \Omega \rightarrow \mathbb{R}^3$  such that for all  $t \in [0, T]$ ,  $\mathcal{Q}^h(t) \in \mathcal{L}^h$  and  $\mathbf{q}^h \in \mathcal{H}^h$  satisfy:

Mixed Method for the Bohmian Quantum Potential

$$\begin{aligned} 1) (\mathcal{Q}_h, \vartheta_h)_\Omega &= \frac{\hbar^2}{m} \left( \frac{\nabla_x \cdot \mathbf{q}_h}{\sqrt{\rho_h}}, \vartheta_h \right)_\Omega, \\ 2) (\mathbf{q}_h, \varsigma_h)_\Omega &= -(\sqrt{\rho_h}, \nabla_x \varsigma_h)_\Omega + (\sqrt{\rho_h}, \varsigma_h n)_\Gamma. \end{aligned} \tag{4.18}$$

Since we wish  $\mathbf{S} \in L^2(\Omega)$ , we choose  $\mathcal{L}^h$  to be a continuous finite element space, and we choose  $\mathcal{H}^h$  to be an  $H(\text{div})$ -conforming space (e.g. Raviart-Thomas elements [221], such that in one dimension, Raviart-Thomas elements collapse to be standard continuous finite elements). Equations (4.14) and (4.18) define our mixed/discontinuous Galerkin method in semi-discrete form. Computationally, we must also discretize time, as shown in §4 and §5.

It is worth noting that in the Lagrangian formulation the primitive variables  $(\rho, \mathbf{u})$  are accompanied by the *quantum action*  $S$  and the *quantum wave function*  $\psi$ . We will explicitly derive these terms in section §5 from the solution (4.14). It is also worth noting that a pure discontinuous Galerkin method was implemented as an alternative approach to the MDG method solution shown in (4.14). This treatment used a dispersive flux formulation as shown in [222]. We found that this formulation depended nonlinearly on the sign of the advective flux term, leading in the naive implementation to the formation of soliton/compacton type behavior; solutions which are well-known in the ‘formally’ equivalent formulation of Korteweg fluids (see [43, 223–225])

– up to turbulence effects etc., as explained in §3 – which model diffuse fluid interfaces as well as having phenomenological interpretation in the context of the nonlinear Schrödinger equation (see [226]) and the Gross-Pitaevskii equation (see [227, 228]) given nearly identical initial conditions to the ones we use in §5. However, in the context of chemical dynamics it is not clear that these types of solutions carry physical significance, and so we have isolated our analysis to the MDG method formulation presented in (4.14).

### 4.3 Boundary Treatment

A recurring difficulty in constructing numerical methods for initial-boundary value systems of partial differential equations for physical systems is the issue of how to prescribe mathematically consistent boundary conditions which accommodate dynamic (physical) boundary data. It turns out that this issue is a cause of both numerical and mathematical difficulties in establishing the formal equivalencies between the TDSE and the QHD system of equations. We show this behavior explicitly in an example in §5, but let us first examine the mathematical source of this difficulty.

Recall that the system presented in (4.1)-(4.2) is derived explicitly from the TDSE. That is, we have set  $\psi = Re^{iS/\hbar}$ , and want to expand the solution of the Schrödinger equation in one unknown and one equation in  $\psi = \psi(t, x)$  into a system of partial differential equations in the unknowns  $R = R(t, x)$  and  $S = S(t, x)$ . To make this a well-posed system we of course need a system of two equations, where both unknowns must be assigned distinct boundary conditions. First take the following form of the Schrödinger equation:

$$\left(-\Delta_x + \frac{2m}{\hbar^2}V\right)\psi = \frac{2mi}{\hbar}\partial_t\psi, \quad (4.19)$$

and plug in  $\psi = Re^{iS/\hbar}$  such that expanding gives for the time derivative,

$$\begin{aligned}\frac{2mi}{\hbar}\partial_t\psi &= \frac{2mi}{\hbar}\frac{\partial}{\partial t}(Re^{iS/\hbar}) \\ &= \frac{2mi}{\hbar}e^{iS/\hbar}\partial_t R - \frac{2m}{\hbar^2}Re^{iS/\hbar}\partial_t S,\end{aligned}\tag{4.20}$$

and for the spatial component

$$\begin{aligned}\Delta_x\psi &= \Delta_x(Re^{iS/\hbar}) = \nabla_x \cdot \nabla_x(Re^{iS/\hbar}) \\ &= \nabla_x \cdot \left( e^{iS/\hbar}\nabla_x R + \frac{i}{\hbar}Re^{iS/\hbar}\nabla_x S \right) \\ &= e^{iS/\hbar} \left( \Delta_x R + \frac{2i}{\hbar}\nabla_x S \nabla_x R - \frac{R}{\hbar^2}(\nabla_x S)^2 + \frac{i}{\hbar}R\Delta_x S \right).\end{aligned}\tag{4.21}$$

Putting (4.20) and (4.21) back into (4.19) and canceling a factor of  $e^{iS/\hbar}$  we obtain:

$$R\frac{2m}{\hbar^2}V = \Delta_x R + \frac{2i}{\hbar}\nabla_x S \nabla_x R - \frac{R}{\hbar^2}(\nabla_x S)^2 + \frac{i}{\hbar}R\Delta_x S + \frac{2mi}{\hbar}\partial_t R - \frac{2m}{\hbar^2}R\partial_t S,\tag{4.22}$$

Now, collecting the imaginary parts of (4.22),

$$-\frac{2mi}{\hbar}\partial_t R - \frac{2i}{\hbar}\nabla_x S \nabla_x R - \frac{i}{\hbar}R\Delta_x S = 0,$$

and multiplying through by  $\hbar^2/2m$  provides:

$$-\partial_t R - \frac{1}{m}\nabla_x R \nabla_x S - \frac{1}{2m}R\Delta_x S = 0.$$

Additionally multiplying through by  $-2mR$  gives,

$$m\partial_t R^2 + \nabla_x R^2 \nabla_x S + R^2 \Delta_x S = 0,$$

where applying the product rule yields the conservation form:

$$m\partial_t R^2 + \nabla_x \cdot (R^2 \nabla_x S) = 0.\tag{4.23}$$

Clearly setting  $R = \sqrt{\varrho}$  and using the Madelung relation  $\mathbf{v} = \frac{1}{m}\nabla_x S$  for  $m$  a constant  $m \in \mathbb{R}$  leads to the usual conservation of mass equation:

$$\partial_t \varrho + \nabla_x \cdot (\varrho \mathbf{v}) = 0. \quad (4.24)$$

Similarly putting together the real parts of (4.22) gives:

$$\frac{2mR}{\hbar^2} \partial_t S - \Delta_x R + \frac{R}{\hbar^2} (\nabla_x S)^2 + \frac{2m}{\hbar^2} RV = 0,$$

such that upon multiplication through by  $\hbar^2/2m^2R$  we have:

$$\frac{1}{m} \partial_t S - \frac{\hbar^2}{2m^2R} \Delta_x R + \frac{1}{2m^2} (\nabla_x S)^2 + \frac{1}{m} V = 0.$$

Taking a derivation in  $x$  then yields

$$\frac{1}{m} \partial_t \nabla_x S - \nabla_x \left( \frac{\hbar^2}{2m^2R} \Delta_x R \right) + \nabla_x \cdot \left( \frac{1}{2m^2} (\nabla_x S)^2 \right) + \frac{1}{m} \nabla_x V = 0.$$

Now again we substitute the important Madelung relation  $\mathbf{v} = \frac{1}{m}\nabla_x S$  giving the form:

$$\partial_t \mathbf{v} + \frac{1}{2} \nabla_x (\mathbf{v} \cdot \mathbf{v}) - \frac{\hbar^2}{2m^2} \nabla_x (R^{-1} \Delta_x R) + \frac{1}{m} \nabla_x V = 0. \quad (4.25)$$

The Madelung relation,  $\mathbf{v} = \frac{1}{m}\nabla_x S$ , is of course equivalent to setting  $\mathbf{v}$  to be an irrotational field, since for *any* field  $S$ ,  $\nabla_x \times \nabla_x S = 0$ . Thus for an irrotational vector field  $\mathbf{v}$ , using that  $\nabla_x (\mathbf{v} \cdot \mathbf{v}) = 2((\mathbf{v} \cdot \nabla_x) \mathbf{v} + \mathbf{v} \times \nabla_x \times \mathbf{v})$ , we may rewrite (4.25) as,

$$\partial_t \mathbf{v} + (\mathbf{v} \cdot \nabla_x) \mathbf{v} - \frac{\hbar^2}{2m^2} \nabla_x (R^{-1} \Delta_x R) + \frac{1}{m} \nabla_x V = 0,$$

so that multiplying by  $\varrho m$  yields,

$$\varrho \partial_t m \mathbf{v} + (\varrho m \mathbf{v} \cdot \nabla_x) \mathbf{v} - \varrho \frac{\hbar^2}{2m} \nabla_x (R^{-1} \Delta_x R) + \varrho \nabla_x V = 0.$$

Combining this equation with (4.24) yields:

$$\partial_t(\varrho m \mathbf{v}) + \nabla_x \cdot (\varrho m \mathbf{v} \otimes \mathbf{v}) - \varrho \nabla_x \mathcal{Q} + \varrho \nabla_x V = 0, \quad (4.26)$$

for  $\mathcal{Q}$  the Bohmian quantum potential given as  $\mathcal{Q} = \left( \frac{\hbar^2}{2m} \Delta_x \sqrt{\varrho} \right) / \sqrt{\varrho}$ . It is important to see that the formal equivalence between 4.19 and 4.26 is entirely dependent on Madelung's irrotational condition, which makes turbulent effects, for example, vanish. In the alternative derivation of the QHD regime, using moment expansions (see for example [20, 42]) this restriction is not necessary.

Thus we have arrived at our system of quantum hydrodynamic equations:

$$\begin{aligned} \partial_t \varrho + \nabla_x \cdot (\varrho \mathbf{v}) &= 0, \\ \partial_t(\varrho m \mathbf{v}) + \nabla_x \cdot (\varrho m \mathbf{v} \otimes \mathbf{v}) - \varrho \nabla_x \mathcal{Q} + \varrho \nabla_x V &= 0, \end{aligned} \quad (4.27)$$

requiring initial conditions

$$\rho|_{t=0} = \rho_0 \quad \text{and} \quad u|_{t=0} = u_0,$$

and numerically requiring explicit boundary conditions  $\rho_b$  and  $u_b$  on an irrotational vector field  $\mathbf{v}$ . Additionally, and as an important aside, the formal equivalence we have derived is constructed without mention of boundary conditions, which is satisfied over  $(0, T) \times \mathbb{R}^3$ , but on a discrete domain  $\Omega \subset \mathbb{R}^3$  is a bit over optimistic, and as we will see below, does not in general hold.

That is, the TDSE code (see §5) sets the initial data  $\psi_{i,b}$  on the boundary as a time-independent condition, so the boundary value  $\psi_b \equiv \psi_b = \psi_{i,b}$  is enforced for all  $t \in [0, T)$ . Since  $\psi_{i,b}$  must be decomposed into  $R_{i,b}$  and  $S_{i,b}$  to make sense for the QHD formulation (4.27), these give Dirichlet conditions which can be implemented, but are unstable in the QHD regime, since  $R_{i,b}$

exponentially decays on the boundary and as a consequence is not numerically invertible; as it must be in the QHD formulation. These may however be approximated by setting  $\rho_{i,b} = \rho_A$ , the ambient density, and  $u_{i,b} = -\frac{1}{m} \int_{\mathcal{G}_b} \nabla S dx$  for  $\mathcal{G}_b$  the boundary element.

However, these BCs still are not well-posed in the QHD regime for the following reason. First we compute the entropy inequality for the rescaled version of (4.27) shown in (4.5) and (4.6). We may compute the important classical/quantum entropy satisfying for non-boundary terms that:

$$\frac{d}{dt} \int_{\Omega} \left( \rho \frac{|\mathbf{v}|^2}{2} + \frac{\hbar^2 (\nabla_x \sqrt{\rho})^2}{4m} + \rho V \right) dx \leq 0. \quad (4.28)$$

We arrive at this system by multiplying the momentum equation from (4.27) by  $\mathbf{v}$  and integrating in space (e.g. the domain is some  $\Omega \subseteq \mathbb{R}^3$ ), such that rearranging we find

$$\int_{\Omega} \mathbf{v} \partial_t (\rho \mathbf{v}) + \mathbf{v} \nabla_x \cdot (\rho \mathbf{v} \otimes \mathbf{v}) dx - \int_{\Omega} \rho \mathbf{v} \nabla_x \mathcal{Q} dx + \int_{\Omega} \rho \mathbf{v} \nabla_x V dx = 0. \quad (4.29)$$

The product rule allows us to expand the first term on the LHS as:

$$\int_{\Omega} |\mathbf{v}|^2 (\partial_t \rho + \nabla_x \cdot (\rho \mathbf{v})) + \rho \mathbf{v} \partial_t \mathbf{v} + \rho |\mathbf{v}|^2 \nabla_x \cdot \mathbf{v} dx,$$

where  $|\mathbf{v}|^2 = \mathbf{v} \cdot \mathbf{v}$ . Using the mass conservation equation twice from (4.27) and applying the divergence theorem we find that,

$$\int_{\Omega} \mathbf{v} (\partial_t (\rho \mathbf{v}) + \nabla \cdot (\rho \mathbf{v} \otimes \mathbf{v})) dx = \frac{d}{dt} \int_{\Omega} \rho \frac{|\mathbf{v}|^2}{2} dx + \frac{1}{2} \int_{\Omega} \nabla_x \cdot (\rho \mathbf{v}^3) dx. \quad (4.30)$$

Next, using the dispersion relation from the Bohm quantum potential the third

term on the left yields:

$$\begin{aligned}
\int_{\Omega} \rho \mathbf{v} \nabla_x \Omega &= \frac{\hbar^2}{2m} \int_{\Omega} \rho \mathbf{v} \nabla_x \left( \frac{\Delta_x \sqrt{\rho}}{\sqrt{\rho}} \right) dx \\
&= -\frac{\hbar^2}{2m} \int_{\Omega} \frac{1}{\sqrt{\rho}} \nabla_x \cdot (\rho \mathbf{v}) \Delta_x \sqrt{\rho} dx + \frac{\hbar^2}{2m} \int_{\Omega} \nabla_x \cdot (\sqrt{\rho} \mathbf{v} \Delta_x \sqrt{\rho}) dx \\
&= \frac{\hbar^2}{2m} \int_{\Omega} \left\{ \nabla_x \left( \frac{1}{\sqrt{\rho}} \nabla_x \cdot (\rho \mathbf{v}) \right) \nabla_x \sqrt{\rho} + \nabla_x \cdot (\sqrt{\rho} \mathbf{v} \Delta_x \sqrt{\rho}) \right\} dx \\
&\quad - \frac{\hbar^2}{2m} \int_{\Omega} \nabla_x \left( \frac{1}{\sqrt{\rho}} \nabla_x \cdot (\rho \mathbf{v}) \nabla_x \sqrt{\rho} \right) dx \\
&= \frac{\hbar^2}{2m} \int_{\Omega} \nabla_x \sqrt{\rho} \partial_t \nabla_x \sqrt{\rho} dx + \text{boundary terms}.
\end{aligned} \tag{4.31}$$

Finally the source term  $V = V(x)$  upon integrating by parts gives

$$\begin{aligned}
\int_{\Omega} \rho \mathbf{v} \cdot \nabla_x V dx &= - \int_{\Omega} V \nabla_x \cdot (\rho \mathbf{v}) dx + \int_{\Omega} \nabla_x \cdot (V \rho \mathbf{u}) dx \\
&= \frac{d}{dt} \int_{\Omega} \rho V dx + \int_{\Omega} \nabla_x \cdot (V \rho \mathbf{v}) dx.
\end{aligned} \tag{4.32}$$

Then we have recovered (4.28) as an equality up to the boundary terms in (4.30), (4.31) and (4.32). To recover the mathematical well-posedness of the system these boundary terms must either vanish or be bounded and positive (or negative) definite. One such choice of boundary data is, for example,  $\mathbf{v}_b \equiv 0$ . Another is the pair of conditions  $\nabla_x \sqrt{\rho_b} \equiv 0$  and  $V_b \equiv 0$  for all  $t \in [0, T)$ , and so forth.

The first set of boundary data, with  $\mathbf{v}_b \equiv 0$ , may be set with  $\rho_b \equiv \rho_A$ . Since the *action* behaves as a phase, this seems a reasonable approximation, since it effectively assumes that up to a constant of integration that the phase is constant over boundary elements  $\nabla S_b \equiv 0$ . These conditions are then mathematically consistent with the system of equations (4.27), but have the



physical effect of generating “inlet/outlet” boundary layers, caused by the value of  $\rho_b$ .

Perhaps a more natural boundary condition is given by setting,

$$\mathbf{U}_h^n|_{\mathcal{K}_{ji}} = \mathbf{U}_h^n|_{\mathcal{K}_{ij}},$$

where  $\mathbf{U}_h^n$  is the numerical solution at timestep  $t_n$ , as explained in detail in §4, and  $\mathcal{K}_{ij} \in \partial\Omega$ . This boundary type is a first order approximation to a transmissive or radiative condition that treats the boundary like a “ghost cell,” and allows density and momentum to leave the domain as though falling into vacuum, while allowing no density or momentum to enter. This condition approximates to the first order, the effect of “not setting boundary conditions at all,” and thus *not badly* perturbing the system (4.27) away from its natural behavior, nor generating reflecting behavior, which in some contexts – such as a chemical reaction occurring in a solvent bath – are difficult to physically interpret.

## 4.4 A Numerical Test Case

We wish to test the accuracy of our MDG method formulation by solving an analytic test solution. In order to do this we choose a numerical flux for (4.14) and restrict to spatial dimension  $l = 1$ . For the inviscid flux  $\Phi$  we implement the local Lax-Friedrich’s flux  $\Phi_{LLF}$  satisfying

$$\begin{aligned} \int_{\mathcal{K}_{ij}} \Phi_{LLF} \cdot \boldsymbol{\varphi}_h d\mathcal{K} &= \frac{1}{2} \int_{\mathcal{K}_{ij}} (\mathbf{f}(\mathbf{U}_h)|_{\mathcal{K}_{ij}} + \mathbf{f}(\mathbf{U}_h)|_{\mathcal{K}_{ji}}) \cdot n_{ij} \boldsymbol{\varphi}_h|_{\mathcal{K}_{ij}} d\mathcal{K} \\ &\quad - \frac{1}{2} \int_{\mathcal{K}_{ij}} (\text{Spec}_r(\mathbf{\Gamma}_0))((\mathbf{U}_h)|_{\mathcal{K}_{ij}} - (\mathbf{U}_h)|_{\mathcal{K}_{ji}}) \cdot n_{ij} \boldsymbol{\varphi}_h|_{\mathcal{K}_{ij}} d\mathcal{K}, \end{aligned}$$

for  $n_{ij}$  the outward unit normal and  $\text{Spec}_r(\mathbf{\Gamma}_0)$  the spectral radius of  $\mathbf{\Gamma}_0$ ; the Jacobian matrix of the inviscid flux  $J_U \mathbf{f}(\mathbf{U}) = \mathbf{\Gamma}_0(\mathbf{U})$  which may be repre-

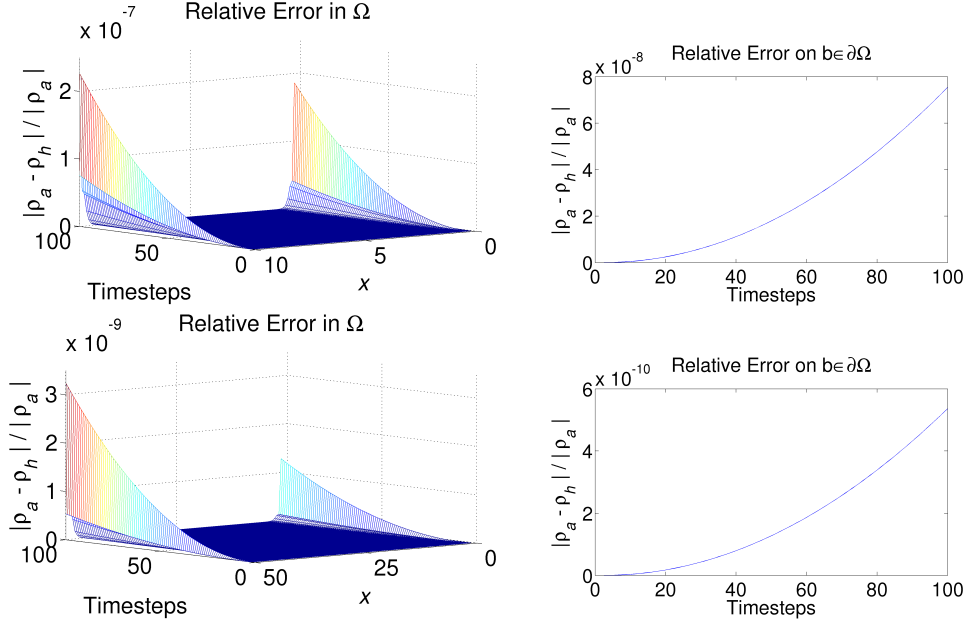


Figure 4.3: Here we show the relative error introduced by the *weak entropy* boundary conditions for  $a = 0$  and both  $b = 10$  and  $b = 50$ . The boundary data (the graphs on the right) show only the relative error on element  $b$  of  $\partial\Omega$  for  $b = 10$  and  $b = 50$ , respectively.

sented by the following  $2 \times 2$  matrix,

$$\mathbf{\Gamma}_0(\mathbf{U}) = \begin{pmatrix} 0 & 1 \\ -u^2 & 2u \end{pmatrix}. \quad (4.33)$$

Summing over the elements of the mesh this term satisfies:

$$\begin{aligned} 2\tilde{\Phi}_{ILF}(\mathbf{U}_h, \boldsymbol{\varphi}_h) &= \sum_{\mathcal{G}_i \in \mathcal{T}_h} \sum_{j \in S(i)} \int_{\mathcal{K}_{ij}} (\mathbf{f}(\mathbf{U}_h)|_{\mathcal{K}_{ij}} + \mathbf{f}(\mathbf{U}_h)|_{\mathcal{K}_{ji}}) \cdot \mathbf{n}_{ij} \boldsymbol{\varphi}_h|_{\mathcal{K}_{ij}} d\mathcal{K} \\ &\quad - \sum_{\mathcal{G}_i \in \mathcal{T}_h} \sum_{j \in S(i)} \int_{\mathcal{K}_{ij}} (\text{Spec}_r(\mathbf{\Gamma}_0))((\mathbf{U}_h)|_{\mathcal{K}_{ij}} - (\mathbf{U}_h)|_{\mathcal{K}_{ji}}) \cdot \mathbf{n}_{ij} \boldsymbol{\varphi}_h|_{\mathcal{K}_{ij}} d\mathcal{K}. \end{aligned} \quad (4.34)$$

Next we discretize in time. That is, we denote a partition of  $[0, T]$  by

$$0 = t^0 < t^1 \dots < t^T = T,$$

for a timestep given as  $\Delta t^n = t^{n+1} - t^n$ , and let  $\mathbf{U}_h^n$  denote the solution at timestep  $t^n$ . Thus we implement the following forward Euler scheme:

$$\frac{\partial \mathbf{U}_h}{\partial t} \approx \frac{\mathbf{U}_h^{n+1} - \mathbf{U}_h^n}{\Delta t^n},$$

which, along with the implementation of a slope limiter in the conservation variables  $(\rho, \rho u)$  given by van Leer's MUSCL scheme (as shown in [196] and [197]), allows us to explicitly solve (4.14). That is, we define an approximate solution as  $\mathbf{U}_h^n$  for all  $t_n$  such that  $n = 0, \dots, T$  satisfying:

$$\begin{aligned} 1) & \mathbf{U}_h^n \in S_h^d, \mathcal{Q}_h^n \in \mathcal{L}_h \text{ and } \mathbf{q}_h^n \in \mathcal{H}_h, \\ 2) & \left( \frac{\mathbf{U}_h^{n+1} - \mathbf{U}_h^n}{\Delta t^n}, \boldsymbol{\varphi}_h \right)_{\Omega_{\mathcal{G}}} + \tilde{\Phi}(\mathbf{U}_h^n, \boldsymbol{\varphi}_h) + \Theta(\mathbf{U}_h^n, \boldsymbol{\varphi}_h) + (\mathbf{S}_h^n, \boldsymbol{\varphi}_h)_{\Omega_{\mathcal{G}}} = 0, \\ 3) & (\mathcal{Q}_h^n, \vartheta_h)_{\Omega} = \frac{\hbar^2}{m} \left( \frac{\nabla_x \cdot \mathbf{q}_h^n}{\sqrt{\rho_h^n}}, \vartheta_h \right)_{\Omega}, \\ 4) & (\mathbf{q}_h^n, \varsigma_h)_{\Omega} = -(\sqrt{\rho_h^n}, \nabla_x \varsigma_h)_{\Omega} + (\sqrt{\rho_h^n}, \varsigma_h n)_{\Gamma}, \\ 5) & \mathbf{U}_0^h = \mathbf{U}_h(0). \end{aligned} \tag{4.35}$$

The above formulation lends itself naturally to a staggered scheme. First, given  $\mathbf{U}_h^n$  one solves step 3 and 4 for  $\mathcal{Q}_h^n$  and  $\mathbf{q}_h^n$ , which provides  $\mathbf{S}_h^n$ , allowing us to solve for  $\mathbf{U}_h^{n+1}$  in step 2.

Now we construct an appropriate test case. Consider the dimension  $N = 1$  case and let  $u \equiv 0$  on  $\Omega$  for (4.5)-(4.6), such that  $\partial_s \rho = 0$ . Up to a choice of boundary conditions, upon integration we have for (4.6) that

$$\mathcal{Q} = C - V,$$

such that choosing a  $C \equiv V$  we find the following second order ordinary differential equation:

$$\rho'' - \rho^{-1}(\rho')^2 = 0,$$

whose solution is  $\rho = e^x$ . We solve for the approximate solution of (4.14) using the above scheme, with initial conditions  $\rho_0 = e^x$ ,  $u = 0$ ,  $V = C$  and  $m = 1836$  the mass of a proton in Hartree atomic units (au). The boundaries are set to the *weak entropy* boundary condition formulation as presented in [162, 185, 186] and [174]. We graph the relative error of our approximate solution  $\rho_h$  to the exact numerical representation  $\rho_a$  in Figure (4.3). We see that the two solutions are numerically exact in the interior of the domain, and error accumulates in the boundary  $\partial\Omega$ , as expected due to the weak entropy boundary conditions. We note that the error on the boundary may be reduced by increasing the absolute size of the interval  $[a, b]$ .

## 4.5 Tunneling in TDSE and QHD

We proceed by testing a relatively standard example in quantum chemistry, given by a propagating Gaussian packet in the direction of a model Eckart potential barrier. We solve the following one dimensional system:

$$\partial_t \rho + \partial_x(\rho u) = 0, \quad (4.36)$$

$$\partial_t(\rho u) + \partial_x(\rho u^2) - \rho \partial_x \Omega + \rho \partial_x V = 0. \quad (4.37)$$

with initial conditions

$$\rho_0 = \rho_A + \left( \frac{1}{\sqrt{2\pi\mu}} \right) e^{\frac{-(x-x_0)^2}{2\mu}} \quad \text{and} \quad u_0 = (\alpha V_0)^{1/2}, \quad (4.38)$$

where the Eckart potential is given by

$$V(x) = V_0 \operatorname{sech}^2 \left( \frac{1}{2}(x - x_1) \right). \quad (4.39)$$

As is conventional in quantum hydrodynamics, the mass is set to approximate the hydrogen (proton) mass  $m \sim 2000$  au (in Hartree atomic units),

Table 4.1: *Runge-Kutta k-th order in time*

Parameter	k=2	k=3
$c_{il}$	$\begin{pmatrix} 1 & 0 \\ 1/2 & 1/2 \end{pmatrix}$	$\begin{pmatrix} 1 & 0 & 0 \\ 3/4 & 1/4 & 0 \\ 1/3 & 0 & 2/3 \end{pmatrix}$
$d_{il}$	$\begin{pmatrix} 1 & 0 \\ 0 & 1/2 \end{pmatrix}$	$\begin{pmatrix} 1 & 0 & 0 \\ 0 & 1/4 & 0 \\ 0 & 0 & 2/3 \end{pmatrix}$

$\rho_A \sim 10^{-10}$  is a numerical background density for division,  $x_0$  centers the Gaussian packet,  $x_1$  centers the potential,  $\mu$  is the variance of the distribution,  $\alpha$  is a constant  $\alpha \in \mathbb{R}$  and  $V_0$  is the barrier height (which we may vary, so some constant  $V_0 \in \mathbb{R}$ ). In the quantum regime (when classical barrier transmission is not present), the initial velocity  $u_0$  is often chosen to satisfy the following condition on the initial kinetic energy  $K_0 = \frac{1}{2}u_0^2 = \frac{1}{4}V_0$ .

The background ambient value  $\rho_A$  is required in order to satisfied the mathematical and numerical well-posedness of the system such that the behavior of the system is not perturbed away from its proper character by compounding residual behavior, as shown in §3. Furthermore, from a phenomenological point of view, this value is nonrestrictive and physically easily justified – for example, for a chemical reaction occurring in a solvent bath, or, similarly, any process occurring away from vacuum.

The discretization proceeds as in section §4.2 and §4.4, where we adopt the local Lax-Friedrich’s inviscid flux with van Leer’s MUSCL slope limiting scheme. Next we implement an explicit Runge-Kutta time discretization (see Ref. [162, 198] and Ref. [3]). That is, we recast (4.14) as the following system

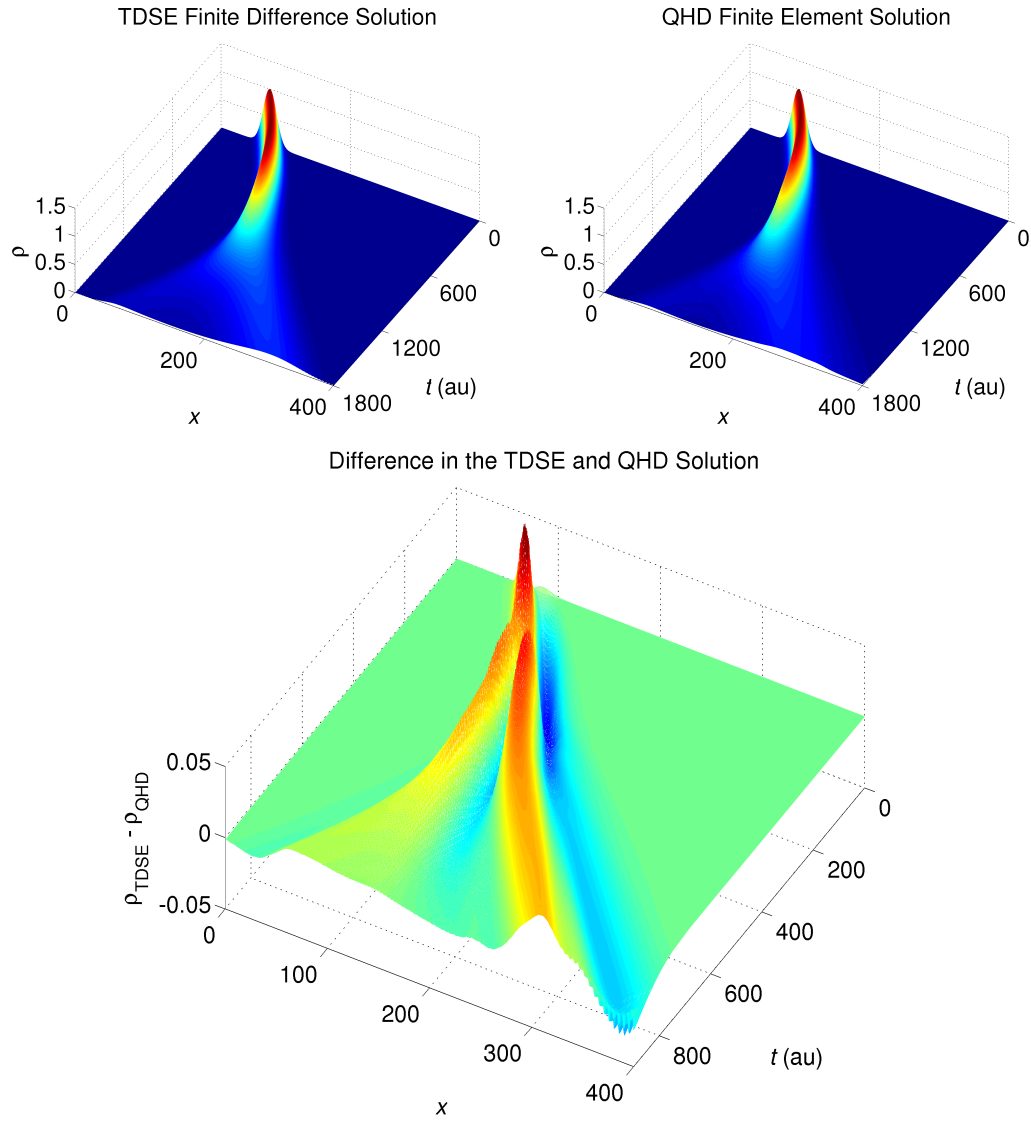


Figure 4.4: The top graphs compare solutions to the TDSE and QHD system in the so-called “eyeball norm,” using the forward Euler scheme. The bottom solution shows the nontrivial formal difference. Here  $x$  refers to the  $x$ -th meshpoint.

of ordinary differential equations,

$$\frac{d}{dt}\mathbf{U}_h = L_h(\mathbf{U}_h).$$

We achieve this by setting the value of the current timestep to  $\mathbf{U}_h^0$ , and decomposing this timestep into  $k$  substeps such that for  $i = 1, \dots, k$  we have the intermediate solutions

$$\mathbf{U}_h^i = \sum_{l=0}^{i-1} c_{il}\mathbf{U}_h^l + d_{il}\Delta t^n L_h(\mathbf{U}_h^l),$$

where the  $c$ 's and  $d$ 's are given in Table 4.1. Then setting  $\mathbf{U}_h^{n+1} = \mathbf{U}_h^k$  we recover a solution such that:

$$\begin{aligned} & 1) \mathbf{U}_h^n \in S_h^d, \mathcal{Q}_h^n \in \mathcal{L}_h \text{ and } \mathbf{q}_h^n \in \mathcal{H}_h, \\ & 2) (\mathbf{U}_h^i, \boldsymbol{\varphi}_h)_{\Omega_g} - \sum_{l=0}^{i-1} \left\{ (c_{il}\mathbf{U}_h^l, \boldsymbol{\varphi}_h)_{\Omega_g} + d_{il}\Delta t^n [\tilde{\boldsymbol{\Phi}}(\mathbf{U}_h^l, \boldsymbol{\varphi}_h) \right. \\ & \quad \left. + \boldsymbol{\Theta}(\mathbf{U}_h^l, \boldsymbol{\varphi}_h) + (\mathbf{S}_h^l, \boldsymbol{\varphi}_h)_{\Omega_g}] \right\} = 0, \quad \text{for } i = 1, \dots, k, \\ & 3) (\mathcal{Q}_h^i, \vartheta_h)_\Omega = \frac{\hbar^2}{m} \left( \frac{\nabla_x \cdot \mathbf{q}_h^i}{\sqrt{\rho_h^i}}, \vartheta_h \right)_\Omega, \quad \text{for } i = 0, \dots, k-1, \\ & 4) (\mathbf{q}_h^i, s_h)_\Omega = \left( \sqrt{\rho_h^i}, s_h n \right)_\Gamma - \left( \sqrt{\rho_h^i}, \nabla_x s_h \right)_\Omega, \quad \text{for } i = 0, \dots, k-1, \\ & 5) \mathbf{U}_0^h = \mathbf{U}_h(0). \end{aligned} \tag{4.40}$$

Now we solve the resultant system using for our initial data (4.38)-(4.39) explicitly that  $\mu = 0.16, \alpha = 2, x_0 = 3$  and  $x_1 = 6$ , such that,

$$\rho_0 = 10^{-10} + \left( \frac{1}{\sqrt{2\pi\mu}} \right) e^{\frac{-(x-3)^2}{0.32}} \quad \text{and} \quad u_0 = (2V_0)^{1/2},$$

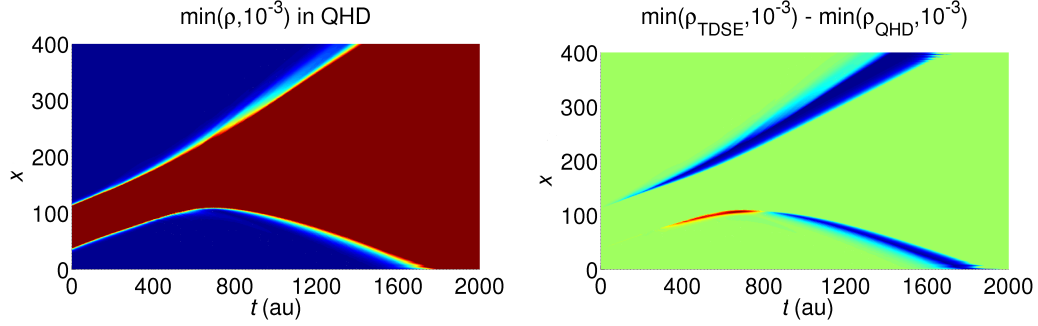


Figure 4.5: We show the diffusive noise profile  $\min(\rho_{\text{QHD}}, 10^{-3})$  in the QHD solution, and the difference  $\min(\rho_{\text{TDSE}}, 10^{-3}) - \min(\rho_{\text{QHD}}, 10^{-3})$ . Here  $x$  refers to the  $x$ -th meshpoint.

with potential:

$$V(x) = V_0 \operatorname{sech}^2 \left( \frac{1}{2}(x - 6) \right).$$

It is worth noting that we have thus chosen a kinetic energy which is in the context of a mixed classical-quantum regime; which is just to say that some classical trajectories transmit over the barrier, in addition to those that tunnel quantum mechanically. For boundary data we use the approximate well-posed Dirichlet conditions discussed in §3:

$$\rho_b = \rho_A = 10^{-10} \quad \text{and} \quad u_b = 0.$$

We compare our solution to a finite difference scheme for the TDSE provided by Prof. Robert E. Wyatt [20] in order to test the accuracy of our formulation. The TDSE has equivalent initial settings, while the boundary conditions are given naturally via  $\psi_b = \psi_{i,b}$  as discussed in §3.

In Figure 4.4 these two solutions are compared. It is clear that the two solutions have the same qualitative behavior. However they do show fundamentally different quantitative behaviors. Analysis has shown that the



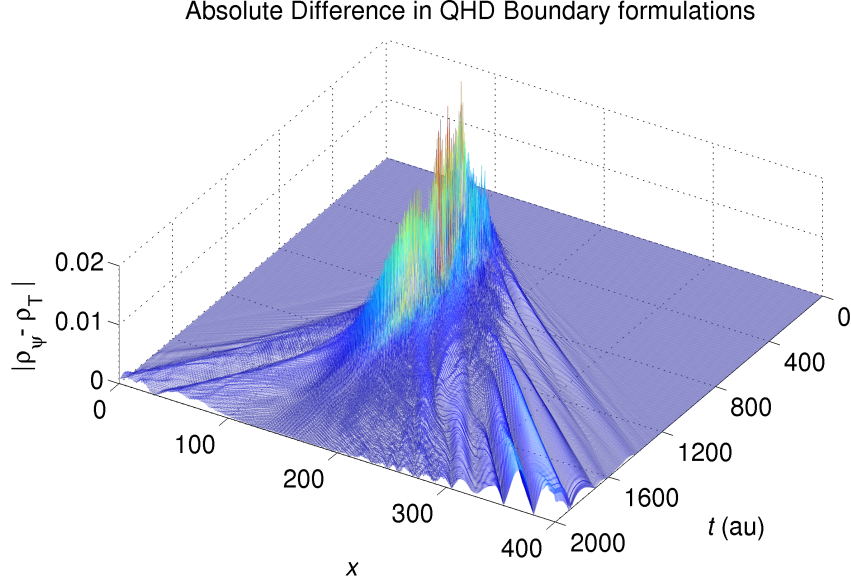


Figure 4.6: We show the absolute difference between the QHD solution using the approximate boundary data from Figure 4.4 denoted  $\rho_\psi$  with the transmissive boundary formulation from (4.44) denoted  $\rho_T$ . Here  $x$  refers to the  $x$ -th meshpoint.

two most prevalent sources of error between these two solutions are diffusion and boundary oscillations. The boundary oscillations clearly occur due to the approximations discussed in §3. The diffusion, on the other hand, is a signature of the slope limiter in the QHD formulation and is shown in greater detail in Figure 4.5. Here we confirm that the MUSCL slope limiting scheme is adding a type of “artificial diffusion” to the QHD solutions. We have found that choosing a less restrictive slope limiter, such as the flux limiter of Osher presented in [229], does stably reduce the diffusion in our solutions.

We may now recover trajectories, or characteristics, of the solution by using the fact that (4.5) is satisfied at every time step (note that we show the alternative method of integrating velocity “pathlines” in §6). We may think of

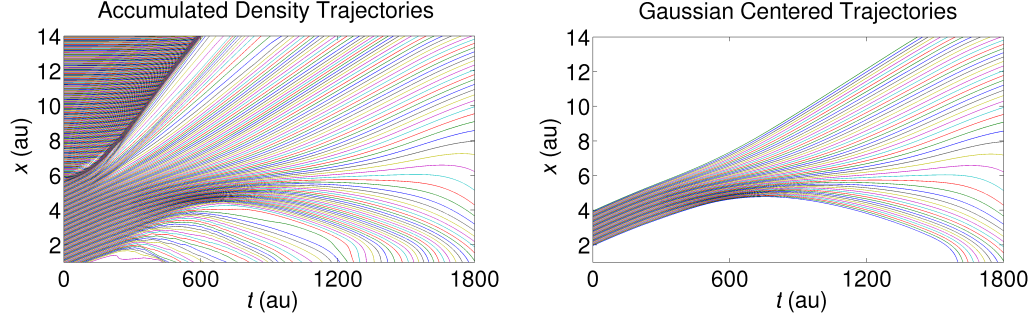


Figure 4.7: We solve the accumulated density trajectories from (4.42) using the transmissive solutions from  $\rho_T$  in Figure 4.6.

this equation as a kind of “conservation of density” here, and thus we simply employ Reynold’s transport theorem (RTT):

$$\frac{\partial}{\partial t} \int_{\tilde{\Omega}(t)} \rho dx + \int_{\tilde{\Gamma}(t)} \rho u_{rel} \cdot n dx = 0, \quad (4.41)$$

where  $u_{rel}$  is the relative velocity of the fluid with respect to the moving boundary  $\tilde{\Gamma}(t)$ . First consider the case when  $u(a) \approx 0$  such that we may choose  $\tilde{\Omega}(t) = (a, y(t))$  where  $y(t)$  is the moving boundary treated as an unknown. By assumption and construction,  $u_{rel}(a) = 0$ , whereas for a trajectory we require  $u_{rel}(y) = 0$ . Then integrating (4.41) in  $t$  we find

$$\int_a^{y(t)} \rho dx = \int_a^{y(0)} \rho dx. \quad (4.42)$$

Let us define for each trajectory  $y(t)$  with  $y(0) = y_0$  the “locally accumulated mass”  $M$  by:

$$M(y_0, t) = \int_a^{y(t)} \rho(x, t) dx.$$

Approximating each trajectory then directly follows from the equation  $M(y_0, t) = M(y_0, 0)$ .

To continue let us denote  $M_i(t) = M(x_i, t)$ , where  $x_i$  is the  $i$ -th mesh-point. To compute  $y(t)$ , we compare  $M(y_0, t)$  to the increasing sequence

$\{M_i(t)\}_{i=0\dots N}$  and find  $j$  such that  $M_{j-1}(t) \leq M(y_0, t) < M_j(t)$ , which gives us that  $y(t) \in [x_{j-1}, x_j]$ . Then to find  $y(t)$  recall that we have from (4.8) an expansion

$$\rho_h(t, x) = \sum_{l=0}^d c_l(t) N_l^j(x), \quad \text{for } x \in (x_{j-1}, x_j)$$

where the  $c_l = c_l(t)$  are constants for every fixed  $t$  and the shape functions  $N_l^j(x)$  in our implementation are translated versions of polynomials  $\{P_l\}_{l=0}^d$  on  $[-1, 1]$ . That is using  $f_j: [x_{j-1}, x_j] \mapsto [-1, 1]$  where

$$f_j(x) = 2 \left( \frac{x - x_{j-1}}{x_j - x_{j-1}} \right) - 1,$$

we find,  $N_l^j(x) = P_l(f_j(x))$ . Then solving for  $y(t)$ , formulated via

$$M(y_0, t) = M_{j-1}(t) + \int_{x_{j-1}}^{y(t)} \rho_h(x, t) dx = M_{j-1}(t) + \int_{x_{j-1}}^{y(t)} \sum_{l=0}^d c_l P_l(f_j(x)) dx,$$

can be recast by a change of variables, as solving for  $X$  in

$$M(y_0, t) = M_{j-1}(t) + \left( \frac{2}{x_j - x_{j-1}} \right) \int_{-1}^X \sum_{l=0}^d c_l P_l(z) dz, \quad (4.43)$$

after substituting  $z = f_j(x)$ . But that just corresponds by the change of variables, to

$$X = 2 \left( \frac{y(t) - x_{j-1}}{x_j - x_{j-1}} \right) - 1.$$

Then a solution to  $X$  exists by the intermediate value theorem, and since the integrand is positive it is uniquely determined as the only solution on  $[-1, 1]$  to the polynomial equation of degree  $d + 1$  arising from (4.43). We may then, for example, in the piecewise linear case (i.e.  $d = 1$ ) use the quadratic formula to recover  $X$  and hence the position of  $y(t)$  within  $\mathcal{G}_j$ .

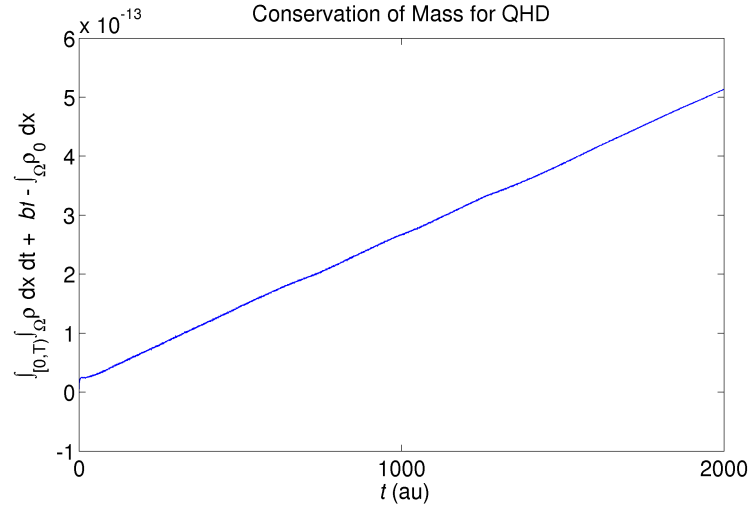


Figure 4.8: Here we show mass conservation in the QHD regime given transmissive boundaries, where  $bf = \int_{[0,T)} \int_{\partial\Omega} \rho dx dt$  is the boundary flux.

Similarly, we also work in the other direction, with the balance of the mass in  $[y(t), x_j]$  such that the analogous integral equation becomes:

$$\int_Y^1 \sum_{l=0}^d c_l P_l(z) dz,$$

which provides for a consistency check on the accumulated density in either direction. Consequently we have that the sequence  $\{y(t)\}_{t=1,\dots,T}$  provides a numerical approximation to the position of a particle initially at  $y_0$  when  $t = 0$  at our given set of later times.

This formulation holds as long as our hypothesis,  $u(a) \approx 0$ , is satisfied. However, we can immediately extend this result to include the case  $u(a) \neq 0$ . That is, after integrating in  $t$  we note that (4.41) becomes:

$$\int_a^{y(t)} \rho dx = \int_a^{y(0)} \rho dx + \int_0^t \rho u(a) dt.$$

This gives us an alternative equation to find  $y(t)$ , where we must only add  $\int_0^t \rho u(a) dt$  to the accumulated density  $M$  at every  $t$ . We further note that this basic framework may also be adapted to higher dimensions (see [230]).

Now, we again solve our system with (4.42) using for (4.38)-(4.39) that  $\mu = 0.16, \alpha = 2, x_0 = 3, x_1 = 6$ , however now we introduce the transmissive boundary condition:

$$\mathbf{U}_h^n|_{\mathcal{K}_{ji}} = \mathbf{U}_h^n|_{\mathcal{K}_{ij}}, \quad (4.44)$$

as discussed in §3. In Figure 4.6 it is clear that the behavior between the solutions with transmissive and approximate solutions is quite distinct, and that boundaries are, so to speak, felt in the interior solution even before significant density has reached  $\partial\Omega$ . We use the transmissive boundary conditions to construct the accumulated mass trajectories derived above, as they seem to represent more physically cogent boundaries. The results are shown in Figure 4.7, where the the “Gaussian centered trajectories” are simply the trajectories containing the majority of the initial density; that is, those trajectories whose initial positions are  $\pm 1$  au from the center of  $\rho_0$ .

We further show that the MDG method is a conservative scheme. That is, in Figure 4.8 we show that the density is effectively (numerically) normalized to one on the domain, when taking into account the boundary flux. That is, we see linear error growth at machine precision over 10,000 timesteps. Another feature of the solution which is attractive in the sense of practical applications, is that the spatial invariance demonstrated by the solutions. In Figure 4.9 we show the this feature, where the same calculation from Figure 4.4 is graphed, where there 400 meshpoints and 10,000 timesteps were used in order to compare with the TDSE. However, as is clear from Figure 4.9, with only 25 meshpoints the solution provides the same qualitative answer. This is an

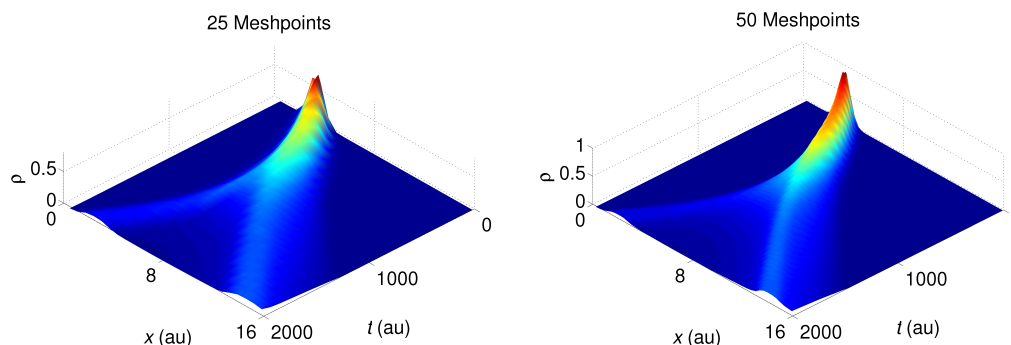


Figure 4.9: Here we show the remarkable spatial invariance of the solution. These represent the same solution as that given in Figure 4.4, except the left graph is with 25 meshpoints and 100 timesteps, and the right at 50 meshpoints and 200 timesteps.

important feature in chemical applications where computations must scale in  $3N$  dimensions, for  $N$  the number of atoms in the molecular system of interest (see for example [231]).

## 4.6 Recovering $\psi$ and $S$ in both frames

Now that we have solutions in the Eulerian and Lagrangian coordinate frames as given in §4 we may recover the important variables  $\psi$  and  $S$  in either frame. First we note that we may alternatively recover the trajectories using the solution  $\mathbf{U}$  from §4 to solve the initial value problem:

$$\frac{d\vec{r}}{dt} = \mathbf{u}(t, \vec{r}) \quad \text{with} \quad \vec{r}|_{t=0} = \vec{r}_0. \quad (4.45)$$

We recover these  $\vec{r}$  by direct integration, and compare them to those computed via (4.42) (see figure 4.10), where we refer to the  $\vec{r}$  trajectories computed in (4.45) as the “velocity pathlines.”

The trajectories computed using the velocity field (4.45) are shown in

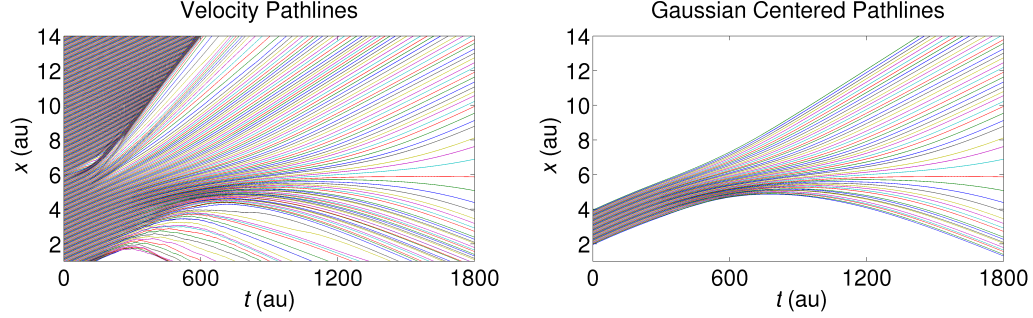


Figure 4.10: We graph the quantum trajectories using (4.45) to solve for  $\vec{r}$ , which can be compared with the accumulated mass trajectories shown in Figure 4.7.

Figure 4.10 and show qualitatively similar behavior to the trajectories computed using the accumulated mass formulation in (4.42). There is no necessarily unique way of arriving at the trajectories one chooses to represent the solution in the Lagrangian frame. For example, one may utilize a method which weights the solutions between (4.42) and (4.45). That is, we may compute the trajectory positions via (4.45) and then offset these by a weighted average of the density conservation in (4.42). We provide details on particular alternative in appendix A and show an example case.

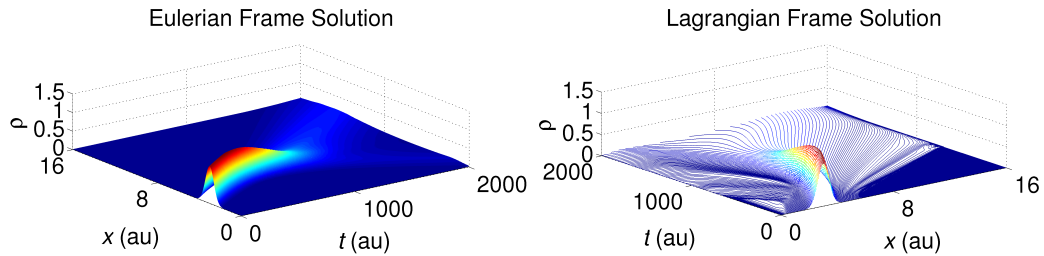


Figure 4.11: The Eulerian solution  $\rho(t, x)$  and the corresponding Lagrangian solution  $\rho(t, \vec{r})$  for the same initial condition settings as in figure 4.7 using the conservation form of the trajectories (4.42)..

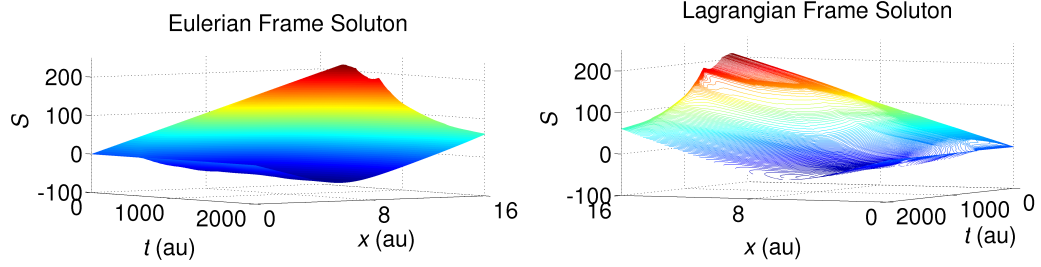


Figure 4.12: A graph of the Eulerian solution  $S(t, x)$  and the corresponding Lagrangian solution  $S(t, \vec{r})$  for the same initial condition settings as in figure 4.11 using the conservation form of the trajectories (4.42).

It is now possible to solve for a number of derived variables in either the Lagrangian or Eulerian frames in order to recover the phase information of the quantum wave-packet associated to each characteristic pathline. First we recover the trajectory-wise solutions  $\rho(s, \vec{r})$  and  $\mathbf{u}(s, \vec{r})$ , and then compute the variables:

$$\nabla_x S = \sqrt{m} \mathbf{u} \quad \text{and} \quad \psi = \sqrt{\rho} e^{iS/\hbar}, \quad (4.46)$$

where  $S(s, \vec{r})$  is the *quantum action* and  $\psi(s, \vec{r})$  is the *quantum wavefunction*. Recall that  $R(s, \vec{r}) = \sqrt{\rho(s, \vec{r})}$  as shown in §3, such that using  $\mathbf{v}$  for the velocity from §2 we recover from (4.46) the more familiar formulation:

$$\nabla_x S = m \mathbf{v} \quad \text{and} \quad \psi = R e^{iS/\hbar}. \quad (4.47)$$

It is important to note that up to a constant of integration,  $S$  and  $\psi$  are completely determined by the solution (4.14). Also, (4.47) is satisfied in both reference frames, so we now have the following solutions:

$$\rho(s, x), \rho(s, \vec{r}), \mathbf{v}(s, x), \mathbf{v}(s, \vec{r}), \psi(s, x), \psi(s, \vec{r}), S(s, x), \text{ and } S(s, \vec{r}). \quad (4.48)$$

These solutions are graphed in figures 4.11–4.12, where it is interesting to note that the two frames draw out different aspects of the solution. While the



Lagrangian frame tracks individual “particle” trajectories across the function profiles, it misses some of the nuance in the continuous structure of the surface; which is naturally recovered by the Eulerian frame solution. Furthermore, as lower resolution, we find that the conservation based trajectories from (4.42) are more well-behaved than the velocity based trajectories from (4.45).

# Chapter 5

## Chemical Reactor Models

### 5.1 Introduction

The study of chemical reactors span many decades of research and a large number of fields of study. Reactors that model complicated dynamics adjoined to chemical kinetics are not only of fundamental importance in applications in chemistry and chemical engineering [30, 45, 184], but also in mechanical and aerospace engineering [232], atmospheric and oceanic sciences [233], astronomy and plasma physics [234, 235], and generally in any number of biologically related fields [236]. That is, the prevalence of reactive chemical systems in each of these fields, makes the ability to model evolutionary systems with functional local pressures, velocities, densities, etc., essential for understanding the way in which many experimental and industrial systems evolve as a function of space and time. In fact, one can generally state that any time-evolving state involving thermodynamic functions with reaction kinetics must, at some level of sophistication, model chemical reactors.

The relative ubiquity of chemical reactor models in dynamic contexts has been somewhat hampered by the mathematical and technical difficulties that arise at the level of modélisation. A good review of approaches related to reactor systems from the point of view of physical chemistry can be found in Ref. [30]. Though the theoretical foundations of the field are quite dense (see for example [30, 237]), the implementational studies of these systems both nu-

merically and in comparison to experimental systems remain relatively sparse. One of the reasons for this, is that reaction-diffusion systems that display complicated chemical kinetics do not satisfy a strict mass conservation property, due to the fact that the components of the flow field have different molecular weights. That is to say, up to the limiting reagent of the reaction, the conservation of atoms in the system does not, strictly speaking, lead to a conservation of mass in the system (though the continuity equation is still satisfied) (see [45]). In addition, the reaction kinetics often occur on substantially different time-scales than the transport dynamics (e.g. such as in a wind-blown spreading flame [238]).

Because of these complicating features that emerge in reactor systems, robust compressible flow models are often required which introduce sophisticated and state-of-the-art applied mathematical and numerical models (see Ref. [47, 66, 69, 134, 184]). Generally, the goal in these fields is to model accurately, consistently, stably and efficiently, reaction dynamics of systems which can accommodate “as much” chemistry and physics as possible.

In this spirit, we introduce a generalized approach to modeling chemical reactors, or reaction-diffusion systems. Our models are largely inspired by Ref. [30, 46, 237, 239, 240]. We find for our explicit examples, that the present approach satisfies the above mentioned conditions, in that they are remarkably stable, accurate, and consistent. The fact that we use the discontinuous Galerkin finite element method additionally makes them – up to parallelization – quite efficient. We obtain the stability in the reaction dynamics by using a novel approach to modeling the reaction parameter; which makes use of solving an ordinary differential equation locally in time for a reaction of arbitrary order. The accuracy follows from the analysis given on the viscous

and inviscid fluxes in chapter 3, and the consistency follows from the fact that our system is mathematically well-posed (up to a source term) as presented in chapter 2.

In §5.2 we present, in some sense, the simplest possible case of a stationary reactor. We present the general solution to these types of problems, and then show explicitly how one may implement this for a given reaction. In §5.3 we expand upon this formalism to include general compressible flow reactors, where we use for simplicity a barotropic pressure law (leading to an isentropic reactive flow equation). Here again we show how to implement this system for a set of examples. Finally, in §5.4 we show how to implement the solutions from §5.2 and §5.3 in higher dimensions.

## 5.2 Basic Stationary Chemical Reactors

Consider the stationary reaction-diffusion system comprised of  $i = 1, \dots, n$  species in one spatial dimension:

$$\begin{aligned} \partial_t \alpha_i - \partial_x (\mathcal{D}_i(\alpha) \partial_x \alpha_i) &= \mathcal{A}_i(\alpha), \\ \mathcal{A}_i(\alpha) &= (\xi_i - \eta_i) \left( k_f \prod_{i=1}^n \alpha_i^{\eta_i} - k_b \prod_{i=1}^n \alpha_i^{\xi_i} \right), \end{aligned} \quad (5.1)$$

with initial conditions

$$\alpha_i(t = 0) = \alpha_{i,0}.$$

Here  $\alpha_i$  is the concentration of the  $i$ -th chemical constituent, the  $\mathcal{D}_i$  are the interspecies diffusion coefficients, and  $\eta_i$  and  $\xi_i$  are the stoichiometric coefficients.

We use the discontinuous Galerkin method here (see Chapter 3 for notation). We thus multiply by a DG test function  $\varphi_h$  locally over elements

$\mathcal{G}_i$  and integrate in space, such that

$$\frac{d}{dt} \int_{\mathcal{G}_i} \varphi_h \alpha_i dx - \int_{\mathcal{G}_i} \varphi_h \partial_x (\mathcal{D}_i(\alpha) \partial_x \alpha_i) dx = \int_{\mathcal{G}_i} \varphi_h \mathcal{A}_i(\alpha) dx. \quad (5.2)$$

The first and second term on the left comprise the usual parabolic system from chapter 2.

Here we solve the reactions by exact integration, which serves as a replacement for the approximate forward Euler step for this piece. That is, we solve (5.1) in two steps, first we analytically solve the ODE for the parts containing the  $i$ -th component of  $\alpha$ . That is, for the  $i$ -th component  $\alpha_i$  let the terms of  $\mathcal{A}_i(\alpha)$  which contain factors of  $\alpha_i$  — which is either in the reactant or product well — be denoted by  $\mathring{\mathcal{A}}_i(\alpha)$ , and the remaining terms be denoted by  $\tilde{\mathcal{A}}_i(\alpha)$ , such that:

$$\mathcal{A}_i(\alpha) = \mathring{\mathcal{A}}_i(\alpha) + \tilde{\mathcal{A}}_i(\alpha), \quad \text{where} \quad \frac{\partial \tilde{\mathcal{A}}_i}{\partial \alpha_i} = 0.$$

Then we define  $\check{\alpha}_i$  as the solution to the following ODE,

$$\partial_t \check{\alpha}_i = \mathring{\mathcal{A}}_i(\alpha), \quad (5.3)$$

and using explicit integration find the rate of change locally in time, which upon plugging back into  $\mathcal{A}_i(\alpha)$  is used to solve:

$$\partial_t \alpha_i - \partial_x (\mathcal{D}_{ij}(\alpha) \partial_x \alpha_i) = \mathcal{A}_i(\alpha), \quad (5.4)$$

using the usual DG methodology.

Now we are ready to solve (5.4). Let the  $\alpha_i$ 's be classical solutions to (5.1). Multiplying by test functions  $\varphi_h$  and  $\vartheta_h$ , and integrating in  $x$  then yields:

$$\begin{aligned} \frac{d}{dt} \int_{\mathcal{G}_i} \varphi_h \alpha_i dx - \int_{\mathcal{G}_i} \varphi_h \partial_x (\mathcal{D}_i(\alpha) \partial_x \alpha_i) dx &= \int_{\mathcal{G}_i} \varphi_h \mathcal{A}_i(\alpha) dx, \\ \int_{\mathcal{G}_i} \sigma_i \vartheta_h dx - \int_{\mathcal{G}_i} (\alpha_{i,h} \vartheta_h)_x dx + \int_{\mathcal{G}_i} \alpha_{i,h} \vartheta_x^h dx &= 0. \end{aligned} \quad (5.5)$$

Index	Species	Viscosity/Pa · s	Mass Diffusion/cm <sup>2</sup> · s <sup>-1</sup>
$\alpha_1$	MMH	$\sim 1.0 \times 10^{-4}$	$\sim 5.9 \times 10^{-6}$ (1)
$\alpha_2$	CH <sub>2</sub> N <sub>2</sub> H <sub>2</sub>	$\sim 9.0 \times 10^{-5}$	$\sim 5.0 \times 10^{-6}$
$\alpha_3$	NO <sub>2</sub>	$\sim 14.9 \times 10^{-6}$ (2)	$\sim 9.0 \times 10^{-2}$ (3)
$\alpha_4$	HNO <sub>2</sub>	$\sim 2.0 \times 10^{-5}$	$\sim 1.2 \times 10^{-2}$ (4)

Table 5.1: All approximate values given at STP. (1) was measured via chronoamperometry as shown in Ref. [241]. (2) was measured using oscillating disc viscometry in Ref. [242]. (3) was determined via the single component Chapman-Enskog experimental fits in Ref. [243]. (4) was calculated using diffusion denuders in Ref. [244]. The remaining approximate coefficients are adapted using relative magnitude arguments from simple collisional theory [12] (viz.  $\nu \propto m$  and  $\mathcal{D} \propto \sigma^{-1}$ ).

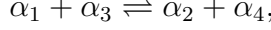
Replacing the viscous term from chapter 2 with the mass diffusion term on the right in (5.5), we may define an approximate solution to (5.5) as functions  $\alpha_{i,h}$  and  $\sigma_h$  for all  $t \in (0, T)$  satisfying:

$$\begin{aligned}
& 1) \ \alpha_{i,h} \in C^1([0, T]; S_h^d), \quad \sigma_h \in S_h^d, \\
& 2) \ \frac{d}{dt}(\alpha_{i,h}, \varphi_h)_{\Omega_g} - \mathcal{G}(\sigma_h, \alpha_{i,h}, \varphi_h) + \mathcal{N}(\sigma_h, \alpha_{i,h}, \varphi_h) \\
& \quad = (\mathcal{A}_{i \neq k}(\alpha_h), \varphi_h)_{\Omega_g} + (\mathcal{A}_k(\alpha_h), \varphi_h)_{\Omega_g}, \\
& 3) \ \mathcal{Q}(\hat{\alpha}, \sigma_h, \alpha_{i,h}, \vartheta_h, \vartheta_x^h) = 0, \\
& 4) \ \alpha_{i,h}(0) = \alpha_{i,0}.
\end{aligned} \tag{5.6}$$

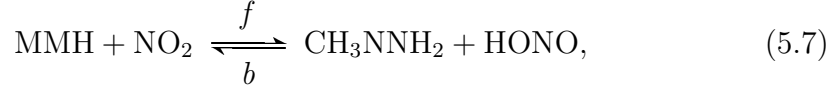
This solution follows for all reactions schemes of arbitrary order which satisfy the *law of mass action* (5.1), whether or not the reactions in  $\mathcal{A}_i(\alpha)$  are elementary.

Let us make this explicit. First consider the second order hypergolic

ignition reaction,



of monomethylhydrazine  $\alpha_1 = \text{MMH} = \text{CH}_3\text{N}_2\text{H}_3$  with nitrogen dioxide  $\alpha_3 = \text{NO}_2$ , given exhaust radical  $\alpha_2 = \text{CH}_3\text{N}_2\text{H}_2$  and nitrous acid  $\alpha_4 = \text{HONO}$ ,



with forward reaction rate (see Ref. [245]):

$$f = k_f = 2.2 \times 10^{11} e^{-5900/R\vartheta} \text{cm}^3(\text{mol} \cdot \text{s})^{-1},$$

where  $\vartheta$  is the temperature at which the reaction occurs and  $R$  is the ideal gas constant in  $\text{cal} \cdot \text{K}^{-1} \text{mol}^{-1}$ . It follows then for  $\alpha_1, \alpha_2, \alpha_3$  and  $\alpha_4$ , that (5.3) becomes:

$$\begin{aligned} \partial_t[\text{MMH}] &= -f[\text{MMH}][\text{NO}_2], & \partial_t[\text{CH}_3\text{N}_2\text{H}_2] &= -b[\text{CH}_3\text{N}_2\text{H}_2][\text{HONO}], \\ \partial_t[\text{NO}_2] &= -f[\text{NO}_2][\text{MMH}], & \partial_t[\text{HONO}] &= -b[\text{HONO}][\text{CH}_3\text{N}_2\text{H}_2]. \end{aligned} \quad (5.8)$$

Since a hypergolic ignition is far from equilibrium  $b = k_b$  is effectively zero in the back reaction, and it will thus be neglected.

Now we discretize in time, denoting a partition of  $[0, T]$  by

$$0 = t^0 < t^1 \dots < t^T = T,$$

for a timestep given as  $\Delta t^n = t^{n+1} - t^n$ . Solving the ordinary differential equations from (5.8) via integration over discrete timesteps then yields the two equations:

$$\begin{aligned} [\text{MMH}(t^{n+1})] &= [\text{MMH}(t^n)] e^{-k_f \Delta t [\text{NO}_2]}, \\ [\text{NO}_2(t^{n+1})] &= [\text{NO}_2(t^n)] e^{-k_f \Delta t [\text{MMH}]}. \end{aligned}$$

However, for ignition reactions, thermal explosions and detonations, which are characterized by shock front propagation and inhomogeneous catalytic expansion, a mass transfer correction  $h_m \in \mathbb{R}$  may be added to the rate constant  $k_f$

(see Ref. [46]), since if such a term is not added, the timestep  $\Delta t$  needed to resolve the solution in bulk concentrations scales inversely with the Arrhenius factor  $\Delta t \sim k_f^{-1}$ , which makes solving in units of cubic centimeters and grams untenable over semiclassical timescales.

This correction-based formulation yields in general that

$$\mathcal{A}_i(\alpha) = (\xi_i - \eta_i) \left( \{k_f + h_m\} \prod_{i=1}^n \alpha_i^{\eta_i} - k_b \prod_{i=1}^n \alpha_i^{\xi_i} \right), \quad (5.9)$$

which provides in our context that,

$$\begin{aligned} [\text{MMH}(t^{n+1})] &= [\text{MMH}(t^n)] e^{-\{k_f + h_m\} \Delta t [\text{NO}_2]}, \\ [\text{NO}_2(t^{n+1})] &= [\text{NO}_2(t^n)] e^{-\{k_f + h_m\} \Delta t [\text{MMH}]}, \end{aligned}$$

which is the new values of  $\alpha_1$  and  $\alpha_3$  at timestep  $t^{n+1}$ . Thus to find the rate of change of  $\alpha_1$  and  $\alpha_3$  at timestep  $t^{n+1}$  requires us to calculate the difference in the concentration from the previous timestep, which is to say generally that for  $i = 1, 3$  and  $\hat{i} = 3, 1$  its complementary reagent,

$$\alpha_i^{n+1} = \left( \alpha_i^n e^{-\{k_f + h_m\} \Delta t \alpha_{\hat{i}}^n} - \alpha_i^n \right),$$

or more explicitly, that we solve for

$$\begin{aligned} [\text{MMH}(t^{n+1})] &= [\text{MMH}(t^n)] \left( e^{-\{k_f + h_m\} \Delta t [\text{NO}_2]} - 1 \right), \\ [\text{NO}_2(t^{n+1})] &= [\text{NO}_2(t^n)] \left( e^{-\{k_f + h_m\} \Delta t [\text{MMH}]} - 1 \right). \end{aligned} \quad (5.10)$$

Generally, in a catalytic expansion of the local volume element, which occurs in an ignition reaction such as (5.7), the mass transport correction  $h_m$  is needed to account for the substantial impact of thermal conduction and diffusion, both of which have a functional dependency on the local temperature gradient of the flow field. In §5.3 we will require such a term in order to model



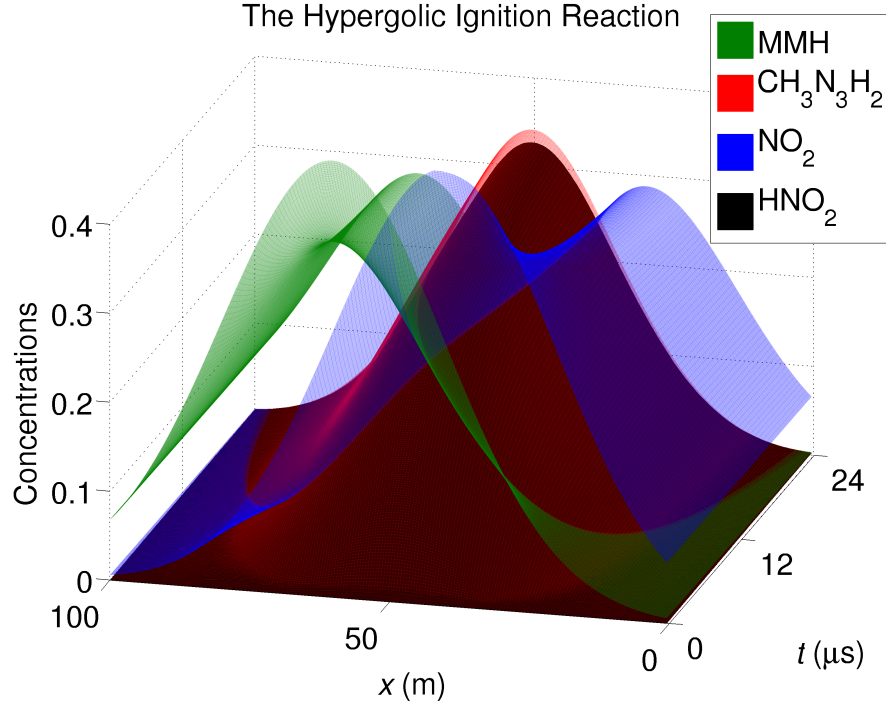


Figure 5.1: We show the hypergolic ignition reaction from 5.7, where initial conditions are given by  $\alpha_{1,0} = 0.49 \exp\left(-\frac{(x-60)^2}{800}\right)$ ,  $\alpha_{2,0} = 1 \times 10^{-5}$ ,  $\alpha_{3,0} = 0.49 \exp\left(-\frac{(x-40)^2}{800}\right)$  and  $\alpha_{4,0} = 1 \times 10^{-5}$ , where transmissive boundaries are used.

high pressure shockwaves. Here, on the other hand, we may simply convert to units of meters and kilograms which allows for stable solutions in  $\mu\text{s}$ , and thus set  $h_m \equiv 0$  for each of our following graphs.

Now we incorporate this analytic correction (i.e. the local solution to (5.10)) into our discontinuous Galerkin scheme. That is, our approximate

solution is formulated to verify: for every  $n \geq 0$  find  $\alpha_{i,h}^{n+1}$  such that:

$$\begin{aligned}
1) \quad & \alpha_{i,h} \in S_h^d, \quad \sigma_h \in S_h^d, \\
2) \quad & \left( \frac{\alpha_{i,h}^{n+1} - \alpha_{i,h}^n}{\Delta t}, \varphi_h \right)_{\Omega_g} + \mathcal{N}(\sigma_h^n, \alpha_{i,h}^n, \varphi_h) - \mathcal{G}(\sigma_h^n, \alpha_{i,h}^n, \varphi_h) \\
& = \left( \tilde{\mathcal{A}}_i(\alpha_h^n), \varphi_h \right)_{\Omega_g} + \frac{1}{\Delta t} \left( \alpha_{i,h}^n e^{-\{k_f+h_m\}\Delta t \alpha_{i,h}^n} - \alpha_{i,h}^n, \varphi_h \right)_{\Omega_g}, \\
3) \quad & \mathcal{Q}(\hat{\alpha}, \sigma_h^n, \alpha_{i,h}^n, \vartheta_h, \vartheta_x^h) = 0, \\
4) \quad & \alpha_{i,0}^h = \alpha_{i,h}(0).
\end{aligned} \tag{5.11}$$

It remains to set the mass diffusion coefficients. The most straightforward way of choosing these  $\mathcal{D}_i$ , is by setting them equal to experimentally determined constants, in which case one may make the additional assumption of pure diffusion, where interspecies diffusion is neglected. In this case the  $\mathcal{D}_i$  reduces to a vector of positive constants,  $\mathcal{D}_i \in \mathbb{R}^+$ . The diffusion coefficients generally occur on a timescale which is significantly slower than the reaction kinetics, in which case their effects are relatively negligible on the dynamics of the stationay solver. Setting the transmissive boundary conditions

$$\mathbf{U}_h^n|_{\mathcal{K}_{ji}} = \mathbf{U}_h^n|_{\mathcal{K}_{ij}}, \tag{5.12}$$

we solve (5.11) for (5.7), and show a graph of the solution in Figure (5.1) using the diffusion constants from Table 5.2, where the initial conditions are given in the figure caption.

However, the diffusion constants may obey complicated dynamics, in which case functional dependencies may be established, such that, for example  $\mathcal{D}_{ij} = \mathcal{D}_{ij}(\alpha, \vartheta)$  for  $\vartheta$  the temperature at which the reaction occurs (thus constant in the isothermal approximation). These may be determined in a number of different ways, including empirically, using basic collisional theory

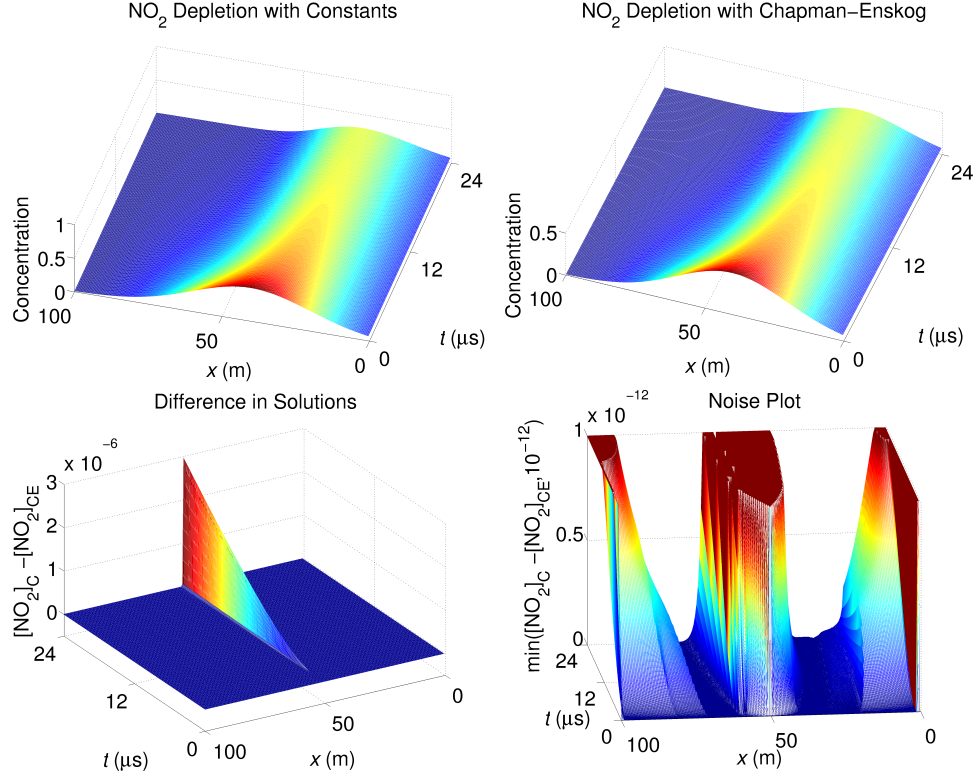


Figure 5.2: The top graphs compare solutions to  $\alpha_3$  with respect to the constant vector  $\mathcal{D}_i$  (on the top left), and the Chapman-Enskog matrix  $\mathcal{D}_{ij}$  (on the top right). The bottom left is a difference map between these two solutions, and the bottom right shows the noise occurring near both the reagent interfaces and near the (*weak entropy*) boundary of the domain,  $\partial\Omega$ .

arguments, or more complicated functional relationships, such as the Stokes-Einstein relation or applying the fluctuation dissipation theory. In any case, the coefficients  $\mathcal{D}_i$  are the row sums over the matrices  $\mathcal{D}_{ij}$ , which is just to say that

$$\mathcal{D}_i = \sum_{j=1}^n \mathcal{D}_{ij}.$$

Let us present functional forms for the mass diffusion, as discussed and

derived in Ref. [30, 31] that arise from the Chapman-Enskog theory of gases. That is, recall that the mass fraction of the  $j$ -th component  $\mu_j$  may be written as  $\mu_j / \sum_i \mu_i$ , such that with respect to the *specific volume*  $\rho^{-1}$  the *total molar concentration* of the mixture  $\tilde{n}$  is given in terms of the *specific molecular weight* of each component  $M_i$ , which yields:

$$\tilde{n} = \sum_i^n \tilde{n}_i = \sum_i^n \mu_i / M_i, \quad (5.13)$$

providing a formula for the molar fraction of the  $j$ -th component of the mixture,  $x_j = \tilde{n}_j / \tilde{n}$ . Then we use the following multicomponent form:

$$\mathcal{D}_{ij} = \left( \frac{1}{M_j} \sum_k x_k M_k \right) \frac{K^{ji} - K^{ii}}{|K|}, \quad (5.14)$$

where the cofactor matrices are given by:

$$K^{ji} = (-1)^{i+j} \begin{vmatrix} 0 & \dots & K_{1,i-1} & K_{1,i+1} & \dots & K_{1,n} \\ \vdots & & \vdots & \vdots & & \vdots \\ K_{j-1,1} & \dots & K_{j-1,i-1} & K_{j-1,i+1} & \dots & K_{j-1,n} \\ K_{j+1,1} & \dots & K_{j+1,i-1} & K_{j+1,i+1} & \dots & K_{j+1,n} \\ \vdots & & \vdots & \vdots & & \vdots \\ K_{n,1} & \dots & K_{n,i-1} & K_{n,i+1} & \dots & 0 \end{vmatrix} \quad (5.15)$$

with entries satisfying,

$$K_{ij} = \frac{x_i}{[\mathcal{D}_{ij}]} + \frac{M_j}{M_i} \sum_{k \neq i} \frac{x_k}{[\mathcal{D}_{ik}]} \text{ if } i \neq j, \quad \text{and zero when } i = j,$$

such that the binary mixtures are set componentwise via,

$$[\mathcal{D}_{ij}] = C_{\mathcal{D}_{ij}} p^{-1} \sqrt{\vartheta^3 (M_i + M_j) / 2 M_i M_j}$$

with empirical binary constants  $C_{\mathcal{D}_{ij}}$ , which may be found semi-explicitly in terms of the reduced temperature of the mixture  $T_{12}^*$ , a measure of the first

order deviation from the idealized rigid sphere model  $\Omega_{1,2}^{(1,1)}$ , and the cross section radius  $\sigma_{1,2}$ , such that:

$$C_{\mathcal{D}_{ij}} = \left( \frac{0.0026280}{\sigma_{1,2}^2 \Omega_{1,2}^{(1,1)} T_{12}^*} \right).$$

Further note that 5.14 can be written using the classical adjoint matrix in order to save significant computational time, so that we obtain the functional scalar valued diffusion mixture:

$$\mathcal{D}_{ij} = \left( \frac{1}{M_j} \sum_k x_k M_k \right) (K^{-1})_{ij} - (K^{-1})_{ii}, \quad (5.16)$$

where  $(K^{-1})_{ij}$  represents the  $ij$ -th entry of the full rank inverse matrix  $K^{-1}$ .

We now compare solutions from setting the constant vector  $\mathcal{D}_i$ , with those obtained from using the Chapman-Enskog treatment giving each component  $\mathcal{D}_{ij}$  separately. Again using the transmissive boundary conditions we solve (5.11) using both these mass diffusion treatments. Graphs of the differences are plotted in Figure 5.2. As can be readily observed, the Chapman-Enskog treatment leads to diffuse stability at the interface between reagent crossings, which is to say that the mixing greatly reduces the effective diffusivity at the point where the concentrated reagents cross. This is due to the fact that the Chapman-Enskog theory effectively “mixes,” or averages in a weighted sense, the componentwise diffusivities where they overlap, while the constant treatment effectively sums them.

### 5.3 Basic Flow Reactors

When the reactions occur along a compressible flow reactor, then in one dimension the system of equations in (5.1), become:

$$\begin{aligned}
\partial_t \rho + \partial_x(\rho u) &= 0, \\
\partial_t(\rho u) + \partial_x(\rho u^2) + \partial_x p - \partial_x(\nu(\rho, \mu) \partial_x u) &= 0, \\
\partial_t(\rho \mu_i) + \partial_x(\rho \mu_i u) - \partial_x(\mathcal{D}_i(\rho, \mu) \partial_x \mu_i) &= \mathcal{A}_i(\rho \mu), \\
\mathcal{A}_i(\rho \mu) &= (\xi_i - \eta_i) \left( k_f \prod_{i=1}^n (\rho \mu_i)^{\eta_i} - k_b \prod_{i=1}^n (\rho \mu_i)^{\xi_i} \right),
\end{aligned} \tag{5.17}$$

with initial conditions,

$$\rho|_{t=0} = \rho_0 > 0, \quad \rho u|_{t=0} = m_0, \quad (\rho \mu_i)|_{t=0} = \rho_{i,0}.$$

The barotropic pressure  $p = p(\rho \mu_1, \dots, \rho \mu_n)$  is chosen to satisfy,

$$p = \sum_{i=1}^n (\rho \mu_i)^{\gamma_i}, \tag{5.18}$$

where  $\sum_{i=1}^n \mu_i = 1$ , and using  $\rho_i = \rho \mu_i$ , the form of the viscosity functional  $\nu = \nu(\rho_1, \dots, \rho_n)$  is fixed to satisfy

$$\nu = \psi'(p) \sum_{i=1}^n \rho_i \partial_{\rho_i} p, \tag{5.19}$$

for  $\psi'(p) = Cp^{-\alpha}$  given  $\alpha \in (0, 1)$  and  $C > 0$  as empirically determined constants.

As shown in equation (3.10) in chapter 2, we can express our system as

$$\begin{aligned}
\mathbf{U}_t + \mathbf{\Gamma} \mathbf{U}_x - (\mathcal{K} \mathbf{U}_x)_x &= \mathbf{S}, \\
\mathbf{\Sigma} - \mathbf{U}_x &= 0,
\end{aligned} \tag{5.20}$$

where  $\mathbf{U}$  and  $\mathbf{\Gamma}$  remain unchanged, while the dissipative flux matrix  $\mathcal{K}$  is now characterized by

$$\mathcal{K} = \frac{1}{\rho} \begin{pmatrix} 0 & 0 & \dots & \dots & \dots & 0 \\ -\nu u & \nu & \dots & \dots & \dots & 0 \\ -\mathcal{D}_1 \mu_1 & 0 & \mathcal{D}_1 & 0 & \dots & 0 \\ -\mathcal{D}_2 \mu_2 & \vdots & 0 & \mathcal{D}_2 & \ddots & \vdots \\ \vdots & \vdots & \vdots & \ddots & \ddots & 0 \\ -\mathcal{D}_n \mu_n & 0 & 0 & \dots & 0 & \mathcal{D}_n \end{pmatrix}, \quad (5.21)$$

and the source term  $\mathbf{S}$  is given by

$$\mathbf{S} = (0, 0, \mathcal{A}_1(\alpha), \dots, \mathcal{A}_n(\alpha))^T,$$

such that it splits in the same way as the  $\mathcal{A}_i$ 's, which is just to say that  $\mathbf{S} = \mathring{\mathbf{S}} + \tilde{\mathbf{S}}$ .

Then recasting (5.6) in the setting of §5.2, we can define an approximate solution to the weak form of (5.20) as functions  $\mathbf{U}_h$  and  $\mathbf{\Sigma}_h$  for all  $t \in (0, T)$  satisfying:

- 1)  $\mathbf{U}_h \in C^1([0, T]; S_h^d)$ ,  $\mathbf{\Sigma}_h \in S_h^d$ ,
- 2)  $\frac{d}{dt}(\mathbf{U}_h, \boldsymbol{\varphi}_h)_{\Omega_{\mathcal{G}}} + \tilde{\Phi}(\mathbf{U}_h, \boldsymbol{\varphi}_h) - \Theta(\mathbf{U}_h, \boldsymbol{\varphi}_h) - \mathcal{G}(\mathbf{\Sigma}_h, \mathbf{U}_h, \boldsymbol{\varphi}_h) + \mathcal{N}(\mathbf{\Sigma}_h, \mathbf{U}_h, \boldsymbol{\varphi}_h) = (\mathbf{S}_h, \boldsymbol{\varphi}_h)_{\Omega_{\mathcal{G}}}, \quad (5.22)$
- 3)  $\mathcal{Q}(\hat{\mathbf{U}}, \mathbf{\Sigma}_h, \mathbf{U}_h, \boldsymbol{\vartheta}_h, \boldsymbol{\vartheta}_x^h) = 0$ ,
- 4)  $\mathbf{U}_h(0) = \mathbf{U}_0$ .

We may now use this to solve for the hypergolic flow reaction (5.7), such that upon discretizing in time and applying of the local Lax-Freidrich's

flux, a solution is obtained such that: for every  $n \geq 0$  find  $\mathbf{U}_h^{n+1}$  such that

$$\begin{aligned}
& 1) \mathbf{U}_h^n \in S_h^d, \quad \boldsymbol{\Sigma}_h^n \in S_h^d, \\
& 2) \left( \frac{\mathbf{U}_h^{n+1} - \mathbf{U}_h^n}{\Delta t^n}, \boldsymbol{\varphi}_h \right)_{\Omega_g} + \tilde{\Phi}_{lLF}(\mathbf{U}_h^n, \boldsymbol{\varphi}_h) - \Theta(\mathbf{U}_h^n, \boldsymbol{\varphi}_h) \\
& \quad - \mathcal{G}_b(\boldsymbol{\Sigma}_h^n, \mathbf{U}_h^n, \boldsymbol{\varphi}_h) + \mathcal{N}(\boldsymbol{\Sigma}_h^n, \mathbf{U}_h^n, \boldsymbol{\varphi}_h) = \left( \mathring{\mathbf{S}}_h^n + \tilde{\mathbf{S}}_h^n, \boldsymbol{\varphi}_h \right)_{\Omega_g}, \quad (5.23) \\
& 3) \mathcal{Q}(\hat{\mathbf{U}}_{RB}, \boldsymbol{\Sigma}_h^n, \mathbf{U}_h^n, \boldsymbol{\vartheta}_h, \boldsymbol{\vartheta}_x^h) = 0, \\
& 4) \mathbf{U}_0^h = \mathbf{U}_h(0).
\end{aligned}$$

Now we can solve (5.23) up to a choice of initial-boundary data. Consider the initial conditions from Figure 5.1 on the mass fractions  $\mu_i$  for  $i = 1, \dots, 4$ , with

$$\rho = 200,000 \text{ kg/Vol},$$

corresponding to an approximate initial pressure of  $\sim 6$  MPa or  $\sim 60$  atm, and given the initial velocity

$$u_0 = 5 \times 10^{-5} \sin\left(\frac{2\pi x}{50}\right) \text{ m}/\mu\text{s},$$

where the viscosity coefficient  $C$  is the average

$$C = \frac{1}{4} \sum_{i=1}^4 (\nu_{\text{approx},i}),$$

from Table 5.2, and again we choose the vector of constants  $\mathcal{D}_i$  as in Figure 5.1. Here, and in the rest of this section, we set the mass transfer correction (as discussed above) to  $h_m \approx -0.9k_f$  in order to rescale solutions in  $\mu\text{s}$ .

Next, we use *weak entropy* boundary conditions, as discussed in chapter 2, and set the transmissive conditions,

$$\rho_h^n|_{\mathcal{K}_{ji}} = \rho_h^n|_{\mathcal{K}_{ij}} \quad \text{and} \quad \mu_{h,i}^n|_{\mathcal{K}_{ji}} = \mu_{h,i}^n|_{\mathcal{K}_{ij}},$$



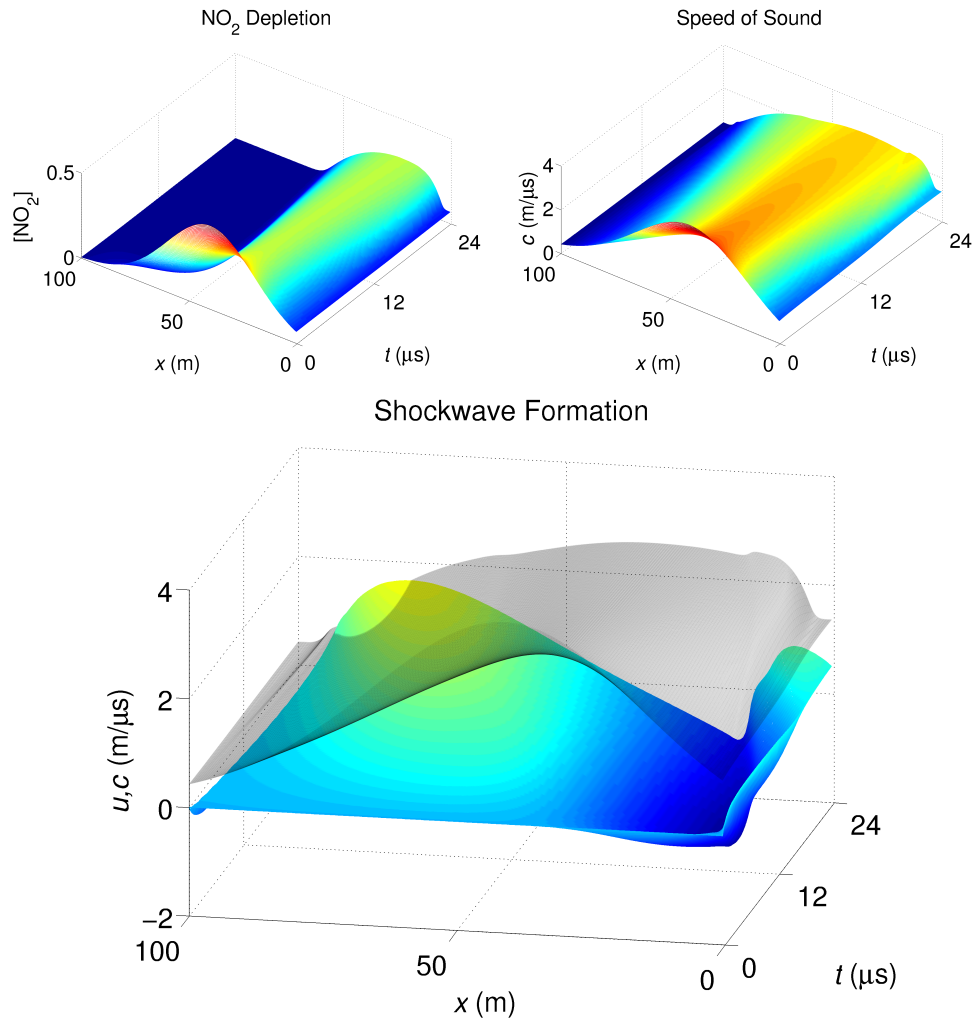


Figure 5.3: The top left graph shows the depletion of the nitrous dioxide, the compound with the largest heat capacity index as approximated by the ideal gas assumption. Hence, the speed of sound is highest in the region of highest NO<sub>2</sub> concentration, as seen in the top right graph. The bottom graph shows that the velocity field  $u$  (*color*) breaks through the speed of sound (*light grey*) in the region containing MMH, causing a shock front to propagate through the solution.

with velocity inlets corresponding to:

$$u_h^n(x=0) = 0.5 \text{ m}/\mu\text{s} \quad \text{and} \quad u_h^n(x=100) = -0.5 \text{ m}/\mu\text{s}.$$

The specific heat capacities are approximated using  $C_v = fR/2$ , for  $f = 3N$  the degrees of freedom of the molecule. Then the ideal gas assumption  $C_p = C_v + R$  is used to calculate  $\gamma = C_p/C_v$ . We show the results in Figure 5.3, where the dynamics of the velocity  $u = u(t, x)$  and pressure  $p = p(t, x)$  cause substantial perturbations in the solution space – leading to shockwaves and increased mixing of the components of the flow.

Let us briefly discuss the origin, from a physical standpoint, of the viscosity functional  $\nu$ . If we replace the constants  $\alpha$  and  $C$  with the standard first approximation (see Ref. [30]):

$$C = C_\nu \vartheta^s \tag{5.24}$$

where  $s \in (0, 1)$  is the empirically determined *temperature index* that takes the place of  $\alpha$ , and  $C_\nu$  is chosen to conform to some temperature dependency; for example, the so-called *Sutherland* form leads to

$$C_{\nu S} = k_{\nu S} / (1 + S/\vartheta),$$

where  $S$  is Sutherland's constant and  $C_{\nu J}$  and  $k_{\nu S}$  are empirically determined. This then leads to the multicomponent viscosity of a mixture (see Ref. [30]), which, upon using the identities associated with 5.13, in the bulk limit gives:

$$\nu_{\text{mix}} = \sum_{i=1}^n \left[ x_i^2 / \left( x_i^2 \nu + C_\nu \sum_{k \neq i} x_i x_k \frac{R\vartheta}{pM_i[\mathcal{D}_{ik}]} \right) \right], \tag{5.25}$$

for  $C_\nu = 1.385$  as determined by collisional analysis (See Ref. [30]). This form of the viscosity is substantially less stable numerically than (5.19), though

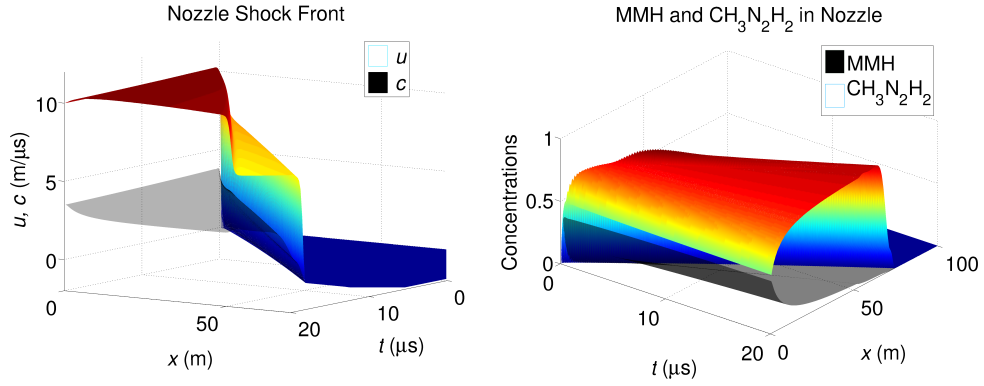


Figure 5.4: Here we show the supersonic nozzle with a propagating hypergolic reaction mechanism.

of a similar form. That is, both formulations can be seen to satisfy Einstein's more general form (see Ref. [30, 246–248]) that may be given as  $\nu_{\text{mix}} = \nu + C_\nu \varphi$ , where  $\varphi = \varphi(\nu_1, \dots, \nu_n, \rho, \vartheta, \mu_1, \dots, \mu_n)$  is a state dependent function. In fact, from this it is clear that the functional form from (5.19),  $\nu_{\text{mix}} = \psi'(p) \sum_{i=1}^n \rho_i \partial_{\rho_i} p$ , alternatively satisfies the Einstein relation, and has the effect of substantially increasing the stability of the system.

Finally let us show a supersonic nozzle with hypergolic reaction kinetics. That is, set the initial conditions homogeneous in the domain, such that the mass fractions satisfy  $\alpha_{i,0} = 10^{-5}$  for  $i = 1, \dots, 4$ , with all other initial conditions set as in Figure 5.3. The boundary conditions are set to satisfy:

$$\begin{aligned} \rho_h^n|_{\mathcal{K}_{ji}} &= \rho_h^n|_{\mathcal{K}_{ij}}, \quad \mu_{h,i}^{n+1}(x=0) = \mu_{h,i}^n(x=0), \\ \text{and } u_h^{n+1}(x=100) &= u_h^n(x=100), \end{aligned}$$

with a supersonic nozzle at the inlet:

$$\mu_{h,1,3}^{n+1}(x=0) = 0.45, \quad \mu_{h,2,4}^{n+1}(x=0) = 0.01 \quad \text{and} \quad u_h^{n+1}(x=0) = 10 \text{ m}/\mu\text{s}.$$

The solution is given in Figure 5.4, where the supersonic inlet is shown with

respect to the speed of sound, and the reaction kinetics from (5.7) are observed to travel along the edge of the shock front.

## 5.4 General Chemical Reactors

Consider the generalized barotropic flow reactor in arbitrary dimension  $N$ , with  $n$  chemical constituents:

$$\begin{aligned}\partial_t \rho + \nabla_x \cdot (\rho \mathbf{u}) &= 0, \\ \partial_t (\rho \mathbf{u}) + \nabla_x \cdot (\rho \mathbf{u} \otimes \mathbf{u}) + \nabla_x \cdot \mathbb{S} &= 0, \\ \partial_t (\rho \mu_i) + \nabla_x \cdot (\rho \mu_i \mathbf{u}) - \nabla_x \cdot (\mathcal{D}_i \nabla_x \mu_i) &= \mathcal{A}_i, \\ \mathcal{A}_i &= (\xi_i - \eta_i) \left( k_f \prod_{i=1}^n (\rho \mu_i)^{\eta_i} - k_b \prod_{i=1}^n (\rho \mu_i)^{\xi_i} \right),\end{aligned}\tag{5.26}$$

with initial conditions,

$$\rho|_{t=0} = \rho_0 > 0, \quad \rho \mathbf{u}|_{t=0} = \mathbf{m}_0, \quad (\rho \mu_i)|_{t=0} = \rho_{i,0},$$

and where the *stress tensor* satisfies

$$\mathbb{S} = p - 2hD(\mathbf{u}) - g\nabla_x \cdot \mathbf{u},\tag{5.27}$$

for  $h = h(\rho, \mu)$  the *shear viscosity*,  $g = g(\rho, \mu)$  the *bulk viscosity*, and the *strain tensor*  $D(\mathbf{u}) = \frac{1}{2}(\nabla_x \mathbf{u} + {}^t \nabla_x \mathbf{u})$ . Let us rewrite (5.27) componentwise via  $S_{ij} = p\delta_{ij} - \tau_{ij}$  where,

$$\tau_{ij} = h \left( \frac{\partial u_i}{\partial x_j} + \frac{\partial u_j}{\partial x_i} \right) + g \nabla_x \cdot \mathbf{u} \delta_{ij}.$$

It is important to note that in Ref. [249] the bulk viscosity  $g$  vanishes in the barotropic setting, though there is no reason to expect this to hold in general. That is, generally we may consider a shear viscosity  $h$  satisfying the

Einstein relation, as discussed above, where we can adapt the coefficient  $g$  via a computation similar to that shown in Ref. [36] to set  $g = 2(\rho\partial_\rho h - h)$  (where it should be noted that such a formulation is known not to satisfy the *second entropy inequailty*, as previously discussed).

Again using that  $\rho_i = \rho\mu_i$  with (5.18) and (5.19) we have the state vector

$$\mathbf{U} = (\rho, \rho u_1, \rho u_2, \rho u_3, \rho_1, \dots, \rho_n)^T,$$

the  $i = 1, \dots, 3$  inviscid flux vectors

$$\mathbf{f}_i = (\rho u_i, \rho u_1 u_i + p\delta_{1i}, \dots, \rho u_N u_i + p\delta_{Ni}, \rho_1 u_i, \dots, \rho_n u_i)^T, \quad (5.28)$$

such that the Jacobian splits into the following three matrices for  $N = 3$ :

$$\mathbf{\Gamma}_1 = \left( \begin{array}{cccc|ccc} 0 & 1 & 0 & 0 & 0 & \dots & 0 \\ -u_1^2 & 2u_1 & 0 & 0 & \partial_{\rho_1} p \delta_{11} & \dots & \partial_{\rho_n} p \delta_{11} \\ -u_2 u_1 & u_2 & u_1 & 0 & 0 & \dots & 0 \\ -u_3 u_1 & u_3 & 0 & u_1 & 0 & \dots & 0 \\ \hline -u_1 \mu_1 & \mu_1 & 0 & 0 & & & \\ \vdots & \vdots & \vdots & \vdots & & & \\ -u_1 \mu_n & \mu_n & 0 & 0 & & & \end{array} \right), \quad (5.29)$$

and

$$\mathbf{\Gamma}_2 = \left( \begin{array}{cccc|ccc} 0 & 0 & 1 & 0 & 0 & \dots & 0 \\ -u_2 u_1 & u_2 & u_1 & 0 & 0 & \dots & 0 \\ -u_2^2 & 0 & 2u_2 & 0 & \partial_{\rho_1} p \delta_{22} & \dots & \partial_{\rho_n} p \delta_{22} \\ -u_3 u_2 & 0 & u_3 & u_2 & 0 & \dots & 0 \\ \hline -u_2 \mu_1 & 0 & \mu_1 & 0 & & & \\ \vdots & \vdots & \vdots & \vdots & & & \\ -u_2 \mu_n & 0 & \mu_n & 0 & & & \end{array} \right), \quad (5.30)$$

and

$$\mathbf{\Gamma}_3 = \left( \begin{array}{cccc|ccc} 0 & 0 & 0 & 1 & 0 & \cdots & 0 \\ -u_3 u_1 & u_3 & 0 & u_1 & 0 & \cdots & 0 \\ -u_3 u_2 & 0 & u_3 & u_2 & 0 & \cdots & 0 \\ -u_3^2 & 0 & 0 & 2u_3 & \partial_{\rho_1} p \delta_{33} & \cdots & \partial_{\rho_n} p \delta_{33} \\ -u_3 \mu_1 & 0 & 0 & \mu_1 & & & \\ \vdots & \vdots & \vdots & \vdots & & & \\ -u_3 \mu_n & 0 & 0 & \mu_n & & & \end{array} \right) u_3 \mathbb{I}_n, \quad (5.31)$$

such that for  $i = 1, \dots, N$ , we have that  $\mathbf{\Gamma}_i \mathbf{U}_i = \mathbf{f}_{i,i}$ , where  $\mathbf{U}_i = \partial \mathbf{U} / \partial x_i$ .

Likewise we have the viscous flux vectors:

$$\mathbf{g}_i = (0, \tau_{i1}, \dots, \tau_{iN}, \mathcal{D}_1 \partial_{x_i} \mu_1, \dots, \mathcal{D}_n \partial_{x_i} \mu_n)^T$$

where setting  $\chi = 2h + g$ , the dissipative flux matrices  $\mathcal{K}_{i,l}$  in  $N = 3$  are:

$$\mathcal{K}_{1,1} = \frac{1}{\rho} \left( \begin{array}{cccccccc} 0 & 0 & \cdots & \cdots & \cdots & \cdots & \cdots & 0 \\ -\chi u_1 & \chi & 0 & 0 & \cdots & \cdots & \cdots & 0 \\ -h u_2 & 0 & h & 0 & \cdots & \cdots & \cdots & 0 \\ -h u_3 & 0 & 0 & h & \cdots & \cdots & \cdots & 0 \\ -\mathcal{D}_1 \mu_1 & 0 & 0 & 0 & \mathcal{D}_1 & 0 & \cdots & 0 \\ -\mathcal{D}_2 \mu_2 & \vdots & \ddots & \ddots & \ddots & \mathcal{D}_2 & \ddots & \vdots \\ \vdots & \vdots & \vdots & \ddots & \ddots & \ddots & \ddots & 0 \\ -\mathcal{D}_n \mu_n & 0 & 0 & \cdots & \cdots & \cdots & 0 & \mathcal{D}_n \end{array} \right), \quad (5.32)$$

$$\mathcal{K}_{1,2} = \frac{1}{\rho} \left( \begin{array}{cccc|c} 0 & 0 & 0 & 0 & \mathbf{0} \\ -g u_2 & 0 & g & 0 & \\ -h u_1 & h & 0 & 0 & \\ 0 & 0 & 0 & 0 & \\ \hline \mathbf{0} & & & & \mathbf{0} \end{array} \right), \quad (5.33)$$

$$\mathcal{K}_{1,3} = \frac{1}{\rho} \left( \begin{array}{cccc|c} 0 & 0 & 0 & 0 & \mathbf{0} \\ -g u_3 & 0 & 0 & g & \\ 0 & 0 & 0 & 0 & \\ -h u_1 & h & 0 & 0 & \\ \hline \mathbf{0} & & & & \mathbf{0} \end{array} \right), \quad (5.34)$$

$$\mathcal{K}_{2,1} = \frac{1}{\rho} \left( \begin{array}{cccc|c} 0 & 0 & 0 & 0 & \mathbf{0} \\ -hu_2 & 0 & h & 0 & \\ -gu_1 & g & 0 & 0 & \\ 0 & 0 & 0 & 0 & \\ \hline \mathbf{0} & & & & \mathbf{0} \end{array} \right), \quad (5.35)$$

$$\mathcal{K}_{2,2} = \frac{1}{\rho} \left( \begin{array}{cccccccc} 0 & 0 & \dots & \dots & \dots & \dots & \dots & 0 \\ -hu_1 & h & 0 & 0 & \dots & \dots & \dots & 0 \\ -\chi u_2 & 0 & \chi & 0 & \dots & \dots & \dots & 0 \\ -hu_3 & 0 & 0 & h & \dots & \dots & \dots & 0 \\ -\mathcal{D}_1 \mu_1 & 0 & 0 & 0 & \mathcal{D}_1 & 0 & \dots & 0 \\ -\mathcal{D}_2 \mu_2 & \vdots & \ddots & \ddots & \ddots & \mathcal{D}_2 & \ddots & \vdots \\ \vdots & \vdots & \vdots & \ddots & \ddots & \ddots & \ddots & 0 \\ -\mathcal{D}_n \mu_n & 0 & 0 & \dots & \dots & \dots & 0 & \mathcal{D}_n \end{array} \right), \quad (5.36)$$

$$\mathcal{K}_{2,3} = \frac{1}{\rho} \left( \begin{array}{cccc|c} 0 & 0 & 0 & 0 & \mathbf{0} \\ 0 & 0 & 0 & 0 & \\ -gu_3 & 0 & 0 & g & \\ -hu_2 & 0 & h & 0 & \\ \hline \mathbf{0} & & & & \mathbf{0} \end{array} \right), \quad (5.37)$$

$$\mathcal{K}_{3,1} = \frac{1}{\rho} \left( \begin{array}{cccc|c} -hu_3 & 0 & 0 & h & \mathbf{0} \\ 0 & 0 & 0 & 0 & \\ -gu_1 & g & 0 & 0 & \\ 0 & 0 & 0 & 0 & \\ \hline \mathbf{0} & & & & \mathbf{0} \end{array} \right), \quad (5.38)$$

$$\mathcal{K}_{3,2} = \frac{1}{\rho} \left( \begin{array}{cccc|c} 0 & 0 & 0 & 0 & \mathbf{0} \\ 0 & 0 & 0 & 0 & \\ -hu_3 & 0 & 0 & h & \\ -gu_2 & 0 & g & 0 & \\ \hline \mathbf{0} & & & & \mathbf{0} \end{array} \right), \quad (5.39)$$

$$\mathcal{K}_{3,3} = \frac{1}{\rho} \begin{pmatrix} 0 & 0 & \dots & \dots & \dots & \dots & \dots & 0 \\ -hu_1 & h & 0 & 0 & 0 & \dots & \dots & 0 \\ -hu_2 & 0 & h & 0 & \dots & \dots & \dots & 0 \\ -\chi u_3 & 0 & 0 & \chi & \dots & \dots & \dots & 0 \\ -\mathcal{D}_1 \mu_1 & 0 & 0 & 0 & \mathcal{D}_1 & 0 & \dots & 0 \\ -\mathcal{D}_2 \mu_2 & \vdots & \ddots & \ddots & \ddots & \mathcal{D}_2 & \ddots & \vdots \\ \vdots & \vdots & \vdots & \ddots & \ddots & \ddots & \ddots & 0 \\ -\mathcal{D}_n \mu_n & 0 & 0 & \dots & \dots & \dots & 0 & \mathcal{D}_n \end{pmatrix}, \quad (5.40)$$

where again the  $\mathbf{0}$ 's are zero matrices of appropriate size such that we may recover the  $\mathbf{g}_i$  for  $i = 1, \dots, 3$  by summing:

$$\mathbf{g}_i = \sum_{l=1}^N \mathcal{K}_{i,l} \mathbf{U}_l.$$

To proceed we must adapt our boundary fluxes to  $N$  dimensions. That is, the inviscid numerical flux  $\Phi_i$  is now given by:

$$\begin{aligned} \tilde{\Phi}_i(\mathbf{U}_h^n|_{\mathcal{K}_{ij}}, \mathbf{U}_h^n|_{\mathcal{K}_{ji}}, \boldsymbol{\varphi}_h) &= \sum_{j \in S(i)} \int_{\mathcal{K}_{ij}} \Phi(\mathbf{U}_h^n|_{\mathcal{K}_{ij}}, \mathbf{U}_h^n|_{\mathcal{K}_{ji}}, n_{ij}) \cdot \boldsymbol{\varphi}_h|_{\mathcal{K}_{ij}} d\mathcal{K} \\ &\approx \int_{\mathcal{K}_{ij}} \sum_{l=1}^N (\mathbf{f}_h^n)_l \cdot (n_{ij})_l \boldsymbol{\varphi}_h|_{\mathcal{K}_{ij}} d\mathcal{K}, \end{aligned} \quad (5.41)$$

for  $n_{ij}$  the unit outward pointing normal. Likewise, the general viscous flux becomes

$$\begin{aligned} \mathcal{G}_i(\boldsymbol{\Sigma}_h^n, \mathbf{U}_h^n, \boldsymbol{\varphi}_h) &= \int_{\mathcal{K}_{ij}} \hat{\mathcal{G}}(\boldsymbol{\Sigma}_h^n|_{\mathcal{K}_{ij}}, \boldsymbol{\Sigma}_h^n|_{\mathcal{K}_{ji}}, \mathbf{U}_h^n|_{\mathcal{K}_{ij}}, \mathbf{U}_h^n|_{\mathcal{K}_{ji}}, n_{ij}) \cdot \boldsymbol{\varphi}_h|_{\mathcal{K}_{ij}} d\mathcal{K} \\ &\approx \int_{\mathcal{K}_{ij}} \sum_{l=1}^N (\mathbf{g}_h^n)_l \cdot (n_{ij})_l \boldsymbol{\varphi}_h|_{\mathcal{K}_{ij}} d\mathcal{K}. \end{aligned} \quad (5.42)$$

And finally the numerical flux is given to satisfy:

$$\begin{aligned} \mathcal{Q}_i(\hat{\mathbf{U}}, \boldsymbol{\Sigma}_h^n, \mathbf{U}_h^n, \boldsymbol{\vartheta}_h, \boldsymbol{\vartheta}_x^h) &= \int_{\mathcal{G}_i} \boldsymbol{\Sigma}_h^n \cdot \boldsymbol{\vartheta}_h dx + \int_{\mathcal{G}_i} \mathbf{U}_h^n \cdot \boldsymbol{\vartheta}_x^h dx \\ &\quad - \sum_{j \in S(i)} \int_{\mathcal{K}_{ij}} \hat{\mathbf{U}}(\mathbf{U}_h^n|_{\mathcal{K}_{ij}}, \mathbf{U}_h^n|_{\mathcal{K}_{ji}}, \boldsymbol{\vartheta}_h|_{\mathcal{K}_{ij}}) d\mathcal{K}, \end{aligned} \quad (5.43)$$



with,

$$\begin{aligned}\mathcal{U}_i(\mathbf{U}_h^n, \boldsymbol{\vartheta}_h) &= \sum_{j \in S(i)} \int_{\mathcal{K}_{ij}} \hat{U}(\mathbf{U}_h^n|_{\mathcal{K}_{ij}}, \mathbf{U}_h^n|_{\mathcal{K}_{ji}}, \boldsymbol{\vartheta}_h|_{\mathcal{K}_{ij}}) d\mathcal{K} \\ &\approx \int_{\mathcal{K}_{ij}} \sum_{l=1}^N (\mathbf{U}_h^n)_l \cdot (n_{ij})_l \boldsymbol{\vartheta}_h|_{\mathcal{K}_{ij}} d\mathcal{K}.\end{aligned}$$

With these definitions in mind, the statement of the approximate solutions satisfies (5.22) in the general case, and upon discretizing, we may solve (5.7) in three dimensions which takes the same form as (5.23).

## Chapter 6

### Conclusions and Future Work

In Chapter 2 we developed a well-posedness argument for the flow of a compressible, miscible, viscous multicomponent fluid. We developed an existence theorem which relied heavily on the short time existence results of Solonnikov, in addition to the derivation of a novel multicomponent entropy inequality. It was found that this *second entropy inequality*, in tandem with the *classical entropy*, was enough to establish global in time  $L^2$  regularity of solutions. We then showed uniqueness of solutions using an application of Gronwall's lemma. We would like to extend these results to higher dimensional settings, to include more physics, such as energy conservation equations, electrodynamics, surface tension effects and turbulence.

In Chapter 3 we have shown an efficient and robust high-order numerical scheme for a mixing compressible barotropic viscous fluid comprised of up to  $n$  distinct components. We began by applying a discontinuous Galerkin method for spacial discretization. The solution was shown to be in very good agreement with two exact solutions derived by a choice of initial conditions, which only demonstrate minimal numerical error at the boundary points. The solution was then shown for two time-explicit schemes, the forward Euler and  $k$ -th order explicit Runge-Kutta schemes. Analysis of the method demonstrated the expected conditional stability up to a restriction by the CFL condition, and that the numerical scheme up to this stability parameter is energy

consistent; and in fact, that the energy consistency holds for a very large family of physically relevant problems. We further provided a large class of free boundary type solutions which are easily implemented, and which are numerically well-behaved. These two classes of boundary conditions were compared, and it was seen that indeed they demonstrate distinctly different behaviors even given (seemingly) equivalent initial data.

A number of examples and potential physical applications were shown and cited in Chapter 3 in order to develop a sense of the large number of applications of this method in chemistry, physics, engineering, and related fields. Future directions of the work include the addition of functional temperature  $\vartheta = \vartheta(t, x)$  dependence into the model (via the energy conservation equation), the addition of fluid-structure interfacing, and the expansion of the modelisation to include ionic and polar species as well as dense plasmas (magnetohydrodynamic effects), surface tensions and gravitational effects.

In Chapter 4 we have presented a numerical solution to the quantum hydrodynamic equations of motion as posited in the context of quantum hydrodynamics with chemical applications. Our approximate solution is rescaled in time from the usual QHD solutions, and is the first model of its type presented in a discontinuous continuous Galerkin or mixed method framework in the context in which it arises in chemical applications. Our solution further shows good stability, up to a *stiffness* of the system of equations which is a well-known feature of the QHD system of equations, and a scale invariance behavior which makes it very appealing for the so-called “fast and dirty computations” often needed in realistic chemistry applications. Additionally we have shown in a rigorous and consistent way how to prescribe proper boundary data, which is often bypassed in the usual Lagrangian formulations of the

system. We have further demonstrated that in the conservation formulation of this system, the *quantum wavefunction*  $\psi$  and *quantum action*  $S$ , which are used as motivation for the derivation of QHD systems to begin with (e.g. [20, 41, 214]), are in fact completely determined (up to a constant of integration) by the solutions  $\varrho$  and  $\mathbf{v}$ .

The solutions in Chapter 4 are very closely related to quantum hydrodynamic solutions which have been extensively studied in other fields (see [42, 215, 216, 220, 250]), but still maintain some important differences. One of the most important and prohibitive aspects of the quantum chemical formulation of QHD, is that the potential surface  $V$  arises from a multiple of  $3N$  degrees of freedom of each quantum subsystem, for  $N$  the number of atoms in each molecular subsystem (for example in an intramolecular rearrangement). This arises from the interpretation of the wavefunction  $\psi$  as being the foundational variable in the dynamics of the quantum subsystem in the chemical models. Clearly, even for relatively small molecules, this immediately leads to extremely difficult numerical problems. In this sense it is important to have a numerical scheme which is easily parallelizable, fast, robust and accurately reflects the mathematical character of the solution. The MDG formulation presented herein is a numerical method that fulfills these requirements, and offers a viable solution to some of the many difficulties which arise in the complicated solution space of chemical quantum hydrodynamics. The scale invariance of the solution makes it even an alternative approach to the Lagrangian formulation; up to the “formal” accuracy of solutions.

In Chapter 5 we have shown a robust, stable, consistent and accurate implementation of reactor models using an adapted discontinuous Galerkin finite element scheme. Our schemes show good stability, and are able to ac-

commodate a wide variety of initial-boundary data, including supersonic inlets, acoustic inlets, and radiative boundaries. The hypergolic reaction was chosen in order to find a “hard” test case for the numerics of the system, since the reaction rate of detonation reactions is so high. We have found that our system was able to deal with this, and was able to accurately model the chemical physics of stationary and flow reactor dynamics.

The discontinuous Galerkin approximate solution to these compressible flow reactors is particularly well-suited for applications in combustion modeling, atmospheric, oceanic and geological modeling, as well as in astronomy and a plethora of experimental studies involving chemical reactor kinetics. The future direction of this work is to include the important physics contained in thermalized turbulence, interfacial surfaces, and electrodynamic into the existing models.

Generally this work has been concerned with expanding the known results of evolution equations, to include systems that contain more parameters of interest to physical chemistry. We have discovered in this process, that modern applied mathematics, though often quite rigorous and complicated, offers substantial advantages in its ability to find consistent and stable models to highly coupled nonlinear systems of equations. Finding “well-posed” model systems further offers the benefit of obtaining deep, careful and closely analyzed mathematical couplings, which very often, we have found, are able to direct “physical intuition” along lines which yield stable and mathematically non-degenerate results. Numerically, these variational form (finite element) solutions demonstrate remarkable accuracy and consistency, strongly conforming to the proper mathematical character of the solution.

What remains to be done, which is of substantial importance in chemi-

cal applications, is the comparison of these numerical experiments to novel experimental systems in the laboratory. Though compressible barotropic flows, quantum hydrodynamics and reaction-diffusion systems have been used to study many experimental systems in many fields (as cited above), the difficulty in developing fully generalized and tractable numerical versions of these solutions has kept them from becoming ubiquitous in the scientific community at large. Many communities, due to the mathematical complications introduced in these systems, have been forced to resort to incompressible and static models, even when the assumptions underlying these models are nonideal for the context of the study performed. It is our hope that this work may serve as a catalyst in overcoming the barrier to the expansive study of generalized evolution equations in physical chemistry.

## Appendices

## Appendix A

We have that  $\mathbf{\Gamma}$  is of the form:

$$\mathbf{\Gamma} = \left( \begin{array}{cc|ccc} 0 & 1 & 0 & \cdots & 0 \\ -u^2 & 2u & Z_1 & \cdots & Z_n \\ \hline -u\mu_1 & \mu_1 & & & \\ \vdots & \vdots & & & \\ -u\mu_n & \mu_n & & & \end{array} \right),$$

where we set for  $i = 1, \dots, n$  the indeterminates  $Z_i = \partial_{\rho_i} p$ . Solving the characteristic equation

$$0 = \left| \begin{array}{cc|ccc} -\varsigma & 1 & 0 & \cdots & 0 \\ -u^2 & 2u - \varsigma & Z_1 & \cdots & Z_n \\ \hline -u\mu_1 & \mu_1 & & & \\ \vdots & \vdots & & & \\ -u\mu_n & \mu_n & & & \end{array} \right|,$$

the eigenvalues counted with multiplicity are,

$$\varsigma_1 = u + c, \varsigma_2 = u - c, \quad \varsigma_3 = u, \quad \underbrace{\varsigma_4 = u, \dots, \varsigma_{n+2} = u}_{n-1}$$

where the speed of sound is given by  $c = \sqrt{\mu_1 Z_1 + \dots + \mu_n Z_n}$ . While  $u$  has multiplicity  $n$  it is better to consider the eigenvalues in the three groups,  $u \pm c$ ,  $u$ , and the remaining  $(n - 1)$  copies of  $u$  as illustrated by the decomposition



of the diagonalizing transformation matrix

$$\mathbf{V}(\mathbf{U}) = (\mathbf{c}_1 \cdots \mathbf{c}_n) = \begin{pmatrix} 1 & 1 & 1 & 0 & \cdots & \cdots & 0 \\ u+c & u-c & u & 0 & \cdots & \cdots & 0 \\ \mu_1 & \mu_1 & 0 & -Z_2 & \cdots & \cdots & -Z_n \\ \mu_2 & \mu_2 & 0 & Z_1 & 0 & \cdots & 0 \\ \vdots & \vdots & \vdots & 0 & \ddots & \ddots & \vdots \\ \vdots & \vdots & \vdots & \vdots & \ddots & \ddots & 0 \\ \mu_n & \mu_n & 0 & 0 & \cdots & 0 & Z_1 \end{pmatrix}$$

whose columns are the corresponding eigenvectors, which we abbreviate for convenience in the  $3 \times 3$  block matrix form

$$\left( \begin{array}{cc|c|c} 1 & 1 & 1 & \mathbf{0} \\ u+c & u-c & u & \mathbf{0} \\ \hline \mu_1 & \mu_1 & 0 & -\mathbf{Y} \\ \hline \mathbf{X} & \mathbf{X} & \mathbf{0} & (Z_1)\mathbb{I}_{n-1} \end{array} \right),$$

where we have set  $\mathbf{X} = (\mu_2, \dots, \mu_n)^T$  and  $\mathbf{Y} = (Z_2, \dots, Z_n)$ .

The inverse transformation matrix is given by

$$\mathbf{V}^{-1}(\mathbf{U}) = \frac{1}{2c^2} \left( \begin{array}{cc|c|c} -uc & c & Z_1 & \mathbf{Y} \\ uc & -c & Z_1 & \mathbf{Y} \\ \hline 2c^2 & 0 & -2Z_1 & -2\mathbf{Y} \\ \hline \mathbf{0} & \mathbf{0} & -2\mathbf{X} & 2Z_1^{-1}(c^2\mathbb{I}_{n-1} - \mathbf{X}\mathbf{Y}) \end{array} \right).$$

Verifying this is a straightforward block matrix multiplication up to the factor of  $2c^2$ , where  $\mathbf{V}\mathbf{V}^{-1}$  is given by

$$\left( \begin{array}{cc|c|c} 1 & 1 & 1 & \mathbf{0} \\ u+c & u-c & u & \mathbf{0} \\ \hline \mu_1 & \mu_1 & 0 & -\mathbf{Y} \\ \hline \mathbf{X} & \mathbf{X} & \mathbf{0} & Z_1\mathbb{I}_{n-1} \end{array} \right) \left( \begin{array}{cc|c|c} -uc & c & Z_1 & \mathbf{Y} \\ uc & -c & Z_1 & \mathbf{Y} \\ \hline 2c^2 & 0 & -2Z_1 & -2\mathbf{Y} \\ \hline \mathbf{0} & \mathbf{0} & -2\mathbf{X} & 2Z_1^{-1}(c^2\mathbb{I}_{n-1} - \mathbf{X}\mathbf{Y}) \end{array} \right).$$

We illustrate the computation only for the lower right portion, where

$$\begin{aligned}
& \left( \begin{array}{c|c|c} & & \\ \hline & 2\mu_1 Z_1 + 2\mathbf{Y}\mathbf{X} & 2\mu_1 \mathbf{Y} - 2Z_1^{-1}(c^2 \mathbf{Y} - \mathbf{Y}\mathbf{X}\mathbf{Y}) \\ \hline & 2Z_1 \mathbf{X} - 2Z_1 \mathbb{I}_{n-1} \mathbf{X} & 2\mathbf{X}\mathbf{Y} + 2(c^2 \mathbb{I}_{n-1} - \mathbf{X}\mathbf{Y}) \\ \hline \end{array} \right) \\
&= \left( \begin{array}{c|c|c} & & \\ \hline & 2c^2 & 2\mu_1 \mathbf{Y} - 2Z_1^{-1}(c^2 - \mathbf{Y}\mathbf{X})\mathbf{Y} \\ \hline & \mathbf{0} & 2c^2 \mathbb{I}_{n-1} \\ \hline \end{array} \right) \\
&= \left( \begin{array}{c|c|c} & & \\ \hline & 2c^2 & 2\mu_1 \mathbf{Y} - 2Z_1^{-1}(\mu_1 Z_1) \mathbf{Y} \\ \hline & \mathbf{0} & 2c^2 \mathbb{I}_{n-1} \\ \hline \end{array} \right) \text{ since } \mu_1 Z_1 + \mathbf{Y}\mathbf{X} = c^2 \\
&= \left( \begin{array}{c|c|c} & & \\ \hline & 2c^2 & \mathbf{0} \\ \hline & \mathbf{0} & 2c^2 \mathbb{I}_{n-1} \\ \hline \end{array} \right).
\end{aligned}$$

For the eigenvalues and eigenvectors of  $\mathbf{\Gamma}$  we obtain with

$$c = \sqrt{\mu_1 \partial_{\rho_1} p + \dots + \mu_n \partial_{\rho_n} p},$$

the pairs

$$u + c, \begin{pmatrix} 1 \\ u + c \\ \mu_1 \\ \mu_2 \\ \vdots \\ \mu_n \end{pmatrix} \quad u - c, \begin{pmatrix} 1 \\ u - c \\ \mu_1 \\ \mu_2 \\ \vdots \\ \mu_n \end{pmatrix} \quad u, \begin{pmatrix} 1 \\ u \\ 0 \\ 0 \\ \vdots \\ 0 \end{pmatrix},$$

while the remaining  $n - 1$  pairs involving the eigenvalue  $u$  are

$$u, \begin{pmatrix} 0 \\ 0 \\ -\partial_{\rho_2} p \\ \partial_{\rho_1} p \\ 0 \\ 0 \\ \vdots \\ 0 \end{pmatrix} \quad u, \begin{pmatrix} 0 \\ 0 \\ -\partial_{\rho_3} p \\ 0 \\ \partial_{\rho_1} p \\ 0 \\ \vdots \\ 0 \end{pmatrix} \quad \cdots \quad u, \begin{pmatrix} 0 \\ 0 \\ -\partial_{\rho_n} p \\ 0 \\ 0 \\ \vdots \\ 0 \\ \partial_{\rho_1} p \end{pmatrix}.$$

## Appendix B

The conservation method of recovering trajectories in (4.42) and the velocity integration method of recovering trajectories in (4.45) in no way exhaust the number of ways of representing solutions in the Lagrangian frame. In fact, there are an infinite number of ways of choosing trajectories. We introduce a way of computing a subset of these, and refer to these as “offset methods.”

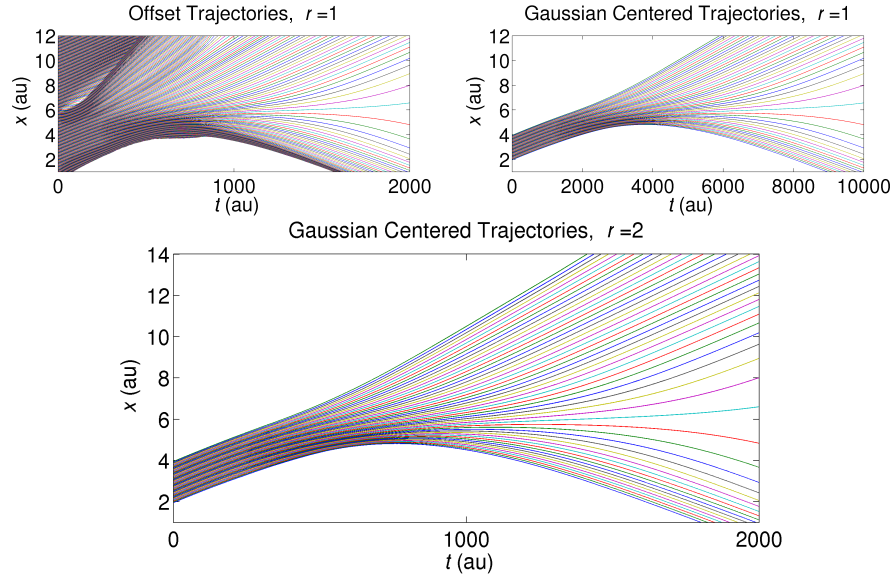


Figure B.1: On the top we show the quantum trajectories using the offset method solution of the same problem in Figure 4.10 with  $r = 1$ ; and on the bottom we show the same trajectories using  $r = 2$ .

The offset solution relies mainly on velocity integration but includes

some information from mass conservation as follows: velocity integration provides an estimated position for each particle at the following time-step. Then one works through particle by particle, starting at the new estimated position and using mass conservation to estimate the new positions of its neighbors (a tunable number of consecutive elements on either side) offset from the velocity estimate of the ‘current’ particle. We set our tuning parameter to  $r$  here on both sides, though there is no reason *a priori* to choose a symmetric (with respect to either side) tuning parameter. Generically this provides a set of estimates for the position of each particle: one directly from integration, and others via the relationship of that estimated position to the relative estimated position of its nearest neighbors.

That is, if  $P_m^m$  is the velocity estimated position, and  $P_{m-r}^m$  and  $P_{m+r}^m$  are the positions of the particles on either side that density conservation requires, and applying our symmetry constraint gives for the new position that:

$$P_{\text{new}} = w_0 P_m^m + \sum_{i=1}^r (w_i P_m^{m-i} + w_i P_m^{m+i}),$$

where the  $w_i$ ’s are the weights for each component, in our examples computed with a Gaussian weighting functions  $\omega_i = e^{-(\ln(2)/r^2)i^2}$  such that:

$$w_i = \omega_i / \sum_{i=0}^r \omega_i \quad \text{for } i = 0, \dots, r.$$

Then for  $r = 1$  we have  $w_0 = 1/2$  and  $w_1 = 1/4$ . We show two examples of obtained offset trajectories in Figure B.1, which are located at distinct locations in the solution space. Also note that these trajectories behave substantially different than those in Figures 4.7 and 4.10.

## Bibliography

- [1] B. Ducomet and E. Feireisl. The equations of magnetohydrodynamics: on the interaction between matter and radiation in the evolution of gaseous stars. *Comm. Math. Phys.*, 266(3):595–629, 2006.
- [2] S. Safran, T. Kuhl, J. Israelachvili, and G. Hed. Polymer induced membrane contraction, phase separation, and fusion via marangoni flow. *Biophysical Journal*, 81(2):659–666, 2001.
- [3] C. Michoski, J.A. Evans, P.G. Schmitz, and A. Vasseur. A discontinuous Galerkin method for viscous compressible multifluids. *J. Comput. Phys.*, Submitted, 2008.
- [4] M. Fujimoto, T. Kado, W. Takashima, K. Kaneto, and S. Hayase. Dye-Sensitized Solar Cells Fabricated by Electrospray Coating Using  $\text{TiO}_2$  Nanocrystal Dispersion Solution. *J. Electrochem. Soc.*, 153(5):A826–A829, 2006.
- [5] E.L. Weitzke and P.J. Ortoleva. Simulating cellular dynamics through a coupled transcription, translation, metabolic model. *Computational Biology and Chemistry*, 27(4-5):469 – 480, 2003.
- [6] H. Iba. Inference of differential equation models by genetic programming. *Information Sciences*, 178(23):4453 – 4468, 2008. Including Special Section: Genetic and Evolutionary Computing.

- [7] R. Engbert, A. Nuthmann, E.M. Richter, and R. Kliegl. SWIFT: A dynamical model of saccade generation during reading. *Psychological Review*, 112(4):p777 – 813, 20051001.
- [8] M. Giuli, F. Gozzi, R. Monte, and V. Vespri. Generation of analytic semigroups and domain characterization for degenerate elliptic operators with unbounded coefficients arising in financial mathematics. II. In *Functional analysis and evolution equations*, pages 315–330. Birkhäuser, Basel, 2008.
- [9] G. Ghirardi. Quantum dynamical reduction and reality: Replacing probability densities with densities in real space. *Erkenntnis: An International Journal of Analytic Philosophy*, 45(2 & 3):349 – 365, 19961101.
- [10] B. F. Wyman. Linear systems over rings of operators. In *Category theory applied to computation and control (Proc. First Internat. Sympos., San Francisco, Calif., 1974)*, pages 218–223. Lecture Notes in Comput. Sci., Vol. 25. Springer, Berlin, 1975.
- [11] P.W. Atkins and J. de Paula. *Physical Chemistry, 7th Edition*. W. H. Freeman, 2001.
- [12] P.L. Houston. *Chemical Kinetics and Reaction Dynamics*. McGraw-Hill Higher Education, New York, NY, 2001.
- [13] H. Ninomiya and M. Taniguchi. Existence and global stability of traveling curved fronts in the Allen-Cahn equations. *J. Differential Equations*, 213(1):204–233, 2005.
- [14] J.W. Cahn and J.E. Hilliard. Free energy of a nonuniform system i. interfacial free energy. *Journal of Chemical Physics*, 30:258–267, 1959.

- [15] G. Ge and L. Brus. Evidence for spinodal phase separation in two-dimensional nanocrystal self-assembly. *The Journal of Physical Chemistry B*, 104(41):9573–9575, 2000.
- [16] E. Kiran. Polymer Miscibility, Phase Separation, Morphological Modifications and Polymorphic Transformations in Dense Fluids. *J. Supercritical Fluids*, 47(3):466–483, 2009. 20th Year Anniversary Issue of the Journal of Supercritical Fluids.
- [17] K. Binder. Collective diffusion, nucleation and spinodal decomposition in polymer mixtures. *Journal of Chemical Physics*, 79(12):6387–6409, 1983.
- [18] D. Bresch and B. Desjardins. Some diffusive capillary models of Korteweg type. *C. R. Acad. Sci., Paris, Section Mécanique*, 332(11):881–886, 2004.
- [19] C. Liu and J. Shen. A phase field model for the mixture of two incompressible fluids and its approximation by a fourier-spectral method. *Physica D-Nonlinear Phenomena*, 179(3–4):211–228, 2003.
- [20] R.E. Wyatt. *Quantum dynamics with trajectories*, volume 28 of *Interdisciplinary Applied Mathematics*. Springer-Verlag, New York, 2005. Introduction to quantum hydrodynamics, With contributions by C.J. Trahan.
- [21] S. O’Sullivan and T.P. Downes. An explicit scheme for multifluid magnetohydrodynamics. *Monthly Notices of the Royal Astronomical Society*, 366(4):1329–1336, 2006.



- [22] V.M. Zhdanov. *Transport Processes in Multicomponent Plasma*. CRC, Taylor and Francis, New York, 2002.
- [23] R.D. Groot and P.B. Warren. Dissipative particle dynamics: Bridging the gap between atomistic and mesoscopic simulation. *The Journal of Chemical Physics*, 107(11):4423–4435, 1997.
- [24] H. Moehwald and D.G. Shchukin. Sonochemical nanosynthesis at the engineered interface of a cavitation microbubble. *Physical Chemistry Chemical Physics*, 8(30):3496–3506, 2006.
- [25] M. E. Ryan, A. M. Hynes, and J. P. S. Badyal. Pulsed plasma polymerization of maleic anhydride. *Chemistry of Materials*, 8(1):37–42, 1996.
- [26] H. Eckert. Structural characterization of noncrystalline solids and glasses using solid state nmr. *Progress in Nuclear Magnetic Resonance Spectroscopy*, 24(3):159 – 293, 1992.
- [27] M.S. Child. *Molecular Collision theory*. Constable and Company, Ltd., London, W6 9ER, 1974.
- [28] B. Perthame. *Kinetic formulation of conservation laws*, volume 21 of *Oxford Lecture Series in Mathematics and its Applications*. Oxford University Press, Oxford, 2002.
- [29] R.E. Heath. *Analysis of the Discontinuous Galerkin Method Applied to Collisionless Plasma Physics*. PhD thesis, 2007.

- [30] J.O. Hirschfelder, C.F. Curtiss, and R.B. Bird. *The Molecular Theory of Gases and Liquids*. Structure of Matter Series. Wiley-Interscience, Revised, New York, 1954.
- [31] S. Chapman and T. G. Cowling. *The Mathematical Theory of Nonuniform Gases*. Cambridge Mathematical Library. Cambridge University Press, Cambridge, third edition, 1990.
- [32] W. Pauli. *Thermodynamics and the Kinetic Theory of Gases (Vol. 3 of Pauli Lectures on Phys.)*. Pauli Lectures on Physics. Dover publications, Basel, 2000.
- [33] H. Struchtrup. Scaling and expansion of moment equations in kinetic theory. *J. Stat. Phys.*, 125(3):569–591, 2006.
- [34] V. A. Solonnikov. The solvability of the initial-boundary value problem for the equations of motion of a viscous compressible fluid. *Zap. Naučn. Sem. Leningrad. Otdel. Mat. Inst. Steklov. (LOMI)*, 56:128–142, 1976. Investigations on linear operators and theory of functions, VI.
- [35] A. Mellet and A. Vasseur. Existence and uniqueness of global strong solutions for one-dimensional compressible Navier-Stokes equations. *SIAM J. Math. Anal.*, 39(4):1344–1365, 2008.
- [36] A. Mellet and A. Vasseur. On the barotropic compressible Navier-Stokes equations. *Comm. Partial Differential Equations*, 32(1-3):431–452, 2007.
- [37] D. Bresch and B. Desjardins. On compressible Navier-Stokes equations with density dependent viscosities in bounded domains. *J. Math. Pures Appl. (9)*, 87(2):227–235, 2007.

- [38] D. Bresch and B. Desjardins. Sur un modèle de Saint-Venant visqueux et sa limite quasi-géostrophique. *C. R. Math. Acad. Sci. Paris*, 335(12):1079–1084, 2002.
- [39] C. Michoski and A. Vasseur. Existence and uniqueness of strong solutions for a compressible multiphase Navier-Stokes miscible fluid-flow problem in dimension  $n=1$ . *Math. Models Methods Appl. Sci.*, 19(3):443–476, 2009.
- [40] D. Bohm. *Quantum Theory (Reprint of Prentice Hall, 1951)*. Dover Publications, 1989.
- [41] D. Bohm. A suggested interpretation of the quantum theory in terms of “hidden variables ”, i and ii. *Phys. Rev.*, 85:166,188, 1952.
- [42] A. Jüngel. *Quasi-hydrodynamic semiconductor equations*. Progress in Nonlinear Differential Equations and their Applications, 41. Birkhäuser Verlag, Basel, 2001.
- [43] S. Benzoni-Gavage, R. Danchin, S. Descombes, and D. Jamet. Structure of Korteweg models and stability of diffuse interfaces. *Interfaces Free Bound.*, 7(4):371–414, 2005.
- [44] C. Michoski, J.A. Evans, P.G. Schmitz, and A. Vasseur. Quantum Hydrodynamics with Trajectories via a Nonlinear Conservation Form Mixed Discontinuous Galerkin method with Chemical Applications. *J. Comput. Phys.*, Submitted, 2009.
- [45] W.C. Gardiner. *Combustion Chemistry*. Springer-Verlag New York Inc., New York, NY, 1984.

- [46] F.A. Williams. *Combustion Theory*. Combustion Science and Engineering Series. The Benjamin/Cummings Publishing Company, Inc., Menlo Park, California, 1985.
- [47] W. Jäger, R. Rannacher, and J. Warnatz, editors. *Reactive flows, diffusion and transport*. Springer-Verlag, Berlin, 2007.
- [48] A. V. Kazhikhov and V. V. Shelukhin. Unique global solution with respect to time of initial-boundary value problems for one-dimensional equations of a viscous gas. *Prikl. Mat. Meh.*, 41(2):282–291, 1977.
- [49] V. V. Shelukhin. Motion with a contact discontinuity in a viscous heat conducting gas. *Dinamika Sploshn. Sredy*, (57):131–152, 1982.
- [50] V. V. Shelukhin. Evolution of a contact discontinuity in the barotropic flow of a viscous gas. *Prikl. Mat. Mekh.*, 47(5):870–872, 1983.
- [51] D. Serre. Sur l’équation monodimensionnelle d’un fluide visqueux, compressible et conducteur de chaleur. *C. R. Acad. Sci. Paris Sér. I Math.*, 303(14):703–706, 1986.
- [52] D. Serre. Solutions faibles globales des équations de Navier-Stokes pour un fluide compressible. *C. R. Acad. Sci. Paris Sér. I Math.*, 303(13):639–642, 1986.
- [53] D. Hoff. Global existence for 1D, compressible, isentropic Navier-Stokes equations with large initial data. *Trans. Amer. Math. Soc.*, 303(1):169–181, 1987.

- [54] V. V. Shelukhin. Boundary value problems for equations of a barotropic viscous gas with nonnegative initial density. *Dinamika Sploshn. Sredy*, (74):108–125, 162–163, 1986.
- [55] D. Hoff. Global solutions of the equations of one-dimensional, compressible flow with large data and forces, and with differing end states. *Z. Angew. Math. Phys.*, 49(5):774–785, 1998.
- [56] A. Matsumura and T. Nishida. The initial value problem for the equations of motion of compressible viscous and heat-conductive fluids. *Proc. Japan Acad. Ser. A Math. Sci.*, 55(9):337–342, 1979.
- [57] A. Matsumura and T. Nishida. The initial value problem for the equations of motion of viscous and heat-conductive gases. *J. Math. Kyoto Univ.*, 20(1):67–104, 1980.
- [58] A. Matsumura and T. Nishida. Initial-boundary value problems for the equations of compressible viscous and heat-conductive fluid. In *Nonlinear partial differential equations in applied science (Tokyo, 1982)*, volume 81 of *North-Holland Math. Stud.*, pages 153–170. North-Holland, Amsterdam, 1983.
- [59] D. Hoff. Strong convergence to global solutions for multidimensional flows of compressible, viscous fluids with polytropic equations of state and discontinuous initial data. *Arch. Rational Mech. Anal.*, 132(1):1–14, 1995.
- [60] P-L. Lions. *Mathematical topics in fluid mechanics. Vol. 2*, volume 10 of *Oxford Lecture Series in Mathematics and its Applications*. The

Clarendon Press Oxford University Press, New York, 1998. Compressible models, Oxford Science Publications.

- [61] B. Desjardins. Regularity results for two-dimensional flows of multi-phase viscous fluids. *Arch. Rational Mech. Anal.*, 137(2):135–158, 1997.
- [62] G-Q. Chen, D. Hoff, and K. Trivisa. Global solutions of the compressible Navier-Stokes equations with large discontinuous initial data. *Comm. Partial Differential Equations*, 25(11-12):2233–2257, 2000.
- [63] E. Feireisl. On the motion of a viscous, compressible, and heat conducting fluid. *Indiana Univ. Math. J.*, 53(6):1705–1738, 2004.
- [64] E. Feireisl. Mathematics of viscous, compressible, and heat conducting fluids. In *Nonlinear partial differential equations and related analysis*, volume 371 of *Contemp. Math.*, pages 133–151. Amer. Math. Soc., Providence, RI, 2005.
- [65] E. Feireisl. Mathematical theory of compressible, viscous, and heat conducting fluids. *Comput. Math. Appl.*, 53(3-4):461–490, 2007.
- [66] G-Q. Chen, D. Hoff, and K. Trivisa. Global solutions to a model for exothermically reacting, compressible flows with large discontinuous initial data. *Arch. Ration. Mech. Anal.*, 166(4):321–358, 2003.
- [67] G-Q. Chen and K. Trivisa. Analysis on models for exothermically reacting, compressible flows with large discontinuous initial data. In *Nonlinear partial differential equations and related analysis*, volume 371 of *Contemp. Math.*, pages 73–91. Amer. Math. Soc., Providence, RI, 2005.

- [68] B. Ducomet and A. Zlotnik. On the large-time behavior of 1D radiative and reactive viscous flows for higher-order kinetics. *Nonlinear Anal.*, 63(8):1011–1033, 2005.
- [69] K. Trivisa. Global existence and asymptotic analysis of solutions to a model for the dynamic combustion of compressible fluids. *Discrete Contin. Dyn. Syst.*, (suppl.):852–863, 2003. Dynamical systems and differential equations (Wilmington, NC, 2002).
- [70] A. A. Zlotnik. Weak solutions of the equations of motion of a viscous compressible reacting binary mixture: uniqueness and Lipschitz-continuous dependence on data. *Mat. Zametki*, 75(2):307–311, 2004.
- [71] A. A. Zlotnik and B. Dyukome. Stabilization of one-dimensional flows of a radiative and a reactive viscous gas for a general rate of reaction. *Dokl. Akad. Nauk*, 403(6):731–736, 2005.
- [72] Y. Amirat and V. Shelukhin. Global weak solutions to equations of compressible miscible flows in porous media. *SIAM J. Math. Anal.*, 38(6):1825–1846 (electronic), 2007.
- [73] D. Hoff and J. Smoller. Non-formation of vacuum states for compressible Navier-Stokes equations. *Comm. Math. Phys.*, 216(2):255–276, 2001.
- [74] B. Das, G. Enden, and A.S. Popel. Stratified multiphase model for blood flow in a venular bifurcation. *Annals of Biomedical Engineering*, 25(1):135–153, 1997.
- [75] J. Fine and L. Waite. *Applied Biofluid Mechanics*. The McGraw-Hill Companies, 2007.

- [76] J. Jung, R.W. Lyczkowski, C. Panchal, and A. Hassanein. Multiphase hemodynamic simulation of pulsatile flow in a coronary artery. *Journal of Biomechanics*, 39(11):2064–2073, 2006.
- [77] G. Lemon, J.R. King, H.M. Byrne, O.E. Jensen, and K.M. Shakesheff. Mathematical modelling of engineered tissue growth using a multiphase porous flow mixture theory. *J. Math. Biol.*, 52(5):571–594, 2006.
- [78] E. Evans. New physical concepts for cell amoeboid motion. *Biophysical Journal*, 64(4):1306–1322, 1993.
- [79] E. Feireisl, P. Laurençot, and H. Petzeltová. On convergence to equilibria for the Keller-Segel chemotaxis model. *J. Differential Equations*, 236(2):551–569, 2007.
- [80] M. Eisenbach. *Chemotaxis*. Imperial College Press, 2004.
- [81] A.B.R. Mayer. Colloidal metal nanoparticles dispersed in amphiphilic polymers. *Polymers for Advanced Technologies*, 12(1–2):96–106, 2001.
- [82] A. Mellet and A. Vasseur. Global weak solutions for a Vlasov-Fokker-Planck/Navier-Stokes system of equations. *Math. Models Methods Appl. Sci.*, 17(7):1039–1063, 2007.
- [83] P. Tartaj, T. Gonzalez-Carreno, and C.J. Serna. Magnetic behavior of gamma-Fe<sub>2</sub>O<sub>3</sub> nanocrystals dispersed in colloidal silica particles. *Journal of Physical Chemistry B*, 107(1):20–24, 1993.
- [84] J. Buajarern, L. Mitchem, and J. P. Reid. Characterizing multiphase organic/inorganic/aqueous aerosol droplets. *Journal of Physical Chemistry A*, 111(37):9054–9061, 2007.



- [85] Shui L., J.C.T. Eijkel, and A. van den Berg. Multiphase flow in microfluidic systems - control and applications of droplets and interfaces. *Advances in Colloid and Interface Science*, (133):35–49, 2007.
- [86] S. Liu, F. Wang, and H. Zhao. Global existence and asymptotics of solutions of the Cahn-Hilliard equation. *J. Differential Equations*, 238(2):426–469, 2007.
- [87] S.Y. Heriot and R.A.L. Jones. An interfacial instability in a transient wetting layer leads to lateral phase separation in thin spin-cast polymer-blend films. *Nature Materials*, 4(10):782–786, 2005.
- [88] E.J. Davis and G. Schweiger. *The Airborne Microparticle*. Springer-Verlag, 2002.
- [89] R.M. Harrison and R.E. van Grieken. *Atmospheric Particles*, volume 5 of *IUPAC Series on Analytical and Physical Chemistry of Environmental Systems*. John Wiley & Sons, New York, NY, 1998.
- [90] J. Pedlosky. *Geophysical fluid dynamics*, volume 2nd Edition. Springer-Verlag New York Inc., New York, NY, 1987.
- [91] G. Vallis. *Atmospheric and oceanic fluid dynamics: fundamentals and large-scale circulation*, volume 2nd Edition. Cambridge University Press, New York, NY, 2006.
- [92] K. Promislow, J. Stockie, and B. Wetton. A sharp interface reduction for multiphase transport in a porous fuel cell electrode. *Proc. R. Soc. Lond. Ser. A Math. Phys. Eng. Sci.*, 462(2067):789–816, 2006.

- [93] U. Pasaogullari and C.Y. Wang. Liquid water transport in gas diffusion layer of polymer electrolyte fuel cells. *Journal of the Electrochemical Society*, 151(3):A399–A406, 2004.
- [94] L.K. Doraiswamy and S.D. Naik. Phase transfer catalysis: chemistry and engineering. *AIChE Journal*, 44(3):612–646, 1998.
- [95] F. Miniati, D.S. Ryu, A. Ferrara, and T.W. Jones. Magnetohydrodynamics of cloud collisions in a multiphase interstellar medium. *Astrophysical Journal*, 510(2):726–746, 1979.
- [96] F.H. Harlow and A.A. Amsden. Numerical-calculation of multiphase fluid-flow. *J. of Comput. Phys.*, 17(1):19–52, 1975.
- [97] J.K. Dukowicz. A particle-fluid numerical-model for liquid sprays. *J. Comput. Phys.*, 35(2):229–253, 1980.
- [98] G.M. Faeth. Evaporation and combustion of sprays. *Progress in Energy and Combustion Science*, 9(1–2):1–76, 1983.
- [99] G.M. Faeth. Mixing, transport and combustion in sprays. *Progress in Energy and Combustion Science*, 14(4):293–345, 1987.
- [100] D.L. Youngs. Numerical-simulation of turbulent mixing by rayleigh-taylor instability. *Physica D*, 12(1–3):32–44, 1984.
- [101] J.H. Hunter, M.T. Sandford, R.W. Whitaker, and R.I. Klein. Star formation in colliding gas-flows. *Astrophysical Journal*, 305(1):309–332, 1986.

- [102] T.E. Ongaro, C. Cavazzoni, G. Erbacci, A. Neri, and M. V. Salvetti. A parallel multiphase flow code for the 3d simulation of explosive volcanic eruptions. *Parallel Computing*, 33(7–8):541–560, 2007.
- [103] C. Hirsch. *Numerical computation of internal and external flows*, volume 1–2 of *Wiley series in numerical methods in engineering*. John Wiley & Sons Ltd., Chichester [England], 1988.
- [104] Shih-I Pai and Shijun Luo. *Theoretical and computational dynamics of a compressible flow*. Beijing: Science Press, New York, NY, 1991.
- [105] M. Feistauer, J. Felcman, and I. Straškraba. *Mathematical and computational methods for compressible flow*. Numerical mathematics and scientific computation. Oxford University Press, 2003.
- [106] M. Bulíček, J. Málek, and K. R. Rajagopal. Navier’s slip and evolutionary Navier-Stokes-like systems with pressure and shear-rate dependent viscosity. *Indiana Univ. Math. J.*, 56(1):51–85, 2007.
- [107] M. Franta, J. Málek, and K. R. Rajagopal. On steady flows of fluids with pressure- and shear-dependent viscosities. *Proc. R. Soc. Lond. Ser. A Math. Phys. Eng. Sci.*, 461(2055):651–670, 2005.
- [108] J. Málek, G. Mingione, and J. Stará. Fluids with pressure dependent viscosity: partial regularity of steady flows. In *EQUADIFF 2003*, pages 380–385. World Sci. Publ., Hackensack, NJ, 2005.
- [109] J. Málek and K. R. Rajagopal. Incompressible rate type fluids with pressure and shear-rate dependent material moduli. *Nonlinear Anal. Real World Appl.*, 8(1):156–164, 2007.

- [110] C.Y. Wong, J.A. Maruhn, and T.A. Welton. Dynamics of nuclear fluids. i. foundations. *Nucl. Phys.*, A253:469–489, 1975.
- [111] P-L. Lions. *Mathematical topics in fluid mechanics. Vol. 1*, volume 3 of *Oxford Lecture Series in Mathematics and its Applications*. The Clarendon Press Oxford University Press, New York, 1996. Incompressible models, Oxford Science Publications.
- [112] S. N. Antontsev and A. V. Kazhikhov. *Matematicheskie voprosy dinamiki neodnorodnykh zhidkosti*. Novosibirsk. Gosudarstv. Univ., Novosibirsk, 1973. Lecture notes, Novosibirsk State University.
- [113] A. V. Kazhikhov. Solvability of the initial-boundary value problem for the equations of the motion of an inhomogeneous viscous incompressible fluid. *Dokl. Akad. Nauk SSSR*, 216:1008–1010, 1974.
- [114] S. N. Antontsev, A. V. Kazhikhov, and V. N. Monakhov. *Boundary value problems in mechanics of nonhomogeneous fluids*, volume 22 of *Studies in Mathematics and its Applications*. North-Holland Publishing Co., Amsterdam, 1990. Translated from the Russian.
- [115] R. J. DiPerna and P.-L. Lions. Ordinary differential equations, transport theory and Sobolev spaces. *Invent. Math.*, 98(3):511–547, 1989.
- [116] A. Nouri and F. Poupaud. An existence theorem for the multifluid Navier-Stokes problem. *J. Differential Equations*, 122(1):71–88, 1995.
- [117] A. Nouri, F. Poupaud, and Y. Demay. An existence theorem for the multi-fluid Stokes problem. *Quart. Appl. Math.*, 55(3):421–435, 1997.

- [118] A. Novotný and I. Straškraba. *Introduction to the mathematical theory of compressible flow*, volume 27 of *Oxford Lecture Series in Mathematics and its Applications*. Oxford University Press, Oxford, 2004.
- [119] N. Tanaka. Global existence of two phase nonhomogeneous viscous incompressible fluid flow. *Comm. Partial Differential Equations*, 18(1-2):41–81, 1993.
- [120] A. Tani and N. Tanaka. Large-time existence of surface waves in incompressible viscous fluids with or without surface tension. *Arch. Rational Mech. Anal.*, 130(4):303–314, 1995.
- [121] V. A. Solonnikov. Unsteady flow of a finite mass of a fluid bounded by a free surface. *Zap. Nauchn. Sem. Leningrad. Otdel. Mat. Inst. Steklov. (LOMI)*, 152(Kraev. Zadachi Mat. Fiz. i Smezhnye Vopr. Teor. Funktsii18):137–157, 183–184, 1986.
- [122] V. A. Solonnikov and A. Tani. A problem with a free boundary for Navier-Stokes equations for a compressible fluid in the presence of surface tension. *Zap. Nauchn. Sem. Leningrad. Otdel. Mat. Inst. Steklov. (LOMI)*, 182(Kraev. Zadachi Mat. Fiz. i Smezh. Voprosy Teor. Funktsii. 21):142–148, 173–174, 1990.
- [123] V. A. Solonnikov. On a nonstationary motion of a finite mass of a liquid bounded by a free surface. In *Differential equations (Xanthi, 1987)*, volume 118 of *Lecture Notes in Pure and Appl. Math.*, pages 647–653. Dekker, New York, 1989.
- [124] V. A. Solonnikov. Unsteady motions of a finite isolated mass of a self-gravitating fluid. *Algebra i Analiz*, 1(1):207–249, 1989.

- [125] V. A. Solonnikov. Unsteady motions of a finite isolated mass of a self-gravitating fluid. *Algebra i Analiz*, 1(1):207–249, 1989.
- [126] D. Bresch, B. Desjardins, and G. Métivier. Recent mathematical results and open problems about shallow water equations. In *Analysis and simulation of fluid dynamics*, Adv. Math. Fluid Mech., pages 15–31. Birkhäuser, Basel, 2007.
- [127] D. Bresch, B. Desjardins, and C-K. Lin. On some compressible fluid models: Korteweg, lubrication, and shallow water systems. *Comm. Partial Differential Equations*, 28(3-4):843–868, 2003.
- [128] A. Valli and W.M. Zajączkowski. Navier-Stokes equations for compressible fluids: global existence and qualitative properties of the solutions in the general case. *Comm. Math. Phys.*, 103(2):259–296, 1986.
- [129] V. A. Solonnikov and A. Tani. Evolution free boundary problem for equations of motion of viscous compressible barotropic liquid. In *The Navier-Stokes equations II—theory and numerical methods (Oberwolfach, 1991)*, volume 1530 of *Lecture Notes in Mathematics*, pages 30–55. Springer, Berlin, 1992.
- [130] D. Hoff and E. Tsyganov. Uniqueness and continuous dependence of weak solutions in compressible magnetohydrodynamics. *Z. Angew. Math. Phys.*, 56(5):791–804, 2005.
- [131] G-Q. Chen and M. Kratka. Global solutions to the Navier-Stokes equations for compressible heat-conducting flow with symmetry and free boundary. *Comm. Partial Differential Equations*, 27(5-6):907–943, 2002.

- [132] B. Ducomet and E. Feireisl. On the dynamics of gaseous stars. *Arch. Ration. Mech. Anal.*, 174(2):221–266, 2004.
- [133] D. Donatelli and K. Trivisa. On the motion of a viscous compressible radiative-reacting gas. *Comm. Math. Phys.*, 265(2):463–491, 2006.
- [134] D. Donatelli and K. Trivisa. A multidimensional model for the combustion of compressible fluids. *Arch. Ration. Mech. Anal.*, 185(3):379–408, 2007.
- [135] D. Bresch and B. Desjardins. On the existence of global weak solutions to the Navier-Stokes equations for viscous compressible and heat conducting fluids. *J. Math. Pures Appl. (9)*, 87(1):57–90, 2007.
- [136] T. Yang and C. Zhu. Compressible Navier-Stokes equations with degenerate viscosity coefficient and vacuum. *Comm. Math. Phys.*, 230(2):329–363, 2002.
- [137] Y. Cho and H. Kim. Existence results for viscous polytropic fluids with vacuum. *J. Differential Equations*, 228(2):377–411, 2006.
- [138] O. A. Ladyženskaja, V. A. Solonnikov, and N. N. Ural'ceva. *Lineinye i kvazilineinye uravneniya parabolicheskogo tipa*. Izdat. “Nauka”, Moscow, 1968.
- [139] R. Abgrall. How to prevent pressure oscillations in multicomponent flow calculations: a quasi-conservative approach. *J. Comput. Phys.*, 125(1):150–160, 1996.
- [140] R. Abgrall and S. Karni. Computations of compressible multifluids. *J. Comput. Phys.*, 169(2):594–623, 2001.

- [141] J.-P. Cocchi and R. Saurel. A Riemann problem based method for the resolution of compressible multimaterial flows. *J. Comput. Phys.*, 137(2):265–298, 1997.
- [142] F. Coquel, K. El Amine, E. Godlewski, B. Perthame, and P. Rascle. A numerical method using upwind schemes for the resolution of two-phase flows. *J. Comput. Phys.*, 136(2):272–288, 1997.
- [143] P. Jenny, B. Müller, and H. Thomann. Correction of conservative Euler solvers for gas mixtures. *J. Comput. Phys.*, 132(1):91–107, 1997.
- [144] S. Karni. Multicomponent flow calculations by a consistent primitive algorithm. *J. Comput. Phys.*, 112(1):31–43, 1994.
- [145] B. Larrouturou. How to preserve the mass fractions positivity when computing compressible multi-component flows. *J. Comput. Phys.*, 95(1):59–84, 1991.
- [146] W. Mulder, S. Osher, and James A. Sethian. Computing interface motion in compressible gas dynamics. *J. Comput. Phys.*, 100(2):209–228, 1992.
- [147] R. Saurel and R. Abgrall. A multiphase Godunov method for compressible multifluid and multiphase flows. *J. Comput. Phys.*, 150(2):425–467, 1999.
- [148] R. Saurel and R. Abgrall. A simple method for compressible multifluid flows. *SIAM J. Sci. Comput.*, 21(3):1115–1145 (electronic), 1999.
- [149] K.-M. Shyue. An efficient shock-capturing algorithm for compressible multicomponent problems. *J. Comput. Phys.*, 142(1):208–242, 1998.



- [150] V.T. Ton. Improved shock-capturing methods for multicomponent and reacting flows. *J. Comput. Phys.*, 128(1):237–253, 1996.
- [151] K. Xu. BGK-based scheme for multicomponent flow calculations. *J. Comput. Phys.*, 134(1):122–133, 1997.
- [152] C.-H. Chang and M.-S. Liou. A robust and accurate approach to computing compressible multiphase flow: stratified flow model and AUSM<sup>+</sup>-up scheme. *J. Comput. Phys.*, 225(1):840–873, 2007.
- [153] V. E. Badalassi, H. D. Cenicerros, and S. Banerjee. Computation of multiphase systems with phase field models. *J. Comput. Phys.*, 190(2):371–397, 2003.
- [154] C. Berthon and B. Nkonga. Multifluid numerical approximations based on a multipressure formulation. *Comput. & Fluids*, 36(2):467–479, 2007.
- [155] T. Y. Hou, J. S. Lowengrub, and M. J. Shelley. Boundary integral methods for multicomponent fluids and multiphase materials. *J. Comput. Phys.*, 169(2):302–362, 2001.
- [156] E. H. van Brummelen and B. Koren. A pressure-invariant conservative Godunov-type method for barotropic two-fluid flows. *J. Comput. Phys.*, 185(1):289–308, 2003.
- [157] J. W. Banks, D. W. Schwendeman, A. K. Kapila, and W. D. Henshaw. A high-resolution Godunov method for compressible multi-material flow on overlapping grids. *J. Comput. Phys.*, 223(1):262–297, 2007.

- [158] D. W. Schwendeman, C. W. Wahle, and A. K. Kapila. The Riemann problem and a high-resolution Godunov method for a model of compressible two-phase flow. *J. Comput. Phys.*, 212(2):490–526, 2006.
- [159] C. Bridges and K. R. Rajagopal. Pulsatile flow of a chemically-reacting nonlinear fluid. *Comput. Math. Appl.*, 52(6-7):1131–1144, 2006.
- [160] J. Hron, J. Málek, and K.R. Rajagopal. Simple flows of fluids with pressure-dependent viscosities. *Proceedings of the Royal Society of London Series A-Math. Phys. Eng. Sciences*, 457(2011):1603–1622, 2001.
- [161] E. Feireisl and J. Málek. On the Navier-Stokes equations with temperature dependent transport coefficients. *Differ. Equ. Nonlinear Mech.*, pages Art. ID 90616, 14 pp. (electronic), 2006.
- [162] B. Cockburn and C.-W. Shu. Runge-Kutta discontinuous Galerkin methods for convection-dominated problems. *J. Sci. Comput.*, 16(3):173–261, 2001.
- [163] B. Cockburn. An introduction to the discontinuous Galerkin method for convection-dominated problems. In *Advanced numerical approximation of nonlinear hyperbolic equations (Cetraro, 1997)*, volume 1697 of *Lecture Notes in Math.*, pages 151–268. Springer, Berlin, 1998.
- [164] B. Cockburn and C.-W. Shu. The local discontinuous Galerkin method for time-dependent convection-diffusion systems. *SIAM J. Numer. Anal.*, 35(6):2440–2463 (electronic), 1998.
- [165] B. Cockburn, S.-Y. Lin, and C.-W. Shu. TVB Runge-Kutta local projection discontinuous Galerkin finite element method for conservation

- laws. III. One-dimensional systems. *J. Comput. Phys.*, 84(1):90–113, 1989.
- [166] B. Cockburn and C.-W. Shu. TVB Runge-Kutta local projection discontinuous Galerkin finite element method for conservation laws. II. General framework. *Math. Comp.*, 52(186):411–435, 1989.
- [167] M. Feistauer and V. Kučera. On a robust discontinuous Galerkin technique for the solution of compressible flow. *J. Comput. Phys.*, 224(1):208–221, 2007.
- [168] V. Dolejší, M. Feistauer, and V. Sobotíková. Analysis of the discontinuous Galerkin method for nonlinear convection-diffusion problems. *Comput. Methods Appl. Mech. Engrg.*, 194(25-26):2709–2733, 2005.
- [169] V. Dolejší and M. Feistauer. A semi-implicit discontinuous Galerkin finite element method for the numerical solution of inviscid compressible flow. *J. Comput. Phys.*, 198(2):727–746, 2004.
- [170] V. Dolejší and M. Feistauer. On the discontinuous Galerkin method for the numerical solution of compressible high-speed flow. In *Numerical mathematics and advanced applications*, pages 65–83. Springer Italia, Milan, 2003.
- [171] V. Dolejší, M. Feistauer, and C. Schwab. A finite volume discontinuous Galerkin scheme for nonlinear convection-diffusion problems. *Calcolo*, 39(1):1–40, 2002.
- [172] V. Dolejší. On the discontinuous Galerkin method for the numerical solution of the Navier-Stokes equations. *Internat. J. Numer. Methods Fluids*, 45(10):1083–1106, 2004.

- [173] F. Shakib, T.J.R. Hughes, and Z. Johan. A new finite element formulation for computational fluid dynamics. X. The compressible Euler and Navier-Stokes equations. *Comput. Methods Appl. Mech. Engrg.*, 89(1-3):141–219, 1991. Second World Congress on Computational Mechanics, Part I (Stuttgart, 1990).
- [174] C. Michoski, P.G. Schmitz, J.A. Evans, and A. Vasseur. A discontinuous Galerkin method for viscous compressible multifluids. *J. Comput. Phys.*, Submitted, 2008.
- [175] D.N. Arnold, F. Brezzi, B. Cockburn, and D. Marini. Discontinuous Galerkin methods for elliptic problems. In *Discontinuous Galerkin methods (Newport, RI, 1999)*, volume 11 of *Lect. Notes Comput. Sci. Eng.*, pages 89–101. Springer, Berlin, 2000.
- [176] J.C. Strikwerda. Initial boundary value problems for incompletely parabolic systems. *Comm. Pure Appl. Math.*, 30(6):797–822, 1977.
- [177] B. Gustafsson and A. Sundström. Incompletely parabolic problems in fluid dynamics. *SIAM J. Appl. Math.*, 35(2):343–357, 1978.
- [178] G. Kreiss, H.-O. Kreiss, and N. A. Petersson. On the convergence to steady state of solutions of nonlinear hyperbolic-parabolic systems. *SIAM J. Numer. Anal.*, 31(6):1577–1604, 1994.
- [179] H.-O. Kreiss. Initial boundary value problems for hyperbolic systems. *Comm. Pure Appl. Math.*, 23:277–298, 1970.
- [180] B. Engquist and A. Majda. Absorbing boundary conditions for the numerical simulation of waves. *Math. Comp.*, 31(139):629–651, 1977.

- [181] T. J. Poinso and S. K. Lele. Boundary conditions for direct simulations of compressible viscous flows. *J. Comput. Phys.*, 101(1):104–129, 1992.
- [182] D.H. Rudy and J.C. Strikwerda. A nonreflecting outflow boundary condition for subsonic Navier-Stokes calculations. *J. Comput. Phys.*, 36(1):55–70, 1980.
- [183] I. Lie. Well-posed transparent boundary conditions for the shallow water equations. *Appl. Numer. Math.*, 38(4):445–474, 2001.
- [184] J.C. Sutherland and C.A. Kennedy. Improved boundary conditions for viscous, reacting, compressible flows. *J. Comput. Phys.*, 191:502–524, 2003.
- [185] C. Bardos, A. Y. le Roux, and J.-C. Nédélec. First order quasilinear equations with boundary conditions. *Comm. Partial Differential Equations*, 4(9):1017–1034, 1979.
- [186] S. Martin. First order quasilinear equations with boundary conditions in the  $L^\infty$  framework. *J. Differential Equations*, 236(2):375–406, 2007.
- [187] A. A. Zlotnik. Parabolicity of a quasihydrodynamic system of equations and the stability of its small perturbations. *Mat. Zametki*, 83(5):667–682, 2008.
- [188] T. G. Elizarova and Yu. V. Sheretov. Theoretical and numerical investigation of quasigasdynamic and quasihydrodynamic equations. *Comput. Math. Math. Phys.*, 41(2):219–234, 2001.
- [189] H. Brenner. Navier-Stokes revisited. *Phys. A*, 349(1-2):60–132, 2005.

- [190] K. O. Kazenkin. Existence of a global generalized solution of a one-dimensional problem of the flow of a viscous barotropic gas. *Fundam. Prikl. Mat.*, 8(4):993–1007, 2002.
- [191] A. Matsumura and K. Nishihara. Large-time behaviors of solutions to an inflow problem in the half space for a one-dimensional system of compressible viscous gas. *Comm. Math. Phys.*, 222(3):449–474, 2001.
- [192] D. Bresch, B. Desjardins, and D. Gérard-Varet. On compressible Navier-Stokes equations with density dependent viscosities in bounded domains. *J. Math. Pures Appl. (9)*, 87(2):227–235, 2007.
- [193] P.B. Mucha and W.M. Zajączkowski. Global existence of solutions of the Dirichlet problem for the compressible Navier-Stokes equations. *ZAMM Z. Angew. Math. Mech.*, 84(6):417–424, 2004.
- [194] Y. Cho, H.J. Choe, and H. Kim. Unique solvability of the initial boundary value problems for compressible viscous fluids. *J. Math. Pures Appl. (9)*, 83(2):243–275, 2004.
- [195] F. Bassi and S. Rebay. A high-order accurate discontinuous finite element method for the numerical solution of the compressible Navier-Stokes equations. *J. Comput. Phys.*, 131(2):267–279, 1997.
- [196] B. van Leer. Towards the ultimate conservative difference scheme. V. A second-order sequel to Godunov’s method [J. Comput. Phys. **32** (1979), no. 1, 101–136]. *J. Comput. Phys.*, 135(2):227–248, 1997. With an introduction by Ch. Hirsch, Commemoration of the 30th anniversary {of J. Comput. Phys.}.

- [197] B. van Leer. Towards the ultimate conservative difference scheme. IV. A new approach to numerical convection. *J. Comput. Phys.*, 135(2):227–248, 1997. With an introduction by Ch. Hirsch, Commemoration of the 30th anniversary {of J. Comput. Phys.}.
- [198] C.-W. Shu and S. Osher. Efficient implementation of essentially nonoscillatory shock-capturing schemes. *J. Comput. Phys.*, 77(2):439–471, 1988.
- [199] T.J. Barth. On discontinuous Galerkin approximations of Boltzmann moment systems with Levermore closure. *Comput. Methods Appl. Mech. Engrg.*, 195(25-28):3311–3330, 2006.
- [200] T.J. Barth and P. Charrier. Energy stable flux formulas for the discontinuous Galerkin discretization of first-order conservation laws. *Tech. Rep. NAS-01-001, NAS Division, NASA Ames Research Center*, 2001.
- [201] G.S. Jiang and C.-W. Shu. On a cell entropy inequality for discontinuous Galerkin methods. *Math. Comp.*, 62(206):531–538, 1994.
- [202] A.P. Abbott, E.G. Hope, and D.J. Palmer. Effects of solutes on the viscosity of supercritical solutions. *J. Phys. Chem. B*, 111:814–8118, 2007.
- [203] V. Vesovic, M.J. Assael, and Z.A. Gallis. Prediction of the viscosity of supercritical fluid mixtures. *International Journal of Thermophysics*, 19(5):1297–1313, 1998.
- [204] K. Rohlfs and T.L. Wilson. *Tools of Radio Astronomy*. Springer-Verlag Telos; 2nd edition, Berlin; New York, 1996.

- [205] J.M.C. Rawlings and T.W Hartquist. Molecular diagnostics of diffusive boundary layers. *The Astrophysical Journal*, 487:672–688, 1997.
- [206] P. Lesaffre, M. Gerin, and P. Hennebelle. Effects of turbulent diffusion on the chemistry of diffuse clouds. *Astronomy & Astrophysics*, 469:949–961, 2007.
- [207] J.J. Martinell, D. del Castillo-Negrete, A.C. Raga, and D.A. Williams. Non-local diffusion and the chemical structure of molecular clouds. *Mon. Notices Royal Astronomical Society*, 372(1):213–218, 2006.
- [208] A.M. Trubachev. Detonation waves in interstellar gas. *Combustion, Explosion, and Shock Waves*, 33(1):72–76, 1997.
- [209] P.R. Holland. *The quantum theory of motion*. Cambridge University Press, Cambridge, 1995. An account of the de Broglie-Bohm causal interpretation of quantum mechanics.
- [210] G. Brunton, D. Griller, L.R.C. Barclay, and K.U. Ingold. Kinetic applications of electron paramagnetic resonance spectroscopy. 26. Quantum-mechanical tunneling in the isomerization of sterically hindered aryl radicals. *J. Am. Chem. Soc.*, 98(22):6803–6811, 1976.
- [211] R.J. McMahon. Chemical reactions involving quantum tunneling. *Science*, 299(5608):833–834, 2003.
- [212] L. Masgrau, A Roujeinikova, L.O. Johannissen, P. Hothi, J. Basran, K.E. Ranaghan, A.J. Mulholland, M.J. Sutcliffe, N.S. Scrutton, and D. Leys. Atomic description of an enzyme reaction dominated by proton tunneling. *Science*, 312:237–241, 2006.



- [213] M. Ito, K. Yabana, T. Nakatsukasa, and M. Ueda. Fusion reaction of halo nuclei: A real-time wave-packet method for three-body tunneling dynamics. *Nuclear Physics A*, 787:267c–274c, 2007.
- [214] V.E. Madelung. Quantentheorie in hydrodynamischer form. *Z. Physik.*, 40:322, 1926.
- [215] C. L. Gardner. The quantum hydrodynamic model for semiconductor devices. *SIAM J. Appl. Math.*, 54(2):409–427, 1994.
- [216] I.M. Gamba and A. Jüngel. Positive solutions to singular second and third order differential equations for quantum fluids. *Arch. Ration. Mech. Anal.*, 156(3):183–203, 2001.
- [217] C.L. Gardner and C. Ringhofer. Dispersive/hyperbolic hydrodynamic models for quantum transport (in semiconductor devices). In *Dispersive transport equations and multiscale models (Minneapolis, MN, 2000)*, volume 136 of *IMA Vol. Math. Appl.*, pages 91–106. Springer, New York, 2004.
- [218] Z. Chen, B. Cockburn, C.L. Gardner, and J.W. Jerome. Quantum hydrodynamic simulation of hysteresis in the resonant tunneling diode. *J. Comp. Phys*, 117:274–280, 1995.
- [219] Z. Chen, B. Cockburn, J.W. Jerome, and C.W. Shu. Mixed-rkdg finite element method for the 2-d hydrodynamic model for semi-conductor device simulations. *VLSI Design*, 3(2):145–158, 1995.
- [220] H. Li and P. Marcati. Existence and asymptotic behavior of multi-dimensional quantum hydrodynamic model for semiconductors. *Comm. Math. Phys.*, 245(2):215–247, 2004.

- [221] P.-A. Raviart and J. M. Thomas. A mixed finite element method for 2nd order elliptic problems. In *Mathematical aspects of finite element methods (Proc. Conf., Consiglio Naz. delle Ricerche (C.N.R.), Rome, 1975)*, pages 292–315. Lecture Notes in Math., Vol. 606. Springer, Berlin, 1977.
- [222] D. Levy, C.-W. Shu, and J. Yan. Local discontinuous Galerkin methods for nonlinear dispersive equations. *J. Comput. Phys.*, 196(2):751–772, 2004.
- [223] M. Kotschote. Strong solutions for a compressible fluid model of Korteweg type. *Ann. Inst. H. Poincaré Anal. Non Linéaire*, 25(4):679–696, 2008.
- [224] R. Danchin and B. Desjardins. Existence of solutions for compressible fluid models of Korteweg type. *Ann. Inst. H. Poincaré Anal. Non Linéaire*, 18(1):97–133, 2001.
- [225] I. Kostin, M. Marion, R. Texier-Picard, and V.A. Volpert. Modelling of miscible liquids with the Korteweg stress. *M2AN Math. Model. Numer. Anal.*, 37(5):741–753, 2003.
- [226] J. Tian and G. Zhou. Soliton-like solutions for higher-order nonlinear Schrödinger equation in inhomogeneous optical fibre media. *Phys. Scr.*, 73(1):56–61, 2006.
- [227] R. Atre, P.K. Panigrahi, and G. S. Agarwal. Class of solitary wave solutions of the one-dimensional Gross-Pitaevskii equation. *Phys. Rev. E (3)*, 73(5):056611, 5, 2006.

- [228] E. Kengne and R. Vaillancourt. Exact solutions of the Gross-Pitaevskii equation in periodic potential in the presence of external source. *J. Math. Phys.*, 48(7):073520, 13, 2007.
- [229] S. Osher. Convergence of generalized MUSCL schemes. *SIAM J. Numer. Anal.*, 22(5):947–961, 1985.
- [230] J.F. Price. Lagrangian and eulerian representations of fluid flow: Kinematics and the equations of motion. *MIT lecture notes online*, 2006.
- [231] J.N. Murrell, S. Carter, S.C. Farantos, P. Huxley, and A.J.C. Varandas. *Molecular Potential Energy Functions*. John Wiley & Sons, Chichester [West Sussex] ; New York, 1984. A Wiley Interscience publication.
- [232] V. N. Snytnikov, G. I. Dudnikova, J. T. Gleaves, S. A. Nikitin, V. N. Parmon, V. O. Stoyanovsky, V. A. Vshivkov, G. S. Yablonsky, and V. S. Zakharenko. Space chemical reactor of protoplanetary disk. *Advances in Space Research*, 30(6):1461 – 1467, 2002.
- [233] S. M. Suh, M. R. Zachariah, and S. L. Girshick. Numerical modeling of silicon oxide particle formation and transport in a one-dimensional low-pressure chemical vapor deposition reactor. *Journal of Aerosol Science*, 33(6):943 – 959, 2002.
- [234] J. Ferris, B. Tran, J. Joseph, V. Vuitton, R. Briggs, and M. Force. The role of photochemistry in titan’s atmospheric chemistry. *Advances in Space Research*, 36(2):251 – 257, 2005. Space Life Sciences: Astrobiology: Steps toward Origin of Life and Titan before Cassini.
- [235] R. Ye, A. Murphy, and T. Ishigaki. Numerical modeling of an arh2 radio-frequency plasma reactor under thermal and chemical nonequilibrium

- conditions. *Plasma Chemistry and Plasma Processing*, 27(2):189–204, April 2007.
- [236] R.R. Pompano, H.-W. Li, and R.F. Ismagilov. Rate of mixing controls rate and outcome of autocatalytic processes: Theory and microfluidic experiments with chemical reactions and blood coagulation. *Biophysical Journal*, 95(3):1531 – 1543, 2008.
  - [237] P. Érdi and J. Tóth. *Mathematical models of chemical reactions*. Non-linear Science: Theory and Applications. Princeton University Press, Princeton, NJ, 1989. Theory and applications of deterministic and stochastic models.
  - [238] K. B. McGrattan, T. Kashiwagi, H. R. Baum, and S. L. Olson. Effects of ignition and wind on the transition to flame spread in a microgravity environment. *Combustion and Flame*, 106(4):377 – 382, 1996.
  - [239] T. Goudon and A. Vasseur. Regularity analysis for systems of reaction-diffusion equations. *Submitted*.
  - [240] M.C. Caputo and A. Vasseur. Global regularity of solutions to systems of reaction-diffusion with sub-quadratic growth in any dimension. *Submitted*.
  - [241] H.M. Nassef, A-E. Radi, and C.K. O’Sullivan. Electrocatalytic oxidation of hydrazine at o-aminophenol grafted modified glassy carbon electrode: Reusable hydrazine amperometric sensor. *Journal of Electroanalytical Chemistry*, 592(2):139 – 146, 2006.
  - [242] M. Takahashi, N. Shibasaki-Kitakawa, C. Yokoyama, and S. Takahashi. Viscosity of gaseous nitrous oxide from 298.15 K to 398.15 K at pressures

- up to 25 MPa. *Journal of Chemical & Engineering Data*, 41(6):1495–1498, 1996.
- [243] W.J. Massman. A review of the molecular diffusivities of  $\text{H}_2\text{O}$ ,  $\text{CO}_2$ ,  $\text{CH}_4$ ,  $\text{CO}$ ,  $\text{O}_3$ ,  $\text{SO}_2$ ,  $\text{NH}_3$ ,  $\text{N}_2\text{O}$ ,  $\text{NO}$ , and  $\text{NO}_2$  in air,  $\text{O}_2$  and  $\text{N}_2$  near STP. *Atmospheric Environment*, 32(6):1111 – 1127, 1998.
- [244] C.L. Benner, N.L. Eatough, E.A. Lewis, D.J. Eatough, A.A. Huang, and E.C. Ellis. Diffusion coefficients for ambient nitric and nitrous acids from denuder experiments in the 1985 nitrogen species methods comparison study. *Atmospheric Environment (1967)*, 22(8):1669 – 1672, 1988.
- [245] L. Catoire, N. Chaumeix, and C. Paillard. Chemical kinetic model for monomethylhydrazine/nitrogen tetroxide gas-phase combustion and hypergolic ignition. *Journal of propulsion and power*, 20(1):87–96, 2004.
- [246] M. Massoudi. A note on the meaning of mixture viscosity using the classical continuum theories of mixtures. *Internat. J. Engrg. Sci.*, 46(7):677–689, 2008.
- [247] K. R. Rajagopal and L. Tao. *Mechanics of mixtures*, volume 35 of *Series on Advances in Mathematics for Applied Sciences*. World Scientific Publishing Co. Inc., River Edge, NJ, 1995.
- [248] A. Einstein. *Investigations on the theory of the Brownian movement*. Dover Publications Inc., New York, 1956. Edited with notes by R. Fürth, Translated by A. D. Cowper.
- [249] D. Bresch, B. Desjardins, J.M. Ghidaglia, and E. Grenier. On global weak solutions to a generic two-fluid model. preprint, 2009.

- [250] N. Crouseilles, P.A. Hervieux, and G. Manfredi. Quantum hydrodynamic model for the nonlinear electron dynamics in thin metal films. *Phys. Rev. B*, 78(15):155412, 2008.

# Vita

Craig Evan Michoski was born in Fort Collins, Colorado on 29 August 1976, the son of Thomas Paul Michoski and Beverly Diane Zeiler Michoski. After graduating from Rocky Mountain High School in 1995, he enrolled at the University of Washington. In 1996 he transferred to the University of Colorado at Boulder and received his Bachelor of Arts degree in Biochemistry in the Spring of 1999 with an emphasis in mathematics. He spent the next four years working in the fields of neurobiology, mycology, microbiology and bioinformatics, until in the Fall of 2003 being admitted to the graduate program in the department of Chemistry and Biochemistry.

Permanent address: 2901 Barton Skyway  
Austin, Texas 78746

This dissertation was typeset with L<sup>A</sup>T<sub>E</sub>X<sup>†</sup> by the author.

---

<sup>†</sup>L<sup>A</sup>T<sub>E</sub>X is a document preparation system developed by Leslie Lamport as a special version of Donald Knuth's T<sub>E</sub>X Program.